DISSERTATION

THE DUAL LENS OF SUSTAINABILITY: ECONOMIC AND ENVIRONMENTAL INSIGHTS INTO NOVEL CARBON REDUCTION TECHNOLOGIES USING SYSTEMS MODELING, DATA SCIENCE, AND MULTI-OBJECTIVE OPTIMIZATION

Submitted by

Braden Jeffery Limb

Department of Systems Engineering

In partial fulfillment of the requirements

For the Degree of Doctor of Philosophy

Colorado State University

Fort Collins, Colorado

Summer 2024

Doctoral Committee:

Advisor: Jason C. Quinn
Co-Advisor: Steven J. Simske

Erika E. Gallegos
Matthew R.V. Ross

ABSTRACT

THE DUAL LENS OF SUSTAINABILITY: ECONOMIC AND ENVIRONMENTAL INSIGHTS INTO NOVEL CARBON REDUCTION TECHNOLOGIES USING SYSTEMS MODELING, DATA SCIENCE, AND MULTI-OBJECTIVE OPTIMIZATION

In an era marked by escalating climate change and increasing energy demands, the pursuit of sustainable solutions in energy production and environmental management is more critical than ever. This dissertation delves into this challenge, focusing on innovative technologies aimed at reducing carbon emissions in key sectors: power generation, wastewater treatment, and aviation.

The first segment of the dissertation explores the integration of thermal energy storage with natural gas power plants using carbon capture, a crucial advancement given the dominant role of fossil fuel-based power plants in electricity generation. Addressing the economic and operational drawbacks of current carbon capture and storage (CCS) technologies, this study evaluates various thermal storage configurations. It seeks to enhance plant performance through energy arbitrage, a novel approach to offset the large heat loads required for carbon capture solvent regeneration. By optimizing these technologies for current and future grid pricing and comparing their feasibility with other production methods, this research aims to strike a balance between maintaining reliable power generation and adhering to stringent environmental targets. Results show that resistively charged thermal storage can both increase CCS flexibility and

power plant profits through energy arbitrage when compared to power plants with CCS but without thermal storage.

Beyond electrical systems, addressing climate change also necessitates improving the energy efficiency of water treatment technologies. Therefore, the dissertation investigates the potential of nature-based solutions as sustainable alternatives to traditional water treatment methods in the second section. This section probes into the efficacy of green technologies, such as constructed wetlands, in reducing costs and emissions compared to conventional gray infrastructure. By quantifying the impact of these technologies across the U.S. and evaluating the role of carbon financing, the research highlights a pathway towards more environmentally friendly and economically viable water treatment processes. Results show that nature-based water treatment technologies can treat up to 37% of future nutrient loading while both decreasing water treatment costs and emissions compared to traditional water treatment techniques.

The transportation sector will play a key role in addressing climate change as it is the largest contributor to greenhouse gas emissions. While most of the transportation sector is expected to transition to electric vehicles to decrease its carbon footprint, aviation remains hard to decarbonize as electric passenger aviation is expected to be range limited. Therefore, the final segment of the dissertation addresses the challenge of meeting the U.S. Department of Energy's Sustainable Aviation Fuel (SAF) goals. It involves a comprehensive analysis of various bioenergy feedstocks for SAF production, using GIS modeling to assess their economic and environmental impacts across diverse land types. The study employs multi-objective optimization to strategize the deployment of these feedstocks, considering factors like minimum fuel selling price, greenhouse gas emissions, and breakeven carbon price. Furthermore, agent-

based modeling is used to identify policy incentives that could encourage farmer adoption of bioenergy crops, a critical step towards meeting the SAF Grand Challenge goals.

This dissertation offers a comprehensive analysis of novel carbon reduction technologies, emphasizing both economic viability and environmental sustainability. By developing integrated models across key sectors affected by climate change, it explores the benefits and trade-offs of various sustainability strategies. Incorporating geospatial and temporal dimensions, the research uses multi-objective optimization and systems thinking to provide targeted investment strategies for the greatest impact. The results provide important insights and actionable plans for policymakers and industry leaders, contributing to a sustainable and low-carbon future in essential areas of the global economy.

ACKNOWLEDGEMENTS

First, I would like to thank my advisor, Dr. Jason Quinn, for providing me with this opportunity and for being an invaluable mentor and friend in all aspects of research and life over the years. I would also like thank Jason's family for graciously allowing him to spend countless hours reviewing my work when he could've been spending time with the family. I also thank my other committee members for their time investment, support, and assistance throughout both my education and research endeavors. Specially, I thank my co-advisor, Dr. Steven Simske, for engaging in thought-provoking discussions about my research and for providing thoughtful feedback and compliments on my work. I thank Dr. Erika Gallegos for opening my eyes to the power of R and enhancing my data visualization skills and thank Dr. Matthew Ross for recommending the work of interdisciplinary thinkers so I can continue to learn and expand my horizons. I also thank Dr. Todd Bandhauer, Dr. Evan Thomas, and Dr. Jordan Kern for their mentorship and feedback on my research.

Thanks to all my amazing research colleagues (Jack Smith, Ethan Markey, Roberto Vercellino, Joe Huyett, Shane Garland, David Quiroz, Jonah Greene, Noah Horesh, Garrett Cole, Anthony Asuega, Brooke Silagy, Reid Maynard, Hailey Summers, Ashley Ryland, Smith Pittman, Evan Sproul, Peter Chen, and David Trinko) for sitting through hours of presentations, providing constructive criticism of my research, being great friends, and striving to make our entire research group better. I also owe a special thanks to Jack Smith for helping me bring our sustainable aviation fuel work to reality as it wouldn’t have been possible without him. I would also like to thank my collaborators at University of Pennsylvania, University of Colorado

Boulder, and North Carolina State University for their assistance and feedback throughout my research.

I would be remiss if I didn't thank my family (Kelli, Owen, Rori, Mary, Breshae, Jared, Oakley, Roland, Taylor, Sherri, Jessica, Braden, Addy, and Erika), friends (Sam, McKenna, Katrina, and countless others), and everyone else I have interacted with during my time at Colorado State University. Each one of these people has played an important part in turning me into the person I am today and have provided the support necessary for me to chase my dreams. I would also like to give a special thank you to Kelli Morrill who tries her hardest to ensure I maintain a healthy work/life balance and has provided more support, companionship, and confidence in me than I could've asked for. I also owe a special thank you to Owen for reminding me to stay curious and appreciate the amazing world we live in, and to Rori for emphasizing the importance of play and ensuring I get my daily exercise.

Lastly, I want to thank the Department of Energy's Advanced Research Projects Agency-Energy (ARPA-E) and the Department of Energy's Bioenergy Technologies Office (BETO) for funding my research projects. None of this research would've been possible without their support.

TABLE OF CONTENTS

ABSTRACT ii

ACKNOWLEDGEMENTS v

CHAPTER 1: INTRODUCTION 1

CHAPTER 2: INTEGRATING THERMAL STORAGE WITH POST COMBUSTION CARBON CAPTURE ON NATURAL GAS POWER PLANTS 4

2.1 Introduction 4

2.2 Materials and methods 8

2.2.1 Thermal Energy Storage Configurations 10

2.2.2 Technology Modeling 12

2.2.3 Optimization 16

2.2.4 Economic Model and Assumptions 17

2.2.5 Electricity Price Profiles 18

2.2.6 Capacity Expansion Modeling Assumptions 21

2.3 Results and discussion 21

2.3.1 Initial Thermal Storage Downselection 22

2.3.2 Feasibility in Future Grid Scenarios 26

2.3.3 Capacity Expansion Modeling 32

2.4 Conclusions 35

CHAPTER 3: ECONOMIC AND ENVIRONMENTAL FEASIBLITY OF GREEN WASTEWATER TREATMENT BASED WATER QUALITY TRADING 37

3.1 Introduction 37

3.2 Materials and methods 43

3.2.1 Wastewater Nutrient Data 43
3.2.2 Gray Treatment Methods 45
3.2.3 Green Treatment Methods 48
3.2.4 Calculation Methods and Assumptions 51
3.3 Results and discussion 56
3.3.1 Nutrient Remediation Potential of Green Infrastructure 57
3.3.2 Global Warming Potential of Gray vs Green Infrastructure 59
3.3.3 Carbon Financing Potential of Green Infrastructure 60
3.4 Discussion 64
3.5 Data and Code Availability 68
CHAPTER 4: PURPOSE-GROWN BIOENERGY FEEDSTOCK OPTIMIZATION FOR UNITED STATES SUSTAINABLE AVIATION FUEL TARGETS WITH ECONOMIC AND ENVIRONMENTAL INSIGHTS 69
4.1 Introduction 69
4.2 Materials and methods 72
4.3 Results 99
4.4 Discussion 109
4.5 Data Availability 112
CHAPTER 5: CONCLUSIONS AND RECOMMENDATIONS 113
5.1 Overall conclusions 113
5.2 Future Directions on Thermal Energy Storage for Natural Gas Combined Cycle Power Plants with Carbon Capture and Sequestration 114
5.3 Future Directions on Green Wastewater Treatment and Water Quality Trading 115

5.4 Sustainable Aviation Fuel from Purpose-Grown Bioenergy Feedstock to Meet U.S. Targets 116
REFERENCES 120
APPENDIX A 156
Appendix A Nomenclature 156
Modeling Assumptions 158
Economic Modeling Details and Governing Equations 159
Technology Modeling Details and Governing Equations 162
Vapor – FG_S/HC Model 170
HRSG IPT – S/HC Model 173
APPENDIX B 177
Nutrient Remediation Potential of Green Infrastructure 177
Optimal Green Infrastructure Deployment Across the US 182
Global Warming Potential of Gray vs. Green Infrastructure 184
Carbon Financing Potential Green Infrastructure 185
Cost and Emissions Comparison Between All Green and Gray Technologies 191
Supplementary Methods Visuals 194
Life Cycle Emissions of Green Treatment Methods 196
Saturated Buffer 197
Woodchip Bioreactor 197
Constructed Wetland 198
Nutrient Rate Reduction 198
Split Nutrient Application 198

Cover Crop 199

No-Till Farming 199

APPENDIX C 200

Discussion on Gasification/Hydroprocessing End Products 200

Impact of biorefinery location on economic and environmental impacts 265

CHAPTER 1: INTRODUCTION

In an era marked by escalating climate change and increasing energy demands, the pursuit of sustainable solutions in energy production and environmental management is more critical than ever. This dissertation, titled "The Dual Lens of Sustainability: Economic and Environmental Insights into Novel Carbon Reduction Technologies Using Systems Modeling, Data Science, and Multi-Objective Optimization," delves into this challenge. It focuses on innovative technologies aimed at reducing carbon emissions in key sectors: power generation, wastewater treatment, and aviation. By addressing the interconnectedness of these sectors, this research highlights the importance of integrated approaches to sustainability.

The global climate crisis necessitates immediate and comprehensive action to reduce greenhouse gas emissions. The energy sector, responsible for a significant portion of these emissions, stands at the forefront of this battle. Fossil fuel-based power generation, which currently accounts for 25% of global emissions [1], must evolve to meet stringent environmental targets. The integration of carbon capture and storage (CCS) with natural gas power plants is a pivotal strategy in this evolution [2–6]. However, the economic and operational drawbacks of CCS, particularly the large parasitic heat loads required for solvent regeneration, present significant challenges [7]. This dissertation explores the integration of thermal energy storage (TES) with CCS to enhance plant performance and economic viability through energy arbitrage [8–16].

Water and wastewater treatment is another critical area requiring sustainable innovation. Traditional gray infrastructure solutions are not only capital-intensive but also contribute substantially to carbon emissions [17]. Nature-based solutions, such as constructed wetlands, offer a promising alternative. These green technologies can reduce costs and emissions, providing a sustainable pathway for water treatment [17–27]. By quantifying the impacts of these technologies across the U.S. and evaluating their role in carbon financing, this research aims to demonstrate the potential of nature-based solutions to transform the water treatment landscape.

The transportation sector, particularly aviation, poses unique challenges for decarbonization. Despite advancements in electric vehicle technology, aviation remains heavily reliant on petroleum fuels due to range limitations [28]. The U.S. Department of Energy's Sustainable Aviation Fuel (SAF) Grand Challenge seeks to address this by expanding domestic SAF production to meet ambitious targets [29–32]. This dissertation conducts a comprehensive analysis of various bioenergy feedstocks for SAF production, utilizing GIS modeling to assess their economic and environmental impacts [33–52]. Multi-objective optimization and agent-based modeling are employed to identify optimal deployment strategies and policy incentives, respectively, to encourage farmer adoption of bioenergy crops [28–44,53–58].

This dissertation employs a range of methodologies to evaluate the economic and environmental implications of carbon reduction technologies. Systems modeling, data science, and multi-objective optimization are integrated to develop comprehensive models across the power generation, wastewater treatment, and aviation sectors. By incorporating geospatial and temporal dimensions, these models provide targeted investment strategies and explore the benefits and trade-offs of various sustainability approaches. The holistic nature of this research

ensures that the solutions proposed are not only technically feasible but also economically viable and environmentally sustainable.

The significance of this dissertation lies in its comprehensive approach to addressing climate change. By focusing on the interconnectedness of power generation, water treatment, and aviation, it underscores the necessity of integrated solutions in achieving sustainability. The findings provide valuable insights for policymakers and industry leaders, offering actionable strategies for reducing carbon emissions and enhancing economic viability.

In power generation, the integration of TES with CCS could revolutionize how natural gas power plants operate, balancing the need for reliable energy with environmental goals [59–69]. In water treatment, the shift towards nature-based solutions represents a paradigm shift, promoting more sustainable and cost-effective practices [70–75]. In aviation, optimizing the production and deployment of SAF from diverse bioenergy feedstocks can significantly reduce the sector's carbon footprint, aligning with global emission reduction targets [33–38,57,58].

This dissertation offers a robust analysis of novel carbon reduction technologies, emphasizing both economic viability and environmental sustainability. By developing integrated models and employing advanced optimization techniques, the research provides critical insights and actionable plans for achieving a sustainable and low-carbon future. The interdisciplinary approach and the focus on real-world applicability make this dissertation a significant contribution to the ongoing efforts to combat climate change. The holistic and unified exploration presented here aims to advance the understanding and implementation of sustainable practices across key sectors, driving progress towards a greener and more resilient global economy.

CHAPTER 2: INTEGRATING THERMAL STORAGE WITH POST COMBUSTION CARBON CAPTURE ON NATURAL GAS POWER PLANTS[1]

2.1 Introduction

Across the world there are a multitude of climate goals designed to reduce the impact of global warming in the coming years. Most of these goals center around reducing greenhouse gas emissions, particularly carbon dioxide (CO_2) [76–79]. Currently, fossil fuel based electricity generation is the largest greenhouse gas emitter of all the economic sectors at 25% of total global emissions [1]. To meet future environmental goals, fossil fuel-based power plants will require the addition of carbon capture and storage (CCS) to reduce their overall environmental impact [2–6]. However, the seamless integration of CCS systems has a variety of hurdles.

One major challenge with the integration of CCS is related to the operation of the power plant. At this time, the real-world feasibility of CCS has only been demonstrated a couple of times on base load power plants fueled by coal and natural gas [80,81]. In the last decade, 121 base load coal fired power plants have been decommissioned or converted to natural gas due to

---

[1]Portions of this chapter were published as a peer-reviewed journal article and as a peer-reviewed conference publication:

Limb, B. J., Markey, E., Vercellino, R., Garland, S., Pisciotta, M., Psarras, P., Herber, D. R., Bandhauer, T., & Quinn, J. C. (2022). Economic viability of using thermal energy storage for flexible carbon capture on natural gas power plants. *Journal of Energy Storage*, 55, 105836. https://doi.org/10.1016/j.est.2022.105836

Limb, B., Markey, E., Vercellino, R., Huyett, J., Garland, S., Pisciotta, M., Psarras, P., Meuleman, E., Fine, N., Abarr, M., Herber, D., Quinn, J., & Bandhauer, T. (2022). Evaluating the economic viability of NGCC-SWITCC: Natural Gas Combined Cycle System With Integrated Thermal storage and Carbon Capture (SSRN Scholarly Paper 4295563). https://doi.org/10.2139/ssrn.4295563

stricter emissions standards and economic constraints [82,83]. Additionally, nuclear plants are not being deployed because of safety concerns, policy changes, and high initial capital costs [84–86]. These plants are being replaced by less expensive renewable generation technologies (i.e. solar and wind) which have intermittent production issues and limited operation flexibility. As environmental policies continue to be adopted and the fraction of renewables increases, it is expected that natural gas power plants with CCS will serve as a technology to replace coal and nuclear loads while also meeting peak demands when renewable energy is not available [87,88]. However, the operation of CCS systems requires a large parasitic heat load from the power plant for the carbon capture solvent regeneration process [7]. This solvent regeneration process is essential to separate and store the captured CO_2 from the chemical-based solvent, but in doing so requires an immense amount of heat from the power plant. The heat load in this process is traditionally supplied via steam taken from the heat recovery steam generator (HRSG) in the natural gas combined cycle (NGCC) power plant. This reduces the power plant's power output to the grid since less steam can be used for power generation in the steam turbines. Overall, this load can reduce the total power generation by 12%, limits the plant's operating flexibility, and reduces the peak power output of the plant. In a scenario where renewable technologies are fully deployed, it is expected that natural gas plants will only represent 3% of the total power generation sector and will primarily be used for highly variable peaking demands caused by the intermittency of renewable technologies [89,90]. This flexible operational mode represents a major challenge to traditional CCS systems which have only been operated on baseload power systems.

Since future power plants will need to incorporate CCS technologies, there is a need to evaluate technologies that can work synergistically with power plants using CCS to overcome

the operational limitations caused by carbon capture. Currently, two areas of research are focused on addressing these concerns: CCS bypass and fluid/energy storage. One of the most studied methods to increase CCS flexibility is to bypass the CCS unit during peak loads [8–13]. This allows the power plant to operate at full power output, but also releases all combustion gases to the environment. Studies have shown that bypassing the CCS is only economically feasible in situations where carbon taxes are between \$20-70/ton-CO_2 which is below expected targets [12,14–16]. As such, bypass is expected to have minimal deployment in future grids [10]. The second area of research aimed at mitigating CCS operation constraints is the use of storage technologies. The primary storage technologies that have been evaluated include solvent storage, hydrogen storage, and oxygen storage [8–13,91–95]. The main benefit of solvent storage is that it allows the energy intensive process of solvent regeneration to be shifted to off-peak power periods. The solvent storage tanks are charged or discharged depending on the operation of the power plant and the energy available for solvent regeneration. During times of peak power demand, the CCS solvent absorbs CO_2 from the flue gas and then stores the solvent in a storage tank. During times of low power demand, the storage tank discharges the CO_2 rich solvent for solvent regeneration using excess plant power. Studies have shown solvent storage to increase plant profits by 9-29% compared to systems without solvent storage [12]. However, solvent storage solutions require specialty equipment which increases capital costs and makes them infeasible in future market conditions [10,96]. Two additional methods to increase flexibility of CCS include hydrogen and oxygen storage [91–95]. Both hydrogen and oxygen storage show promise by taking advantage of electricity price arbitrage. Hydrogen and oxygen can be produced and stored using low-cost electricity, then burned to produce additional electricity and profits at high prices. These storage methods show economic promise, but have limited real

world testing which has led to concerns about their feasibility [97]. Another storage technology that has shown significant economic promise is thermal energy storage (TES). Previous studies have found TES to have promising economic potential to stabilize the electricity grid, increase NGCC peak power generation, and increase NGCC combustion efficiency through inlet chilling [59,60,98,99,61–69]. However, the interconnection between TES and CCS has not been explored. Therefore, this study evaluates the feasibility of TES solutions to be used in combination with NGCC power plants and CCS technologies.

TES systems can be made up of both hot and cold thermal storage units and provide many benefits to the NGCC+CCS system. First, hot thermal storage can be used to supply steam to the CCS regeneration process during times of peak power demand which eliminates the steam requirement from the NGCC and therefore increase the NGCC's power output to the grid. Second, cold thermal storage can be generated concurrently with hot thermal storage using a Brayton Cycle heat pump or tiered vapor compression heat pump. This cold energy can be used to chill the air entering the NGCC power plant which increases the inlet air's density, thus improving the plant's efficiency and net power output [59]. Third, future electricity grids are expected to have large price variability which TES systems can leverage [100,101]. TES units can charge during times of low electricity demand (low electricity prices) and discharge during peak demand (high electricity prices) which increase overall power plant profits since more power will be output at higher electricity costs. Lastly, the charging and discharging of the TES system allows the power plant to have a more flexible power output range (i.e. lower minimum power output and higher maximum power output) than comparable NGCC+CCS systems.

This research evaluates multiple TES configurations (Brayton cycle heat pump, vapor compression heat pump, HRSG steam extraction for storage, and resistive heating for storage)

over thousands of real-world and future electricity price signals to determine the optimal thermal storage solution to overcome current limitations with NGCC+CCS systems. Additional results use capacity expansion modeling to compare future deployment of NGCC+CCS+TES to existing power generation technologies to assess its feasibility. Discussion focuses on the impact of electricity pricing on the optimal thermal storage system and the advantages and disadvantages of the systems evaluated.

2.2 Materials and methods

The methods are broken down into the subsections representing each component necessary for the completion of this analysis. Evaluation of the proposed thermal storage technologies required three interconnected models to simulate the power plant's operation and evaluate the economic feasibility of TES coupled with NGCC+CCS. These models include a technology model which simulates the thermodynamic performance of each of the key components (NGCC, CCS, and TES), an optimization model which determines how the power plant should operate based off a given electricity price signal and calculates optimum TES storage sizing, and an economics model which evaluates the net present value (NPV) of the system based off the profits and costs (including all capital and operational costs). Descriptions of the each of these models are presented in the following sections. The following subsections detail the TES configurations, the technology model, optimization, economics model, electricity price signals used, and capacity expansion modeling assumptions.

For all TES configurations, the NGCC+CCS+TES's operation mechanics are dependent on whether the TES units are charging, discharging, or neutral (Figure 1). The "neutral phase" refers to the operation mode where the power plant is running as a standard NGCC+CCS plant and no charging or discharging of thermal storage is taking place. During the "charging phase", net power

plant output is decreased and the extra energy is used to charge the thermal storage reservoirs. Charging of the TES units can be done via heat from the NGCC or grid electricity depending on the configuration. Configurations that charge using grid electricity can charge during periods when electricity prices are near zero for greater arbitrage opportunity. During the "discharge phase", peak power output is being sent to the grid and both thermal storage reservoirs are being depleted. The hot TES is providing steam to the CCS unit and cold TES is chilling the ambient air entering the NGCC to increase combustion efficiency. Last, there is an additional "boost phase," which is only available for configurations that include an independently refrigerated cold storage and refers

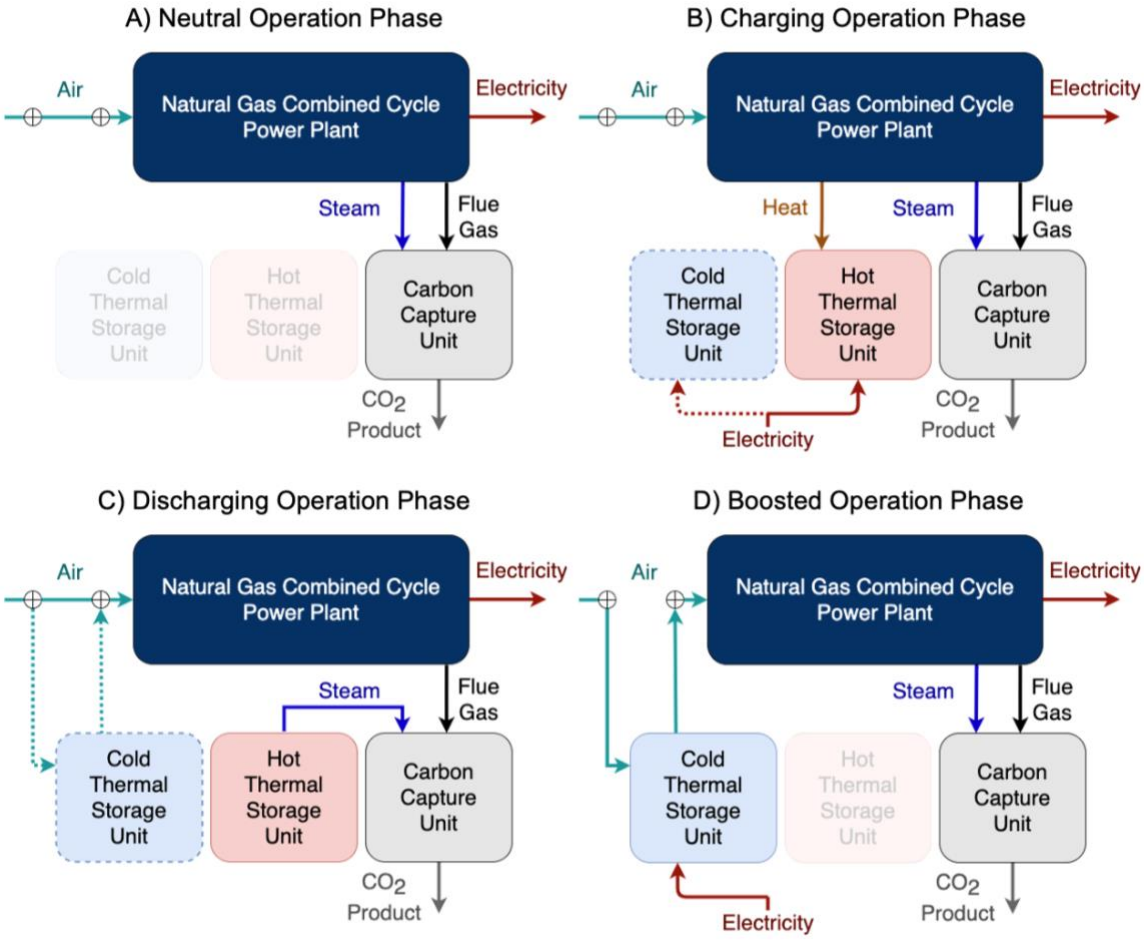

Figure 1. Four operation phases that were simulated for the thermal energy storage configurations evaluated: A) neutral operation phase, B) charging operation phase, C) discharging operation phase, and D) boosted operation phase (only available if cold TES is used). Dotted lines to/from cold thermal storage unit represent optional paths if cold TES is used. Cold TES is not required on all configurations.

to the operation mode where the cold TES is simultaneously being charged and discharged. For some configurations, this results in a slight power boost above the neutral power output and incurs an increase in natural gas consumption.

2.2.1 Thermal Energy Storage Configurations

In total, seventeen unique thermal storage configurations coupled with a NGCC+CCS were evaluated for this study. These configurations were identified through a preliminary economic and thermodynamic analysis that confirmed real-world feasibly. The configurations are broken down into 4 main categories of thermal storage heat pump design: Brayton cycle heat pump, vapor compression heat pump, HRSG steam extraction for storage, and resistive heating. Diagram of the thermal storage categories can be found in publications by Limb et al. [102,103]. Regardless of the thermal storage category used, all configurations interact with the NGCC+CCS in a similar way. Each configuration stores thermal energy during times of low electricity prices and discharges that thermal energy during high electricity prices to generate maximum profits. In all cases, hot thermal energy is taken from the NGCC plant or generated using electricity to charge the hot TES. The hot TES is discharged to provide steam to the CCS unit for solvent regeneration such that the NGCC can output maximum power to the grid. If used, cold TES is charged using electricity and discharged to chill NGCC inlet air which increases combustion efficiency. The main operational difference between the unique configurations is the thermal energy source or generation method. The thermal energy source or generation method is based on the combination of thermal storage category, working fluid, and hot and/or cold thermal storage that is used. A list of all the thermal storage configurations is presented in Table 1.

Table 1. Breakdown of each of the thermal storage configurations evaluated in this study. All systems are coupled with a natural gas combined cycle power plant with carbon capture sequestration for evaluation.

Name	Heat Pump Type	Working Fluid	Hot	Cold
Brayton - FG/HC	Brayton Cycle	Flue Gas	✓	✓
Brayton - FG/H	Brayton Cycle	Flue Gas	✓	✗
Brayton - A/HC	Brayton Cycle	Ambient Air	✓	✓
Brayton - A/H	Brayton Cycle	Ambient Air	✓	✗
Brayton - FA/HC	Brayton Cycle	Flue Gas Heated Air	✓	✓
Brayton - FA/H	Brayton Cycle	Flue Gas Heated Air	✓	✗
Vapor - FG/HC	Vapor Compression	Flue Gas Heated Steam	✓	✓
Vapor - FG/H	Vapor Compression	Flue Gas Heated Steam	✓	✗
Vapor - S/HC	Vapor Compression	Steam Heated Steam	✓	✓
Vapor - S/H	Vapor Compression	Steam Heated Steam	✓	✗
Tiered VC - S/HC	Tiered Vapor Compression	Heat Pumped Steam	✓	✓
HRSG LPT - S/HC	Steam from LPT	Steam	✓	✓
HRSG LPT - S/H	Steam from LPT	Steam	✓	✗
HRSG IPT - S/HC	Steam from IPT	Steam	✓	✓
HRSG IPT - S/H	Steam from IPT	Steam	✓	✗
Resistive - A/HC	Resistive Heating TES	Air	✓	✓
Resistive - A/H	Resistive Heating TES	Air	✓	✗

Each TES configuration shown in Table 1 has been designated a simplified name for reference in this paper. Each name starts with the heat pump type, followed by the working fluid used, and finishes with a designation for the type of thermal storage used (hot and/or cold). The heat pump types used are Brayton cycle heat pump (Brayton), vapor compression heat pump (Vapor), tiered vapor compression heat pump with interconnected hot and cold storage (Tiered VC), steam extraction from the low-pressure turbine in the heat recovery steam generator for storage (HRSG LPT), steam extraction from the intermediate-pressure turbine in the heat recovery steam generator for storage (HRSG IPT), and resistive heating (Resistive). The working fluids used are flue gas (FG), steam (S), flue gas heated air (FG_A), flue gas heated steam (FG_S), and steam heated steam (S_S). Lastly, there were two types of thermal storage used: hot storage (H) or hot and cold storage (HC). For example, Brayton – A/HC is a Brayton cycle heat pump that uses ambient air as the working fluid and has both hot and cold storage. This cycle

differs from Brayton – FG_A/HC in that Brayton – FG_A/HC is a Brayton cycle heat pump that also uses air as the working fluid, but it is preheated by the flue gas leaving the HRSG before entering the Brayton cycle. For all vapor compression (besides Tiered VC – S/HC) and HRSG configurations that use both hot and cold storage, a vapor compression unit is used to generate the cold thermal energy for inlet chilling.

2.2.2 Technology Modeling

The technology model is designed to simulate the key components of the NGCC+CCS+TES configurations in the different phases of operation. The following sections detail how each of the main components (NGCC, CCS, and TES) are modeled and validated.

2.2.2.1 NGCC + CSS Modeling

The base power plant selected for this analysis was the NGCC power plant with CCS as specified in the National Energy Technology Laboratory's (NETL) 2019 report (Case B31B) [104]. Case B31B uses Shell's proprietary and patented CANSOLV CO_2 capture technology which utilizes a regenerable amine solvent [105]. As such, all assumptions listed for both the NGCC and CCS units in the NETL report were used for this analysis unless otherwise noted. In some scenarios, the NGCC power plant without CCS in the NETL 2019 report was used (Case B31A) and ION Clean Energy's ICE-31 solvent was evaluated as a next generation CCS technology [106]. The TES configurations were coupled with the base power plant and compared to the base power plant without TES to determine the value of TES used with CCS. A thermodynamic model of this plant was constructed in Engineering Equation Solver (EES) to properly represent the effect that each TES configuration has on the base plant's operation. This model calculates the heat transfer, power production/consumption, and thermodynamic states on either side of the primary components (heat exchangers, pumps, compressors, turbines, etc.) for

both the gas and the steam cycles. The model assumes constant volumetric air flowrate, combustor temperature, heat of combustion, and component isentropic efficiencies. The net power output and flowrates of the gas and steam plant calculated in the model were compared to those specified by the NETL report. All calculated values were within 5% of the specified NETL value. The technology model governing equations, detailed process flow diagram, assumption list, and mass, power, and heat flows are included in Appendix A. The CANSOLV CCS steam reboiler duty and electrical parasitic load (as specified by NETL) were held constant for all operation modes. Since the steam reboiler duty is held constant, the percent of CO_2 sequestered was assumed to vary with natural gas flowrate according to data in the literature [107,108].

To evaluate the TES configurations, models were created for each of the individual configurations. Like the base model, the surrogate models calculate the heat transfer, power consumption/production, and thermodynamic states of the main heat pump components, including the storage mediums, heat exchangers, compressors, turbines, expansion valves, and pumps. The surrogate models output the heat rate to/from the thermal storages, flow rates of the working fluids, total mechanical power required to run individual configurations, and sizes of each component. The TES medium was assumed to be concrete and was based off those designed by Storworks Power [109].

2.2.2.2 TES Modeling

To evaluate the TES configurations, models were created for each of the individual configurations. Like the base model, the surrogate models calculate the heat transfer, power consumption/production, and thermodynamic states of the main heat pump components, including the storage mediums, heat exchangers, compressors, turbines, expansion valves, and pumps. The surrogate models output the heat rate to/from the thermal storages, flow rates of the

working fluids, total mechanical power required to run individual configurations, and sizes of each component. The process flow diagram, assumption list, and mass, power, and heat flows for configuration Vapor – FG_S/HC are included in Appendix A as a representative case for all configurations.

The base NGCC+CCS model was modified to incorporate the charging and discharging modes of TES operation. During the charging mode, the working fluid streams in the base model were adjusted to account for the fluid extraction in the TES configuration and re-combination at the corresponding location in the base plant. For example, in the HRSG IPT – S/HC configuration steam is extracted from the intermediate-pressure turbine (IPT) inlet, condensed in the hot storage, pumped to a high pressure, and then recombined with the inlet to the HRSG. This results in lower flow rates through multiple components in the steam cycle, lower power outputs from the IPT and low-pressure turbine (LPT), and higher HRSG steam inlet/gas outlet temperatures. The process flow diagram, assumption list, and mass, power, and heat flows are included in the Appendix A for HRSG IPT – S/HC to show the alterations to the base B31B model. During the discharging mode, the hot storage is used to provide the CANSOLV reboiler steam requirement. As such, the steam used for the CANSOLV reboiler during normal operation is instead routed through the LPT, consequently increasing power output for all configurations. The cold storage heat rate is used to calculate increased gas and steam flowrates. The total increase in gas and steam generator sizes and costs are calculated in discharging mode of the model.

The thermal storage medium assumed for this research was modular concrete blocks based on Storworks' BolderBloc™ Module [109]. Modular concrete blocks were selected due to their low cost and ability to be configurable with every thermal generation design. The

thermophysical properties of pure concrete were assumed for modeling purposes (thermal conductivity of 0.5 W m^{-1} °K^{-1} and specific heat of 0.96 kJ kg^{-1} °K^{-1}) [110,111]. Additionally, it was assumed that the heat exchanger effectiveness was 0.85 and the required CCS reboiler steam temperature was 152°C. The focus of this study was to determine if adding TES to NGCC+CCS power plants was feasible, not to determine the best TES medium to use. Therefore, it is recommended that future work evaluate additional thermal storage mediums to determine if they can further optimize the NGCC+CCS+TES design and improve NPV.

2.2.2.3 Carbon Capture Options

This research considered two carbon capture technologies. Case B31B uses Shell's proprietary and patented CANSOLV® CO_2 capture technology [105]. As such, all assumptions listed for the CCS unit in the NETL report were used for CANSOLV® in this analysis. Additionally, ION Clean Energy's ICE-31 solvent was evaluated as a next generation CCS technology [106]. Both are proprietary solvent absorption technologies that have the similar operation principles. As such, the CCS unit in the technology model was represented as a black box with clearly defined inputs and outputs. These inputs and outputs include: flue gas flowrate, composition, and temperature; steam flowrate, temperature, and pressure; CO_2 capture percent and electricity requirement; and CAPEX and OPEX. The CCS unit performance was validated for CANSOLV® CCS using the NETL 2019 report. CCS parameters were adjusted for ION CCS based on publicly available data. The primary difference between the two technologies is that ION CCS has a 38% reduction in CAPEX, 28% reduction in OPEX, and capture rate of 99% (compared to 90% for CANSOLV® CCS) [106,112]. The CCS steam reboiler duty and electrical parasitic load were held constant for all operation modes. Since the steam reboiler duty is held

constant, the percent of CO_2 sequestered was assumed to vary with natural gas flowrate according to data in the literature [107,108].

2.2.3 Optimization

The optimization model is designed to simulate the behavior of a NGCC+CCS responding LMP electricity price signals by making hourly dispatch decisions. The design and operation of this model builds upon the dispatch methodology used by Limb et al. and incorporates the optimization framework created by Vercellino et al. [102,113]. In addition to simulating the NGCC+CCS behavior, the optimization model optimizes TES sizing to maximize NPV. Figure 2 provides an example of the NPV benefit that can be seen by incorporating optimization into TES sizing. In this example, the optimization found that both longer hot and cold TES durations resulted in an increase in NPV of $35 million. Optimization was performed using both the base NGCC+CCS power plant and the NGCC+CCS+TES system to determine the economic benefit provided by TES. Additionally, optimization was performed on all electricity price signals independently such that optimum design and operation could be found in all scenarios.

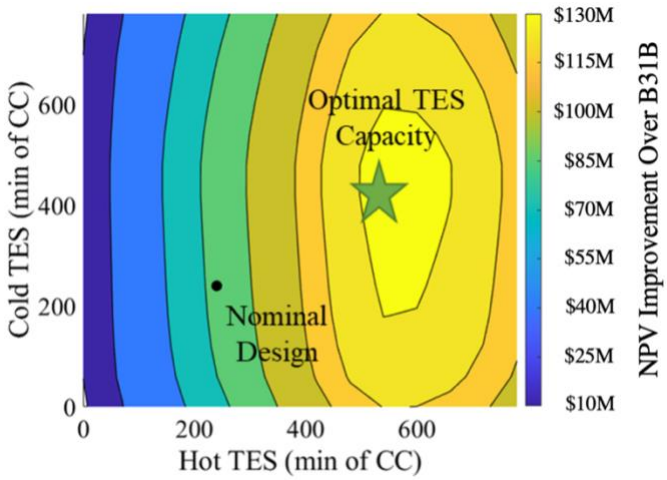

Figure 2. Example of the impact on NPV by optimizing both hot and cold thermal energy storage (TES) capacities.

2.2.4 Economic Model and Assumptions

A 30-year discounted cash flow analysis was used to evaluate which TES technology had the highest NPV based on simulations of the power plant using future electricity grid pricing. NPV was selected as the primary economic metric over other commonly used indicators such as levelized cost of electricity (LCOE) because NPV accounts for variations in the electricity pricing structure, which are critical to understand the benefit of storage technologies. LCOE does not account for these variations. Standard economic assumptions are used and presented in Table 2 [114,115]. All dollar values were adjusted to December 2018 dollars based on historical inflation rates as calculated by the Bureau of Labor Statistics using the Consumer Price Index [116]. A full list of equations used to calculate the 30-year discounted cash flow analysis and the NPV can be found in Appendix A.

Table 2. Economic Analysis Assumptions

Item	Value	Units	Source
Loan Interest Rate	5	%	ABT
Loan Term	30	years	ABT
Financed Amount	80	%	ABT
Equity Amount	20	%	ABT
Construction Interest Rate	3.5	%	ABT
Construction Period	3	Years	ABT
Construction Build Rate	80, 10, 10	%	ABT
MARCS Depreciation	15	Years	ABT
Tax Rate (Federal and State	25.7	%	ABT
Internal Rate of Return	10	%	ABT
Natural Gas Price Increase	3.5	%/year	EIA
Price Increase	2.2	%/year	EIA

Cost assumptions for each of the technologies varied by the individual components. Depending on the components that were added or removed for a given system, the prices of the components were scaled accordingly. All costs associated with new TES components were based on the same components used within NETL's B31B power plant. Similarly, when the CCS unit was scaled to accommodate the higher power outputs, costs were scaled based off the CANSOLV® CCS system used for B31B. Lastly, thermal storage component costs were based on Storworks' project capital costs of $25/kW-thermal for a 100° K temperature change during charging/discharging [109]. Both fixed and variable operation costs were based on the values provided by NETL for B31B and scaled depending on the thermal storage configuration. All system components were assumed to last a 30-year life, except those replaced through routine maintenance.

2.2.5 Electricity Price Profiles

In estimating the economic feasibility of NGCC+CCS+TES systems, both real-world and future pricing scenarios were evaluated. The following sections detail each.

2.2.5.1 Real-World Price Profiles

To simulate real world performance of the NGCC+CCS+TES systems, electricity Locational Marginal Pricing (LMP) profiles were used. Real-world LMP data is available for the major wholesale electricity markets in the United States. For this analysis, the New York Independent System Operator (NYISO) and the California Independent System Operator (CAISO) electricity regions were used as the primary source for LMP profiles [117,118]. Natural gas fuel prices for the first year were assumed to be those reported in the New York and California regions over the 2018 calendar year as provided by U.S. Energy Information Administration [119].

Since the selected electricity LMP profiles and natural gas prices only represented one years' worth of data, the operation model outputs (revenue generated, operation costs, total profits, etc.) were duplicated for every subsequent year for the 30-year life of the system. To approximate increasing energy prices over time, the price increases of 3.5% annually and 2.2% annually were used for natural gas and electricity, respectively, as expected by the Energy Information Administration's Annual Energy Outlook 2020 [115]. Fixed and variable operation costs associated with the NGCC, CCS, and TES were assumed to remain constant over the 30-year life of the system.

These real-world LMP profiles were used to downselect from all considered TES technologies to the most promising. After downselection, the most promising technologies were then evaluated with future price signals.

2.2.5.2 Future Price Profiles

To simulate future performance of the NGCC+CCS+TES systems, fourteen future electricity market scenarios were evaluated in this study, all of which include one year of hourly electricity prices. Four electricity market scenarios were generated by Princeton and MIT's GenX capacity expansion model and ten scenarios were generated by NREL's ReEDs capacity expansion model [120,121]. The GenX scenarios utilize a CO_2 tax of $60 per tonne and represent a possible mix of future generators (i.e. high amounts of wind or solar generation). The ReEDs scenarios consider existing regional electricity markets under carbon taxes of $100 per tonne and $150 per tonne of CO_2. All fourteen electricity price signals are meant to simulate future electricity grids with high renewable energy deployment. A summary of the electricity price scenarios is shown in Table 3. The future price signals analysis was designed to further downselected TES configures to the most promising. The most promising configuration was then evaluated with capacity expansion modeling.

Table 3. Summary of the future electricity market scenarios evaluated.

Scenario Name	Source	Model	CO_2 Tax ($/tonne)	Situation/Region
G60-Base	Princeton	GenX	60	Base Case
G60-HighWind	Princeton	GenX	60	High Wind Generation
G60-HighSolar	Princeton	GenX	60	High Solar Generation
G60-Winter	Princeton	GenX	60	Winter/New York
R100-CAISO	NREL	ReEDS	100	California Independent System Operator
R150-CAISO	NREL	ReEDS	150	California Independent System Operator
R100-ERCOT	NREL	ReEDS	100	Electricity Reliability Council of Texas
R150-ERCOT	NREL	ReEDS	150	Electricity Reliability Council of Texas
R100-MISO	NREL	ReEDS	100	Midcontinent Independent System Operator
R150-MISO	NREL	ReEDS	150	Midcontinent Independent System Operator
R100-NYISO	NREL	ReEDS	100	New York Independent System Operator
R150-NYISO	NREL	ReEDS	150	New York Independent System Operator
R100-PJM	NREL	ReEDS	100	PJM Interconnection
R150-PJM	NREL	ReEDS	150	PJM Interconnection

2.2.6 Capacity Expansion Modeling Assumptions

To understand the feasibility of the most promising NGCC+CCS+TES system compared to existing and future power generation technologies, capacity expansion modeling was used. This research was completed as part of the Department of Energy's Advanced Research Projects Agency–Energy (ARPA-E) FLExible Carbon Capture and Storage (FLECCS) project [122]. Therefore, the FLECCS version of Princeton's GenX model was used for capacity expansion modeling of this research [120,123].

2.3 Results and discussion

The results of this research chapter are presented in three different sections, 1) initial TES downselection using real-world price signals, 2) final downselection using future electricity price signals, and 3) capacity expansion modeling results.

2.3.1 Initial Thermal Storage Downselection

The goal of this task was to determine the economic viability of adding TES to an NGCC+CCS system. To understand the economic viability of the TES configurations, the NPV of each NGCC+CCS+TES configuration was compared to the base NGCC+CCS power plant over real-world LMP profiles. The comparison between NPVs of the base plant and TES configurations is shown in Figure 3. This figure presets a range of NPVs for each TES configuration evaluated on NYISO nodes using box and whisker plots. The bounds of the box in the box and whisker plot represents the 25th and 75th percentile results. The base NGCC+CCS power plant was found to have a range of NPVs from -$1.15 billion to $41.9 million. All thermal storage configurations were evaluated with Figure 3 showing the net improvement compared to the base plant. Scenarios that have a higher NPV than the base plant fall above the breakeven line and data points that fall below the breakeven line have a lower NPV. To be economically viable, the TES configurations need a portion of the results to fall above the breakeven line.

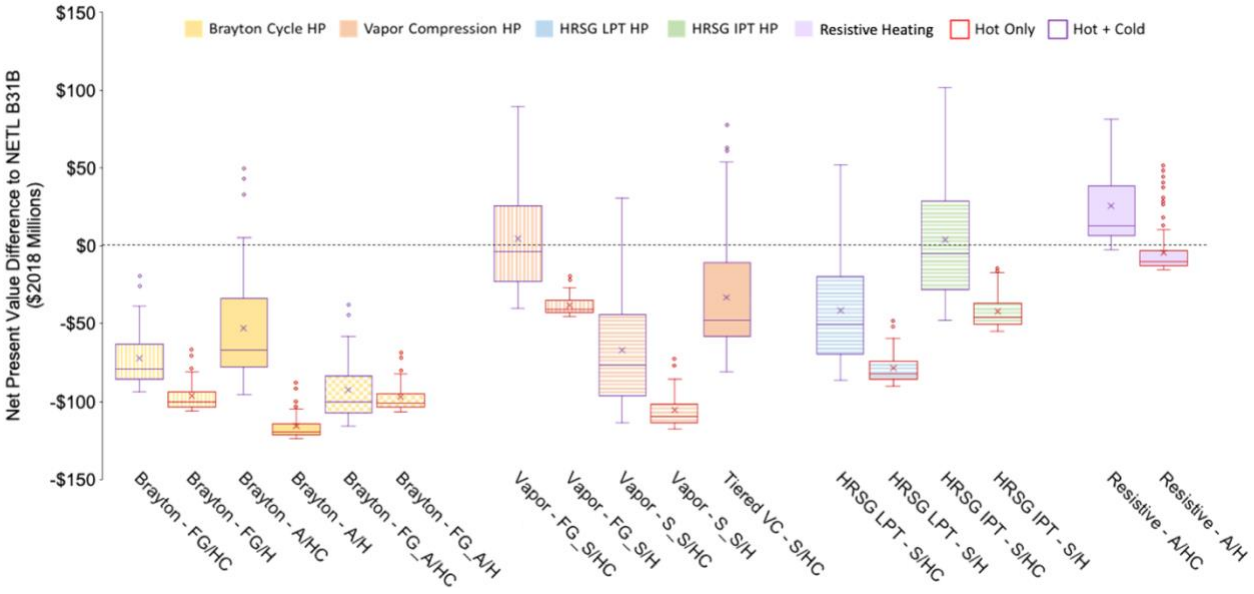

Figure 3. Net Present Value difference between each thermal storage configuration and NETL's B31B based on simulation with NYISO nodal data.

In general, the Brayton cycle configurations yielded lower NPVs than the base power plant due to their large capital costs. Of the Brayton cycle options, the configuration using air as the working fluid with both hot and cold storage (Brayton – A/HC) performed the best. It had a higher NPV than the base plant on 12.6% of the NYISO LMP profiles, the seventh highest percentage of the configurations evaluated. This configuration performed better than the other Brayton cycle configurations because it was able to charge the thermal storage independently of the power plant's operation. In order to charge the other configurations, the power plant needed to be in operation as they used heat from the NGCC flue gas or steam to heat the TES working fluid. Conversely, Brayton – A/HC pulls electricity directly from the grid and uses ambient air as the working fluid. Therefore, it is capable of charging at electricity prices lower than the breakeven cost of NGCC operation and the other Brayton cycle configurations. Charging independently of the NGCC power plant is particularly helpful in locations of low electricity prices and low NGCC capacity factors. That being said, the large capital costs of all the Brayton cycle configurations limited the overall benefit that was seen from the TES system. While this configuration was not the best performing overall due to high capital costs, it indicated that having a TES option capable of charging independent of the base plant could be valuable.

Based on the Brayton cycle results, a tiered vapor compression heat pump (Tiered VC – S/HC) was designed. This configuration uses interconnected vapor compression cycles to achieve the hot and cold temperatures required of the CCS and NGCC, respectively. Tiered VC – S/HC had a higher NPV than the base plant on 15.7% of the NYISO LMP profiles evaluated, the fifth highest percentage of the TES configurations. Tiered VC – S/HC performed better than Brayton – A/HC primarily due its lower capital costs. Both Vapor Compression heat pumps that included hot and cold thermal storage (Vapor – FG_S/HC and Vapor – S_S/HC) performed

better than the base power plant over some of the NYISO profiles. The vapor compression configuration using steam as the working fluid and both hot and cold storage (Vapor – S_S/HC) performed similarly to the best Brayton cycle configuration with 11.5% of the nodes having a higher NPV than the base plant, the eighth highest percent of the configurations evaluated. The other vapor compression configuration (Vapor - FG_S/HC) had the third highest NPVs of all the configurations evaluated. This configuration had a higher NPV than the base plant on 38.7% of the NYISO profiles. This can be attributed to the configuration's low capital cost and ability to utilize waste heat from the plant.

The thermal storage configuration using steam extraction from the intermediate pressure turbine in the HRSG with both hot and cold storage (HRSG IPT – S/HC) was the fourth best performing configuration. It had a higher NPV than the base plant on 36.9% of the LMP profiles. Additional benefits to this configuration include: the simple design, low capital cost, and that it does not require additional power to run compressors during TES charging. The low-pressure turbine HRSG configuration with both hot and cold storage (HRSG LPT – S/HC) performed the sixth best in this analysis by having a higher NPV than the base plant on 13.7% of the nodes.

The two thermal storage configuration that use resistive heating to generate heat performed the best overall, with the resistive heating with cold storage performing better than the base power plant in 98% of the NYISO LMP profiles. Even though resistive heating is relatively inefficient compared to the other TES methods, it performed the best due to its very low capital costs and its ability to charge independently of the NGCC power plant.

In addition to the evaluation over NYISO LMP profiles, the same analysis was performed on CAISO LMP profiles. However, the best performing configurations did not change during this analysis. The resistive heating configurations were the best performing configurations on the

CAISO nodes with Resistive – S/HC performing better than the base plant on 99% of the LMP profiles. After resistive heating, Vapor – FG_S/HC and HRSG IPT – S/HC performed the best. These two configurations had a higher NPV than the base plant on 28.3% and 27.8% of CAISO LMP profiles, respectively. Tiered VC – S/HC once again had the fifth highest percent of LMP profiles with a higher NPV than the base plant at 24.6%. Brayton – A/HC performed sixth best of the configurations by having a higher NPV than the base plant on 20.7% of the CAISO nodes. The main takeaway from the CAISO analysis is that the TES configurations that can charge independently of the NGCC increased their performance compared to the NYISO results, whereas the configurations dependent on NGCC performed worse in CAISO than in NYISO. This is because CAISO LMP profiles have a lower average electricity cost than the NYISO LMP profiles which decreases the overall capacity factor of the NGCC and limits the charging/discharging window of the TES configurations dependent on the NGCC's flue gas or steam for heat.

These results show that the thermal storage configurations with the lowest capital costs tend to perform the best across the price signals evaluated. Based on these results, Resistive – S/HC, Vapor – FG_S/HC, HRSG IPT – S/HC, and Tiered VC – S/HC are the best potential technologies to overcome the operational limitations caused by the large heat load needed for CCS solvent regeneration on NGCC power plants. Resistive – S/HC, Vapor – FG_S/HC, and HRSG IPT – S/HC will be kept in future analysis because they performed the best overall and Tiered VC – S/HC will be kept because it adds the flexibility of charging independently of the power plant which could be important for future electricity LMP profiles where NGCC power plants are expected to operate with a lower capacity factor [124–126]. As mentioned previously, having a lower capacity factor will limit the time window where charging and discharging of the

TES can take place for configurations dependent on heat from the NGCC. Configurations independent of the NGCC can operate more easily because they only need to discharge the TES when the NGCC is in operation.

Based on the results of the real-world LMP analysis, Resistive – S/HC, Vapor – FG_S/HC, HRSG IPT – S/HC, and Tiered VC – S/HC were selected during downselection and were evaluated using future grid price signals. For easier comprehension, these configurations will be referred to as Resistive Heating (Resistive – S/HC), HRSG Steam (HRSG IPT – S/HC), Heat Pump VC (Vapor – FG_S/HC), and Tiered VC (Tiered VC – S/HC) in the following sections.

2.3.2 Feasibility in Future Grid Scenarios

The results for this task are broken down into two subsections representing the key findings of this analysis. The first subsection details the economic performance of the four TES configurations evaluated over future electricity price signals and includes a discussion on the value of optimization. The second subsection presents detailed NPV results for the Resistive Heating TES configuration working in conjunction with both CANSOLV® and ION CCS systems.

2.3.2.1 Economic performance of TES in Future Electricity Markets

Figure 4 presents a NPV comparison between the four TES technologies evaluated and NETL's B31B power plant. Results also show the improvement in NPV gained through optimization (blue) vs the downselection TES sizing of 4 hours found in Task 1.1 [127]. Results are separated between GenX and ReEDS future electricity price signals because of their varying assumptions and carbon taxes. All configurations incorporate Cold TES, but results focus on hot

TES technologies since previous studies have shown Cold TES to be a valuable solution [60,66–68,98,128].

The results in Figure 4 clearly show the economic value of adding TES to NGCC+CCS systems. On average, TES improved the NPV of the NGCC+CCS system by $67 million and $26 million for the GenX and ReEDS future price scenarios, respectively. Additionally, scenario specific optimization dramatically improved the NPV of the NGCC+CCS+TES system when compared to the downselection configurations used by Limb et al. [127]. Optimization improved the average NPVs by $38 million and $76 million for the GenX and ReEDS future price scenarios, respectively. There are two primary reasons why optimization had such a large impact. First, the dispatch strategy used is specific to each price profile, whereas previous work assigned the same operation strategy to each profile and configuration. Secondly, the TES component sizes are specific to each profile and configuration. For example, ReEDS price profiles are better suited for longer TES storage durations because of the longer periods of price variation. This is also why there is a larger gap between optimized and unoptimized results for the ReEDS pricing scenarios compared to the GenX ones. The nature of the GenX price signals result in optimized TES sizes near the 4 hours of duration assumed in Task 1.1 but ReEDS price signals typically have optimized sizes closer to 10 hours of storage duration.

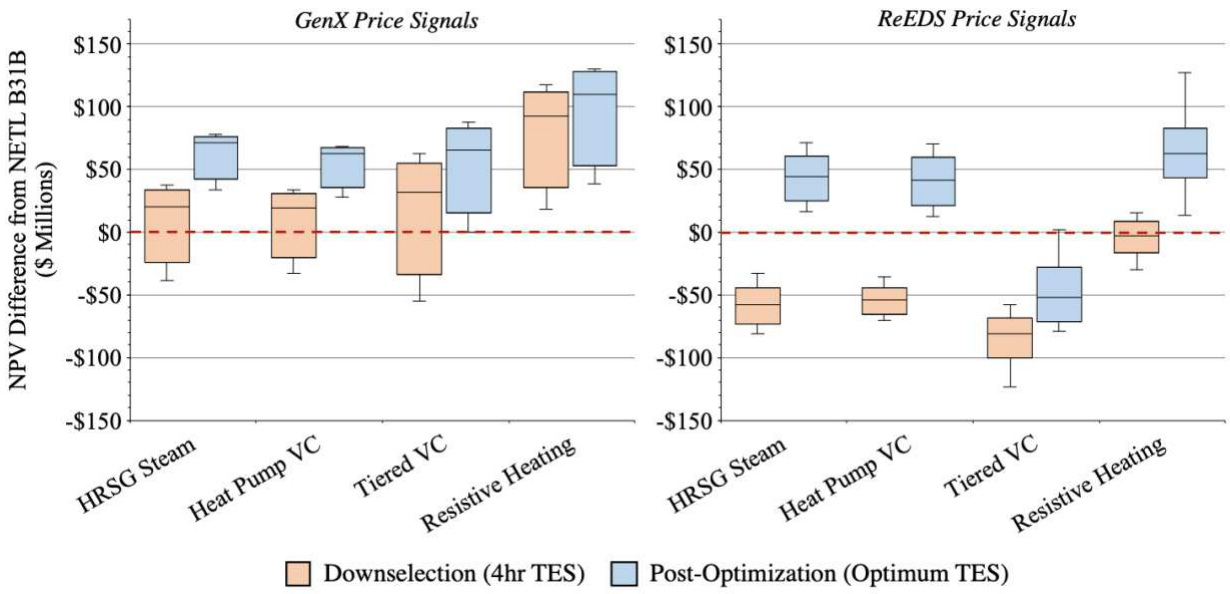

Figure 4. NPV comparison between the four thermal energy storage (TES) technologies evaluated for both GenX and ReEDS future electricity price signals compared to NETL's B31B power plant. Results are shown for the improvement in NPV gained through optimization (blue) vs the assumed scenario of 4 hours of TES (orange).

In all scenarios evaluated, Resistive Heating was the best performing TES configuration. Since the future scenarios in this study focused on situations with high renewable energy deployment, the lower round-trip efficiency associated with Resistive Heating was negated because since the TES could charge at very low electricity prices when renewable energy is plentiful. Alternatively, the HRSG Steam and Heat Pump VC configurations rely on the NGCC plant operation to charge their hot TES and therefore couldn't take advantage of low-cost renewable energy. Additionally, the Tiered VC configuration has the capability to charge using low-cost renewable electricity, but its high CAPEX costs only make it feasible in certain scenarios. For example, Tiered VC is the 2nd best performing configuration for the GenX scenarios, but the worst performing configuration for the ReEDS scenarios. Tiered VC also has the limitation that it has hot and cold combined storages which limits optimization potential since the hot and cold storages need to be sized together. Optimization results presented by Vercellino

et al. show that the optimal hot TES duration is usually much larger than that of the cold TES because cold TES is used primarily for boosting [113]. Resistive Heating provides low CAPEX, independent charging from the NGCC, and separate hot and cold storages at the expense of decreased efficiency. However, these results show that the downside of decreased efficiency is minimal in a future electricity market with plentiful low-cost renewable energy. Since Resistive Heating not only outperforms all other TES configurations, but also improves NGCC+CCS NPV in every scenario evaluated, it is recommended that Resistively Heated TES be added to NGCC+CCS systems when increased flexibility and profitability is desired. The Resistive Heating configuration is used for capacity expansion modeling in the following section.

2.3.2.2 TES Performance with Multiple CCS Technologies

Figure 5 presents the NPV improvement of adding the Resistive Heating TES configuration to both NETL B31B (B31A with CANSOLV® CCS) and B31A with ION Clean Energy CCS. Subplots show NPV values compared to (a) NETL B31B to show the NPV improvement from adding TES and ION CCS or (b) NETL B31B (CANSOLV® CCS) and NETL B31A+ION CCS (ION Clean Energy CCS) to show the NPV improvement from TES only. NPV results in Figure 5a show a dramatic increase in NPV when ION CCS is used. This is due to the reduced CAPEX and OPEX costs and increased carbon capture rate compared to CANSOLV® CCS. When NPV results are simplified to only show the impact of TES on NGCC+CCS performance (Figure 5b), Resistive Heating + Cold TES is found to have a very similar impact regardless of CCS technology used. Minor differences between the results stem from the different steam requirements (flow rate & desired temperature) of each CCS technology. Higher required flowrates as are required by CANSOLV® CCS indicate higher capacity thermal storages and a higher potential for thermal storage to offset the parasitic load.

Lower flowrates as are found using ION CCS indicate a more efficient CCS unit that doesn't require as much TES to offset the parasitic power.

The real value of TES can be seen when the NPV improvement on individual electricity market scenarios is evaluated. Table 4 shows NPV improvement or detriment of adding CCS and TES to NETL B31A (NGCC without CCS or TES). NPV values are provided for both NETL B31B (B31A with CANSOLV® CCS) and B31A with ION CCS. In three of the fourteen scenarios evaluated, TES made the difference between NGCC with CCS being more economical than a NGCC without CCS. In ReEDS price signals, B31B has a lower NPV than B31A for both R100-CAISO and R150-NYISO price signals. However, B31B+TES for the same price signals has a higher NPV than B31A. The same is seen for B31A+ION CCS vs B31A+ION CCS+TES on the GenX G60-HighWind scenario. Therefore, regardless of the CCS technology used, TES could be the difference between CCS technologies being economically feasible in future electricity markets.

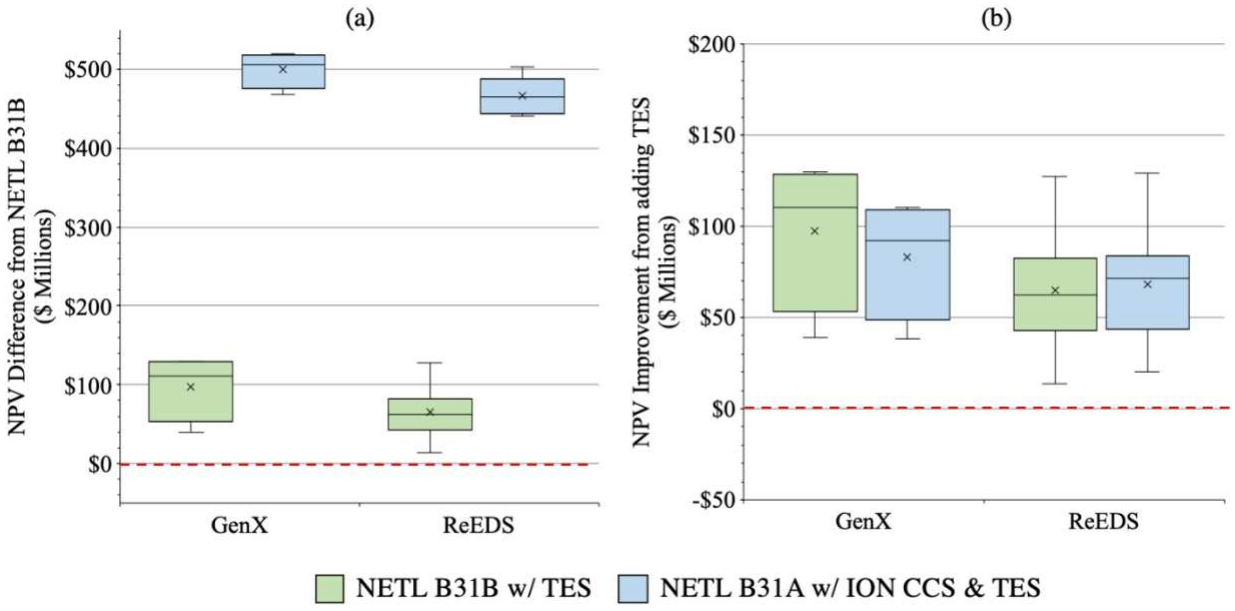

Figure 5. NPV improvement of adding thermal energy storage to NGCC+CCS for both NETL B31B (B31A w/ CANSOLV® CCS) and B31A w/ ION Clean Energy CCS. NPV values are compared to (a) NETL B31B to show the NPV improvement from adding TES and ION CCS or (b) NETL B31B (CANSOLV® CCS) and NETL B31A+ION CCS (ION Clean Energy CCS) to show the NPV improvement from TES only.

Table 4. NPV improvement/detriment of adding carbon capture and storage (CCS) and thermal energy storage (TES) to NETL B31A (NGCC without CCS or TES). NPV values are provided for both NETL B31B (B31A with CANSOLV® CCS) and B31A with ION CCS. Highlighted rows identify scenarios where TES made NGCC+CCS become economical compared to a NGCC without CCS.

	Price Profile	B31B	B31B+TES	TES Impact	B31A+ION	B31A+ION+TES	TES Impact
GenX	G60-Base	($ 273 M)	($ 177 M)	+$ 96 M	+$ 144 M	+$ 225 M	+$ 80 M
	G60-HighWind	($ 433 M)	($ 303 M)	+$ 130 M	($ 24 M)	+$ 87 M	+$ 111 M
	G60-HighSolar	($ 344 M)	($ 219 M)	+$ 124 M	+$ 67 M	+$ 171 M	+$ 104 M
	G60-Winter	($ 213 M)	($ 174 M)	+$ 39 M	+$ 216 M	+$ 254 M	+$ 38 M
ReEDS	R100-CAISO	($ 9 M)	+$ 118 M	+$ 127 M	+$ 365 M	+$ 494 M	+$ 129 M
	R150-CAISO	+$ 115 M	+$ 222 M	+$ 107 M	+$ 490 M	+$ 603 M	+$ 113 M
	R100-ERCOT	($ 206 M)	($ 153 M)	+$ 53 M	+$ 235 M	+$ 281 M	+$ 46 M
	R150-ERCOT	+$ 21 M	+$ 69 M	+$ 48 M	+$ 429 M	+$ 477 M	+$ 48 M
	R100-MISO	($ 45 M)	($ 16 M)	+$ 29 M	+$ 361 M	+$ 397 M	+$ 36 M
	R150-MISO	($ 21 M)	($ 7 M)	+$ 14 M	+$ 404 M	+$ 423 M	+$ 20 M
	R100-NYISO	($ 158 M)	($ 84 M)	+$ 75 M	+$ 211 M	+$ 285 M	+$ 74 M
	R150-NYISO	($ 40 M)	+$ 30 M	+$ 70 M	+$ 332 M	+$ 405 M	+$ 72 M
	R100-PJM	+$ 118 M	+$ 182 M	+$ 63 M	+$ 521 M	+$ 593 M	+$ 71 M
	R150-PJM	+$ 361 M	+$ 422 M	+$ 61 M	+$ 779 M	+$ 851 M	+$ 72 M

2.3.3 Capacity Expansion Modeling

The following figures show the deployment and generation results that were generated using Princeton's GenX capacity expansion model. The "FLECCS" technology shows the deployment and electricity generation from the proposed technology. For the GenX results, four technologies were evaluated. These include CSUBASE: NGCC with CANSOLV CCS and no TES, CSUTES: NGCC with CANSOLV CCS and TES, CSUION: NGCC with ION CCS and no TES, and CSUTESION: NGCC with ION CCS and TES.

By using these combinations of technologies in the model, the benefit of switching from the state-of-the-art CANSOLV CCS to ION CCS and the benefit added through TES can be easily and independently observed. For the capacity expansion results, the scenarios evaluated are shown in Table 5.

Table 5. Capacity Expansion Scenarios Evaluated

Name	Description
S1: Deployment	Favorable for deployment (cheap gas, expensive renewables, expensive batteries, high electrification)
S2: Flexibility	Favorable for flexibility (cheap gas, cheap renewables, expensive batteries, high electrification)
S3: Reference	Reference (moderate gas, moderate renewables, moderate batteries, moderate demand)
S4: UnfavorableNoNET	Unfavorable for deployment, but excludes negative emissions tech (expensive gas, cheap renewables, cheap batteries, moderate demand)
S5: Unfavorable	Unfavorable for deployment, but includes negative emissions tech (expensive gas, cheap renewables, cheap batteries, moderate demand)

Overall, significant capacity of the NGCC+CCS+TES technology is deployed, and power is generated by it. Figure 6 and Figure 7 show the capacity deployment and power generation, respectively, for all resources in the "Deployment" "Flexibility" and "Reference" scenarios using

carbon taxes $150/ton-CO2 and $300/ton-CO2. $225/ton-CO2 results were omitted for space and clarity as they fall between the two edge cases.

The results in Figure 6 show significant capacity deployment of the NGCC+CCS+TES technology in Deployment, Flexibility, and Reference cases. In particular, the technology option that includes both ION CCS and TES is deployed in every combination of scenario and carbon tax. Comparatively, the state-of-the-art technology (NGCC with CANSOLV CCS and no TES) is deployed both less than the proposed technology and is not deployed in the $150/ton-CO2 scenarios. The addition of both ION CCS and TES to NGCC plants shows both increased deployment of the technology and a decrease in the overall system capacity due to the high-capacity factor of these systems. Similarly, the results in Figure 7 show significant power generation by the proposed technology in Deployment, Flexibility and Reference cases. The addition of both ION CCS and TES to NGCC plants shows increased power generation to non-ION or non-TES systems. In the Reference $300/ton-CO2 scenario, the FLECCS system represents 8.9% of the total system capacity and generates 11.3% of the power generated by the system. Similarly, the other natural gas technologies represent 14.4% of the system capacity, but only generate 1.4% of the power generated.

Results were also generated for “Unfavorable” scenarios but were excluded because they did not show any deployment of the NGCC+CCS+TES technology. In the “Unfavorable” case, the model chooses to deploy DAC and BECCS instead of NGCC+CCS+TES. In the “UnfavorableNoNet”, hydrogen plants are selected over gas due to the high cost of natural gas.

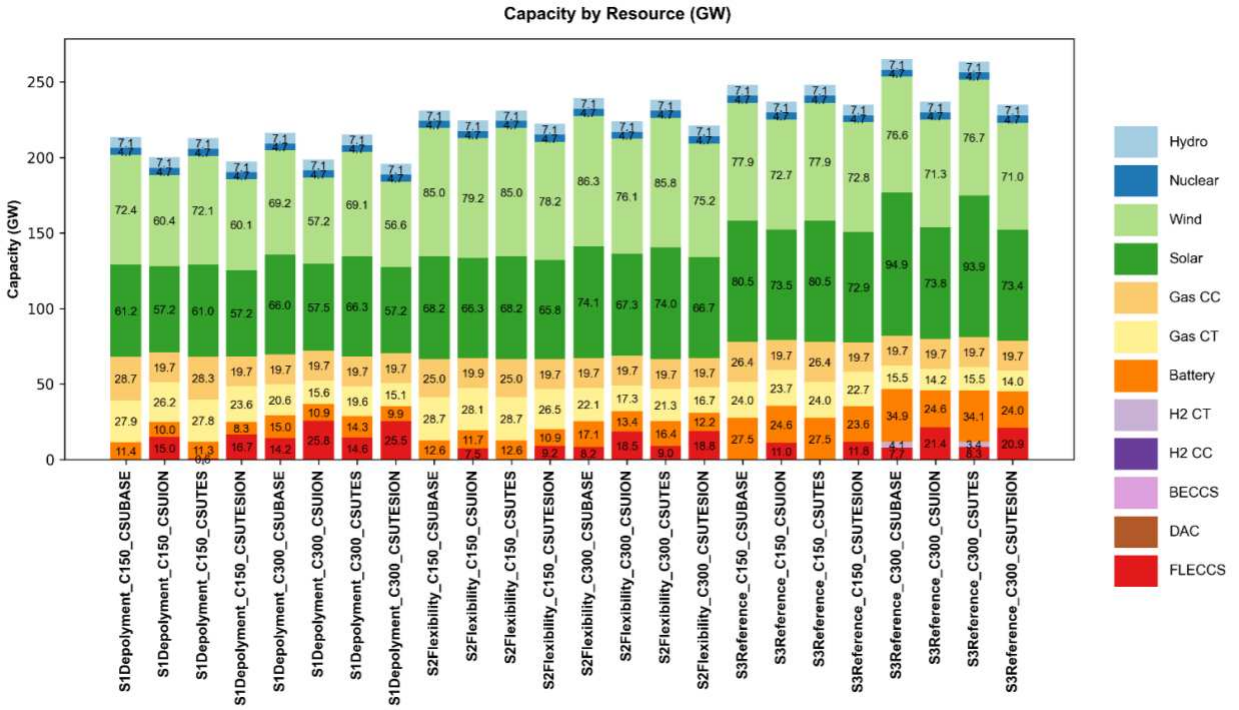

Figure 6. Results for capacity deployment using GenX.

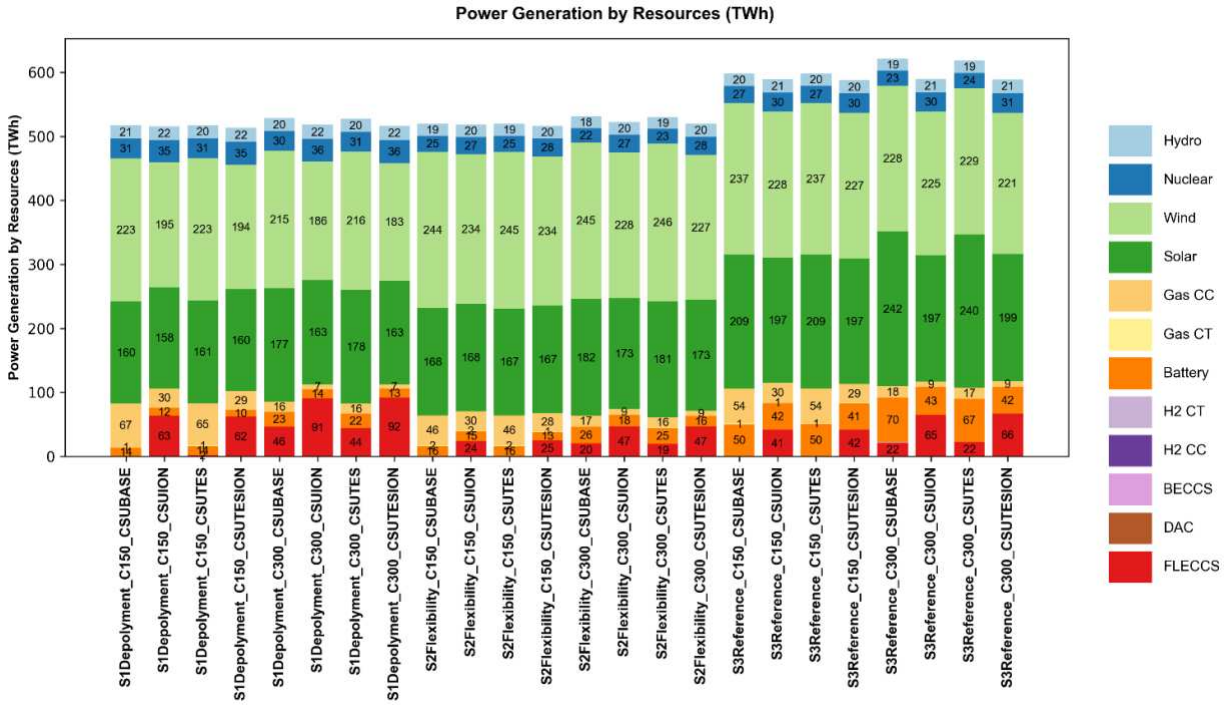

Figure 7. Results for power generation by resource using GenX.

2.4 Conclusions

Currently, fossil fuel-based power plants generate the majority of the United States' electricity and provide a reliable generation source for both base and peak power demands. However, future emissions standards are expected to require these power plants to use CCS, which has a detrimental impact on the power plant's performance. Therefore, this study evaluated TES configurations designed to overcome the operational limitation placed on the NGCC by CCS due to the large heat load required for solvent regeneration.

Results from this analysis clearly show the economic value of adding TES to NGCC+CCS systems. Specifically, resistively heated TES performs the best on NGCC+CCS systems. On average, TES improved the NPV of the NGCC+CCS system by $67 million and $26 million for GenX and ReEDS future price scenarios, respectively. Additionally, a resistively heated hot TES system was found to be the best performing TES configuration in all future scenarios evaluated. Since the future scenarios in this study focused on situations with high renewable energy deployment, the lower round-trip efficiency associated with resistive heating was negated because the TES could charge at very low electricity prices when renewable energy was plentiful. Results confirmed previous findings which illustrated that low CAPEX is more important than increased round trip efficiency in future electricity markets. This study also evaluated the impact of TES on two CCS technologies: CANSOLV® CCS and ION Clean Energy's CCS. Results showed that TES has similar performance regardless of CCS system used. Further, ION CCS system was found to have a more efficient system design which results in a slightly reduced NPV benefit for TES because the ION system's regeneration parasitic load is smaller. Lastly, this work also found that TES can make the difference between CCS being profitable in future grid environments. In many of the scenarios evaluated, TES made the

difference between NGCC with CCS being more economical than a NGCC without CCS. This is a key finding and should be investigated further in future studies.

CHAPTER 3: ECONOMIC AND ENVIRONMENTAL FEASIBLITY OF GREEN WASTEWATER TREATMENT BASED WATER QUALITY TRADING[2]

3.1 Introduction

Half of America's rivers are impaired and today do not meet Clean Water Act standards [18]. Point-source river discharges (i.e. Wastewater Treatment Facilities) are regulated by the United States Environmental Protection Agency (EPA) and state agencies under the Clean Water Act, while non-point sources are largely unregulated. These environmental and regulatory realities are subsequently putting increasing pressure on water and wastewater utilities to address riverine water quality. However, a substantial source of freshwater contamination in the United States is attributable to non-point source pollution from land-use change, agricultural and forestry practices, soil erosion, and urbanization as well as large-scale, short-and-medium term shocks associated with wildfires and other impacts of climate change. A dominant form of water quality impairment is fertilizer application and subsequent runoff to streams [19]. The most prominent water quality impacts of fertilizer are harmful algae blooms and subsequent anoxic zones either in lakes or in near-coastal environments [20].

[2]This chapter was published as a peer-reviewed journal article: Limb, B. J., Quinn, J. C., Johnson, A., Sowby, R. B., & Thomas, E. (2024). The potential of carbon markets to accelerate green infrastructure based water quality trading. Communications Earth & Environment, 5(1), 1–12. https://doi.org/10.1038/s43247-024-01359-x

Wastewater Treatment Facilities must construct gray infrastructure to reduce their pollutant loads under the National Pollutant Discharge Elimination System (NPDES). Waste load allocations in an individual NPDES permit are often calculated in response to pollutant levels in a river via the establishment of Total Maximum Daily Loads. Given the success of the Clean Water Act since the 1970s, the percentage of instream pollutant loads directly attributable to NPDES permittees has become proportionately low in many watersheds [21,22].

Typically, water and wastewater utilities meet their NPDES water quality regulatory obligations by constructing gray infrastructure, such as secondary, tertiary and reverse osmosis treatment plants, requiring substantial capital and operational costs as well as embodied emissions from materials and indirect emissions from energy use throughout their operational lifetimes. Though point-source pollutant inputs from Wastewater Treatment Facilities are often proportionately low, a high overall level of a given pollutant in a river of concern often leads to substantially lower point-source waste load allocations that may force a utility to the limits of existing wastewater treatment technology[4]. While there are other regulatory and nonregulatory pathways and attempts to improve instream water quality outside of Point Source permitting (such as conservation funding from the United States Department of Agriculture), none have had the levels of success over the last 50 years as the NPDES part of the Clean Water Act. While improving the quality of an NPDES permittee's discharge is not the only means to improve instream water quality, it has long been the dominant mechanism in the United States to drive public investments in regional water quality [23].

Water and wastewater treatment plants currently account for about 2% of energy use and 45 million tonnes of carbon dioxide equivalent (CO_{2e}) emissions per year in the United States [17]. Further gray infrastructure technology upgrades would continue to increase overall energy

demand and emissions. However, in many cases, further upgrades to gray infrastructure driven by current regulatory pressures and impaired riverine water quality could be substituted through regulator-approved water quality trading programs with green infrastructure including riparian, floodplain, and wetlands restoration; regenerative agricultural practices; improved forestry management; and other efforts to reduce non-point source contamination. Existing water quality trading (WQT) programs are governed by the EPA toward compliance with a NPDES permit. The EPA allows for what is known as Point Source to Non-Point Source water quality trading. This has been practiced in the United States for over three decades. These water quality trading programs enable point dischargers to meet regulated water quality obligations and in the process restore and sustain freshwater ecosystems [24]. These types of formal, market-based water quality trading programs were established and recently strengthened by the EPA [23,25] and several state-level regulators, but have not achieved large scale, despite often being much more cost effective [26,27,129].

Two recent studies have analyzed factors that contribute to the existence of water quality trading programs. In one study, a negative association between urban activity and the presence of WQT markets was observed, aligning with the historical context of WQT evolving as a tool to incentivize reductions in agricultural runoff. Further, this study identifies a substantial relationship between certain types of permit approaches taken by regulators and the likelihood of WQT market activity. Interestingly, the presence of impaired waterways does not consistently correlate with WQT markets, leading the authors to suggest a potential policy lag in addressing water quality issues [130]. In another recent analysis, insights on active and inactive WQT programs were drawn from 19 reviews. Eighty-four factors were identified in regulatory, institutional, environmental, economic, and social categories. Regulatory barriers, encompassing

official rules set by government or regulatory agencies, were most frequently mentioned in 31% of cases. Economic, institutional, and environmental factors were considered relatively equally important in 19%, 19%, and 18% of cases, respectively. Specifically, the ability to directly monitor the success of WQT programs in addressing water quality was highlighted as a major institutional barrier[14]. Emerging technologies may support improved monitoring and management of green infrastructure water quality solutions (e.g. [70–75]). These studies emphasize the significance of regulatory support and utility technical capacity to enable WQT programs.

Paired with increase technical capacity and regulator interest, we propose that carbon markets may provide a private capital source to motivate utilities and regulators using green infrastructure to take pre-permit, early action. In this light, one way to view carbon market mechanisms is that they offer the potential to redirect climate-damaging capital toward water infrastructure and create a sustainable, performance-based funding stream to move away from fossil-fuel dependent infrastructure. For this to hold, the financing needs to occur in locations where the transition to renewables is slow and where existing efforts to switch from energy intensive infrastructure to nature based solutions is lacking. The Voluntary Carbon Market (VCM) facilitates the reduction of greenhouse gas emissions worldwide through economic incentives. A voluntary carbon credit is a financial commodity, currently worth about $10 for many nature-based projects [131], and over $1,000 for some direct air capture projects [132], that represents the reduction or removal of one tonne of carbon dioxide. Many corporations are interested in buying carbon credits through the VCM to compensate for a proportion of their remaining emissions to achieve sustainability targets. The VCM is designed to financially incentivize voluntary action supporting climate change solutions. VCM projects include both

nature-based solutions, such as improved forest management and reforestation, and technology-based solutions, such as renewable energy installations and improved cookstoves. While there is a growing, multi-billion dollar global market for carbon credits, water, as a local management challenge, has not typically been fungible in the same way. This local feature of water has made it challenging to create effective financing and trading mechanisms and has limited the value, transactability, and liquidity of various forms of so-called water credits, such as those developed to demonstrate compliance with the United States Clean Water Act or the Gold Standard Water Benefit Certificates [133,134]. Alternatively, if the financial instrument is a carbon credit that motivates improved water quality, that credit accesses a liquid market and can be bought and sold and create revenue, incentivizing water security actions.

Market research conducted in 2022 projected a 20-fold increase in the demand for carbon credits by 2035, with prices rising to an estimated $80-$150 per tonne from the current $25 [135]. However, the VCM has recently faced several challenges, calling into question the additionality, permanence, and volume of credits issued, primarily those associated with REDD+ programs. Yet, there are also clear signals that the VCM may recover, including the strengthening of activities led by the Voluntary Carbon Markets Initiative and the Integrity Council for Voluntary Carbon Markets. Further, recent research suggested that corporations purchasing carbon credits decarbonize twice as fast as companies not participating in the VCM, belying suggestions that carbon credits enable greenwashing [136].

The VCM represents a fraction of overall climate finance, at about $2 billion per year. In 2022, more than $60 billion dollars in climate finance was provided by multilateral development banks to low- and middle-income economies, including loans (61 percent), policy-based financing (14 percent), and grants (10 percent). Of this, 15 percent of global climate adaptation

finance, more than $3.3 billion, was directed to the water and wastewater sector, preceded only by energy, transport, and other built environment and infrastructure (30 percent), and by cross-cutting operations (17 percent), suggesting large existing commitments [1]. Among high-income economies, the investment is even more substantial, with 29 percent of adaptation funds applied toward energy, transport, and other built environment and infrastructure, and 28 percent toward water and wastewater systems. In least-developed countries, 14 percent of adaptation funds are applied to the water and wastewater sector, ahead of crop and food production at 13 percent. Total climate adaptation finance allocations for water and wastewater in least-developed countries totaled nearly $900 million in 2023, with nearly 89 percent allocated to Sub-Saharan Africa [137].

In this research, we evaluate the economic and environmental potential of water quality trading programs. The economic and life-cycle greenhouse gas (GHG) emissions savings by using green infrastructure methods in place of gray wastewater treatment methods is evaluated. The primary analysis evaluates the benefits seen by nutrient (nitrogen and phosphorus) reduction. The United States EPA defines five target effluent nutrient concentration levels for wastewater treatment technologies. Nutrient removal requirements vary state-by-state but have generally trended toward increased stringency, requiring water treatment plant technology upgrades and corresponding increases in energy demand [138–140]. Given this trend, we consider nutrient concentration limits ranging from Level 2 (removal of nitrogen to 8 mg L^{-1} and phosphorus to 1 mg L^{-1}) to Level 5 (removal of nitrogen to 2 mg L^{-1} and phosphorus to 0.02 mg L^{-1}) [138]. Geospatially resolved nutrient impaired water data is combined with the performance of various gray and green infrastructure alternatives to determine the total cost and environmental impact (GHG emissions) associated with various solutions to water quality

targets. The discussion focuses on the potential impact of carbon markets (carbon credits) to support the development and deployment of green infrastructure.

3.2 Materials and methods

This study evaluates the economics and emissions of water treatment technologies in the CONUS. The CONUS was divided into smaller sections as designated by the United States Geological Survey's Hydrological Unit Code (HUC) regions. To maximize geographic resolution of this analysis, HUC 12 sub-watersheds were used wherever possible. However, it was assumed that nutrient trading could take place at the HUC 6 waterbasin level and, therefore, all results were aggregated to the waterbasin level [141]. Geodatabase files for various HUC regions were downloaded from the United States Geological Survey's Watershed Boundary Dataset [142]. Data associated with HUC 12 sub-watersheds was aggregated from United States EPA's EnviroAtlas database [143]. EnviroAtlas provides national data layers at the HUC 12 sub-watershed level with many of these data layers being derived from data with a resolution of 30 m. Full details of which data was required is discussed in each subsection. It was assumed that nutrient trading could take place within each waterbasin (HUC 6), therefore stricter requirements placed on existing facilities could only be satisfied by gray or green treatment methods within the same waterbasin.

3.2.1 Wastewater Nutrient Data

Geographically resolved nutrient loading data compared to water quality targets for point source dischargers in the CONUS motivates the water treatment trade study. Therefore, 2022 data from the Nutrient Model (Hypoxia Task Force Search) created by the EPA was used [144]. This data is provided through the EPA's Water Pollutant Loading Tool [145]. The Nutrient

Model was created by EPA to provide access to aggregated nitrogen and phosphorus loads (including modeled loads) for facilities across the United States. As such, data is provided for wastewater treatment facilities with current EPA NPDES permits with facility information, total annual wastewater flow, total nutrient loads, and maximum allowable nutrient loads (if applicable). In total, 53,055 data entries were provided for 29,335 unique facilities. Data consists of both discharge monitoring report (28,318) and modeled (24,737) nutrient loads for both nitrogen (27,238) and phosphorus (25,817). Additionally, each data point was associated with a HUC 12 sub-watershed code so analysis could be evaluated on a geospatially resolved level. An overview of the input data including number of facilities, mean daily wastewater flow, mean nitrogen concentration, and mean phosphorus all aggregated to the waterbasin level can be viewed in Figure 8. For analysis of all technologies in this study, a 40-year time horizon was assumed.

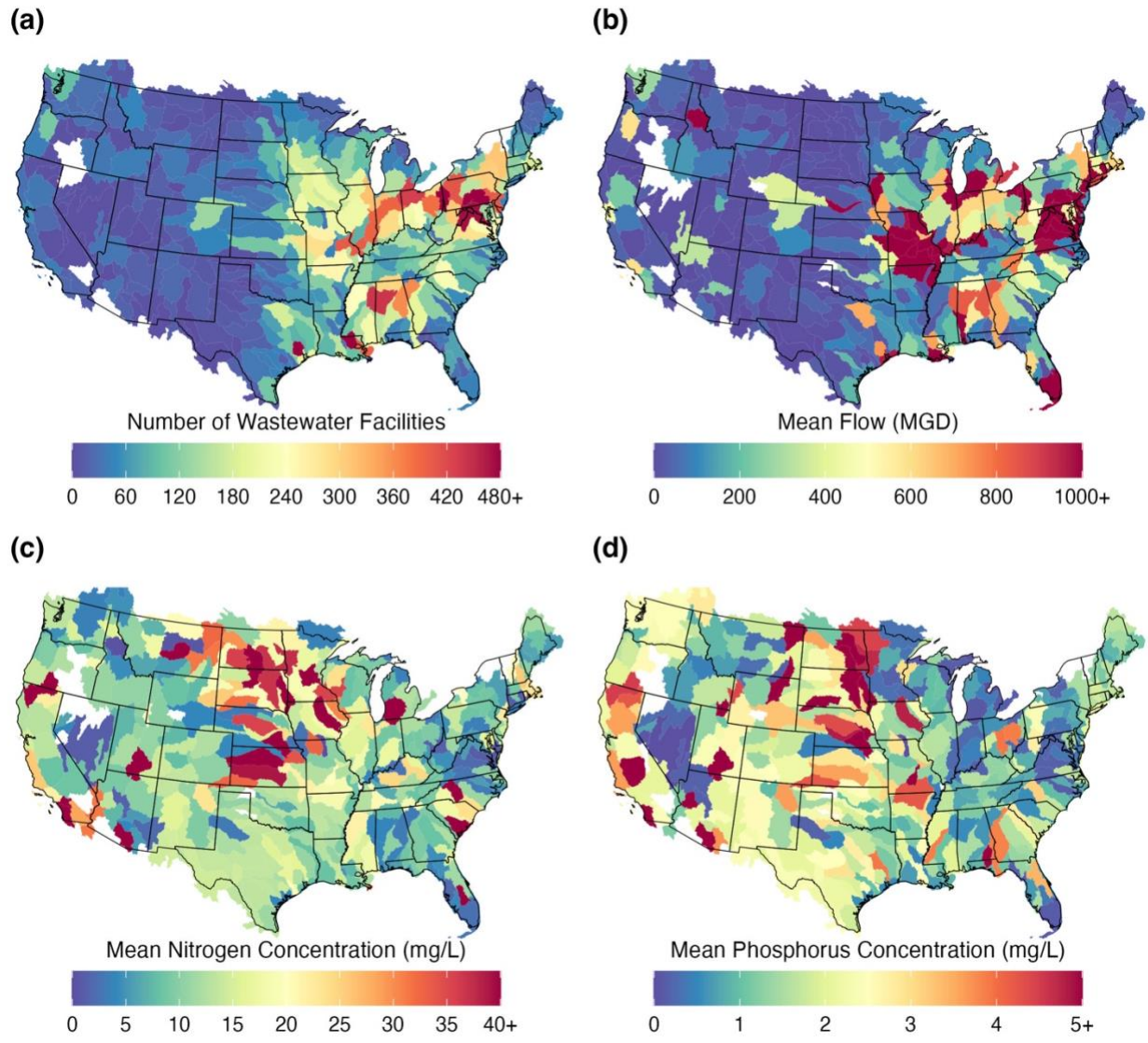

Figure 8. Wastewater treatment facility data in the contiguous United States: (a) Number of wastewater facilities in each waterbasin (b) Total mean flow in millions of gallons per day in each waterbasin (c) Mean Nitrogen concentration of the wastewater (mg/L) in each waterbasin (d) Mean Phosphorus concentration of the wastewater (mg/L) in each waterbasin.

3.2.2 Gray Treatment Methods

Gray nutrient treatment technologies outlined in the EPA's report title *Life Cycle and Cost Assessments of Nutrient Removal Technologies in Wastewater Treatment Plants* were used in this analysis [138]. The EPA report estimated the costs and GWP of 8 alternative wastewater

treatment technologies to treat excess nitrogen and phosphorus in wastewater streams. Costs and GWP were also provided for a 9th 'baseline' technology, but it was excluded from this analysis because its primary design was not focused on nutrient removal and had low nutrient remediation potential. Details of the gray treatment methods can be seen in Table 6. Each gray nutrient treatment technology was assigned a treatment level in the EPA report. These levels range from Level 2 to Level 5 based on their ability to achieve target effluent nutrient concentrations. These concentration levels are 8 mgN L^{-1} and 1 mgP L^{-1} for Level 2, 6 mgN L^{-1} and 0.2 mgP L^{-1} for Level 3, 3 mgN L^{-1} and 0.1 mgP L^{-1} for Level 4, and 2 mgN L^{-1} and 0.02 mgP L^{-1} for Level 5. Level 1 designates that no effluent concentration is specified and has been excluded from this analysis accordingly.

Table 6. Costs and Emissions of Gray Treatment Methods. Treatment "Level" refers to the EPA's target effluent nutrient concentration levels for wastewater treatment technologies.

Name	*Abbr.*	*Level*	*N Cost (2022$/kgN)*	*P Cost (2022$/kgP)*	*N GWP (kg-CO2eq/kgN)*	*P GWP (kg-CO2eq/kgP)*	*N Removal (mg/L)*	*P Removal (mg/L)*
Anaerobic/Anoxic/Oxic	A2O	2	$ 28.59	$ 194.64	24.06	163.83	32	4.7
Activated Sludge, 3-Sludge System	AS3	2	$ 46.36	$ 370.86	28.75	230.00	32	4.0
5-Stage Bardenpho	B5	3	$ 30.54	$ 216.34	29.41	208.33	34	4.8
Modified University of Cape Town Process	MUCT	3	$ 31.27	$ 221.49	28.24	200.00	34	4.8
5-Stage Bardenpho with Denitrification Filter	B5/Denit	4	$ 31.41	$ 237.15	29.73	224.49	37	4.9
4-Stage Bardenpho Membrane Bioreactor	MBR	4	$ 29.74	$ 224.54	29.73	224.49	37	4.9
5-Stage Bardenpho with Sidestream Reverse Osmosis	B5/RO	5	$ 44.38	$ 346.14	46.15	360.00	39	5.0
5-Stage Bardenpho Membrane Bioreactor with Sidestream Reverse Osmosis	MBR/RO	5	$ 42.29	$ 321.41	47.37	360.00	38	5.0

To perform a geographically resolved analysis, costs and GWP of each gray treatment technology were adjusted based on the location of the facility being evaluated. For gray treatment technologies, only the electricity grid mix was assumed to vary geographically. Treatment costs and GWP presented in the EPA report assumed the 2010 United States average electrical grid mix was used for water treatment and all cost information was presented in 2014 dollars. We assumed a linear increase in energy demand between Level 2 and Level 5, which is likely conservative as some estimates suggest an exponential increase in energy use approaching Level 5 [140]. Electricity prices were updated using the mean state electricity prices as reported

by the United States Energy Information Administration's 2021 Annual Energy Outlook, which is the most recent annual outlook available [115]. To approximate the emissions associated with electricity use in various geographic regions in the United States, the United States EPA's Emissions & Generation Resource Integrated Database (eGRID) was used [146]. Since Energy Information Administration electricity prices and eGRID mixes are not aggregated to the sub-watershed level, the GeoPandas library in Python was used to compare the shapefiles for United States states and eGRID regions to HUC 12 sub-watersheds [147]. If two states or eGRID regions overlapped a sub-watershed region, the state or eGRID region which overlapped a larger area of the sub-watershed was assigned to the sub-watershed. All technology costs and electricity prices were converted to 2022 dollars using historical Consumer Price Index data provided by the United

States Bureau of Labor Statistics using the mean annual Consumer Price Index values for all items and the United States city average was used [148,149]. The electricity prices and GWP was updated for each gray treatment method in each HUC region using the total electricity demand (kWh m^{-3}) presented in the EPA report and 2021 electricity values using Equation 1:

$$X_{i,w} = X_{i,US} - ElectricDemand_i * Y_{US} + ElectricDemand_i * Y_w \quad (1)$$

where X represents the technology's cost or GWP, i represents the gray technology method, w represents the waterbasin value, US represents the United States mean value, $ElectricDemand$ represents electricity demand of nutrient treatment for each gray technology, and Y represents the geographic specific cost or GWP of electricity.

3.2.3 Green Treatment Methods

Green non-point source nutrient treatment methods range from minimally invasive nutrient fertilizer reduction to land altering constructed wetlands [150,151]. For this analysis, 7 green treatment methods were considered, all of which are implemented on agricultural farmland (Table 7). These include 3 barrier treatment methods which are applied at the edge of the field (saturated buffers, woodchip bioreactors, and constructed wetlands) and 4 land treatment methods (nutrient rate reduction, split nutrient application, cover crops, and no-till farming). Some of these treatment methods treat both nitrogen and phosphorus, while others only treat one of the two nutrients considered. Mean nutrient removal percentages and treatment costs came from the 2016 *Illinois Nutrient Loss Reduction Strategy* report [151]. All values used within this analysis fall within the range of values reported in the literature [150,152–163].

Table 7. Costs and Emissions of Green Treatment Methods. Treatment" Type" designates if the green treatment method is applied at the edge of the field (Barrier) or applied across the entire farm (Land).

Name	*Abbr.*	*Type*	*N Cost (2022$/kgN)*	*P Cost (2022$/kgP)*	*N GWP (kg-CO2eq/kgN)*	*P GWP (kg-CO2eq/kgP)*	*N Removal (%)*	*P Removal (%)*
Saturated Buffers	BU	Barrier	$ 1.95	$ 14.63	0.10	3.98	90%	50%
Woodchip Bioreactors	BR	Barrier	$ 2.68	$ -	0.70	-	25%	0%
Constructed Wetland	W	Barrier	$ 4.88	$ -	(3.90)	-	50%	0%
N Rate Reduction	NR	Land	$ 0.00	$ 0.00	(9.21)	(105.72)	10%	7%
Split N Application	NS	Land	$ 7.56	$ -	11.10	-	10%	0%
Cover Crop	CC	Land	$ 3.90	$ 158.52	0.55	8.10	30%	30%
No-till	NT	Land	$ -	$ 0.00	-	(91.35)	0%	50%

One limitation to published values on green treatment methods is that they are presented in terms of the cost for the farmer to implement the technology, not the costs that would be incurred by a utility encouraging the adoption of these technologies to avoid new gray infrastructure upgrades. Therefore, some of the technology costs (i.e. applied nutrient reduction and no-till farming) are negative because they are cheaper than conventional farming practices. Since this analysis was performed from the utilities perspective, it was assumed that the utility would incur the costs of technology adoption, but would not claim the benefits of cost saving

practices. Therefore, it was assumed that the technology costs of the negative cost technologies would be zero.

Additionally, it was assumed that farmers would need to be financially incentivized by the utility to implement green nutrient treatment methods. Therefore, it was assumed that the utility would pay farmers \$31 $acre^{-1}$ $year^{-1}$ for land treated with green treatment methods, which is the mean value reportedly paid to farmers in 2021 by the Soil and Water Outcomes Fund [164]. This incentive payment is in addition to the green technology costs paid for by the utility. Barrier treatment methods which only need to be installed once, were only assumed to pay incentive fees during the first year of operation. Land treatment methods are applied yearly and, as such, the incentive fees were paid out annually. Lastly, constructed wetlands require up to 6% of the treated farmland acres to be converted to a wetland [150]. As a conservative estimate, it was assumed that this land was productive farmland and the utility would need to rent the land from the farmer at the mean land rental prices as reported by the USDA's 2022 land cash rental prices in order to compensate farmers for reducing their farm size [165]. Farmland rental prices were reported at a state level and were applied to each waterbasin based on the states which the waterbasin resided in. If the waterbasin covered land in multiple states, the land rental prices were calculated using a weighted mean based on the number of agricultural acres in each state. Land rental prices were assumed to stay constant over the life of the project.

Similar to the costs of gray treatment technologies, the costs of green treatment technologies were received in 2016 dollars and were converted to 2022 dollars using historical Consumer Price Index data provided by the United States Bureau of Labor Statistics [148,149]. The GWP of each green treatment method were estimated using life-cycle inventory data from the EcoInvent 3.71 database, using cut-off analysis, accessed through the software openLCA

1.10.3 (https://openlca.org), and calculated using the Traci 2.1 impact assessment methodology [166,167]. The GWP estimate for constructed wetlands includes direct land use change effects which were calculated using IPCC methodology [168]. Details of LCA calculations for each treatment method are discussed in Appendix B.

Since each green nutrient treatment method requires different topology, infrastructure, or climate in order to be implemented; not every green treatment method could be applied in every waterbasin. Therefore, land limitations were added to green infrastructure on a waterbasin basis. These land limitations included the availability of tile-drained soil (saturated buffers and woodchip bioreactors), the availability of riparian buffer between agricultural land and discharge waterways (saturated buffers), the soil and climate to support wetlands (constructed wetlands), and the requirement of supplemental fertilizer application (nutrient rate reduction and split nutrient application). It was assumed that if the requirements were met in one part of the waterbasin, the requirements could be implemented in the rest of the waterbasin and the nutrient reduction strategy could be applied. For example, if tile drains were used on agricultural land in one part of the waterbasin, it was assumed that they could be added to all agricultural land in the waterbasin. Data for tile drain locations was acquired from Nakagaki et al. (2016) based on analysis from Sugg (2007) and data for riparian buffers, wetlands, and fertilizer application were acquired from the EPA's EnvironAtlas [143,169,170]. Details of each green treatment method's requirements is provided in Table B1 and maps of tile drainage, riparian buffers, wetlands, and fertilizer application availability in each waterbasin is presented in Figure B13.

One of the benefits of green nutrient treatment methods is that they can be used in combination with each other [150]. This analysis considered all combinations of the 7 treatment methods proposed. Since each of the barrier treatment methods are applied at the edge of the

field before discharge to the waterway, it was assumed that only one barrier treatment method could be used at a time. Conversely, no limitations were placed on the land treatment methods. Therefore, 63 unique combinations of green treatment methods were evaluated to find the best performing treatment methods in each watershed. For combined green treatment methods, it was assumed that costs, GWP, and nutrient removal efficiency were compounded. For example, if saturated buffers were combined with cover crops, their nitrogen cost would be $\$1.95 kgN^{-1} + \$3.90 kgN^{-1} = \$5.85 kgN^{-1}$, nitrogen GWP would be $0.10 kg - CO_{2eq} kgN^{-1} + 0.55 kg - CO_{2eq} kgN^{-1} = 0.65 kg - CO_{2eq} kgN^{-1}$, and their nitrogen removal efficiency would be $90\% + 30\% * (100\% - 90\%) = 93\%$.

3.2.4 Calculation Methods and Assumptions

In order to estimate the nutrient trading potential of green versus gray nutrient reduction technologies, multiple scenarios were assumed. The first scenario assumed that each of the wastewater treatment facilities evaluated were required to meet Level 2 nitrogen and phosphorus concentration limits of 8 mgN L^{-1} and 1 mgP L^{-1}, respectively. These values were selected because they are the conservative limit that all gray treatment technologies can achieve based on their treatment level in the EPA report. The second scenario assumed that each of the wastewater treatment facilities evaluated were required to meet Level 5 nitrogen and phosphorus concentration limits of 2 mgN L^{-1} and 0.02 mgP L^{-1}, respectively. These values were selected because they are the limit that the advanced reverse osmosis gray treatment technologies can achieve based on their treatment level in the EPA report. Two additional scenarios (Level 3 and Level 4) were also run to evaluate the sensitivity of results between the conservative Level 2 and advanced Level 5 scenarios. Concentration limits for nitrogen and phosphorus were 6 mgN L^{-1} and 0.2 mgP L^{-1} for the Level 3 scenario and 3 mgN L^{-1} and 0.1 mgP L^{-1} for the Level 4 scenario.

Each scenario was evaluated independently of the other scenarios. For all treatment methods, analysis was performed on the facility level and nutrient trading was assumed to occur within each waterbasin.

For each scenario, all facilities where both nitrogen and phosphorus concentrations were lower than the specified limits were excluded from analysis. Additionally, each gray nutrient treatment technology had maximum concentration limits which they could decrease the effluent during treatment. It was assumed that the wastewater could be treated multiple times when the concentration was above this limit, but costs and GWP would increase by the multiple of the number of treatments required. To avoid the highest concentration scenarios which would exaggerate the gray treatment costs, facilities which required a mean nutrient concentration reduction greater than 5X the Level 2 treatable concentration limit were excluded from analysis. Facilities located outside CONUS (i.e. Alaska, Hawaii, Puerto Rico, Guam, United States Virgin Islands, and American Samoa) were also excluded due to their lack of HUC 12 sub-watershed data provided by the EPA's EnviroAtlas [143]. After data filtration to remove facilities residing outside the CONUS or with nutrient concentrations lower than treatable limits, 18,534 unique facilities remained for the Level 2 analysis (16,686 facilities treated for nitrogen, 14,444 facilities treated for phosphorus, and 12,633 facilities treated for both); 20,989 unique facilities remained for the Level 3 analysis (17,634 facilities treated for nitrogen, 19,369 facilities treated for phosphorus, and 16,045 facilities treated for both); 21,828 unique facilities remained for the Level 4 analysis (19,207 facilities treated for nitrogen, 20,110 facilities treated for phosphorus, and 17,514 facilities treated for both); and 22,386 unique facilities remained for the Level 5 analysis (19,769 facilities treated for nitrogen, 20,785 facilities treated for phosphorus, and 18,192 facilities treated for both).

In addition to gray treatment facility limitations, green treatment methods were limited by agricultural land availability within each waterbasin. Total area within each sub-watershed was calculated using the GeoPandas' area function in Python. The percentage of crop land and pasture land in each sub-watershed as reported by EnviroAtlas were used to approximate the total agricultural land in each sub-watershed [143]. Since nutrient trading was performed at the waterbasin level, sub-watershed values were aggregated to the waterbasin level to determine the maximum nutrient treatment of the waterbasin as a whole.

Additionally, some of the green treatment methods considered are already in use on farms throughout the CONUS, but limited information exists on their prevalence. The USDA's 2017 agricultural census provides state-level tillage and cover crop data, but geographically resolved data is unavailable for the other green treatment methods [171]. The most recent non-census data coverage data is provided by the Iowa Department of Agriculture and Land Stewardship in their *Iowa Nutrient Reduction Strategy 2018-19 Annual Progress Report* [160]. The report states that of the total 30,600,000 acres of farm land in Iowa, 8,200,000 acres (26.8%) were no-till farmed, 5,700,000 acres (18.6%) were treated with nutrient management strategies (nitrogen rate reduction and split nitrogen applications), 973,000 acres (3.2%) used cover cropping, 107,000 acres (0.35%) were treated with wetlands, and 2,000 acres (0.35%) were treated with either saturated buffers or woodchip bioreactors [160,172]. To fill the gaps between the USDA census data and treatment methods considered, these values were applied to their respective green treatment methods across all waterbasins in the CONUS to provide a conservative estimate of land availability for additional green treatment applications. While accounting for land limitations, the maximum nutrient treatment potential of each green technology in each waterbasin was calculated using Equation 2:

$$NT_{i,w} = A_w * (Pct_{crop,w} + Pct_{past,w}) * (1 - Pct_{tech,i}) * N_{mean-loss,w} * Pct_{N-removal,i} \quad (2)$$

where $NT_{i,w}$ represents the possible nutrient treatment for each green technology (subscript i) in each waterbasin (subscript w), A_w represents the waterbasin total area, $Pct_{crop,w}$ represents the percent of waterbasin area which is crop land, $Pct_{pasture,w}$ represents the percent of waterbasin area which is pasture land, $Pct_{tech,i}$ represents the percent of agricultural land currently treated with each green treatment method, $N_{mean-loss}$ represents the mean nutrient loss per land area of agricultural land in the waterbasin, and $Pct_{N-removal,i}$ represents the percent of nutrient removal for each green technology. The state-level nutrient runoff values as predicted by the 2012 regional United States Geological Survey's Spatially Referenced Regression On Watershed attributes models were used to quantify nutrient loading from agricultural land in each water-basin [173–178].

Analysis was performed first for all green treatment methods and combinations. The required nutrient treatment and the possible nutrient treatment were calculated on a waterbasin level as described in the previous paragraphs. If the available agricultural land in a waterbasin could not support the removal of the required nutrient load to meet the desired concentration limits, it was assumed that the maximum possible treatment would be applied based on the land available. The percentage of maximum nutrient treatment compared to the desired nutrient treatment was calculated and was used for nutrient treatment of all facilities within the waterbasin. Total land area required for nutrient remediation was also recorded to calculate farmer incentive payments. After the nutrient treatment loads were calculated for each wastewater facility, the new mean nutrient concentrations were calculated based on annual wastewater discharge. After final nutrient treatment loads were determined, the treatment costs (including farmer incentive and wetland costs) and GWP were calculated for both nutrients.

Lastly, if both nitrogen and phosphorus were being treated, the total treatment costs and GWP of the facility were set by the nutrient which required more infrastructure. For example, if nitrogen required 500 ha of treatment to meet concentration limits and phosphorus required 1,000 ha, the phosphorus treatment costs and GWP were assumed for treatment of both nutrients at the facility since both nutrients can be treated simultaneously for certain treatment methods. Comparison of the nutrient treatment levels for each green treatment method are presented in Figure B4.

After treatment costs and GWP were calculated for every wastewater treatment facility and each green treatment method (including combinations), an optimization was run to determine the maximum amount of nutrients that could be treated using green treatment methods in each waterbasin. In many waterbasins, multiple green treatment methods could treat the required nutrient load to reach the desired concentration limits. Therefore, a secondary optimization was performed to determine the minimum cost scenario and minimum GWP scenario when the maximum amount of nutrients were treated. Results for the minimum cost scenario are used for comparison to the gray treatment methods in the results section. The minimum GWP scenario was excluded from the primary results section because it has a breakeven carbon cost of $939 per tonne-$CO_{2e}$ when compared to the minimum cost scenario which is more expensive than direct air carbon capture technologies [179]. Detailed results for both optimization scenarios is discussed in Appendix B.

Once costs and GWP were determined for each green treatment method, costs and GWP were calculated for each of the gray treatment methods. In order to ensure green and gray treatments were compared evenly, the gray nutrient treatment levels were set equal to those of the green maximum treatment scenarios even though they are not limited by agricultural land constraints. If these limitations were not placed on gray treatment technologies, they would treat

more nutrients than the green treatment methods which would increase their treatment costs and emissions and exaggerate the benefit of green treatment methods. Costs for all treatment methods were originally calculated at the wastewater facility level using sub-watershed characteristics. For analysis purposes, results were aggregated from the facility level to the waterbasin level. Figure B14 provides a diagram of the analysis process.

3.3 Results and discussion

The outcomes of the work are presented in three subsections: 1. nutrient treatment potential of green infrastructure, 2. global warming potential (GWP) of gray compared to green treatment technologies, and 3. total costs and carbon markets potential for gray and green treatment technologies. A summary table of key results from this analysis are shown in Table 8. All results are presented for the minimum cost technology for both green and gray technologies. The minimum costs gray technologies were Anaerobic/Anoxic/Oxic for Level 2, 4-Stage Bardenpho Membrane Bioreactor for Levels 3 and 4, and 5-Stage Bardenpho Membrane Bioreactor with Sidestream Reverse Osmosis for Level 5 treatment scenarios.

Table 8. Aggregated results for the national deployment of gray or green technologies to meet regulated water quality obligations (Levels 2 thru 5 for gray infrastructure, compared to water quality trading based green infrastructure alternatives)

	Level 2	**Level 3**	**Level 4**	**Level 5**
Treatment Target mg N/L	8	6	3	2
Treatment Target Limits mg P/L	1	0.2	0.1	0.02
Gray Electricity Use (Tera Wh/yr)	8.1	8.9	10.1	21.2
Gray Emissions (MtCO2e/Year)	11.9	17.4	18.5	29.8
Gray Cost ($B/Year)	$14.9	$18.3	$19.5	$28.5
Green Emissions (MtCO2e/Year)	-3.4	-3.8	-3.9	-4.2
Green Cost ($B/Year)	$10.0	$12.4	$13.2	$13.6
Net Emissions (MtCO2e/Year)	15.3	21.2	22.4	33.9
Carbon Revenue				
Total ($M/Year)	$307	$424	$449	$679
Green Net Savings w/ Carbon Revenue ($B/Year)	$5.2	$6.3	$6.8	$15.6
Mean Carbon Revenue vs Green Waterbasin Costs	5.4%	6.0%	5.8%	8.6%
StDev of Carbon Revenue vs Green Waterbasin Costs	5.7%	6.8%	6.7%	10.5%
Max Carbon Revenue vs Green Waterbasin Costs	20.9%	26.2%	26.5%	43.7%

3.3.1 Nutrient Remediation Potential of Green Infrastructure

In total, we find that 31.7% (530,255 tonnes N yr^{-1}) and 20.8% (54,110 tonnes P yr^{-1}) of the desired nitrogen and phosphorus treatment could be achieved using green infrastructure, for the Level 5 scenario (Figure 9).

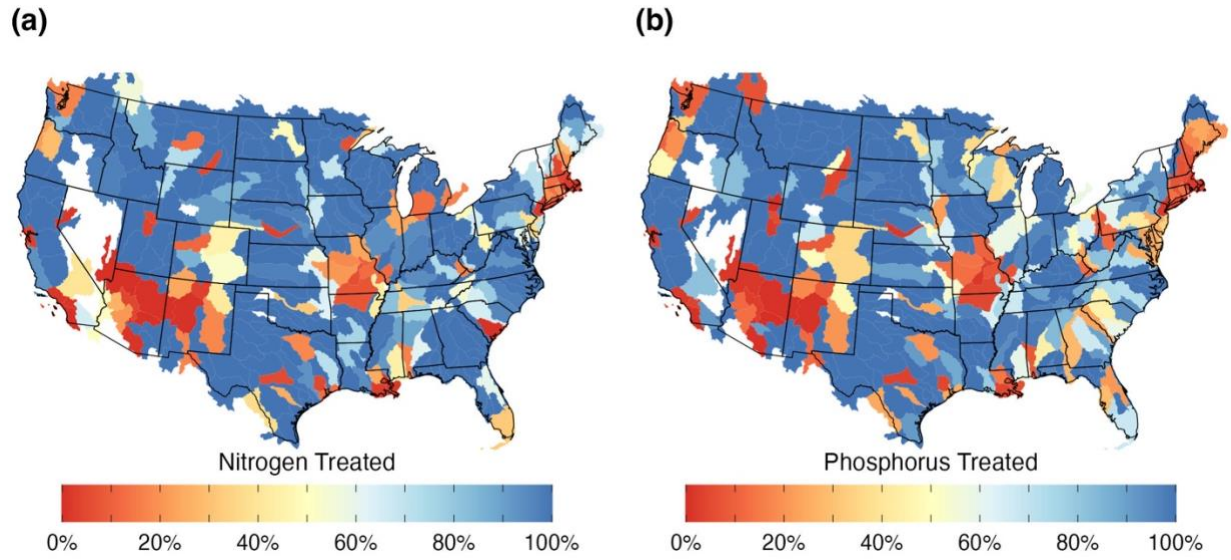

Figure 9. Percent of Nitrogen (a) and Phosphorus (b) treatment possible for green treatment technologies in each waterbasin for the Level 5 scenario of reducing mean nutrient concentrations to 2 mgN/L and 0.02 mgP/L. White space designates waterbasins which didn't have wastewater treatment facilities or didn't require nutrient treatment.

For the Level 2 scenario, Level 3 scenario, and Level 4 scenario; results show that 36.8% (403,913 tonnes N yr^{-1}) and 22.5% (39,453 tonnes P yr^{-1}), 35.3% (447,888 tonnes N yr^{-1}) and 21.1% (50,147 tonnes P yr^{-1}), and 32.4% (505,953 tonnes N yr^{-1}) and 21.0% (52,457 tonnes P yr^{-1}) of the desired nitrogen and phosphorus treatment could be achieved using green infrastructure, respectively (Figures B1, B2, and B3). The primary reason why green treatment methods cannot achieve higher nutrient treatment loads is due to limited agricultural land in the waterbasins and limitations on geographic deployment. For example, saturated buffers and woodchip bioreactors can only be used in locations with tile drainage, but are also two of the treatment methods with the highest nutrient reduction effectiveness. These agricultural land limitations are seen in the desert southwest where limited agriculture land exists, in Missouri where high wastewater flow rates exist, and in the northeast where land availability is limited due to high population densities. While green treatment methods can only treat less than 40% of nitrogen and 25% of phosphorus needed in the United States, this would still represent a large decrease in infrastructure compared to the scenario where green treatment methods are not used.

This is particularly true at the higher treatment levels where more advanced gray water treatment technologies are required. According to the EPA report, the only treatment technologies which can reach Level 5 concentration levels are those that use sidestream reverse osmosis filtration systems that suffer from issues of frequent fouling which both decreases treatment efficiency and increases operation expenses [138,180,181]. Therefore, reducing the need for any gray wastewater treatment infrastructure would be of benefit. Figure B4 illustrates the effectiveness of each of the green treatment methods (and combinations of methods) at meeting desired nutrient treatment goals.

3.3.2 Global Warming Potential of Gray vs Green Infrastructure

Annually, we find that gray treatment technologies would emit 29.8 MtCO2e while green treatment technologies would sequester 4.2 MtCO2e for the Level 5 scenario (Figure 2). This results in a annual carbon credit potential of 33.9 MtCO2e. Our results also show that green treatment technologies can reduce emissions compared to gray treatment technologies in every waterbasin.

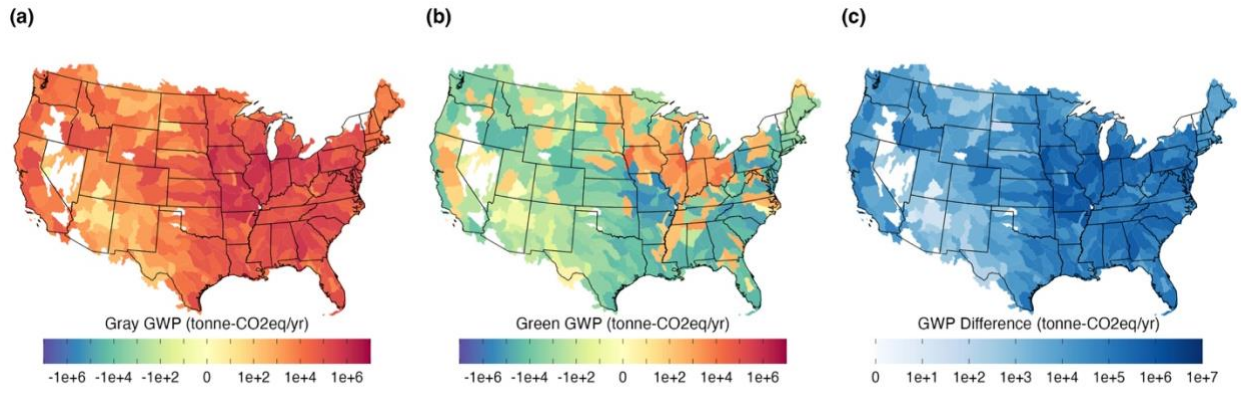

Figure 10. Continental United States global warming potential (GWP) in tonnes of CO_2 equivalent emissions per year for removal of nitrogen (to 2 mg/L) and phosphorus (to 0.02 mg/L) using (a) gray treatment technologies (29.8 $MtCO_{2e}$/year) and (b) green treatment technologies (-4.2 MtCO2e/year), and (c) net GWP representing potential carbon credit generation (33.9 MtCO2e/year). White space designates waterbasins which didn't have wastewater treatment facilities or didn't require nutrient treatment.

Depending on the optimal green treatment technologies used (Figure B5), waterbasin greenhouse gas emissions can be either positive or negative. When optimized for both minimum cost and maximum nutrient treatment, our results show that the primary green treatment technology to use in the Corn Belt is saturated buffers which has a positive GWP. Conversely, the primary treatment technologies to use in the western United States are constructed wetlands, nutrient rate reduction, and no-till farming which all have a negative GWP and therefore allow the waterbasin to also have negative nutrient treatment GWP compared to conventional practices. Similar results were observed for the Level 2 scenario, Level 3 scenario, and Level 4 scenario (Figures B6, B7, and B8). In the Level 2 scenario, gray treatment technologies emit 11.9 MtCO2e while green treatment technologies sequester 3.4 MtCO2e annually which results in a annual carbon credit potential of 15.3 MtCO2e. In the Level 3 scenario, gray treatment technologies emit 17.4 MtCO2e while green treatment technologies sequester 3.8 MtCO2e annually which results in a annual carbon credit potential of 21.2 MtCO2e. In the Level 4 scenario, gray treatment technologies emit 18.5 MtCO2e while green treatment technologies sequester 3.9 MtCO2e annually which results in a annual carbon credit potential of 22.4 MtCO2e. Overall, GWP values are reduced in the Level 2-4 scenarios compared to the Level 5 scenario due to the reduction in nutrient treatment required.

3.3.3 Carbon Financing Potential of Green Infrastructure

Nutrient treatment costs for the Level 5 scenario were found to be \$28.5B year^{-1} and \$13.6B year^{-1} for gray and green technologies, respectively, when costs are normalized over the life of the technology. Additionally, we found the carbon financing potential is \$679M year^{-1} assuming a carbon credit price of \$20 tonne-CO2eq^{-1} which results in the total savings of green treatment technologies when compared to gray treatment and including carbon financing

potential of \$15.6B year^{-1} (Figure 3). Contrary to the GWP results, green treatment technologies are not cheaper than gray treatment technologies in all waterbasins. Of the 316 waterbasins in the Contiguous United States (CONUS) which required nutrient treatment, 222 (70%) had green treatment costs cheaper than the gray treatment technologies when excluding carbon financing revenues. If carbon financing revenue is added, 232 (73%) of waterbasins had green treatment costs cheaper than gray treatment technologies. However, when evaluated as a percent of total nutrients treated in the CONUS, 93.4% of nitrogen and 90.2% of phosphorus is treated in waterbasins where green treatment costs are cheaper than gray treatment technologies when carbon financing revenues are excluded. These values increase to 94.6% of nitrogen and 91.9% of phosphorus treated in the CONUS in waterbasins which green technologies are cheaper when carbon financing revenues are included. The primary driver for increased green treatment costs compared to gray technologies in some waterbasins is farmer incentive payments. These waterbasins are those where the optimum green treatment technology is land based (nutrient rate reduction, split nutrient application, cover crops, and no-till farming) which incurs annual farmer incentive payments, compared to the one-time farmer incentive payments for other green treatment methods. On a national level, farmer incentive payments make up 49% (\$6.7B year^{-1}) of the total green treatment costs in the Level 5 scenario.

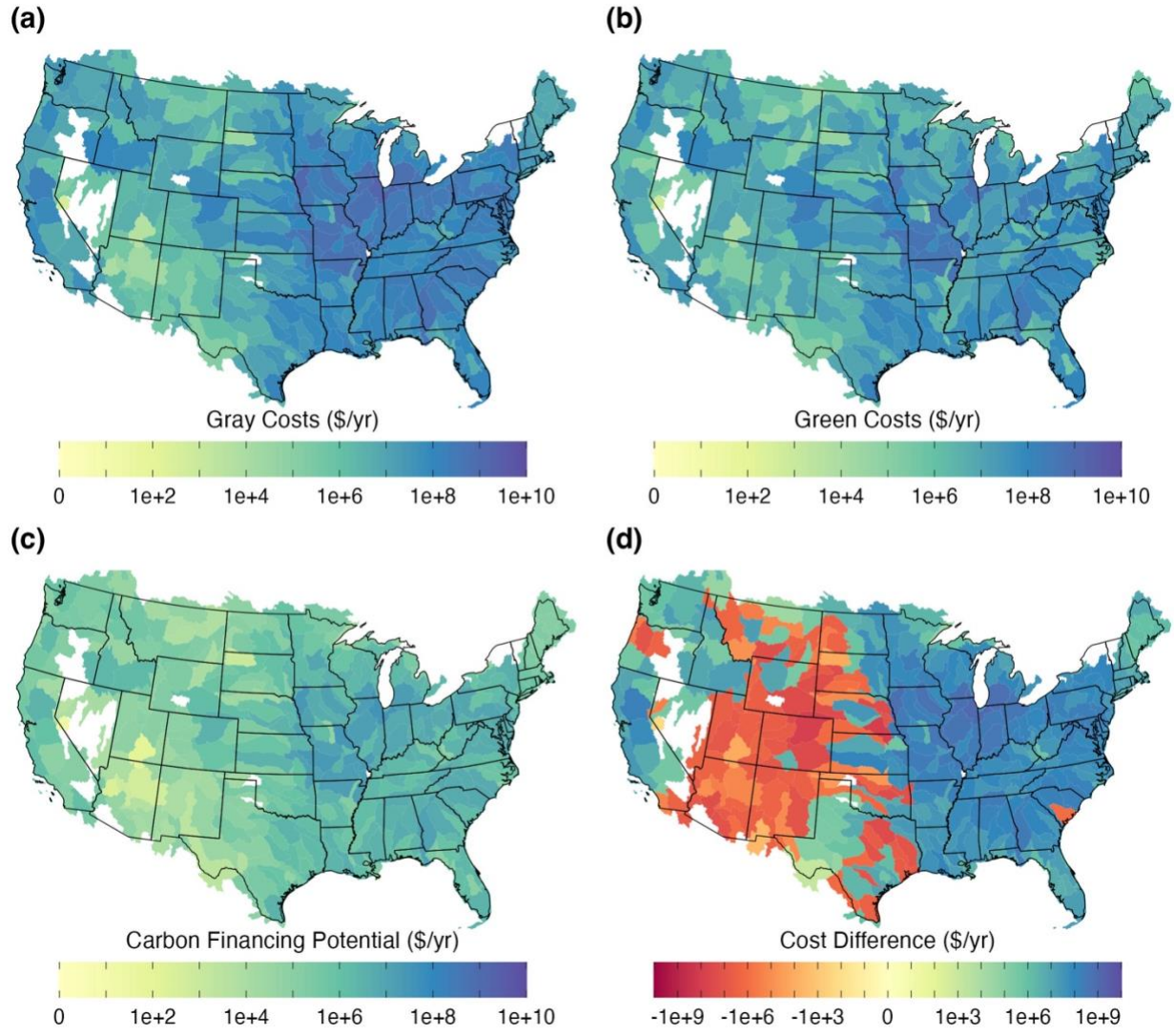

Figure 11. Continental United States water treatment costs for removal of nitrogen (to 2 mg/L) and phosphorus (to 0.02 mg/L) using (a) gray treatment technologies ($28.5B/year) and (b) green treatment technologies ($13.6B/year), (c) Potential carbon markets revenue ($679 M/year at $20/credit), and (d) net cost difference between gray and green treatment technologies when including carbon financing revenue ($15.6B/year). Negative cost differences show waterbasins where green technologies are more expensive than gray technologies. White space designates waterbasins which didn't have wastewater treatment facilities or didn't require nutrient treatment.

Nutrient treatment costs for the Level 2 scenario were found to be \$14.9B year^{-1} and \$10.0B year^{-1} for gray and green technologies, respectively, when costs are normalized over the life of the technology. Additionally, we found the carbon financing potential is \$307M year^{-1} assuming a carbon credit price of \$20 tonne-CO2eq^{-1} and a 40 year lifespan. This results in the total savings of green treatment technologies when compared to gray treatment and including

carbon financing potential of \$5.2B year^{-1} (Figure B9). Of the 314 waterbasins in the CONUS which required nutrient treatment, 166 (53%) had green treatment costs cheaper than those of the gray treatment technologies when excluding carbon financing revenues. If carbon financing revenue is added, 172 (55%) of waterbasins had green treatment costs cheaper than gray treatment technologies. However, when evaluated as a percent of total nutrients treated in the CONUS, 80.9% of nitrogen and 66.2% of phosphorus is treated in waterbasins where green treatment costs are cheaper than gray treatment technologies when carbon financing revenues are excluded. These values increase to 85.6% of nitrogen and 72.0% of phosphorus treated in the CONUS in waterbasins which green technologies are cheaper when carbon financing revenues are included. Similar to the Level 5 scenario, green treatment costs were largely impacted by the farmer incentive payments. On a national level, farmer incentive payments make up 53% (\$5.3B year^{-1}) of the total green treatment costs.

The nutrient treatment costs for both Level 3 and Level 4 scenario fall between those of the Level 2 and Level 5 scenarios. In the Level 3 scenario, treatment costs were found to be \$18.3B year^{-1} and \$12.4B year^{-1} for gray and green technologies, respectively, with a carbon financing potential of \$424M year^{-1} assuming a carbon credit price of \$20 tonne-CO2eq^{-1} and a 40 year lifespan. This results in the total savings of green treatment technologies when compared to gray treatment and including carbon financing potential of \$6.3B year^{-1} (Figure B10). In the Level 4 scenario, treatment costs were found to be \$19.5B year^{-1} and \$13.2B year^{-1} for gray and green technologies, respectively, with a carbon financing potential of \$449M year^{-1} assuming a carbon credit price of \$20 tonne-CO_{2eq}^{-1} and a 40-year lifespan. This results in the total savings of green treatment technologies when compared to gray treatment and including carbon financing potential of \$6.8B year^{-1} (Figure B11). Additional information about the waterbasin level

economic feasibility of Level 3 and Level 4 scenarios is in Appendix B. A costs and emissions comparison between all green and gray treatment methods is shown in Figure B12.

3.4 Discussion

River water quality improvements in the United States have been often delayed because of cost, complexity and litigation, with alternative compliance solutions, like nutrient trading, established but limited in scale. Meanwhile, carbon credits are designed to use market mechanisms to accelerate the energy transition. Combining this challenge and opportunity, there is a window of opportunity now to accelerate the improvement of America's rivers using these market mechanisms, as we transition to a renewable energy and restored watershed future.

Water and wastewater treatment in the United States already accounts for 2% of energy use and 45 million tonnes of CO_{2e} emissions. We estimate these values could almost double over the coming years as utilities are obligated to increase treatment levels, even as states transition to renewable energy sources. Our results also indicate potential feasibility, effectiveness, and cost savings associated with green infrastructure alternatives to gray infrastructure to meet water quality goals and obligations. The EPA has recently revitalized their commitment to market-based water quality trading, emphasizing the role of the private sector in enabling improved river water quality in the United States, and encouraging regulators to embrace these opportunities and methodologies [23]. Yet, water quality trading programs in the United States have been limited in part by a reliance on regulator support, high transaction costs and a lack of pooled risk mitigation potential between programs. Fundamentally, local water problems have never benefited from a global, liquid economy. Carbon markets have been used extensively in the past fifteen years to deliver measurable clean drinking water services in low-income countries globally and could be

applied in the United States to further motivate early, pre-permit green alternatives to meet water quality obligations [181].

International carbon credit markets are designed to financially incentivize early, voluntary action toward climate change mitigation, adaptation, and reduced emissions. Some estimates suggest that carbon credit markets can, "double climate ambition relative to current Paris pledges (NDCs) over 2020–2035, without increasing total costs," [182]. In 2022, some market research estimates that the volume of carbon credits in demand will increase at least 20x by 2035, with credits increasing in value from around $25 per tonne to a central estimate of $80-$150 per tonne by 2035 [135]. Toward this opportunity, new methodologies are needed which enable the generation of carbon credits, salable for revenue, associated with replacing gray infrastructure with green infrastructure to improve watershed health and river water quality. In this approach, the GHG emissions envisioned are avoided, rather than sequestered or removed, through the avoided construction of electricity consuming infrastructure. These avoided emissions, when achieved early and voluntarily, can have substantial social benefits [183], while generating a potential $679 million annually in carbon credit revenue (at $20 per credit), representing an opportunity to further motivate green infrastructure solutions within water quality trading programs to meet regulated obligations in lieu of new gray infrastructure.

The results we've presented in this study are the best estimates possible with currently available data, but we acknowledge that some limitations exist with green nutrient technology research that should be addressed through future studies. Importantly the results and model presented here is not intended for top-down planning, it was developed to try and better understand the scope of the problem and opportunity. Any green infrastructure development must be done in a way that incorporates the local communities considerations, opportunities,

values, and rights. Additionally, green infrastructure projects are notable for creating local jobs that do not require advanced degrees, and that are inherently 'local'. Disadvantaged communities are also disproportionately impacted by water rate increases, as well as emissions and the effects of accelerating climate change on watersheds and the resulting wildfire risks. In contrast to expensive, high-technology gray infrastructure construction, estimates suggest that approximately 20 jobs are created for every $1M of public investment in green infrastructure, and investment in forest and watershed restoration is multiplied in local economic activity between 1.7 and 2.6 times [184].

Limited data exists on the current prevalence and effectiveness of green technologies across the United States which represents the largest uncertainty associated with this work. Existing research on these technologies is focused in the Midwestern United States (i.e. Corn Belt) and have found non-point source nutrient treatment methods to have a wide range of nutrient reduction efficiencies based on geographic location, agricultural techniques used, and local climate patterns. Studies need to be performed on each of the green treatment methods to evaluate their effectiveness in more geographically diverse regions across the United States. However, it should be noted that regions in the United States which are currently studying green treatment technologies correlate with those found in this study to have the largest economic incentive from implementing these technologies. Therefore, regions that we find to have receive the largest benefit from green treatment technologies are also those with the lowest uncertainties. Additionally, surveys need to be completed to provide better estimates of the current prevalence of these technologies throughout the United States to better estimate future potential. United States Department of Agriculture (USDA) census data is available for cover cropping and no-till farming across the United States, but limited data is available for saturated buffers, woodchip

bioreactors, constructed wetlands, and smart fertilizer application strategies. Literature shows that green treatment methods can be used in combination with each other, but it is unknown how the benefits of these technologies compound. Research should be performed to evaluate the effectiveness of these technologies when used in combination with each other to ensure nutrient treatment isn't saturated and to maximize the nutrient reduction of the technologies being implemented. The LCA estimates made for green technologies in this study should also be evaluated in specific case studies to capture nuances of the local installations and performance data should be used to accurately determine the GHG emissions. Additionally, it is important to acknowledge the evolution of the grid in terms of carbon emissions will impact the carbon financing potential of green nutrient treatment technologies. As the grid evolves with less environmental impact, carbon credits generated by offsetting gray infrastructure with green infrastructure will be reduced, which means that the window of opportunity for leveraging carbon markets to incentivize a shift from gray to green infrastructure may be limited.

Extending this opportunity globally, there are many examples of watershed and water quality trading programs in Canada, Australia, New Zealand, the United Kingdom, the Netherlands, Honduras, India, China, and Kenya. Extending the findings of the United States study globally and assuming that an indicative 10 percent of irrigated croplands outside of the United States could be used to generate instream water quality benefits and thereby avoid facility-based treatment, the global potential for this approach could be close to 80 million tonnes of CO2e reduced or removed per year.

3.5 Data and Code Availability

The primary data used in this study consisted of geographically resolved nutrient loading data a from the Nutrient Model (Hypoxia Task Force Search) created by the EPA which was acquired through the EPA's Water Pollutant Loading Tool [144,145]. Using the data analysis techniques described in this paper and the Python code available in the Code Availability section, the results were generated for this study. All results data presented in this study is available on Zenodo [185]: https://doi.org/10.5281/zenodo.10456151. All code used in this analysis is available on Zenodo [186]: https://doi.org/10.5281/zenodo.10790349. Any updates to the code will be publicly available on GitHub: https://github.com/bradenlimb/Green-Wastewater-Treatment

CHAPTER 4: PURPOSE-GROWN BIOENERGY FEEDSTOCK OPTIMIZATION FOR UNITED STATES SUSTAINABLE AVIATION FUEL TARGETS WITH ECONOMIC AND ENVIRONMENTAL INSIGHTS[3]

4.1 Introduction

In 2023, the U.S. Department of Energy, along with the U.S. Department of Agriculture and the U.S. Department of Transportation, released the Sustainable Aviation Fuel (SAF) Grand Challenge [28]. The SAF Grand Challenge aims to expand domestic production of SAF to 3 billion gallons by 2030 and satisfy 100% of the aviation fuel demand with domestically produced SAF by 2050 (estimated to be 35 billion gallons). To qualify as SAF, the fuel must attain at least a 50% reduction in life cycle emissions compared to conventional jet fuel. These emission targets are similar to the International Air Transport Association's resolution to reach net zero carbon emissions by 2050, which requires a 50% reduction in aviation emissions compared to 2005 levels [29]. The SAF Grand Challenge is supported by the Clean Fuels & Products Shot™, the seventh initiative of the Department of Energy's Energy Earthshots™ program [30,31]. These initiatives are imperative to reduce carbon emissions in the hard to decarbonize aviation sector which accounts for 2% of U.S. carbon dioxide equivalent emissions [28]. As part of the SAF Grand Challenge, the previously mentioned governmental organizations released the SAF

[3]This chapter was submitted for publication as a peer-reviewed journal article: Limb, B. J., Smith, J. P., Simske, S. J., & Quinn, J. C. Addressing the Sustainable Aviation Fuel Grand Challenge: Economic and Environmental Insights from Feedstock Optimization (Manuscript In Review)

Grand Challenge Roadmap, which outlines potential pathways for achieving the SAF targets [28]. In this roadmap, many feedstocks are identified that could help achieve these production targets, such as municipal solid wastes, wet wastes (animal waste, food waste, wastewater solids), agricultural residues, and purpose grown bioenergy feedstocks. Of these feedstocks and fuels pathways, it's estimated that the U.S. will have enough future biomass to support 50-60 billion gallons of advanced biofuels without impacting current agriculture systems [28,32]. This estimate is a high-level assessment and there is a need to evaluate the potential of purpose-grown bioenergy feedstocks for SAF production across the U.S. that considers costs, emissions, and land use.

Many previous studies have evaluated the costs or emissions of bio-jet fuels [53–56]. However, fewer studies have evaluated the production of SAFs from bioenergy feedstocks or waste streams at a geographically resolved resolution, particularly at the national scale [33–38,57,58]. Additionally, few studies have evaluated the production potential of marginal lands for bioenergy production at large scales [32,33,39–44]. Previous studies have found that biofuel economics and emissions are sensitive to geographic location [38,45,46,56]. However, limited research exists on the impact of bio-jet economics and environmental impact at a geographically resolved level considering multiple feedstocks for the U.S. To the author's knowledge, the most comprehensive studies that have evaluated the economics and environmental impact of bio-jet fuels have only evaluated three or less feedstocks (miscanthus, switchgrass, and sorghum) simultaneously [33,47].

Uludere Aragon et al. (2022) evaluated the deployment of miscanthus and switchgrass on marginal lands to meet SAF production targets in the United States [33]. This study highlighted a novel model for prediction of miscanthus and switchgrass yields east of the 104th Meridian West

(eastern U.S.). However, their simulated yields were notably higher than those published in other known literature. For example, the Department of Energy's Billion Ton Study [32,44], which is commonly accepted as the foremost treatment of the subject, uses the Parameter-elevation Regressions on Independent Slopes Model (PRISM) datasets [48]. The PRISM data sets have mean yields that are approximately 20% lower than those reported by Uludere Aragon et al. Because of this, Uludere Aragon et al.'s land requirements are much lower than would be seen with the PRISM datasets. Critically, Uludere Aragon et al. also assume that 100% of the produced liquid fuel is suitable for drop-in replacement of jet fuel which represents an unrealistic assumption. It is infeasible to convert 100% of the produced hydrocarbons into the SAF range through repeated hydro-processing, and that a non-trivial portion of the produced fuel will be in the diesel, gasoline, or naphtha range [49–52]. Appendix C provides an extended literature review and discussion on this subject. Due to this, it is our assessment that the results presented in Uludere Aragon et al. are considerably understated in terms of land requirements and are optimistic in terms of economics and environmental impact due to unrealistic optimal yields. Gautam et al. (2023) presents a nation-wide analysis of bio-jet fuels, however their feedstocks were limited to miscanthus, switchgrass, and sorghum which only encapsulates a single biomass feedstock category (herbaceous energy crops) as defined by the SAF Grand Challenge Roadmap [28,47].

This study addresses the limitations in existing literature by evaluating the potential of multiple purpose grown bioenergy feedstocks to meet targeted SAF production volumes at a geographically resolved level across the U.S. In total, nine feedstocks and seven land types are considered for SAF production which cover 5 feedstock categories identified by the SAF Grand Challenge Roadmap (corn grain, seed oils, herbaceous energy crops, woody energy crops, and

algae). Geographically resolved results are presented for economic and environmental impacts of the bio-jet fuels. Additionally, optimization is performed to evaluate the best deployment of purpose-grown bioenergy feedstocks to meet SAF requirements while minimizing fuel costs, fuel emissions, land use, or carbon price. Finally, agent-based modeling is used to evaluate the feasibility of achieving SAF targets through policy incentives and farmer education.

4.2 Materials and methods

A flow diagram of the process used to complete this study is shown in Figure 12. The methods section of this paper includes eight subsections: an overview of the GIS analysis and model for estimating land availability for feedstocks, process models for converting feedstocks to SAF, and economic, environmental, carbon pricing, and biorefinery assumptions. The seventh subsection discusses optimization techniques for deploying feedstocks to meet SAF Grand Challenge targets. The final subsection details agent-based modeling assumptions.

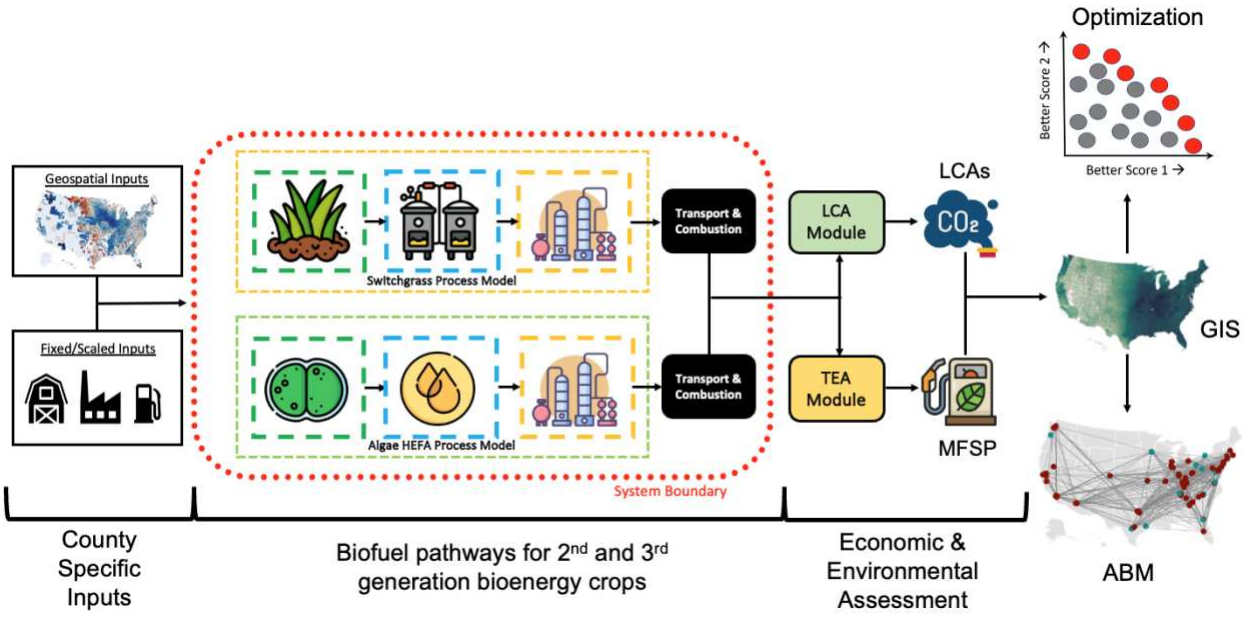

Figure 12. Flow diagram of research methodology.

4.2.1 GIS Model

To evaluate the feasibility of purpose-grown feedstocks for SAF production across the U.S., we first needed to evaluate the total production potential of different bioenergy feedstocks across the U.S. To do this, a multistep approach was taken. First, the desired bioenergy feedstocks and land classifications were identified. Second, the U.S. was broken up into small land parcels. Third, certain land regions were excluded due to unfeasible crop cultivation. Lastly, the crop productivities were overlaid on the possible land regions to calculate total biomass productivity potential. The following paragraphs detail each of these steps.

The purpose grown bioenergy feedstocks considered for this study include corn, soybeans, upland and lowland switchgrass, miscanthus, sorghum, poplar, willow, and microalgae grown in open raceway ponds. Corn and soy beans are limited to the fraction of land currently dedicated to bioenergy cultivation and do not compete with cropland for food production [187]. These feedstocks were selected based the availability of feedstock productivities across the U.S. and potential for SAF production. Biomass yields for switchgrass, miscanthus, sorghum, poplar, and willow were obtained from the PRISM-ELM dataset [48]. The United States Department of Agriculture's (USDA's) National Agricultural Statistics Service was used for county-level corn and soybean yields from the 2017 USDA crop census [188]. The 2017 USDA crop census data was used for this analysis as it is the most recent USDA crop census data available and annual USDA survey data often has data discrepancies in geographic areas important for this research. Microalgae yields were obtained utilizing the biological growth model developed by Greene et al. (2021) and Quiroz et al. (2021) [189,190].

This study did not consider the conversion of existing cropland to bioenergy cultivation due to the need for continued food production and the complications associated with indirect land use changes [191]. Therefore, it was assumed that only marginal land could be used for bioenergy feedstock cultivation. Marginal land is defined for this work as land that is not being used for productive purposes and includes grasslands, shrublands, barren lands, and forests not being used for timber or paper industries. Portions of the United States have productive forestry industries (e.g. southeastern U.S. and the northwest U.S.). Therefore, forest land considered for bioenergy feedstock cultivation was limited based on the amount of products that are currently produced on that forest land annually [192]. Forestry data was limited to the county level, therefore, if greater than 3% of forest biomass is harvested for forestry products annually, then that entire county was assumed to not have any forestry land available for biomass cultivation [193]. Additionally, cultivated cropland currently being used for corn ethanol and soybean biodiesel production was assumed to be available for all bioenergy feedstocks based on the assumption that the transportation sector is moving towards electrified vehicles and the need for corn ethanol and soybean biodiesel will be reduced [187,194]. The geographic variability of different land classifications in the U.S. was obtained from the National Land Cover Database and generated by Dewitz [195]. Land was also excluded from consideration if it had a protected status or was a key biodiversity area [196,197]. Land areas were also excluded with steep land grades which would make feedstock cultivation infeasible. Land was excluded if it had a slope greater than 5% for non-woody terrestrial crops, greater than 2% for algae facilities, and greater than 25% for poplar and willow [37,198–202]. Land slope data was retrieved from the USGS LANDFIRE program [203]. In total, nine different purpose-grown bioenergy feedstocks were evaluated across seven land classifications, Table 9.

Table 9. National land cover database land types considered for each bioenergy crop. Table options include No, Yes, Excluded, Limited, and Bioenergy. "No" means that the crop could not be cultivated on the land type. "Yes" means that the crop could be cultivated on the land type. "Excluded" means that feedstocks could feasibly be grown on pastureland, but pastureland was excluded from this analysis due to indirect land use change effects. "Limited" refers to the fact that feedstocks could be grown on forested land, but only forested land not currently used for forestry products was considered. "Bioenergy" refers feedstocks only being grown on cultivated cropland if it is currently used for bioenergy (corn ethanol or soybean biodiesel). [187]

NLCD Land Cover Type	Corn	Soybeans	Switchgrass	Miscanthus	Sorghum	Poplar	Willow	Algae
Water	No	No	No	No	No	No	No	No
Perennial Ice Snow	No	No	No	No	No	No	No	No
Developed Land	No	No	No	No	No	No	No	No
Barren Land	No	No	No	No	No	No	No	Yes
Deciduous Forest	No	No	Limited	Limited	Limited	Limited	Limited	Limited
Evergreen Forest	No	No	Limited	Limited	Limited	Limited	Limited	Limited
Mixed Forest	No	No	Limited	Limited	Limited	Limited	Limited	Limited
Shrubland	No	No	Yes	Yes	Yes	Yes	Yes	Yes
Grassland Herbaceous	No	No	Yes	Yes	Yes	Yes	Yes	Yes
Pasture Hay	No	No	Excluded	Excluded	Excluded	Excluded	Excluded	Excluded
Cultivated Crops	Bioenergy	Bioenergy	Bioenergy	Bioenergy	Bioenergy	Bioenergy	Bioenergy	Bioenergy
Wetlands	No	No	No	No	No	No	No	No

In order to evaluate the potential of the U.S. to grow purpose-grown feedstocks for SAF, the contiguous United States was divided into 200 meter by 200 meter land parcels. This resolution was chosen to strike a balance between high-resolution land characteristics and manageable file sizes. After the contiguous United States was broken up into parcels, multiple characteristics were applied to each parcel. Mean feedstock yields were assigned to each parcel using nearest neighbor resampling of the PRISM-ELM dataset or calculated using the algae growth model [48,189,190]. Land cover type, as defined by National Land Cover Database, was also assigned to each parcel using nearest neighbor resampling of the dataset compiled by Dewitz [195]. County FIPS number, protection status, and key biodiversity status were assigned to each parcel based on reprojecting their shapefiles [196,197,204]. Land slope percentage was assigned to each parcel using bilinear resampling of the LANDFIRE dataset [203]. Above ground carbon density of the parcel was assigned using bilinear resampling of the carbon density

dataset compiled by Spawn et al. (2020) [205]. Global Ecological Zones were assigned to each parcel by reprojection of shapefile data [206]. Soil type was assigned to each parcel by using nearest neighbor resampling of the dataset compiled by Batjes [207].

After each land parcel was characterized, data was aggregated to the county level based on feedstock and land cover type. This aggregation involved several steps: first, all parcels within a given county were identified. Parcels containing protected lands or key biodiversity areas were excluded. Next, parcels with steep land grades were excluded for a given feedstock. For each land cover type and feedstock combination, the remaining parcels were aggregated, calculating the mean feedstock yield and above-ground carbon density to produce county-level values. The number of aggregated parcels was recorded to determine the total land area available. The resulting dataset consisted of county-level total land availability, mean feedstock yield, and mean above-ground carbon density for every feedstock and land type combination.

Once land availability for feedstocks was calculated and the feedstock productivities were known from the listed sources, these values could be multiplied together to calculate the maximum biomass production potential of different purpose-grown bioenergy feedstocks on different land types at the county level throughout the U.S. All county level values were passed to the process models to calculate SAF production potential along with associated fuel costs and emissions.

4.2.2 Process Modeling

To evaluate the economic and environmental impacts associated with converting purpose-grown feedstocks to SAF, process models were developed for every feedstock-to-SAF pathway. Process models consisted of three primary steps: feedstock cultivation, feedstock

conversion to fuels, and upgrading the fuels to SAF. The cultivation phase includes all inputs and outputs associated with growing and harvesting the biomass as well as transporting the biomass from the farm to the biorefinery. The conversion phase includes all inputs and outputs to convert the biomass into fuel components. The upgrading phase includes all inputs and outputs to convert the fuel components into fuel products as well as transporting the jet fuel to the nearest airport with one million annual passenger enplanements. The model applied to this work is an extension of the one presented in Smith et al. (2023) [45]. A flow diagram of the feedstocks and conversion pathways used in this study are shown in Figure 13.

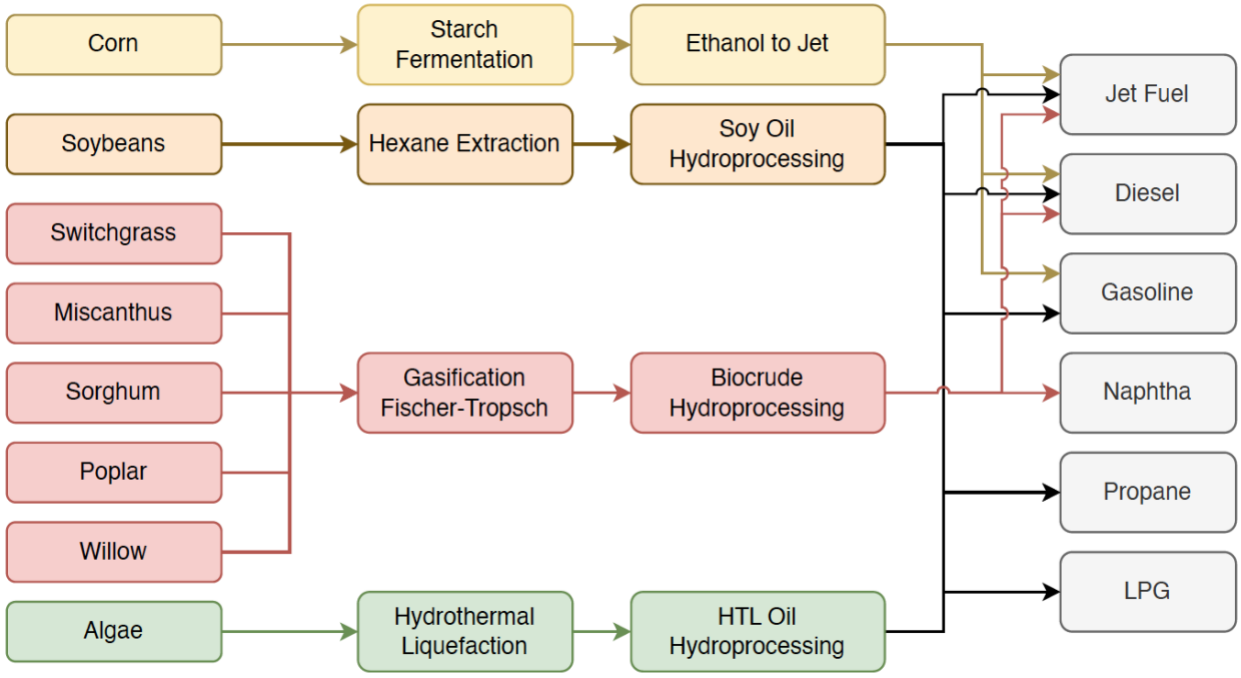

Figure 13. Feedstocks and conversion pathways to sustainable jet fuel considered for this study. Yellow blocks represent the ethanol-to-jet pathway, orange blocks represent the soybean hexane extraction pathway, red blocks represent the gasification Fischer-Tropsch pathway, and green blocks represent the algae hydrothermal liquefaction (HTL) pathway. Superscripted numbers identify references used for each of the process model blocks.

Four primary pathways were used in this study: ethanol-to-jet, hexane extraction, gasification Fischer-Tropsch, and hydrothermal liquefaction. In the ethanol-to-jet pathway, corn was cultivated, converted to ethanol through starch fermentation, and upgraded to SAF using an

ethanol-to-jet process. Full input and output values associated with the corn to SAF process can be seen in Figure C1. In the hexane extraction process, soybeans were cultivated, soy oil recovered through hexane extraction, and upgraded to SAF using soy oil hydroprocessing. Full input and output values associated with the soybean to SAF process can be seen in Figure C2. The gasification Fischer-Tropsch pathway encapsulated most of the feedstocks in this study. In this process, switchgrass, miscanthus, sorghum, poplar, or willow were cultivated, converted to biocrude through gasification Fischer-Tropsch, and upgraded to SAF using biocrude hydroprocessing. Full input and output values associated with the woody and herbaceous energy crop to SAF processes can be seen in Figure C3-C7. In the hydrothermal liquefaction process, microalgae was cultivated, converted to biocrude oil through hydrothermal liquefaction (HTL), and upgraded to SAF through HTL oil hydroprocessing. Full input and output values associated with the microalgae to SAF process can be seen in Figure C8. Additional details of each process model pathway block are provided in the following paragraphs.

Process model blocks were constructed to characterize the most generic case of a given process (e.g., corn grain cultivation in the Mid-West on established land). Where possible, we integrated geographic data to improve the characterizations of the cultivation pathway blocks, as agricultural systems are diverse based on geographic location.

We retrieved values for the corn grain (*Zea mays*) cultivation pathway block from the model presented in Beal et al. (2021), which in turn is based on the extension work presented by Plastina (2018) and Wright et al. (2015) [208–210]. To improve the resolution of the model, we integrated geographically specific data (e.g., yield) from the 2017 U.S. Census of Agriculture, we obtained land cost and rental frequencies from Bigelow et al. (2016), and we incorporated

data presented in Pelton et al. (2017) to characterize nitrogen fertilizer application rates [46,211,212].

The soybean (*Glycine max*) cultivation pathway block is also based on the model presented in Beal et al. (2021), which in turn is based on Chen et al. (2017) [208,213]. We brought in land cost and rental frequencies from Bigelow et al. (2016) and integrated geographically specific data from Pelton et al. (2017) and the 2017 U.S. Census of Agriculture to characterize fertilizer rates and estimated yields, respectively [46,211,212].

We retrieved values for the switchgrass (*Panicum virgatum L.*) cultivation pathway block from the extension work presented by Duffy (2008) [214]. The PRISM-ELM datasets present yield estimates for two ecotypes of switchgrass (upland- and lowland-switchgrass) [48]. We assumed that there is not a meaningful difference in management requirements or practices between the two ecotypes of switchgrass modeled in this work (i.e., upland- and lowland-switchgrass are assumed to require many of the same base inputs). However, geographically specific data is integrated where available to improve these characterizations. Because switchgrass is a perennial crop, we performed amortization of input and management requirements assuming a 10-year stand before replanting and reestablishment is required [214].

We integrated the information presented in the extension work by Hoque et al. (2014) for the miscanthus cultivation pathway block [215]. The species presented in this work is *Miscanthus x giganteus*. Because miscanthus is a perennial crop, we performed amortization of input and management requirements assuming a 20-year stand is achieved before replanting and reestablishment is required [215]. During establishment, we assumed that only 50% of the established yield is achieved in the second year [215]. The management and input requirements

are consistent with a winter-cover crop (e.g., oats). However, this winter-cover crop is outside of the system boundary, so we did not include these requirements in our analysis. Geographically specific yields were integrated from the PRISM-ELM dataset [48].

We constructed the sorghum (*Sorghum bicolor*) cultivation pathway block based on the information presented by Moore et al. (2020) [216]. We assumed a seeding rate of 4.1 kg ha^{-1} and a similar nutrient requirement profile to that of corn [216]. Because the whole biomass is applied to biofuel production applications, we assumed that the harvesting costs are similar to those of miscanthus and switchgrass, rather than corn grain. This assumption impacts the diesel use, labor, and capital cost rates for this pathway block. Geographically specific yields were integrated from the PRISM-ELM dataset [48].

We applied the extension work of Buchman et al. (2020) to build the poplar cultivation pathway block [217]. In this analysis, we assume a hybrid of cottonwood (*Populus deltoides*) and black poplar (*Populus nigra*), which produces a breed referred to as *P. x canadensis* [217]. We assumed that un-rooted cuttings are used for planting, in a 10 foot by 10 foot planting grid, and that the stand is harvested after 12 years [217]. Geographically specific yields were integrated from the PRISM-ELM dataset [48].

We integrated values presented in the extension work of Heavey and Volk (2015) to construct the willow (*Salix spp.)* cultivation pathway block [218]. We assumed coppice management techniques were applied for harvest cycles of three years, and that the stand could support seven harvest cycles before replanting and reestablishment was required [218]. We assumed that whips for planting were seven feet long, and eight-inch cuttings were used from

these whips for planting (1,295 whips ha^{-1}). Geographically specific yields were integrated from the PRISM-ELM dataset [48].

We based the algae cultivation pathway block on the biological growth model developed by Greene et al. (2021) and Quiroz et al. (2021) [189,190]. This work assumes an open-channel raceway pond facility design operated with paddlewheels, and a three-step biomass dewatering process (gravity settling, followed by hollow-fiber membrane filtration, followed by centrifugation). The characterized species is *Scenedesmus obliquus* (UTEX 393), and geographic yield estimates are obtained from this model [189,190].

The starch fermentation pathway block used to convert corn grain to ethanol was based off of the work presented in Smith et al. (2023), which in turn is based on the work of McAloon et al. (2000) [45,219]. The modeled conversion pathway block characterizes a dry mill starch fermentation process, with Dried Distiller's Grains produced as a coproduct. We assumed that each kilogram of corn grain biomass would produce 0.32 kg ethanol, 0.34 kg of Dried Distiller's Grains, and 0.34 kg of carbon dioxide [219].

The hexane extraction pathway block used to convert soybeans to soy oil is based off of the information presented in Beal et al. (2021), which in turn references the work of Cheng and Rosentrater (2017) [208,220]. The modeled process includes cracking, dehulling, conditioning and flaking as pre-treatment steps, heating/flaking as conditioning steps, and continuous countercurrent percolation of hexane as the solvent extraction step [220]. Soybean meal is the only coproduct of the system, and we assumed that each kilogram of soybean biomass would produce 0.22 kg soybean oil, and 0.77 kg of soybean meal [220].

The gasification and Fischer-Tropsch pathway block used to convert herbaceous and woody feedstocks into biocrude is based on the information presented in Beal et al. (2021), which in turn references the work of Swanson et al. (2010) [208,221]. We integrated values that correspond to the high-temperature scenario presented in the Swanson report, that utilizes a "pressurized, oxygen-blown, entrained-flow gasification" system, a cobalt catalyst, and an on-site air separation unit to meet gasifier requirements [221]. We assumed that each kilogram of inserted biomass will produce 0.15 kilograms of biocrude [221].

The hydrothermal liquefaction pathway block used to convert microalgae into algae oil is based off the information presented in Beal et al. (2021), which in turn references the work of Jiang et al. (2019) and Zhu et al. (2014) [208,222,223]. Because the input algae biomass is assumed to be at 20% weight after harvesting/dewatering (steps included in the biomass cultivation pathway block), we assumed that no pretreatment steps were required [189,190]. The modeled HTL system is a plug flow reactor with a shell-and-tube design operated at 350°C and 20 MPa. We assumed that each kilogram of dewatered algal biomass (20% weight) would produce 0.5 kg biocrude [223].

The ethanol-to-jet upgrading pathway block is based on the information presented in Beal et al. (2021), which in turn references the work of Tao et al. (2017) [208,224]. We incorporated values that corresponded to a tubular reactor, homogeneous catalyst system, and that the produced fuels may be used as a blendstock for jet fuel, diesel, and gasoline [224]. We assumed that each kilogram of processed biomass will produce 0.39 kilograms of jet fuel, 0.05 kilograms of diesel fuel, and 0.08 kilograms of gasoline [224].

The hydro-processing of biocrude upgrading pathway block was based on the information presented in Michaga et al. (2021) [225]. We integrated values into our model that corresponded to hydro-treating designed to minimize wax production and maximize jet fuel production. We assumed that the hydrogen requirement for the pathway block would be obtained from the input Fischer-Tropsch liquids, and that each kilogram of input biocrude would produce 0.59 kilograms of jet fuel, 0.31 kilograms of diesel fuel, and 0.1 kilograms of naphthalene [225].

The hydro-processing of oils (i.e., algae and soybean oil) pathway block was based on the information presented in Pearlson et al. (2013) [49]. This analysis presents yield values and input requirements associated with maximizing jet fuel production. We assumed that each kilogram of input oil could be converted to 0.49 kilograms of jet fuel, 0.04 kilograms of propane, 0.06 kilograms of LPG, 0.23 kilograms of diesel, and 0.07 kilograms of gasoline [49].

4.2.3 Techno-Economic Assessment

The techno-economic assessment performed in this work executed a 30-year, discounted cash flow rate-of-return analysis, which is standard practice in the TEA and biofuel research community [38,45]. The methodology determines the minimum price at which the final product (SAF and other liquid fuels) must be sold to attain a net present value of zero over a 30-year production lifespan considering an internal rate of return of 10%. Operational and Capital Expenditure (OPEX and CAPEX, respectively) are calculated with the input/output table produced by the process models. Process inputs (e.g., grid electricity) are multiplied by the location-specific unit cost values ($USD kWh^{-1}, in the case of electricity) for that flow. A comprehensive list of all unit cost values is available in the associated open data package [226]. As numerous fuels were generated, the TEA assessed the Minimum Fuel Selling Price (MSFP) per megajoule of produced liquid fuel (i.e., MJ of SAF, diesel, gasoline, propane, and naphtha),

and the fuel-specific selling prices presented in this work correspond to this $USD MJ^{-1} selling price scaled by the specific Higher Heating Value of each fuel. This approach was taken for two reasons. First, the real-world volatility of liquid fuel selling prices makes it difficult to assign a consistent coproduct value for each fuel, particularly given the timeframe of analysis. Potentially over- or under-estimating the value of any of the secondary transportation fuels (i.e., diesel, gasoline, propane, and naphtha) would cause a similar over- or under-estimation in the expected cost of SAF production. Furthermore, this analysis is focused on the cost of production rather than the anticipated retail price of the generated fuels. Second, it is more consistent with the selected functional unit and coproduct burden-attribution approach (i.e., energy allocation) of the LCA to determine the minimum cost in $USD MJ^{-1} of generated fuel. Relevant parameters used in this TEA include a federal tax rate of 21%, a state tax rate of 6.1%, an investor equity share of 40%, a loan interest rate of 8%, a loan term of 10 years, a maintenance rate equal to 3% of the OPEX, and an insurance rate equal to 1% of the OPEX. No construction period and no tax credits were assumed in this analysis, and a seven-year modified accelerated cost recovery system schedule was used to evaluate equipment depreciation.

Since existing cropland currently used for corn ethanol and soybean biodiesel cultivation was considered for all feedstocks, land rental prices associated with this cropland was also included. Land rental prices for cropland were paid based on county-level USDA data [165,227,228]. Specifically, county-level land rent prices were provided by USDA for both irrigated and non-irrigated land in each county. Accordingly, county-level rental prices were calculated as a weighted-average of irrigated and non-irrigated land rental prices based on the respective land area harvested for corn and soybeans in each county [211]. Productivity estimates for all other feedstocks were presumed unirrigated, so non-irrigated land rental prices were used

[48]. When county-level land rental price data was unavailable, state-level land rental prices were used. Both county- and state-level land rental prices were used from 2023 USDA data [227,228]. Non-cropland land types were assumed to have no land rental prices because they are not considered currently productive land.

Where possible, geographically diverse energy input costs were incorporated into the model. Mean values for the 2021 calendar year were used for all energy inputs. Costs from 2021 were used since they fell between the lower energy prices in 2020 caused by the Coronavirus pandemic and the higher prices of 2022 caused by the Russo-Ukrainian War. All energy inputs are dynamic in the real world, so the values input in the model were designed to represent the median values seen in the previous years. Historical state level electricity prices were used from the U.S. Energy Information Administration [229]. State level electricity prices were assigned uniformly to each county within the state.

Historical state-level industrial natural gas prices were used from the U.S. Energy Information Administration [230]. State level natural gas costs were assigned uniformly to each county within the state. Industrial prices were used because natural gas is primarily consumed in the conversion and upgrading phases of the process model.

Historical retail gasoline and diesel prices were used from the U.S. Energy Information Administration at the state level when available and the Petroleum Administration for Defense District (PADD) region level when state level data was unavailable [231]. PADD region values were uniformly assigned to each state within that region based on the definition of PADD regions from the U.S. Energy Information Administration [232]. State level values were then assigned uniformly to each county within the state. Retail prices were used since gasoline and

diesel are primarily consumed during the cultivation phase from farm equipment. PADD 5 prices excluding California were used for the PADD 5 region states as prices were provided for California separately.

Historical wholesale propane prices were used from the U.S. Energy Information Administration at the state level when available and the PADD region level when state level data was unavailable [233]. PADD region values were uniformly assigned to each state within that region based on the definition of PADD regions from the U.S. Energy Information Administration [232]. State level values were then assigned uniformly to each county within the state. No data was available for the PADD 5 region, so the U.S. mean prices was used for PADD 5 states and counties. Additionally, no data was available for the PADD 1A region, so the PADD 1 mean price was used for PADD 1A states and counties. Wholesale prices were used since propane is primarily consumed during the refining phase. Liquified petroleum gas prices were assumed to be equal to propane prices.

4.2.4 Life Cycle Analysis

The life cycle analysis (LCA) performed in this work applied a farm-to-wake system boundary and a functional unit of megajoules of transportation fuel produced. Greenhouse gas intensity (GHGi) was calculated in units of grams of $CO_{2\text{-eq}}$ per megajoule of fuel produced, as is common practice in biofuel LCAs [38,45]. Units of $gCO_{2\text{-eq}}$ are used as different gases (specifically, methane and nitrous oxide) possess different global warming potential profiles. Equivalence factors from the Intergovernmental Panel on Climate Change's Sixth Assessment Report were applied based on 100 year warming potentials (27 $gCO_{2\text{-eq}}$ gCH_4^{-1} and 273 $gCO_{2\text{-eq}}$ gN_2O^{-1}) [234]. The model incorporates life cycle inventory (LCI) data from EcoInvent 3.8 Database [166]. A comprehensive list of all unit LCI values is available in the associated open

data package [226]. Cutoff allocation methods were used for this LCI data and the TRACI v2.1 impact assessment methodology was utilized to obtain the unit emissions intensity of each substance [167]. To address the multiple products generated, the LCA applied an energy allocation approach, in which the GHGi of a product (e.g., liquid fuel) is calculated as the total emissions intensity of the system multiplied by the percentage of megajoules attributable to that product compared to the total megajoules produced by the system.

The handling of biogenic carbon uptake requires careful consideration in LCAs associated with bioenergy products [235]. Therefore, we used a -1/+1 biogenic carbon methodology in accordance with ISO 21930:2017 [236]. According to this methodology, when biogenic carbon enters the product system (biomass carbon uptake) it is assigned a life cycle inventory factor of -1 kg $CO_{2\text{-eq}}$ per kg CO_2. When biogenic carbon leaves the product system as CO_2 emissions (fuel combustion), it is assigned a life cycle inventory factor of +1 kg $CO_{2\text{-eq}}$ per kg CO_2.

Where possible, geographically diverse energy input emissions were incorporated into the model. Electricity emissions were used from United States EPA's Emissions & Generation Resource Integrated Database (eGRID) [146]. eGRID datasets are provided for annual values for 21 regions in the CONUS. eGRID regions were disaggregated to the county level based on which region the county resided. If a county covered multiple eGRID regions, a weighted average of GHGi was assigned on a weighted mean basis using land area in each region. Additional energy inputs included natural gas, gasoline, diesel, liquified petroleum gas, and propane. Constant emissions factors were assigned to each of these fuel sources based on the EcoInvent 3.8 Database and had values of 65.0 $gCO_2eq\ MJ^{-1}$ for natural gas, 82.7 $gCO_2eq\ MJ^{-1}$

for gasoline, 123.2 $gCO_2eq\ MJ^{-1}$ for diesel, and 86.2 $gCO_2eq\ MJ^{-1}$ for propane [166]. Emissions for liquified petroleum gas were assumed to be the same as those for propane.

When considering biofuels, a key component of the embodied emissions of the fuel is the land use change (LUC) impacts [56,237]. LUC is typically broken up into direct and indirect LUC effects [237,238]. Indirect land use change impacts are those associated with the unintended impacts of converting non-cropland to cropland, typically due to the displacement of another crop or industry. Indirect land use change impacts were excluded from this study due to their large and persistent uncertainties [191,239,240]. Additionally, the land types considered for crop cultivation were specifically selected to limit indirect LUC effects (See Section 4.2.1).

Direct land use change (dLUC) impacts are those associated with converting existing non-cropland into viable cropland for feedstock cultivation. This involves removing all the existing biomass on the land, disposing of that biomass, and preparing the land for the desired feedstock. Specifically, two categories of dLUC impacts were included in this study: above ground carbon change and soil carbon change.

The above ground carbon dLUC was estimated using the Spawn et al. (2020) database [205]. This database estimated the above ground biomass carbon density across the contiguous U.S. for the 2010 year using satellite imagery and advanced data analysis. As a conservative estimate for the study, it was assumed that all land that was being converted to cultivated cropland was clear-cut and burned. The emissions associated with burning this biomass and removing this biomass from the field was assumed to be allocated over the 30-year life of the biomass cultivation and processing facilities.

The soil carbon dLUC values were gathered from the Carbon Calculator for Land Use and Land Management Change from Biofuels Production (CCLUB) database within the GREET model produced by Argonne National Laboratory [241,242]. The CCLUB module inside of GREET estimates the soil carbon change (sequestration or removal) by planting different purpose-grown feedstocks on various land types throughout the U.S. at the county level. CCLUB includes corn, soybeans, switchgrass, miscanthus, poplar, and willow feedstocks in their database. The U.S. average values for tillage and 30% "residue or biomass removal rate" was used. Cropland values were used for cultivated cropland, "Pasture/hay/grasslands" values were used for both grasslands and shrublands, and "Forests" values were used for each of the forest lands considered. When a CCLUB value didn't exist for a county, the values associated with the representative agro-ecological zone (AEZ) value was used. CCLUB does not report soil dLUC values for sorghum or algae. Therefore, a constant soil carbon gain of 0.043 Mg C ha^{-1} yr^{-1} was used for all land types based on analysis by Kent et al [243]. who used DAYENT modeling methods similar to CCLUB. The Intergovernmental Panel on Climate Change methodology was for dLUC emissions associated with algae cultivation and was based on methods used by Handler et al. (2017) and Quiroz et al. (2023) [38,234,244].

4.2.5 Carbon Pricing

To estimate the price of carbon required to make sustainable aviation fuel economically competitive with petroleum jet fuel, Equation 3 was used:

$$Carbon\ Price = \frac{SAF\ Cost - Jet\ Fuel\ Cost}{Jet\ Fuel\ Emissions - SAF\ Emissions} \quad (3)$$

SAF Cost represents the minimum fuel selling price calculated for bioenergy based SAF as discussed in the previous paragraphs, *Jet Fuel Cost* represents the cost of petroleum jet fuel, *Jet Fuel Emissions* represents the well-to-wake emissions associated with petroleum jet fuel, and *SAF Emissions* represents the farm-to-wake emissions calculated for bioenergy based SAF as discussed in the previous paragraphs. Petroleum jet fuel emissions were assumed to be 84.8 $gCO_2\ MJ^{-1}$ as calculated by GREET for a the well-to-wake system boundary [241]. Petroleum jet fuel cost was assumed to be \$1.89 $gallon^{-1}$ which is the mean price for 2021 as reported by the U.S. Energy Information Administration [245]. Fuel prices from 2021 were used since they align with the stable jet fuel prices of 2019, and are in between the lower prices in 2020 caused by the Coronavirus pandemic and the higher prices of 2022 caused by the Russo-Ukrainian War. However, it should be noted that petroleum jet fuel prices are dynamic and breakeven carbon prices for SAF fuels are impacted by that. Higher petroleum jet prices result in lower breakeven carbon prices for bio-jet fuels and vice versa.

4.2.6 Future Biorefinery Location Assumptions

Due to the uncertainty of future biorefinery locations needed to satisfy SAF demands, multiple transportation scenarios were evaluated. In both scenarios, the biomass was assumed to be transported from the farm it was cultivated to the county center of the county in which the farm resided. The transportation distance to the county center was assumed to be the mean distance from transporting biomass to the county center from any location within the county (calculated as ¼ the mean width and length of the county).

In the primary scenario, biorefineries were placed at the agricultural district center and all biomass within the agricultural district fed to that biorefinery [246]. Therefore, biomass was

transported to the county center then transported to the agricultural district center (as defined by the USDA) for all counties within the agricultural district. The biomass was processed and converted to SAF at the agricultural distance center and then transported to the nearest airport with one million passenger enplanements annually [247].

To test the sensitivity to this assumption, an alternate scenario assumed biorefineries were placed at county centers. Therefore, the biomass was transported to the county center, processed and converted into sustainable aviation fuel at the county center, and then transported to the nearest airport with one million passenger enplanements annually [247].

It was assumed that all biomass and fuel was transported via truck to the end destination due to the lack of railway connections between every county and associated airports. Truck transportation costs were assumed to be $0.17 per kilometer-tonne and had associated emissions of 139 $gCO_{2\text{-eq}}$ per kilometer-tonne [166,248]. County-specific transportation distances and associated destination airports are provided in the associated open data package [226]. For the results presented in the main article and Appendix C, the agricultural district center biorefinery assumptions were used. Additional results including those for the county center biorefinery scenario are provided in the associated open data package [226]. The impact of the biorefinery location assumptions on minimum fuel selling price and fuel emissions is discussed in Appendix C.

4.2.7 Optimization

This section outlines the optimization methods employed in our study to evaluate the deployment of purpose-grown bioenergy feedstocks across the U.S. Our approach leveraged both population selection and genetic algorithms to derive the most efficient solutions for achieving

the SAF Grand Challenge targets. Given the vast scale of our analysis (nine feedstocks across seven land types and 3,108 counties), a traditional linear optimization algorithm proved computationally prohibitive thus the evolutionary approach was used. The genetic evolutionary algorithm was implemented in Python using the Distributed Evolutionary Algorithms in Python (DEAP) framework [249]. Individual optimization decision variables were each unique feedstock, land type, and county combination. Therefore, if the optimization selected one of these combinations, all feasible land in that county of that land type was assumed to be converted to that feedstock for SAF production as identified in the GIS model. In total, four optimum solutions were evaluated for each SAF quota or land requirement scenario. These included minimum fuel selling price, minimum fuel emissions, minimum breakeven carbon price, and minimum land requirements for feedstock cultivation.

To identify seed populations for the genetic algorithm, we aggregated all data points produced by the process modeling and organized them by the parameter of interest (i.e. fuel selling price, fuel emissions, fuel carbon price, or land requirements), ranging from minimum to maximum values. This preliminary sorting facilitated the identification of the most promising variables to use as seed populations for the subsequent genetic algorithm. The minimum values for each county across different land types were selected until the desired SAF quota or land use was achieved. In cases where multiple favorable values emerged within the same county and land type, they were earmarked for further evaluation by the genetic algorithm to balance potential trade-offs between optimal values and higher production quantities.

Due to the large uncertainty in which feedstocks will satisfy SAF demand in the future, a variety of SAF quotas were evaluated for optimization. Based on current biomass availability quantities presented in the SAF Grand Challenge Roadmap and biomass-to-jet conversion factors

from literature, we estimate 36.6 billion gallons of SAF could be produced with the feedstocks outlined in the SAF Grand Challenge Roadmap (Table C89). Of that 36.6 billion, 28.8 billion could be produced from seed oil crops, corn grain, woody energy crops, herbaceous energy crops, and algae. Intermediate seed oil crops (Camelina, Pennycress, Carinata, etc.) were excluded from this study due to lack of geospatially resolved yield data, but studies estimate these crops could produce 4.0 billion gallons of fuel annually [250,251]. Therefore, feedstocks included in this study could be expected to make up approximately 25 billion gallons of SAF annually and optimization results in the main article reflect this assumption. Additional optimization quotas include 3 billion (2035 SAF Grand Challenge Target), 5 billion, 10 billion, 15 billion, 20 billion, 25 billion, 30 billion, and 35 billion gallons (2050 SAF Grand Challenge Target) annually. Additional optimization was run considering land limitations based on historical National Land Cover Database land conversions from noncrop land to cultivated cropland [195]. These land-limited scenarios considered three situations: First, land was limited to current cropland dedicated to bioenergy crops, defined as land used for corn ethanol and soybean biodiesel [187]. Second, land was limited to the mean historical annual conversion from noncrop land to cultivated cropland, as reported by the National Land Cover Database, and this conversion was assumed to occur annually over the next 30 years, with starting land availability in the first year assumed to be current cropland dedicated to bioenergy crops [187,195]. Annual conversion factors were applied on a county-by-county basis. Third, land was limited to the maximum historical annual conversion from non-crop land to cultivated cropland, also reported by the National Land Cover Database, and this conversion was similarly assumed to occur annually over the next 30 years, with the same assumptions for starting land availability and

county-by-county annual conversion factors [187,195]. County-level annual land conversion quantities are available in the associated open data package [226].

4.2.8 Agent Based Modeling

In agent-based modeling (ABM), a system is modeled as a collection of autonomous decision-making entities called agents and the relationships between them [252]. An ABM was developed to understand the bioenergy feedstock adoption by farms to achieve U.S. SAF targets.

Based on the results gathered from the process modeling, a county-level scale analysis was used for ABM. While each county contains multiple farms in the real world, the total cropland and marginal land was used to generate approximate yields per crop per county per land cover type. Therefore, each county in the U.S. was assumed to represent a "farmer" who could decide which crop(s) to plant on their given land type. To make their decisions, both the farmer and the crop have weighting factors for each decision variable. The weighting factors are multiplied together and normalized to find the percent of crops each farmer will plant. Literature reviews have identified familiarity, profitability, and environmental impact as the key decision-making factors when determining which crops farmers plant [253]. Therefore, those are the weighting factors were used for farmers and feedstocks in the ABM. An example of farmer decision making is shown in Figure 14.

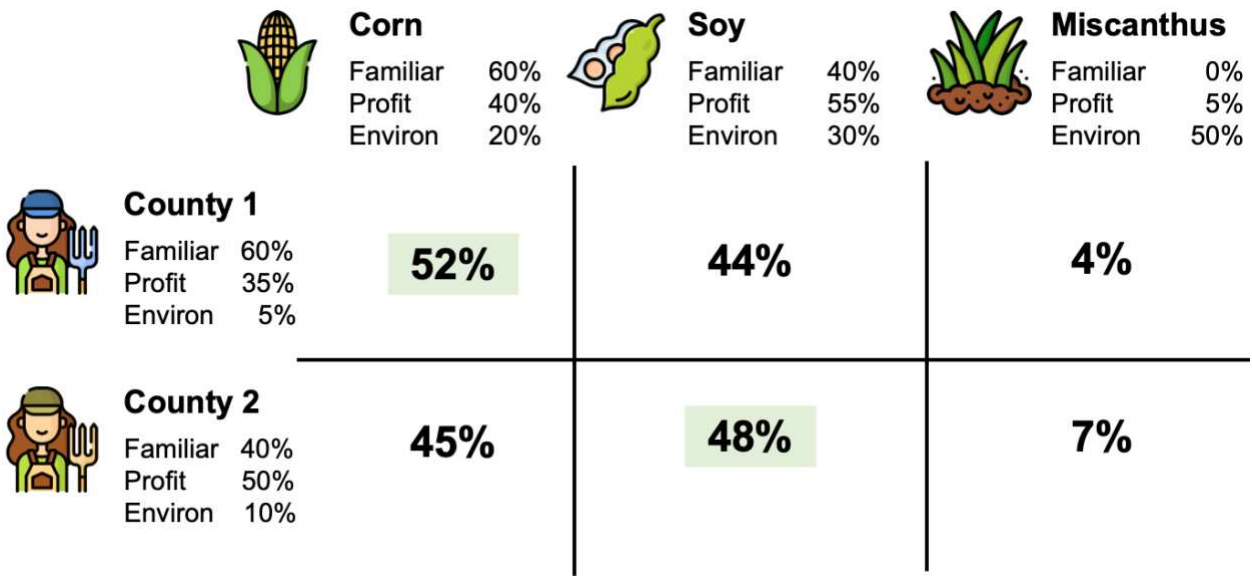

Figure 14. Example of farmer decision making in the agent-based model

Each of the three crop weighting factors will be calculated in different ways. Profitability weighting factors was based on the biomass yield per area. The crop with the highest yield was given a weighting factor of 1 and the other crops was given a weighting factor less than 1 based on their yield compared to the highest yield crop. For example, if we assume the farmer can choose to plant corn, soy, or miscanthus and they have biomass yields of 70 kg/ha, 80 kg/ha, and 100 kg/ha, respectively, then these crops will have profitability weighting factors of 0.7, 0.8, and 1.0, respectively. Environmental impact weighting factors will be calculated in a similar way to profitability weighting factors, but instead of biomass yield, greenhouse gas emissions was used and the lowest value will have the highest weighting factor. For example, if the farmer can plant corn, soy, and miscanthus which have GWP of 150 $gCO_{2\text{-}eq}$/kg-biomass, 125 $gCO_{2\text{-}eq}$/kg-biomass, and 100 $gCO_{2\text{-}eq}$/kg-biomass, respectively, then the crops will have weighting factors of 0.67, 0.8, and 1.0.

Lastly, the familiarity weighting factors were determined by the crops planted in surrounding counties in the previous year. Multiple weighting methods have been incorporated

to evaluate the relationships between farms. Typically, this familiarity weighting factor is taken as the average of neighboring farmers planted crops in the previous year. The number of farmers that impact familiarity is usually taken to be those farmers within a specified "radius of influence" from the farm. As such, this research includes a familiarity factor based on the average of farmers within a specified radius of influence to the farm. Additionally, other studies have assessed a familiarity score using the average of all farmers in the study or the weighted average of all the farmers in study based on their distance to the farm. Both methods have also been implemented into the ABM for comparison purposes. To determine the weighted average of each farmer, the inverse square law was used to determine influence based on the distance between the geographic centers of each county. A comparison between the weighted average of all farmers (inverse square) and radius of influence can be seen in Figure 15 for Larimer County, Colorado. Additionally, these two methods could be combined such that only counties within a 100-mile radius have an impact, but their weighting is based on the inverse square of their distance to the county of influence.

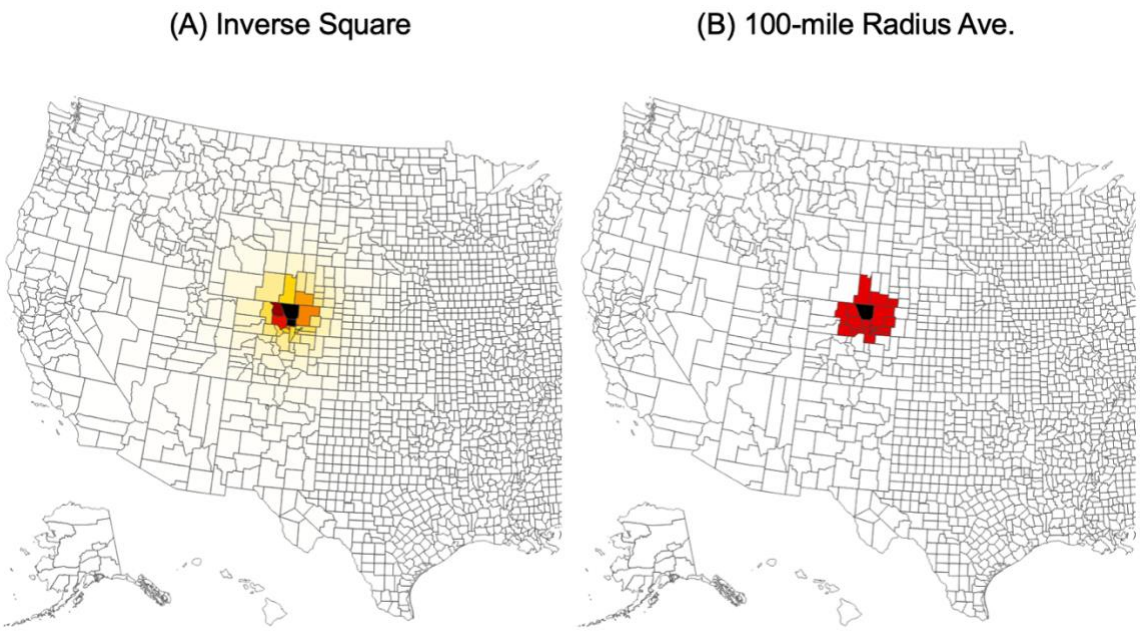

Figure 15. Example of familiarity weighting for Larimer County, CO based on the surrounding counties. Darker counties have a larger influence on the familiarity of crops. (A) shows weighting using an inverse square relationship and (B) uses an average of the surrounding counties withing a 100-mile radius.

In addition to crop weighting factors, farmer weighting factors also needed to be decided. Unfortunately, the best method of farmer weighting factor calculation is unclear. Literature reviews identified that most studies which use an ABM for farmer/crop planting either present the farmer weighting factors as a result of their analysis or use predefined weighting factors to explore different scenarios [253,254]. As this study is designed to approximate real world scenarios, weighting factors need to be designated at the front end that can be adjusted to simulate the impact of policy changes and incentives. As such, a brute force analysis of the three weighting factors was performed to evaluate which weighting factors resulted in the lowest error compared to real world results Figure 16. For this analysis, prior USDA crop census data was used. Since the ABM needs the planted area per crop for the prior year to assign familiarity values, consecutive USDA crop census datasets were used. The earlier dataset was used as an input to the ABM and the ABM's predicted results were compared to the real-world planted area

by crop in the latter USDA dataset. Error was calculated by the absolute value difference between the predicted crop plantings compared to the real-world crop plantings given by the USDA crop census. For example, the USDA crop census is performed in years ending in "2" and "7". Therefore, the last two publish census are 2012 and 2017. For the analysis shown in Figure 16, the area planted by crop was input to the ABM from the 2012 census data. The ABM was then run using updated crop profitability, familiarity, and environmental impact and the predicted crop plantings were calculated. These predicted values were compared to the 2017 census data and the error was calculated between them. Each combination of weighting factors was simulated 1,000 times to generate a representative sample of results.

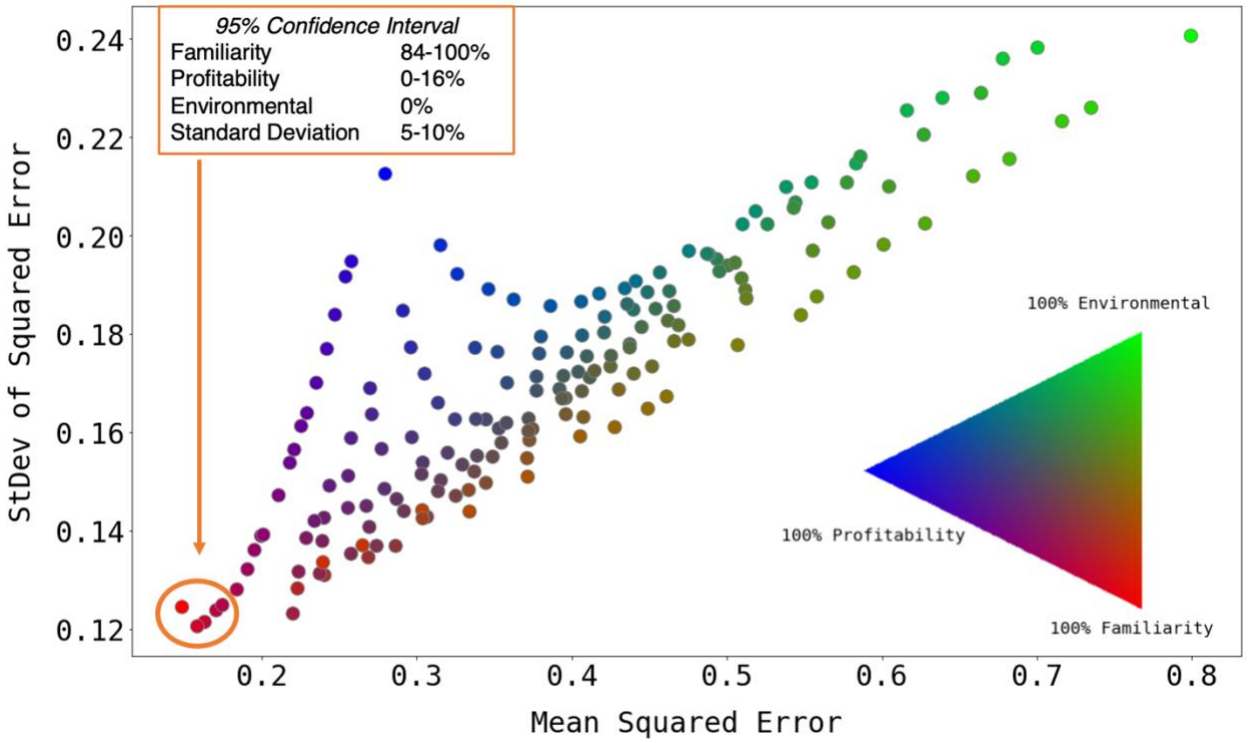

Figure 16. Analysis of the best farmer weighting factors to use to predict future crop cycles. Error was calculated by the absolute value difference between the predicted crop plantings compared to the real-world crop plantings for USDA crop census years. Desired results have low mean squared error and low standard deviation of squared error. Each combination of weighting factors was simulated 1,000 times to generate a representative sample of results. Farmer weighting factors of 100% environmental impact, 100% profitability, and 100% familiarity are shown by green, blue, and red dots respectivly. Combinations of weighting factors are shown by the gradient between the colors.

Results show that farmer weighting factors high in familiarity were the best predictor of future crop plantings. Alternatively, the environmental impact weighting factor was found to have the highest error and the worst prediction of future crop plantings. Based on the results received, it was found that farmer weights for familiarity of 84-100%, profitability of 0-16%, and environmental impact of 0% were the best predictor of real-world crop planting behavior using a 95% confidence interval. Additionally, it was found that a low standard deviation was also desired so a standard deviation of 5-10% will be used in this study. For the results presented here, farmer weighting factors were used for 95% familiarity, 5% profitability, 0% environmental impact, and 5% standard deviation. Farmer weighting factors were randomly assigned based on these mean and standard deviation values.

For each ABM analysis, a 30-year simulation was performed. It was assumed that the current cropland dedicated to bioenergy cultivation was initial cultivation land available for SAF production under the assumption that electric vehicles are reducing the need for corn ethanol and soybean biodiesel [187,194]. To approximate realistic land conversion scenarios, cropland increase limits were placed on each county based on historically available data from the National Land Cover Database [195]. Options included mean historical annual land conversion and maximum annual land conversion, similar to what was used for the optimization results discussed in the previous section.

4.3 Results

The results are presented in two main sections. The first provides aggregated values for the total SAF production potential for each of the bioenergy feedstocks on varying land types throughout the U.S. Also presented in this section are the median minimum fuel selling price and the median fuel emissions from each feedstock on each different land classification based on the

total quantity of SAF production potential. The second section provides the optimized deployment of bioenergy feedstocks for meeting 25 billion gallons of SAF across the U.S. in terms of minimum fuel price, minimum fuel emissions, minimum carbon price, and minimum land area requirement.

4.3.1 Aggregated Results

The aggregated results for SAF production potential, minimum fuel selling price, and environmental impact are presented in Figure 17. These results are based on the assumption that 100% of the potential land is transitioned to purpose grown bioenergy feedstocks with a primary end product of SAF. As can be seen in Figure 17a, algae has the highest fuel potential of all the bioenergy feedstocks (627 billion gallons annually) due to its very high areal productivity compared to the terrestrial crops. When comparing the terrestrial crops, miscanthus and sorghum exhibit the highest production potential across the U.S. (66 and 76 billion gallons, respectively) due to their high yields and the amount of land that they can be grown on. Poplar and willow also perform well (76 and 69 billion gallons, respectively), but primarily on forested regions of the U.S. It is important to note, the technology readiness level of the feedstocks considered are different. Algae has not been deployed commercially for fuels while the other feedstocks have been demonstrated at pilot-scale, if not commercial scale.

The median minimum fuel selling price in dollars per gallon of SAF for the contiguous U.S., based on purpose-grown bioenergy feedstock and land cover type is shown in Figure 17b. Minimum fuel selling price is defined as the breakeven selling price required to recoup production costs including a return capital investment. These results assume that 100% of the land that can be converted is converted to bioenergy feedstocks. The median per gallon value

was found for each feedstock considering all SAF produced with the error bars representing the range between the 25th and 75th percentiles. The results show that algae has the highest SAF minimum fuel selling prices of the feedstocks evaluated ($9.32 gal^{-1} to $16.42 gal^{-1}). These high fuel prices are driven by the large capital costs associated with building an open raceway pond algae facility. The other feedstocks do not require substantial capital investments, so algae-derived SAF is more expensive. On the other end, miscanthus ($3.21 gal^{-1} to $4.15 gal^{-1}) and sorghum ($3.26 gal^{-1} to $3.92 gal^{-1}) have the lowest median minimum fuel selling prices of the feedstocks evaluated. These feedstocks have low fuel prices because of their higher feedstock yields than other terrestrial crops. The remaining feedstocks (upland and lowland switchgrass, poplar, and willow) have similar minimum fuel selling prices (all range between $3.64 gal^{-1} to $6.76 gal^{-1}).

The median environmental impact, in grams of carbon dioxide equivalent ($CO_{2\text{-eq}}$) emissions per megajoule of fuel, across the evaluated feedstocks and land classifications is presented in Figure 17c. These results incorporate both above ground and soil direct land use change effects. As the figure shows, direct land use change emissions have a dramatic impact on the overall results. Many conclusions can be drawn from these results. First, converting existing forest land to grow purpose-grown feedstocks for SAF is a non-starter due to the high direct land use change emissions caused by the removal of existing biomass and soil carbon disruption. In almost every case, cutting down forests to grow purpose-grown bioenergy feedstocks results in higher net emissions compared to petroleum-based jet fuel (84.8 $gCO_{2\text{-eq}}$ MJ^{-1}) [241]. Additionally, SAF derived from algae has high emissions due to energy consumption during algae cultivation (63.5 $gCO_{2\text{-eq}}$ MJ^{-1} to 72.9 $gCO_{2\text{-eq}}$ MJ^{-1} excluding forested land). In most cases, SAF derived from algae only has an emissions reduction of ~20% when compared to petroleum-

based aviation fuel. Therefore, the SAF Grand Challenge's requirement of a 50% emissions reduction would not be met by algae. Algae is also a nascent technology and advancements in productivity or optimization of cultivation systems would improve results. Similar to the economic results, miscanthus (1.3 $gCO_{2\text{-}eq}$ MJ^{-1} to 31.1 $gCO_{2\text{-}eq}$ MJ^{-1}) and sorghum (28.7 $gCO_{2\text{-}eq}$ MJ^{-1} to 35.4 $gCO_{2\text{-}eq}$ MJ^{-1}) perform well on non-forested land in terms of emissions reduction. Miscanthus performs well due to its large soil carbon increase on cultivated cropland, grassland, and shrubland. Miscanthus has large root systems compared to other bioenergy feedstocks which results in adding carbon back to the soil, especially in cultivated cropland soil which has been depleted by conventional farming practices [47]. SAF derived from sorghum also has low carbon emissions driven by its high productivities in the southeastern U.S. Both feedstocks have emission reductions greater than the 50% requirement from the SAF Grand Challenge when grown on non-forested land.

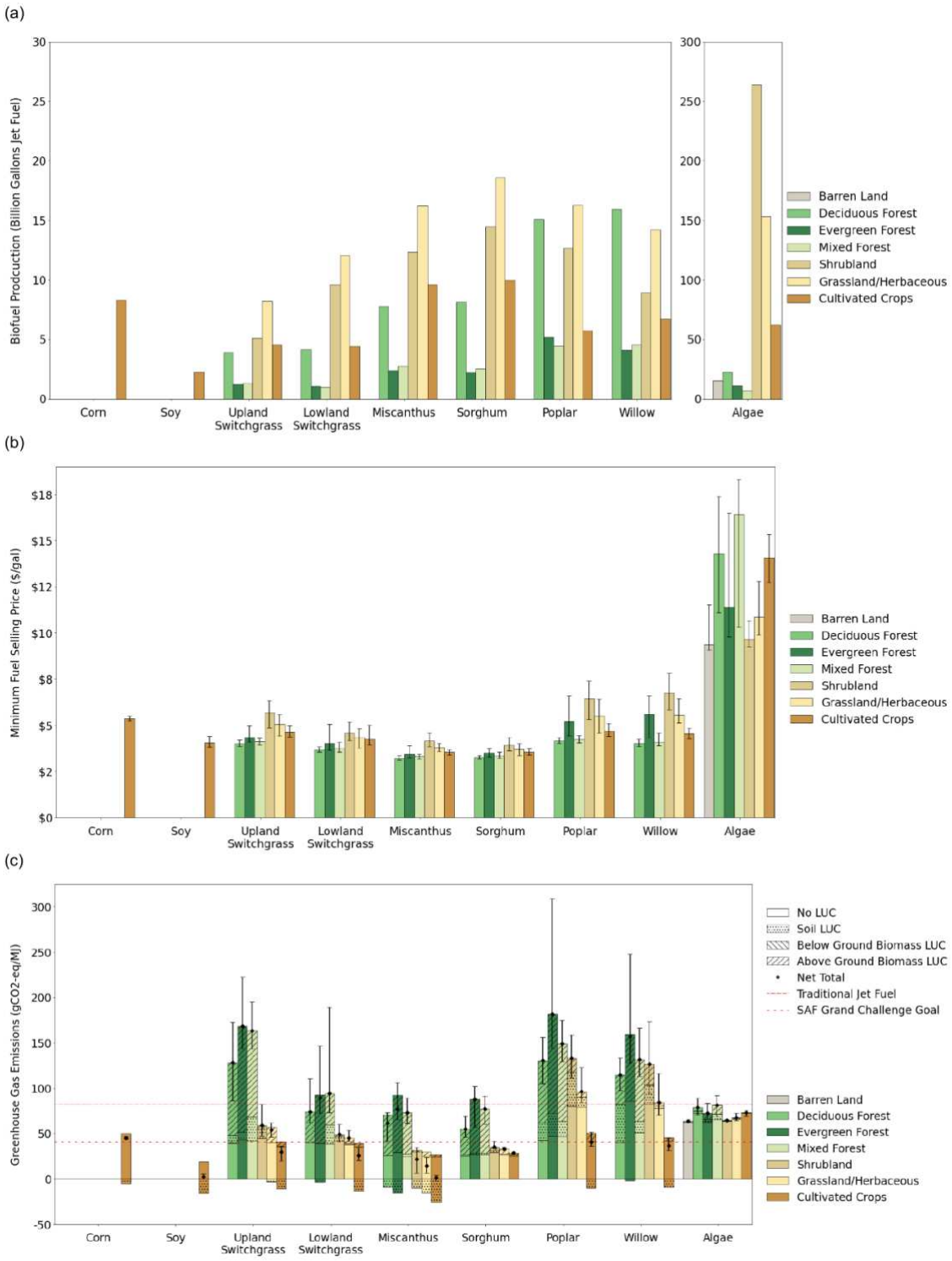

Figure 17. Aggregated results for sustainable aviation fuel (SAF) metrics for the contiguous U.S. based on bioenergy feedstock and land cover type. Subfigures show (a) total SAF production potential in billions of gallons fuel (note the axis scale of Algae is 10X that of the other bioenergy crops due to increased productivity per land area), (b) median minimum fuel selling price in dollars per gallon of SAF, and (c) median environmental impact in grams of CO_2 equivalent emissions per megajoule of SAF. Error bars in subplots (b) and (c) represent the range between the 25th and 75th percentiles for fuel cost/emissions when all possible fuel produced is considered.

4.3.2 Optimal Bioenergy Feedstock Deployment across the United States.

The optimized deployment of purpose grown feedstocks across the U.S. to meet a SAF quota of 25 billion gallons by 2050 is presented in Figure 18. This figure also shows the additional fuel products that are produced in achieving the 25 billion gallons along with the mean fuel selling price, the mean fuel emissions, the mean carbon price of SAF compared to petroleum jet fuel prices, and the total percent of land required to deploy the optimum feedstock(s) across the contiguous U.S.

The optimum deployment of feedstocks when minimizing for SAF price is presented in Figure 18. We find soy makes up 1% of total SAF production and is grown in the corn belt on cropland currently used for bioenergy production and will not impact food supply [187]. Sorghum makes up 49% of SAF production and is grown in the southeast due to its high aerial productivity in that region. Lastly, we see Miscanthus makes up 50% of SAF production and is grown in the northeast (Table C1). Both miscanthus and sorghum are grown on forested land because this land has high productivities compared to other land types and reduces fuel selling price. In total, 47% of SAF production comes from feedstocks grown on forested land, 26% on grassland, 17% on cultivated cropland, and 10% on shrubland (Table C2). Overall, this scenario results in a mean SAF price of \$3.24 gallon^{-1}, mean fuel emissions of 47 $gCO_{2\text{-}eq}$ MJ^{-1}, mean carbon price compared to petroleum jet fuel of \$273 $tCO_{2\text{-}eq}^{-1}$ and would require 5.3% of total contiguous U.S. land for feedstock cultivation. The mean fuel emissions found for this scenario (47 $gCO_{2\text{-}eq}$ MJ^{-1}) would not meet the SAF Grand Challenge targets (50% fuel emissions

reduction) as it is only a 44% reduction from petroleum jet fuel emissions (84.8 $gCO_{2\text{-}eq}$ MJ^{-1}) due to forest land cultivation.

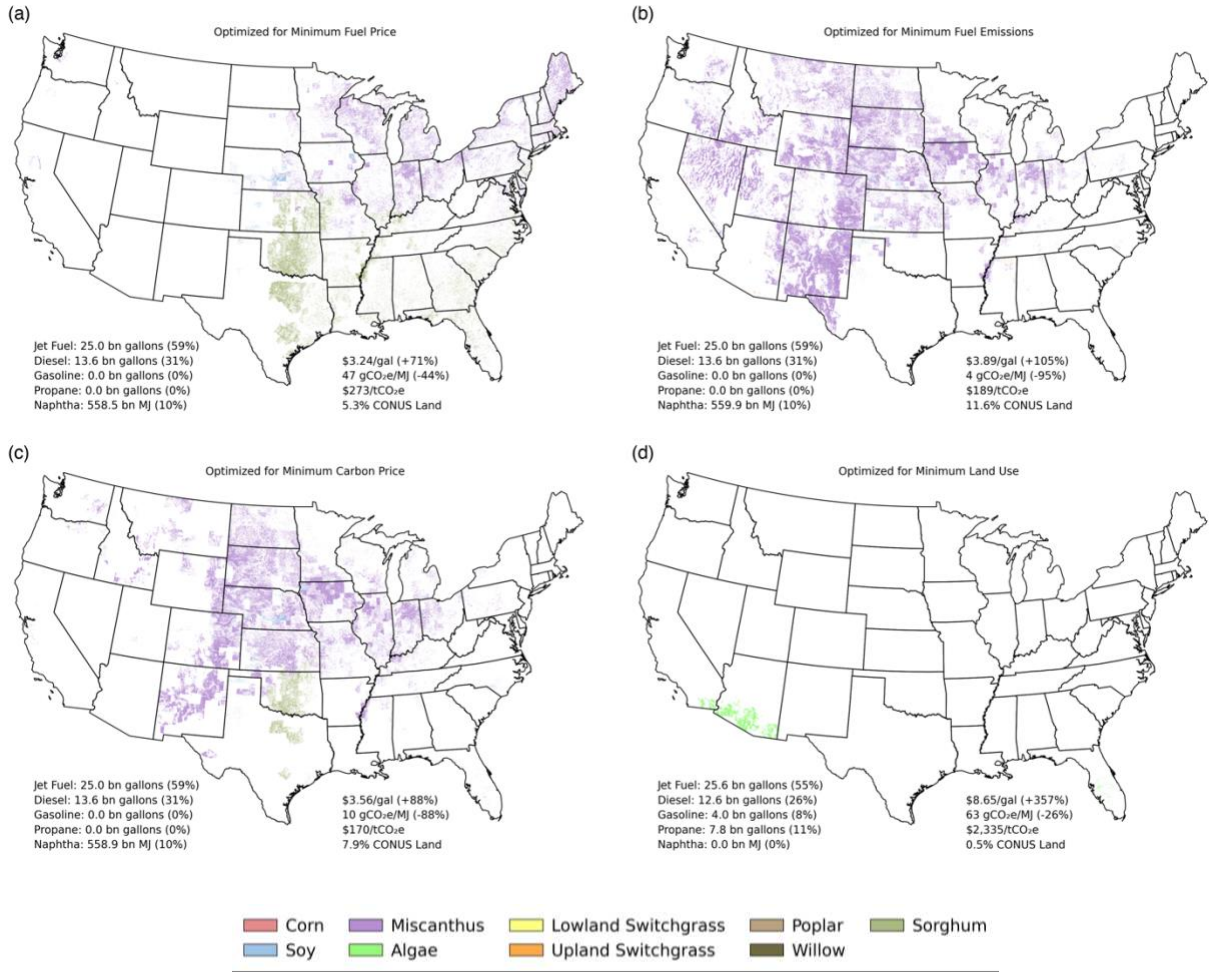

Figure 18. Multi-objective optimization maps of the optimal geographic feedstock deployment to meet 25 billion gallons of annual SAF production while minimizing fuel price (a), fuel emissions (b), breakeven carbon price (c), and land area (d). Percentages in parentheses for the fuel products represent the total percent of megajoules produced for that fuel type as a percentage of total megajoules of fuel produced by the feedstocks. Percentages in parentheses for the mean fuel selling price and mean fuel emissions represent the percent cost increase and percent emissions reduction, respectively, compared to petroleum jet fuel.

The optimized feedstock deployment to produce 25 billion gallons of SAF while minimizing for fuel emissions is presented in Figure 18b. This result has much less diversity in terms of feedstocks deployed and is dominated by miscanthus across the western U.S. The optimization selects miscanthus in the western U.S. due to the increased land availability of

grasslands and shrublands where miscanthus derived SAF has low emissions due to its soil carbon sequestration. Miscanthus makes up 99.5% of SAF production in this scenario with an additional 99 million gallons derived from soy and 14 thousand gallons from upland switchgrass (Table C3). The feedstocks are cultivated on grassland (40%), cultivated cropland (38%), and shrubland (22%) (Table C4). Overall, this scenario results in a mean SAF price of \$3.89 gallon^{-1}, mean fuel emissions of 4 $gCO_{2\text{-}eq}$ MJ^{-1}, mean carbon price compared to petroleum jet fuel of \$189 $tCO_{2\text{-}eq}^{-1}$ and would require 11.6% of total contiguous U.S. land for feedstock cultivation.

The optimized results for producing 25 billion gallons of SAF while minimizing carbon price compared to petroleum jet fuel is presented in Figure 18c. Carbon price in this scenario is defined as the cost of carbon required to make SAF economically competitive with petroleum jet fuel. This scenario is used to highlight the tradeoffs between the minimal fuel cost (Figure 18a) and minimal fuel emissions (Figure 18b) scenario when trying to minimize both fuel prices and emissions. The minimum carbon price scenario features soy and sorghum from the minimum cost scenario and miscanthus from the minimum emissions scenario. In total, 88% of SAF is produced from miscanthus, 11% from sorghum, and 1% from soy (Table C5). Additionally, 45% of SAF is from feedstocks grown on grassland, 38% cultivated cropland, 8% shrubland, 8% deciduous forest, and 1% mixed forest (Table C6). Overall, this scenario results in a mean SAF price of \$3.56 gallon^{-1}, mean fuel emissions of 10 $gCO_{2\text{-}eq}$ MJ^{-1}, mean carbon price compared to petroleum jet fuel of \$170 $tCO_{2\text{-}eq}^{-1}$, and would require 7.9% of total contiguous U.S. land for feedstock cultivation.

The optimum feedstock deployment when minimizing land for feedstock cultivation is presented in Figure 18d. Due to its high productivity, algae is the only feedstock deployed in this scenario (Table C7). Algae is deployed in southwestern U.S. (Arizona and California) and

Florida where algae's productivity is the highest. Due to its very high productivity, only 0.5% of total contiguous U.S. land is required to meet the 25-billion-gallon requirement (65% shrubland, 18% grassland, 15% barren land, and 2% evergreen forest [Table C8]). Even though the land requirement is low, this comes at the cost of high emissions (63 $gCO_{2\text{-}eq}$ MJ^{-1}) and high fuel prices (\$8.65 $gallon^{-1}$). In this scenario, fuel emissions are only 26% lower than petroleum jet fuel and do not meet the SAF Grand Challenge targets. Carbon price (\$2,335 $tCO_{2\text{-}eq}^{-1}$) is also substantially greater than existing carbon reduction technologies today, such as biomass burial or direct air carbon capture, and would not be feasible from a carbon reduction perspective.

Due to uncertainty in the portion of future SAF demand which will be satisfied by purpose grown feedstocks, additional results are presented in the Supplementary Information for annual SAF quotas from purpose-grown bioenergy feedstocks ranging between 3 billion gallons and 35 billion gallons (Figure C9-C15 and Table C9-C64) and land limitation scenarios based on historical cultivated cropland conversion rates (Figure C16-C18 and Table C65-C88).

4.3.3 Agent Based Modeling Results

The agent-based modeling results are presented in Figure 19. This figure shows the total deployment of bioenergy-feedstocks for SAF production after 30 years using (a) mean land conversion factors, (b) maximum land conversion factors, (c) three times the maximum land conversion factors, and (d) maximum land conversion factors and 50% cheaper algae based SAF.

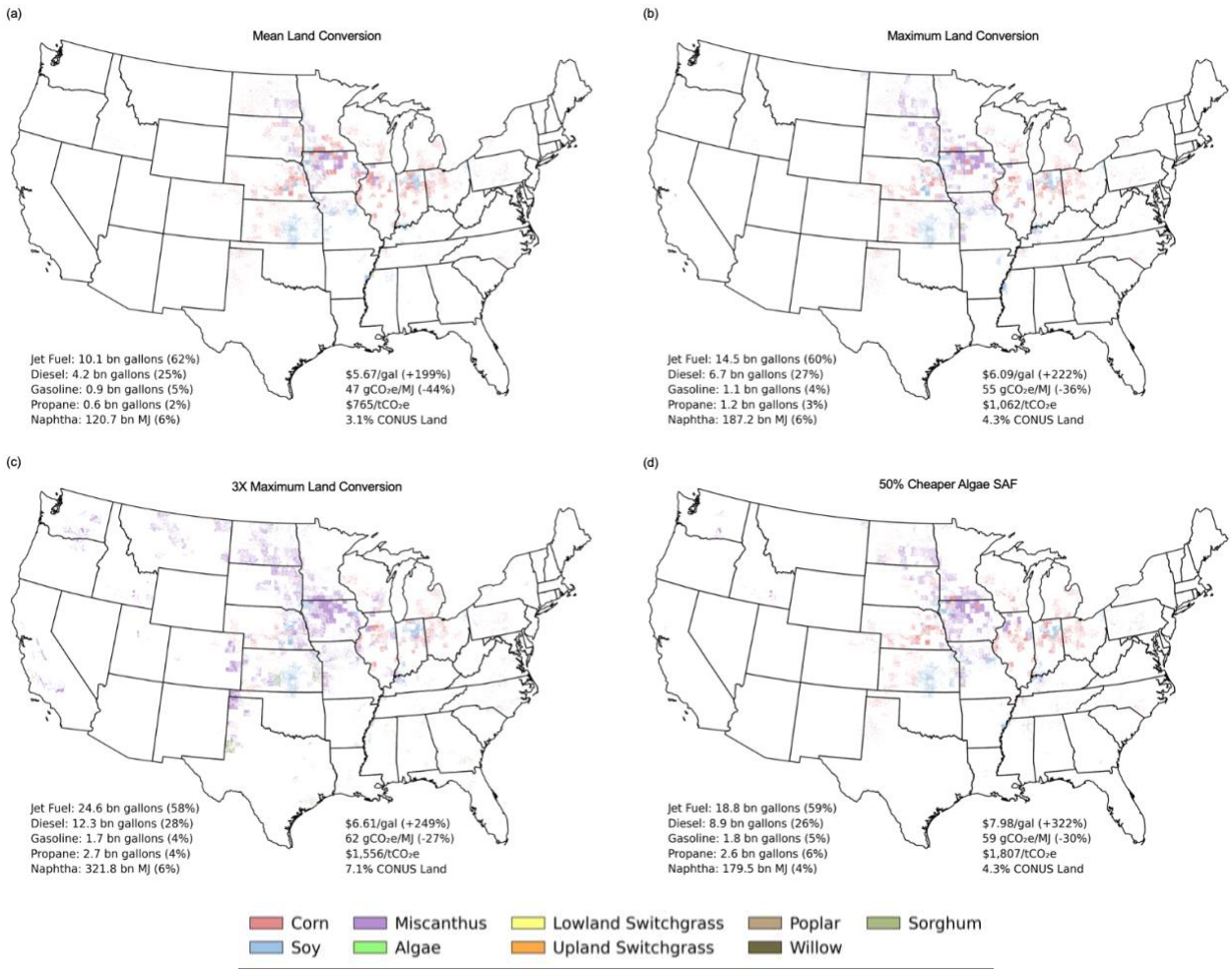

Figure 19. Agent-based modeling results

The agent-based modeling results show that the land conversion required to meet SAF targets will be challenging. In both the mean and max land conversion scenarios (Figure 19a and Figure 19b, respectively) will not meet the 25-billion gallon SAF target needed from purpose grown bioenergy feedstocks. The mean land conversion scenario will only achieve 10 billion gallons in annual SAF production potential after 30 years and the max land conversion scenario will only achieve 14.5 billion gallons annually. To get close to the 25-billion-gallon target, three times the historical maximum land conversion from non-cropland to cropland would be required every year over the next 30 years (Figure 19c). Due to its low commercial development, an alternative scenario would be the maximum land conversion factors with algae-based SAF costs

were reduced by 50% (Figure 19d). However, even with the large reduction in algae-based SAF pricing, the 25-billion-gallon SAF target is not achieved.

These results illustrate the difficulty in expanding purpose-grown bioenergy feedstock cultivation in the U.S. to meet SAF targets. This research finds that farmers typically plant crops which they are familiar with and are similar to those around them, which leads to slow deployment of unproven feedstock types. If purpose-grown feedstocks are going to play a large role in achieving SAF targets, additionally education or incentives will be required.

4.4 Discussion

This is the first national scale study evaluating a variety of purpose-grown feedstocks simultaneously across the U.S. for SAF production. The findings highlight the trade-offs required to utilize these feedstocks to meet SAF Grand Challenge targets which include sacrificing land to save on fuel costs and fuel emissions. Any scenario which doesn't prioritize land area, suffers from a large increase in land use for biomass cultivation. Current U.S. land use for crop cultivation is 16.2% of CONUS land [195]. Therefore, existing cultivated land would need to increase by 35.2% in the minimum carbon price scenario or 58.0% in the minimum fuel emissions scenario to meet SAF Grand Challenge targets (minimum fuel price scenario doesn't meet emissions targets) assuming that 25 billion gallons of the 35 billion gallon goal will be met by purpose grown bioenergy feedstocks.

These large land requirements could be a significant inhibitor to allowing purpose-grown feedstocks to be used for sustainable aviation fuel on a large scale in the future. To achieve SAF Grand Challenge targets by 2050, an unprecedented land use change from non-cropland to cropland will be required. Based on historical National Land Cover Database data, if the

maximum annual historical land type change from non-cropland to cropland seen in the prior 20 years was observed every year over the next 30 years only 5.0% of CONUS land would be used for biomass cultivation for SAF including the 2.2% of CONUS land currently used for corn ethanol and soybean biodiesel [187,195]. In the optimized minimum fuel price scenario, results show 23.8 billion gallons of SAF could be produced annually on 5.0% of CONUS land (Figure C18 and Table C81-C88). Similarly in the optimized minimum fuel emissions scenario, 9.5 billion gallons of SAF could be produced annually on 5.0% of CONUS land. The remainder of the required 35 billion gallons would need to be provided by other pathways such as agricultural residues, waste streams, or power-to-jet liquids. By our estimates, agricultural residues and waste streams can provide approximately 8 billion gallons annually (Table C89). Therefore, power-to-jet liquids could be necessary to meet SAF Grand Challenge targets, but are expensive and require significant clean energy scaling to meet aviation sector demands [255]. While the U.S. Department of Energy's Billion Ton Study found the U.S. has the potential to produce enough biomass for 60 billion gallons of annual fuel, the results of this study show that providing even 25 billion gallons of from purpose-grown feedstocks while meeting economic and environmental targets would have substantial land change requirements which could lead to biodiversity loss and water quality degradation [32,256,257]. These findings are more in line with those of the International Civil Aviation Organization who found biomass and its derivatives may only be able to meet approximately 50% of the total jet fuel demand annually [258].

In recent years there has also been a push towards ethanol-to-jet as a way to utilize ethanol as ground transportation is moving towards electrification, despite the uncertainty surrounding its environmental impact [259]. Optimization results in this study used limited corn as a SAF feedstock, instead favoring miscanthus and sorghum due to their lower costs and

environmental impact and ability to be grown on marginal lands. However, cultivation of miscanthus and sorghum is not at the scales necessary to meet aviation sector demands and miscanthus/sorghum biorefineries are not currently available at commercial scales unlike ethanol-to-jet [260]. Therefore, the tradeoffs identified in this analysis are essential for the U.S. Department of Energy, U.S. Department of Transportation, and the U.S. Department of Agriculture to take into consideration when investing in purpose-grown feedstocks and technologies in the coming years.

Many limitations were encountered during this study with the main one being data availability. The primary assumptions associated with the model, and the highest sensitivity to the results, are the purpose-grown feedstocks yields across the U.S. These purpose-grown feedstocks are not cultivated widely across the U.S., so the input yield data required for this analysis had to come from simulated sources. These simulated yields were based on the best available data, but it is likely that some of the aerial productivities that were estimated in this data set may not come to fruition in future climates. Similarly, the feedstock inputs required for cultivation are not available with the geographic resolution desired for this analysis due to their limited cultivation nationally. Limited research also exists on the commercial scale conversion of many of these feedstocks to SAF. We used the best literature available, but often found confounding values for conversion efficiencies. Before any of these technologies are deployed on large scales, additional case studies and pilots need to be performed to verify both the feedstock inputs and productivities, as well as the conversion efficiency to SAF.

Lastly, the environmental impacts associated the modeled pathways were substantially influenced by direct land-use change emissions. The authors excluded indirect land-use change emissions by assuming that existing land was not used for productive purposes, but if included it

could have an impact on the overall emissions of the study. The data availability for direct land-use change emissions for purpose-grown feedstocks is limited and the authors had to rely on simulated data for each of these different feedstocks across the U.S. based on modeling done using the DAYCENT model. Further research needs to be done in these areas to verify purpose-grown feedstock yields, direct land-use change emissions over the life of the biorefinery, and the costs, emissions, and conversion efficiencies for converting these purpose-grown feedstocks to SAF at the commercial scales required to decarbonize the aviation sector by 2050.

4.5 Data Availability

This study integrated primary data from many sources as discussed in the Methods section. Using the modeling and data analysis techniques described in this paper, the results were generated for this study. All input data and results data is available on Zenodo [226]: https://doi.org/10.5281/zenodo.11521694

CHAPTER 5: CONCLUSIONS AND RECOMMENDATIONS

5.1 Overall conclusions

This dissertation has explored the dual lens of sustainability by examining the economic and environmental impacts of innovative carbon reduction technologies across the power generation, wastewater treatment, and aviation sectors. The comprehensive analysis presented highlights the critical importance of integrating technological advancements with sustainability goals to address the pressing challenges of climate change and resource management.

Based on the findings, each of these technologies shows potential to significantly contribute to reducing overall greenhouse gas emissions and help achieve net zero targets by 2050. However, several limitations are associated with these technologies. Primarily, they are still novel or in their early stages compared to where they need to be by 2050 to meet our sustainability targets. The research was conducted from a systems modeling and data analysis perspective, facing limitations in data availability and quality across all three sectors.

Many of these technologies have not been deployed at large scales and lack pilot studies or commercial-scale facilities, necessitating numerous assumptions to evaluate their economic and environmental feasibility. Despite these challenges, the analysis demonstrated that these technologies are promising in both economic and environmental terms compared to the incumbent technologies they aim to replace.

Moving forward, pilot-scale deployments of these technologies need to be evaluated across the U.S. through pilot studies. Data from these studies should be integrated into existing

models or similar frameworks to continuously iterate and update these models, ensuring they accurately reflect the evolving landscape. A major concern is the rapid deployment required to meet the 2050 net zero goals. The current pace of scaling up these technologies may not be sufficient to meet these targets.

Additionally, the lack of geographically resolved data for some of these technologies is a concern. Transitioning to a sustainable future will require addressing these data gaps and accelerating the deployment of promising technologies. The following sections detail future directions for each of the technologies considered in this dissertation, focusing on implementation challenges and potential solutions.

5.2 Future Directions on Thermal Energy Storage for Natural Gas Combined Cycle Power Plants with Carbon Capture and Sequestration

Integrating TES with NGCC+CCS proves to be a viable solution for reducing the burden of the CCS plant on the host power plant. However, more work needs to be done to verify that the interaction between TES and CCS is accurate as modeled. The modeling in this dissertation shows that using a resistively heated TES unit is viable in both real-world and future price profiles. Capacity expansion results indicate that TES provides a proven benefit over a power plant without resistively heated TES.

However, the results also reveal that integrating more advanced CCS technologies, such as Ion Clean Energy's solvents, has a larger economic impact than integrating TES alone. This holds true when optimizing for electricity price signals and in capacity expansion modeling. Therefore, it is recommended that additional research be conducted on both integrating TES with

CCS facilities and further exploring advanced CCS technologies to ensure they perform as expected at both pilot and commercial scales.

It is also recommended that further research compare CCS technologies on fossil fuel plants to more sustainable technologies, such as renewable energy combined with battery storage. As the costs of solar and wind technologies decrease, along with the cost of batteries, they will become more cost-competitive with fossil fuel generation and CCS. Thus, additional research needs to identify the break-even threshold for these different technologies and determine when it becomes more economically viable to build new renewable energy facilities with battery energy storage rather than retrofitting existing fossil fuel power plants with CCS.

5.3 Future Directions on Green Wastewater Treatment and Water Quality Trading

Green wastewater treatment options and water quality trading within different watershed regions prove to be a very feasible alternative to retrofitting existing wastewater treatment facilities. However, there are significant limitations associated with current research around green wastewater treatment solutions, specifically related to nutrient remediation, that need to be addressed before these methods can be adopted on a large scale. Additionally, policy implementation is necessary to allow for water quality trading across different regions, and more incentives are needed for individuals to adopt green wastewater treatment facilities on their agricultural farms.

The biggest limitation associated with this research is the lack of data on existing green wastewater treatment options, particularly for nutrient remediation. Current research is predominantly conducted in the Corn Belt and the Mississippi River Basin due to algal blooms and dead zones in the Gulf of Mexico and the high nutrient loads in that region. This analysis

evaluated green wastewater treatment across the continguous U.S. and had to apply values found in the Corn Belt to different geographic regions. Therefore, a significant limitation is the insufficient research on green wastewater treatment technologies elsewhere in the United States. It is known that these treatment options can vary significantly based on geographic location, making this a vital area of study before these technologies and policies are implemented on a large scale.

Additionally, there is a lack of research and literature on the compounding effects of different green wastewater treatment technologies applied in agricultural fields. While it is expected that multiple green wastewater treatment solutions could be applied in combination, it is unclear what the added value of each additional treatment method would be. Further research is needed in this area.

Despite these limitations, the results show that green infrastructure is both economically and environmentally friendly. Significant cost reductions and emissions reductions are observed compared to existing wastewater treatment infrastructure, making this a very promising alternative. Additional research and case studies are needed to verify the accuracy of nutrient remediation across the United States, ensuring that this technology can be implemented on a larger scale to meet the various water quality requirements nationwide.

5.4 Sustainable Aviation Fuel from Purpose-Grown Bioenergy Feedstock to Meet U.S. Targets

Decarbonizing the aviation sector may be one of the hardest challenges the United States faces to achieve a net-zero economy by 2050. The United States SAF Grand Challenge, initiated by the Department of Energy, Department of Transportation, and Department of Agriculture, is a

great first step in identifying targets to achieve these goals. However, there are concerns about the availability of feedstocks to meet the demand for sustainable aviation fuel.

The first goal of the SAF Grand Challenge is to produce 3 billion gallons by 2030. Currently, there is enough corn ethanol and soybean biodiesel being produced in the U.S. that, if redirected to SAF production, could meet this initial target. However, achieving the more ambitious target of 35 billion gallons of SAF will be much more challenging, as this will require a significant portion of SAF production to come from purpose-grown bioenergy feedstocks, such as miscanthus, switchgrass, poplar, willow, and algae. While corn and soy are grown extensively in the U.S. today, the optimization results in this study show limited deployment of these crops for SAF, instead favoring more advanced bioenergy crops not currently grown at large scales.

To meet the SAF Grand Challenge targets, a rapid and substantial increase in the deployment of crops like miscanthus and sorghum is necessary. This raises land use concerns, as implementing these crops on a large scale without impacting the existing food supply or cropland used for export is challenging. Some optimization scenarios suggest nearly doubling the amount of cropland in the contiguous U.S. to grow enough bioenergy feedstocks to meet SAF targets. Historical land conversion data indicate that converting the required amount of land within the necessary timeframe will be difficult, if not impossible. Even if achievable, this could lead to significant biodiversity loss and water quality issues due to increased nutrient loads from agricultural fields.

An interesting finding from this study is the optimization showing very little use of corn and soybeans for SAF, contradicting the current momentum of transitioning ethanol to jet fuels. While the ethanol industry is moving towards jet fuels, results indicate that corn ethanol-based

SAF will play a minimal role in future scenarios due to cost, emissions, carbon price, and land use considerations. This discrepancy needs further evaluation.

The agent-based model results show that while corn and soy could be used for SAF, farmers are likely to prefer familiar crops over new, riskier bioenergy feedstocks. High carbon prices associated with SAF also pose a challenge compared to other carbon reduction technologies. The break-even carbon price for SAF is around $170 per tonne of CO_2 equivalent, significantly higher than the targets for other carbon reduction technologies, such as biomass burial, which can achieve reductions at closer to $50 per tonne of CO_2 equivalent. Additional research needs to be done on if using bioenergy feedstock for SAF would be better suited for biomass burial if the goal is increased carbon reduction.

Meeting the SAF production targets will likely rely on residues or waste streams, which could provide about 8 billion gallons of SAF. The remaining amount would need to come from power-to-liquid fuels, which currently have low technical readiness levels and high energy requirements. While these fuels are unproven at commercial scales, they offer potential if technological advancements are made.

Algae-based SAF presents another interesting option, avoiding land use concerns but resulting in higher costs and less emissions reduction compared to petroleum jet fuel. With additional research to improve economic feasibility and environmental benefits, algae could also become a more competitive option.

There is a broader question of whether SAF is the best method to decarbonize the aviation sector. Given the high energy or land intensity required for SAF, it may be more economical to focus on decarbonizing the electricity grid and using technologies like direct air

capture to offset emissions. Investing in renewable energy, battery storage, and direct air capture could maximize carbon removal per dollar spent, deferring large-scale SAF investment until the technologies are more mature.

Finally, there are significant challenges in optimizing feedstock deployment, balancing fuel cost and emissions reductions, and aligning bioenergy feedstock production with fuel consumption locations. To address these issues and achieve the SAF Grand Challenge targets, significant policy incentives and careful consideration by stakeholders and policymakers are essential.

REFERENCES

[1] U.S. Environmental Protection Agency. Global Greenhouse Gas Emissions Data 2016. https://www.epa.gov/ghgemissions/global-greenhouse-gas-emissions-data (accessed April 21, 2021).

[2] Capturing carbon: Can it save us? Chemical & Engineering News n.d. https://cen.acs.org/environment/greenhouse-gases/Capturing-carbon-save-us/97/i8 (accessed April 20, 2021).

[3] Babaee S, Loughlin DH. Exploring the role of natural gas power plants with carbon capture and storage as a bridge to a low-carbon future. Clean Techn Environ Policy 2018;20:379–91. https://doi.org/10.1007/s10098-017-1479-x.

[4] Mignone BK, Showalter S, Wood F, McJeon H, Steinberg D. Sensitivity of natural gas deployment in the US power sector to future carbon policy expectations. Energy Policy 2017;110:518–24. https://doi.org/10.1016/j.enpol.2017.08.012.

[5] Du Y, Gao T, Rochelle GT, Bhown AS. Zero- and negative-emissions fossil-fired power plants using CO2 capture by conventional aqueous amines. International Journal of Greenhouse Gas Control 2021;111:103473. https://doi.org/10.1016/j.ijggc.2021.103473.

[6] Chao C, Deng Y, Dewil R, Baeyens J, Fan X. Post-combustion carbon capture. Renewable and Sustainable Energy Reviews 2021;138:110490. https://doi.org/10.1016/j.rser.2020.110490.

[7] Global CCS Institute. CO2 Capture Technologies - Post Combustion Capture (PCC). 2012.

[8] Tait P, Buschle B, Ausner I, Valluri P, Wehrli M, Lucquiaud M. A pilot-scale study of dynamic response scenarios for the flexible operation of post-combustion CO2 capture. International Journal of Greenhouse Gas Control 2016;48:216–33. https://doi.org/10.1016/j.ijggc.2015.12.009.

[9] Chen Q, Kang C, Xia Q, Kirschen D s. Optimal Flexible Operation of a CO2 Capture Power Plant in a Combined Energy and Carbon Emission Market. IEEE Transactions on Power Systems 2012;27:1602–9.

[10] Oates DL, Versteeg P, Hittinger E, Jaramillo P. Profitability of CCS with flue gas bypass and solvent storage. International Journal of Greenhouse Gas Control 2014;27:279–88. https://doi.org/10.1016/j.ijggc.2014.06.003.

[11] Cohen SM, Rochelle GT, Webber ME. Optimal operation of flexible post-combustion CO2 capture in response to volatile electricity prices. Energy Procedia 2011;4:2604–11. https://doi.org/10.1016/j.egypro.2011.02.159.

[12] Cohen S, Rochelle G, Webber M. Optimizing post-combustion CO2 capture in response to volatile electricity prices. International Journal of Greenhouse Gas Control 2012;8:180–95. https://doi.org/10.1016/j.ijggc.2012.02.011.

[13] Cohen S, Rochelle G, Webber M. Optimal CO2 Capture Operation in an Advanced Electric Grid. Energy Procedia 2013;37:2585–94. https://doi.org/10.1016/j.egypro.2013.06.142.

[14] OECD. Effective Carbon Rates 2021: Pricing Carbon Emissions through Taxes and Emissions Trading. OECD; 2021. https://doi.org/10.1787/0e8e24f5-en.

[15] BloombergNEF. Carbon Offset Prices Could Increase Fifty-Fold by 2050. BloombergNEF 2022. https://about.bnef.com/blog/carbon-offset-prices-could-increase-fifty-fold-by-2050/ (accessed January 31, 2022).

[16] Bhat P. Carbon needs to cost at least $100/tonne now to reach net zero by 2050: Reuters poll. Reuters 2021.

[17] EPA. Energy Efficiency for Water Utilities. Sustainable Water Infrastructure 2016.

[18] Environmental Integrity Project. The Clean Water Act at 50. 2022.

[19] Cheng FY, Van Meter KJ, Byrnes DK, Basu NB. Maximizing US nitrate removal through wetland protection and restoration. Nature 2020;588:625–30. https://doi.org/10.1038/s41586-020-03042-5.

[20] Díaz RJ, Rosenberg R. Introduction to Environmental and Economic Consequences of Hypoxia. International Journal of Water Resources Development 2011;27:71–82. https://doi.org/10.1080/07900627.2010.531379.

[21] Tomczyk N, Naslund L, Cummins C, Bell EV, Bumpers P, Rosemond AD. Nonpoint source pollution measures in the Clean Water Act have no detectable impact on decadal trends in nutrient concentrations in U.S. inland waters. Ambio 2023;52. https://doi.org/10.1007/s13280-023-01869-6.

[22] Murchison KM. Learning from More than Five-and-a-Half Decades of Federal Water Pollution Control Legislation: Twenty Lessons for the Future. C Envtl Aff L Rev 2005;527.

[23] Ross D. Updating the Environmental Protection Agency's Water Quality Trading Policy to Promote Market-Based Mechanisms for Improving Water Quality. USEPA; 2019.

[24] Chung MG, Frank KA, Pokhrel Y, Dietz T, Liu J. Natural infrastructure in sustaining global urban freshwater ecosystem services. Nat Sustain 2021;4:1068–75. https://doi.org/10.1038/s41893-021-00786-4.

[25] USEPA. Water Quality Trading Policy. USEPA; 2003.

[26] Liu Y, Engel BA, Collingsworth PD, Pijanowski BC. Optimal implementation of green infrastructure practices to minimize influences of land use change and climate change on hydrology and water quality: Case study in Spy Run Creek watershed, Indiana. Science of The Total Environment 2017;601–602:1400–11. https://doi.org/10.1016/j.scitotenv.2017.06.015.

[27] Jaffe M. Environmental Reviews & Case Studies: Reflections on Green Infrastructure Economics. Environmental Practice 2010;12:357–65. https://doi.org/10.1017/S1466046610000475.

[28] U.S. Department of Energy, U.S. Department of Transportation, U.S. Department of Agriculture, U.S. Environmental Protection Agency. SAF Grand Challenge Roadmap. 2022.

[29] IATA. Resolution on the Industry's Commitment to Reach Net Zero Carbon Emissions by 2050. 2021.

[30] U.S. Department of Energy. Clean Fuels & Products Shot™: Alternative Sources for Carbon-based Products. EnergyGov 2023. https://www.energy.gov/eere/clean-fuels-products-shottm-alternative-sources-carbon-based-products (accessed April 18, 2024).

[31] U.S. Department of Energy. Energy Earthshots Initiative. EnergyGov 2021. https://www.energy.gov/energy-earthshots-initiative (accessed April 18, 2024).

[32] Langholtz MH, Stokes BJ, Eaton LM. 2016 Billion-Ton Report: Advancing Domestic Resources for a Thriving Bioeconomy. 2016. https://doi.org/10.2172/1271651.

[33] Uludere Aragon NZ, Parker NC, VanLoocke A, Bagley J, Wang M, Georgescu M. Sustainable land use and viability of biojet fuels. Nat Sustain 2022:1–11. https://doi.org/10.1038/s41893-022-00990-w.

[34] Chandrasekaran S, Salah NB, Posada JA. European Union's biomass availability for Sustainable Aviation Fuel production and potential GHG emissions reduction in the aviation sector: An analysis using GIS tools for 2030. In: Kokossis AC, Georgiadis MC, Pistikopoulos E, editors. Computer Aided Chemical Engineering, vol. 52, Elsevier; 2023, p. 3055–60. https://doi.org/10.1016/B978-0-443-15274-0.50487-X.

[35] Guarenghi MM, Santos JL, Walter A, Rocha JV, Seabra JE, Vieira ND, et al. SAFmaps: the WebGIS for sustainability assessment of aviation biofuels in Brazil. GEOINFO, 2021, p. 120–31.

[36] Ullah KM, Masum FH, Field JL, Dwivedi P. Designing a GIS-based supply chain for producing carinata-based sustainable aviation fuel in Georgia, USA. Biofuels, Bioproducts and Biorefining 2023;n/a. https://doi.org/10.1002/bbb.2483.

[37] Quinn JC, Catton KB, Johnson S, Bradley TH. Geographical Assessment of Microalgae Biofuels Potential Incorporating Resource Availability. Bioenerg Res 2013;6:591–600. https://doi.org/10.1007/s12155-012-9277-0.

[38] Quiroz D, Greene JM, Limb BJ, Quinn JC. Global Life Cycle and Techno-Economic Assessment of Algal-Based Biofuels. Environ Sci Technol 2023. https://doi.org/10.1021/acs.est.3c02892.

[39] Liu T, Huffman T, Kulshreshtha S, McConkey B, Du Y, Green M, et al. Bioenergy production on marginal land in Canada: Potential, economic feasibility, and greenhouse gas emissions impacts. Applied Energy 2017;205:477–85. https://doi.org/10.1016/j.apenergy.2017.07.126.

[40] Stoof CR, Richards BK, Woodbury PB, Fabio ES, Brumbach AR, Cherney J, et al. Untapped Potential: Opportunities and Challenges for Sustainable Bioenergy Production

from Marginal Lands in the Northeast USA. Bioenerg Res 2015;8:482–501. https://doi.org/10.1007/s12155-014-9515-8.

[41] Yang P, Zhao Q, Cai X. Machine learning based estimation of land productivity in the contiguous US using biophysical predictors. Environ Res Lett 2020;15:074013. https://doi.org/10.1088/1748-9326/ab865f.

[42] Gelfand I, Sahajpal R, Zhang X, Izaurralde RC, Gross KL, Robertson GP. Sustainable bioenergy production from marginal lands in the US Midwest. Nature 2013;493:514–7. https://doi.org/10.1038/nature11811.

[43] Zhuang D, Jiang D, Liu L, Huang Y. Assessment of bioenergy potential on marginal land in China. Renewable and Sustainable Energy Reviews 2011;15:1050–6. https://doi.org/10.1016/j.rser.2010.11.041.

[44] U.S. Department of Energy, Langholtz MH. 2023 Billion-Ton Report: An Assessment of U.S. Renewable Carbon Resources. Oak Ridge, TN: Oak Ridge National Laboratory; 2024.

[45] Smith JP, Limb BJ, Beal CM, Banta KR, Field JL, Simske SJ, et al. Evaluating the sustainability of the 2017 US biofuel industry with an integrated techno-economic analysis and life cycle assessment. Journal of Cleaner Production 2023;413:137364. https://doi.org/10.1016/j.jclepro.2023.137364.

[46] Pelton REO, Spawn-Lee SA, Lark TJ, Kim T, Springer N, Hawthorne P, et al. Land use leverage points to reduce GHG emissions in U.S. agricultural supply chains. Environmental Research Letters 2021;16:115002. https://doi.org/10.1088/1748-9326/ac2775.

[47] Gautam S, Baral NR, Mishra U, Scown CD. Impact of bioenergy feedstock carbon farming on sustainable aviation fuel viability in the United States. Proceedings of the National Academy of Sciences 2023;120:e2312667120. https://doi.org/10.1073/pnas.2312667120.

[48] Daly C, Halbleib MD, Hannaway DB, Eaton LM. Environmental limitation mapping of potential biomass resources across the conterminous United States. GCB Bioenergy 2018;10:717–34. https://doi.org/10.1111/gcbb.12496.

[49] Pearlson M, Wollersheim C, Hileman J. A techno-economic review of hydroprocessed renewable esters and fatty acids for jet fuel production. Biofuels Bioprod Bioref 2013;7:89–96. https://doi.org/10.1002/bbb.1378.

[50] de Jong S, Hoefnagels R, Faaij A, Slade R, Mawhood R, Junginger M. The feasibility of short-term production strategies for renewable jet fuels – a comprehensive techno-economic comparison. Biofuels, Bioproducts and Biorefining 2015;9:778–800. https://doi.org/10.1002/bbb.1613.

[51] Atsonios K, Kougioumtzis M-A, D. Panopoulos K, Kakaras E. Alternative thermochemical routes for aviation biofuels via alcohols synthesis: Process modeling, techno-economic assessment and comparison. Applied Energy 2015;138:346–66. https://doi.org/10.1016/j.apenergy.2014.10.056.

[52] Ekbom T, Hjerpe C, Hagstroem M, Hermann F. Pilot study of Bio-jet A-1 fuel production for Stockholm-Arlanda Airport; Foerstudie foer biobaserat flygbraensle foer Stockholm-Arlanda Flygplats 2009.

[53] Watson MJ, Machado PG, da Silva AV, Saltar Y, Ribeiro CO, Nascimento CAO, et al. Sustainable aviation fuel technologies, costs, emissions, policies, and markets: A critical review. Journal of Cleaner Production 2024;449:141472. https://doi.org/10.1016/j.jclepro.2024.141472.

[54] Shahriar MF, Khanal A. The current techno-economic, environmental, policy status and perspectives of sustainable aviation fuel (SAF). Fuel 2022;325:124905. https://doi.org/10.1016/j.fuel.2022.124905.

[55] Dahal K, Brynolf S, Xisto C, Hansson J, Grahn M, Grönstedt T, et al. Techno-economic review of alternative fuels and propulsion systems for the aviation sector. Renewable and Sustainable Energy Reviews 2021;151:111564. https://doi.org/10.1016/j.rser.2021.111564.

[56] Jeswani HK, Chilvers A, Azapagic A. Environmental sustainability of biofuels: a review. Proceedings of the Royal Society A: Mathematical, Physical and Engineering Sciences 2020;476:20200351. https://doi.org/10.1098/rspa.2020.0351.

[57] Seiple T, Jiang Y, Snowden-Swan LJ, Betzsold N, Ramasamy KK, Fuller C. Cost-Effective Opportunities to Produce Sustainable Aviation Fuel from Low-Cost Wastes in the U.S. ACS Sustainable Chem Eng 2023;11:12326–35. https://doi.org/10.1021/acssuschemeng.3c02147.

[58] Masum FH, Coppola E, Field JL, Geller D, George S, Miller JL, et al. Supply chain optimization of sustainable aviation fuel from carinata in the Southeastern United States. Renewable and Sustainable Energy Reviews 2023;171:113032. https://doi.org/10.1016/j.rser.2022.113032.

[59] Paudel A, Bandhauer T. Techno-economic analysis of waste heat recovery systems for wet-cooled combined cycle power plants. Applied Thermal Engineering 2018;143:746–58. https://doi.org/10.1016/j.applthermaleng.2018.07.138.

[60] Eveloy V, Rodgers P, Popli S. Power generation and cooling capacity enhancement of natural gas processing facilities in harsh environmental conditions through waste heat

utilization. International Journal of Energy Research 2014;38:1921–36. https://doi.org/10.1002/er.3197.

[61] Gil A, Medrano M, Martorell I, Lázaro A, Dolado P, Zalba B, et al. State of the art on high temperature thermal energy storage for power generation. Part 1—Concepts, materials and modellization. Renewable and Sustainable Energy Reviews 2010;14:31–55. https://doi.org/10.1016/j.rser.2009.07.035.

[62] Medrano M, Gil A, Martorell I, Potau X, Cabeza LF. State of the art on high-temperature thermal energy storage for power generation. Part 2—Case studies. Renewable and Sustainable Energy Reviews 2010;14:56–72. https://doi.org/10.1016/j.rser.2009.07.036.

[63] Chang J, Lee G, Adams D, Ahn H, Lee J, Oh M. Multiscale modeling and integration of a combined cycle power plant and a two-tank thermal energy storage system with gPROMS and SimCentral. Korean J Chem Eng 2021;38:1333–47. https://doi.org/10.1007/s11814-021-0789-1.

[64] Malta Inc. Malta's Electro-Thermal Energy Storage System: A Better Way to Enable Cleaner Reliable Electricity on the Grid. Malta Inc n.d. https://www.maltainc.com/our-solution (accessed January 31, 2022).

[65] Smallbone A, Jülch V, Wardle R, Roskilly AP. Levelised Cost of Storage for Pumped Heat Energy Storage in comparison with other energy storage technologies. Energy Conversion and Management 2017;152:221–8. https://doi.org/10.1016/j.enconman.2017.09.047.

[66] Gkoutzamanis V, Chatziangelidou A, Efstathiadis T, Kalfas A, Traverso A, Chiu JNW. Thermal Energy Storage For Gas Turbine Power Augmentation. J Glob Power Propuls Soc 2019;3:592–608. https://doi.org/10.33737/jgpps/110254.

[67] Barigozzi G, Perdichizzi A, Gritti C, Guaiatelli I. Techno-economic analysis of gas turbine inlet air cooling for combined cycle power plant for different climatic conditions. Applied Thermal Engineering 2015;82:57–67. https://doi.org/10.1016/j.applthermaleng.2015.02.049.

[68] Palestra N, Barigozzi G, Perdichizzi A. Inlet Air Cooling Applied to Combined Cycle Power Plants: Influence of Site Climate and Thermal Storage Systems. Journal of Engineering for Gas Turbines and Power 2008;130. https://doi.org/10.1115/1.2771570.

[69] Zhang H, Baeyens J, Cáceres G, Degrève J, Lv Y. Thermal energy storage: Recent developments and practical aspects. Progress in Energy and Combustion Science 2016;53:1–40. https://doi.org/10.1016/j.pecs.2015.10.003.

[70] Bedell E, Harmon O, Fankhauser K, Shivers Z, Thomas E. A continuous, in-situ, near-time fluorescence sensor coupled with a machine learning model for detection of fecal contamination risk in drinking water: Design, characterization and field validation. Water Research 2022;220:118644. https://doi.org/10.1016/j.watres.2022.118644.

[71] Brown CJ, Jupiter SD, Albert S, Klein CJ, Mangubhai S, Maina JM, et al. Tracing the influence of land-use change on water quality and coral reefs using a Bayesian model. Sci Rep 2017;7:4740. https://doi.org/10.1038/s41598-017-05031-7.

[72] Ahearn DS, Sheibley RW, Dahlgren RA, Anderson M, Johnson J, Tate KW. Land use and land cover influence on water quality in the last free-flowing river draining the western Sierra Nevada, California. Journal of Hydrology 2005;313:234–47. https://doi.org/10.1016/j.jhydrol.2005.02.038.

[73] Hohner AK, Rhoades CC, Wilkerson P, Rosario-Ortiz FL. Wildfires Alter Forest Watersheds and Threaten Drinking Water Quality. Acc Chem Res 2019;52:1234–44. https://doi.org/10.1021/acs.accounts.8b00670.

[74] Basso M, Vieira DCS, Ramos TB, Mateus M. Assessing the adequacy of SWAT model to simulate postfire effects on the watershed hydrological regime and water quality. Land Degradation & Development 2020;31:619–31. https://doi.org/10.1002/ldr.3476.

[75] Loiselle D, Du X, Alessi DS, Bladon KD, Faramarzi M. Projecting impacts of wildfire and climate change on streamflow, sediment, and organic carbon yields in a forested watershed. Journal of Hydrology 2020;590:125403. https://doi.org/10.1016/j.jhydrol.2020.125403.

[76] United Nations. Adoption of the Paris Agreement, 2015.

[77] Schleussner C-F, Rogelj J, Schaeffer M, Lissner T, Licker R, Fischer EM, et al. Science and policy characteristics of the Paris Agreement temperature goal. Nature Clim Change 2016;6:827–35. https://doi.org/10.1038/nclimate3096.

[78] UNFCCC Climate Goal by Country 2017. https://www4.unfccc.int/sites/submissions/indc/Submission%20Pages/submissions.aspx (accessed April 13, 2021).

[79] Australia Climate Change Authority. Comparing countries' emissions targets n.d. https://www.climatechangeauthority.gov.au/comparing-countries-emissions-targets (accessed May 4, 2021).

[80] International Energy Agency. CCUS in Power – Analysis. IEA n.d. https://www.iea.org/reports/ccus-in-power (accessed June 6, 2021).

[81] NS Energy. What are the top carbon capture and storage projects around the world? n.d. https://www.nsenergybusiness.com/features/top-carbon-capture-storage-projects/ (accessed June 2, 2021).

[82] U.S. Energy Information Administration (EIA). More than 100 coal-fired plants have been replaced or converted to natural gas since 2011 - Today in Energy n.d. https://www.eia.gov/todayinenergy/detail.php?id=44636 (accessed June 1, 2021).

[83] U.S. Energy Information Administration (EIA). More U.S. coal-fired power plants are decommissioning as retirements continue - Today in Energy n.d. https://www.eia.gov/todayinenergy/detail.php?id=40212 (accessed June 1, 2021).

[84] Jacobson, Mark Z. The 7 reasons why nuclear energy is not the answer to solve climate change | Heinrich Böll Stiftung | Brussels office - European Union. Heinrich-Böll-Stiftung n.d. https://eu.boell.org/en/2021/04/26/7-reasons-why-nuclear-energy-not-answer-solve-climate-change (accessed May 15, 2021).

[85] Wilkerson, Jordan. Reconsidering the Risks of Nuclear Power. Science in the News 2016. https://sitn.hms.harvard.edu/flash/2016/reconsidering-risks-nuclear-power/ (accessed May 15, 2021).

[86] Stauffer, Nancy W. Building nuclear power plants. Massachusetts Institute of Technology n.d. https://energy.mit.edu/news/building-nuclear-power-plants/ (accessed May 15, 2021).

[87] Gürsan C, de Gooyert V. The systemic impact of a transition fuel: Does natural gas help or hinder the energy transition? Renewable and Sustainable Energy Reviews 2021;138:110552. https://doi.org/10.1016/j.rser.2020.110552.

[88] Delborne JA, Hasala D, Wigner A, Kinchy A. Dueling metaphors, fueling futures: “Bridge fuel” visions of coal and natural gas in the United States. Energy Research & Social Science 2020;61:101350. https://doi.org/10.1016/j.erss.2019.101350.

[89] National Renewable Energy Laboratory. Renewable Electricity Futures Study. Volume 1: Exploration of High-Penetration Renewable Electricity Futures 2012:280.

[90] Leslie M. The Next Energy Battle: Cheap Natural Gas versus Renewables. Engineering 2021;7:133–5. https://doi.org/10.1016/j.eng.2020.12.008.

[91] Ajiwibowo M, Darmawan A, Aziz M. A conceptual chemical looping combustion power system design in a power-to-gas energy storage scenario. International Journal of Hydrogen Energy 2018;44. https://doi.org/10.1016/j.ijhydene.2018.11.177.

[92] Szima S, Cormos A-M, Cormos C-C. Flexible Hydrogen and Power Co - generation based on Dry Methane Reforming with Carbon Capture. In: Friedl A, Klemeš JJ, Radl S, Varbanov PS, Wallek T, editors. Computer Aided Chemical Engineering, vol. 43, Elsevier; 2018, p. 1281–6. https://doi.org/10.1016/B978-0-444-64235-6.50225-4.

[93] Davison J, Arienti S, Cotone P, Mancuso L. Co-production of hydrogen and electricity with CO2 capture. Energy Procedia 2009;1:4063–70. https://doi.org/10.1016/j.egypro.2009.02.213.

[94] Hu Y, Li X, Li H, Yan J. Peak and off-peak operations of the air separation unit in oxy-coal combustion power generation systems. Applied Energy 2013;112:747–54. https://doi.org/10.1016/j.apenergy.2012.12.001.

[95] Mitchell C, Avagyan V, Chalmers H, Lucquiaud M. An initial assessment of the value of Allam Cycle power plants with liquid oxygen storage in future GB electricity system.

International Journal of Greenhouse Gas Control 2019;87:1–18. https://doi.org/10.1016/j.ijggc.2019.04.020.

[96] Domenichini R, Mancuso L, Ferrari N, Davison J. Operating Flexibility of Power Plants with Carbon Capture and Storage (CCS). Energy Procedia 2013;37:2727–37. https://doi.org/10.1016/j.egypro.2013.06.157.

[97] David Yellen. Carbon capture and the Allam Cycle: The future of electricity or a carbon pipe(line) dream? Atlantic Council 2020. https://www.atlanticcouncil.org/blogs/energysource/carbon-capture-and-the-allam-cycle-the-future-of-electricity-or-a-carbon-pipeline-dream/ (accessed January 31, 2022).

[98] Mohapatra AK, Sanjay. Thermodynamic assessment of impact of inlet air cooling techniques on gas turbine and combined cycle performance. Energy 2014;68:191–203. https://doi.org/10.1016/j.energy.2014.02.066.

[99] Li D, Hu Y, He W, Wang J. Dynamic modelling and simulation of a combined-cycle power plant integration with thermal energy storage. 2017 23rd International Conference on Automation and Computing (ICAC), 2017, p. 1–6. https://doi.org/10.23919/IConAC.2017.8081972.

[100] Ela E, Billimoria F, Ragsdale K, Moorty S, O'Sullivan J, Gramlich R, et al. Future Electricity Markets: Designing for Massive Amounts of Zero-Variable-Cost Renewable Resources. IEEE Power and Energy Magazine 2019;17:58–66. https://doi.org/10.1109/MPE.2019.2933281.

[101] Gomez T, Herrero I, Rodilla P, Escobar R, Lanza S, de la Fuente I, et al. European Union Electricity Markets: Current Practice and Future View. IEEE Power and Energy Magazine 2019;17:20–31. https://doi.org/10.1109/MPE.2018.2871739.

[102] Limb BJ, Markey E, Vercellino R, Garland S, Pisciotta M, Psarras P, et al. Economic viability of using thermal energy storage for flexible carbon capture on natural gas power plants. Journal of Energy Storage 2022;55:105836. https://doi.org/10.1016/j.est.2022.105836.

[103] Limb B, Markey E, Vercellino R, Huyett J, Garland S, Pisciotta M, et al. Evaluating the economic viability of NGCC-SWITCC: Natural Gas Combined Cycle System With Integrated Thermal storage and Carbon Capture 2022. https://doi.org/10.2139/ssrn.4295563.

[104] James R, Zoelle A, Keairns D, Turner M, Woods M, Kuehn N. Cost And Performance Baseline for Fossil Energy Plants Volume 1: Bituminous Coal and Natural Gas To Electricity. National Energy Technology Laboratory (NETL); 2019.

[105] Shell CANSOLV® CO_2 Capture System n.d. https://www.shell.com/business-customers/catalysts-technologies/licensed-technologies/emissions-standards/tail-gas-treatment-unit/cansolv-co2.html (accessed August 20, 2021).

[106] The ION Systems Solution. ION Clean Energy n.d. https://ioncleanenergy.com/our-technology/ (accessed August 10, 2022).

[107] Wilcox J. Carbon Capture. New York: Springer-Verlag; 2012. https://doi.org/10.1007/978-1-4614-2215-0.

[108] Carnegie Mellon University (CMU). Integrated Environmental Control Model n.d. https://www.cmu.edu/epp/iecm/ (accessed March 15, 2021).

[109] Storworks Power. Economic Benefits. Storworks n.d. https://storworks.com/economic-benefits/ (accessed April 15, 2021).

[110] Solids - Specific Heats n.d. https://www.engineeringtoolbox.com/specific-heat-solids-d_154.html (accessed September 13, 2022).

[111] Solids, Liquids and Gases - Thermal Conductivities n.d. https://www.engineeringtoolbox.com/thermal-conductivity-d_429.html (accessed September 13, 2022).

[112] Fine N. Validation of Transformational CO2 Capture Solvent Technology with Revolutionary Stability 2021.

[113] Vercellino R, Markey E, Limb BJ, Pisciotta M, Huyett J, Garland S, et al. Control Co-Design Optimization of Natural Gas Power Plants with Carbon Capture and Thermal Storage, St. Louis, Missouri: ASME; 2022, p. 14.

[114] National Renewable Energy Laboratory. 2020 Electricity Annual Technology Baseline n.d. https://atb-archive.nrel.gov/electricity/2020/data.php (accessed October 1, 2020).

[115] U.S. Energy Information Administration (EIA). Annual Energy Outlook 2021 2021. https://www.eia.gov/outlooks/aeo/ (accessed March 6, 2021).

[116] U.S. Bureau of Labor Statistics. Consumer Price Index Data n.d. https://data.bls.gov/timeseries/CUUR0000SA0 (accessed December 15, 2020).

[117] New York Independent System Operator. Energy Market & Operational Data - NYISO n.d. https://www.nyiso.com/energy-market-operational-data (accessed October 30, 2020).

[118] California Independent System Operator. California ISO OASIS n.d. http://oasis.caiso.com/ (accessed October 30, 2020).

[119] U.S. Energy Information Administration (EIA). New York Natural Gas Prices n.d. https://www.eia.gov/dnav/ng/ng_pri_sum_dcu_sny_m.htm (accessed October 30, 2020).

[120] Jesse D Jenkins SC. Summary Report of the GenX and PowerGenome runs for generating Price Series (for ARPA-E FLECCS Project) 2021. https://doi.org/10.5281/ZENODO.5765797.

[121] Cohen S, Durvasulu V. NREL Price Series Developed for the ARPA-E FLECCS Program 2021:2 files. https://doi.org/10.7799/1838046.

[122] ARPA-E. FLECCS 2019. http://arpa-e.energy.gov/technologies/programs/fleccs (accessed June 12, 2024).

[123] GenX. FLECCS branch of GenX 2022. https://github.com/fc4uk/GenX/tree/fleccs (accessed June 12, 2024).

[124] Nunes P, Brito MC. Displacing natural gas with electric vehicles for grid stabilization. Energy 2017;141:87–96. https://doi.org/10.1016/j.energy.2017.09.064.

[125] Papaefthymiou G, Grave K, Dragoon K. Flexibility options in electricity systems. 2014.

[126] Hunter CA, Penev MM, Reznicek EP, Eichman J, Rustagi N, Baldwin SF. Techno-economic analysis of long-duration energy storage and flexible power generation technologies to support high-variable renewable energy grids. Joule 2021;5:2077–101. https://doi.org/10.1016/j.joule.2021.06.018.

[127] Limb, BJ, Markey E, Vercellino R, Garland S, Pisciotta MD, Psarras P, et al. Economic Viability of Thermal Energy Storage on Natural Gas Power Plants with Carbon Capture. Journal of Energy Storage n.d.

[128] Gillespie M, Erickson B. Duke Energy Hines Chiller Uprate Project. Power Engineering 2017. https://www.power-eng.com/gas/duke-energy-hines-chiller-uprate-project/ (accessed July 29, 2022).

[129] Shakya R, Ahiablame L. A Synthesis of Social and Economic Benefits Linked to Green Infrastructure. Water 2021;13:3651. https://doi.org/10.3390/w13243651.

[130] Liu H, Brouwer R. What is the future of water quality trading? Contemporary Economic Policy 2023;41. https://doi.org/10.1111/coep.12583.

[131] Ecosystem Marketplace. Ecosystem Marketplace Insights Report: Paying for Quality. State of the Voluntary Carbon Markets. 2023.

[132] IEA. Unlocking the potential of direct air capture: Is scaling up through carbon markets possible? – Analysis - IEA 2023.

[133] Johnson AH, Whitworth JS. Enabling ecological restoration through quantification. Broken Pumps and Promises: Incentivizing Impact in Environmental Health, 2016. https://doi.org/10.1007/978-3-319-28643-3_7.

[134] The Gold Standard. Gold Standard Water Benefit Certificates 2022.

[135] Ernst and Young. Essential, expensive and evolving: The outlook for carbon credits and offsets An EY Net Zero Centre report. 2022.

[136] Ecosystem Marketplace. 2023 All in on Climate: The Role of Carbon Credits in Corporate Climate Strategies. 2023.

[137] European Investment Bank. 2022 Joint Report on Multilateral Development Banks' Climate Finance. 2023.

[138] Cashman S, Arden S, Morelli B, Gray J, Bartram D, Falatko D. Life Cycle and Cost Assessments of Nutrient Removal Technologies in Wastewater Treatment Plants. EPA, Eastern Research Group; 2021.

[139] US EPA. Nutrient Reduction Progress Tracker 2018. https://www.acwa-us.org/wp-content/uploads/2018/03/Nutrient-Reduction-Progress-Tracker-Version-1.0-2017-Report.pdf (accessed August 2, 2023).

[140] Falk MW, Reardon DJ, Neethling JB, Clark DL, Pramanik A. Striking the Balance between Nutrient Removal, Greenhouse Gas Emissions, Receiving Water Quality, and Costs. Water Environment Research 2013;85:2307–16.

[141] United States Geological Survey. Hydrologic Unit Codes (HUCs) Explained 2023. https://nas.er.usgs.gov/hucs.aspx (accessed June 25, 2023).

[142] United States Geological Survey. Watershed Boundary Dataset (WBD) 2022.

[143] US EPA. EnviroAtlas Data Download 2015. https://www.epa.gov/enviroatlas/forms/enviroatlas-data-download (accessed June 23, 2023).

[144] US EPA. Nutrient Model (Hypoxia Task Force Search) 2022.

[145] US EPA. Water Pollutant Loading Tool - Data Downloads | ECHO | US EPA 2023. https://echo.epa.gov/trends/loading-tool/get-data (accessed August 1, 2023).

[146] US EPA. Emissions & Generation Resource Integrated Database (eGRID) 2020.

[147] Bossche JV den, Jordahl K, Fleischmann M, McBride J, Wasserman J, Richards M, et al. geopandas/geopandas: v0.13.2 2023. https://doi.org/10.5281/zenodo.8009629.

[148] United States Bureau of Labor Statistics. Consumer Price Index (CPI) 2023. https://www.bls.gov/cpi/ (accessed May 18, 2023).

[149] United States Bureau of Labor Statistics. Bureau of Labor Statistics Data 2023. https://data.bls.gov/pdq/SurveyOutputServlet (accessed May 18, 2023).

[150] Christianson L, Frankenberger J, Hay C, Helmers M, Sands G. Ten Ways to Reduce Nitrogen Loads from Drained Cropland in the Midwest. 2016. http://draindrop.cropsci.illinois.edu/wp-content/uploads/2016/09/Ten-Ways-to-Reduce-Nitrate-Loads_IL-Extension-_2016.pdf (accessed May 17, 2023).

[151] Illinois Water Resources Center. Nutrient loss reduction: Using science to find the right practices for your field. 2016.

[152] Christianson L, Tyndall J, Helmers M. Financial comparison of seven nitrate reduction strategies for Midwestern agricultural drainage. Water Resources and Economics 2013;2–3:30–56. https://doi.org/10.1016/j.wre.2013.09.001.

[153] Christianson L. Nitrogen Loss Reduction Practices: What Do They Cost? Farmdoc Daily 2018;8.

[154] Christianson LE. Woodchip Bioreactor: A science-based option to reduce nitrate loss 2018. http://draindrop.cropsci.illinois.edu/wp-content/uploads/2019/12/Christianson-et-al_2018_Woodchip-Bioreactor_2pg-Factsheet.pdf (accessed June 12, 2023).

[155] Gu B, Zhang X, Lam SK, Yu Y, van Grinsven HJM, Zhang S, et al. Cost-effective mitigation of nitrogen pollution from global croplands. Nature 2023;613:77–84. https://doi.org/10.1038/s41586-022-05481-8.

[156] Zhou Q, Sun H, Jia L, Wu W, Wang J. Simultaneous biological removal of nitrogen and phosphorus from secondary effluent of wastewater treatment plants by advanced treatment: A review. Chemosphere 2022;296:134054. https://doi.org/10.1016/j.chemosphere.2022.134054.

[157] Jaynes DB, Isenhart TM. Performance of Saturated Riparian Buffers in Iowa, USA. Journal of Environmental Quality 2019;48:289–96. https://doi.org/10.2134/jeq2018.03.0115.

[158] Jaynes DB, Isenhart TM. Reconnecting Tile Drainage to Riparian Buffer Hydrology for Enhanced Nitrate Removal. Journal of Environmental Quality 2014;43:631–8. https://doi.org/10.2134/jeq2013.08.0331.

[159] Utt N, Jaynes D, Albertsen J. Demonstrate and Evaluate Saturated Buffers at Field Scale to Reduce Nitrates and Phosphorus from Subsurface Field Drainage Systems. 2015.

[160] Iowa Department of Agriculture and Land Stewardship, Iowa Department of Natural Resources, Iowa State University. Iowa Nutrient Reduction Strategy 2018-19 Annual Progress Report. 2020.

[161] Harrold J. Indiana's State Nutrient Reduction Strategy. 2021.

[162] Arkansas Department of Agriculture Natural Resources Division. 2022 Arkansas Nutrient Reduction Strategy. 2022.

[163] Iowa State University. Reducing Nutrient Loss: Science Shows What Works 2017. https://www.cals.iastate.edu/files/misc/183758/reducing-nutrient-loss-science-shows-what-works.pdf (accessed August 1, 2023).

[164] Soil and Water Outcomes Fund. Soil and Water Outcomes Fund Produces More Than Tenfold Increase in Environmental Outcomes in 2021. Soil and Water Outcomes Fund 2021. https://theoutcomesfund.com/news-release-2021-environmental-outcomes (accessed July 25, 2023).

[165] United States Department of Agriculture. 2022 USDA/NASS QuickStats Land Rent Costs 2022. https://quickstats.nass.usda.gov/results/58B27A06-F574-315B-A854-9BF568F17652#7878272B-A9F3-3BC2-960D-5F03B7DF4826 (accessed July 25, 2023).

[166] Wernet G, Bauer C, Steubing B, Reinhard J, Moreno-Ruiz E, Weidema B. The ecoinvent database version 3 (part I): overview and methodology. Int J Life Cycle Assess 2016;21:1218–30. https://doi.org/10.1007/s11367-016-1087-8.

[167] Bare J, Young D, Qam S, Hopton M, Chief S. Tool for the Reduction and Assessment of Chemical and other Environmental Impacts (TRACI). US Environmental Protection Agency: Washington, DC, USA 2012.

[168] IPCC. 2006 IPCC Guidelines for National Greenhouse Gas Inventories 2006. https://www.ipcc-nggip.iges.or.jp/public/2006gl/index.html (accessed January 10, 2023).

[169] Nakagaki N, Wieczorek M, Qi SL. Estimates of Subsurface Tile Drainage Extent for the Conterminous United States, early 1990s 2016. https://doi.org/10.5066/F7RB72QS.

[170] Sugg Z. Assessing U.S. Farm Drainage. 2007.

[171] United States Department of Agriculture. National Agricultural Statistics Service: Quick Stats 2022.

[172] United States Department of Agriculture National Agricultural Statistics Service. Iowa Ag News - Farms and Land in Farms. 2021.

[173] US EPA. Estimated Total Nitrogen and Total Phosphorus Loads and Yields Generated within States 2023. https://www.epa.gov/nutrient-policy-data/estimated-total-nitrogen-and-total-phosphorus-loads-and-yields-generated (accessed July 18, 2023).

[174] Ator SW. Spatially referenced models of streamflow and nitrogen, phosphorus, and suspended-sediment loads in streams of the northeastern United States. vol. 2019–5118. Reston, VA: U.S. Geological Survey; 2019. https://doi.org/10.3133/sir20195118.

[175] Hoos AB, Roland II VL. Spatially referenced models of streamflow and nitrogen, phosphorus, and suspended-sediment loads in the southeastern United States. vol. 2019–5135. Reston, VA: U.S. Geological Survey; 2019. https://doi.org/10.3133/sir20195135.

[176] Saad DA, Robertson DM. SPARROW model inputs and simulated streamflow, nutrient and suspended-sediment loads in streams of the Midwestern United States, 2012 Base Year 2020. https://doi.org/10.5066/P93QMXC9.

[177] Wise DR, Anning DW, Miller OL. Spatially referenced models of streamflow and nitrogen, phosphorus, and suspended-sediment transport in streams of the southwestern United States. vol. 2019–5106. Reston, VA: U.S. Geological Survey; 2019. https://doi.org/10.3133/sir20195106.

[178] Wise DR. Spatially referenced models of streamflow and nitrogen, phosphorus, and suspended-sediment loads in streams of the Pacific region of the United States. vol. 2019–5112. Reston, VA: U.S. Geological Survey; 2019. https://doi.org/10.3133/sir20195112.

[179] Fasihi M, Efimova O, Breyer C. Techno-economic assessment of CO2 direct air capture plants. Journal of Cleaner Production 2019;224:957–80. https://doi.org/10.1016/j.jclepro.2019.03.086.

[180] Ghernaout D. Short Communication: Requiring Reverse Osmosis Membranes Modifications – An Overview. AJCHE 2017;5:81. https://doi.org/10.11648/j.ajche.20170504.15.

[181] Tałałaj IA, Biedka P, Bartkowska I. Treatment of landfill leachates with biological pretreatments and reverse osmosis. Environ Chem Lett 2019;17:1177–93. https://doi.org/10.1007/s10311-019-00860-6.

[182] Piris-Cabezas P, Lubowski RN, Leslie G. Estimating the potential of international carbon markets to increase global climate ambition. World Development 2023;167:106257. https://doi.org/10.1016/j.worlddev.2023.106257.

[183] Groom B, Venmans F. The social value of offsets. Nature 2023:1–6. https://doi.org/10.1038/s41586-023-06153-x.

[184] Nielsen-Pincus M, Moseley C. The Economic and Employment Impacts of Forest and Watershed Restoration. Restoration Ecology 2013;21. https://doi.org/10.1111/j.1526-100X.2012.00885.x.

[185] Limb BJ, Quinn JC, Johnson A, Sowby RB, Thomas E. Results Dataset for Greening America's Rivers: The Potential of Climate Financing for Nature-Based Water Quality Improvement 2024. https://doi.org/10.5281/zenodo.10456151.

[186] Limb B. bradenlimb/Green-Wastewater-Treatment: Green Wastewater Treatment Code v1.0.0 2024. https://doi.org/10.5281/zenodo.10790349.

[187] Limb BJ, Smith JP, Simske SJ, Quinn JC. Estimating geographic origins of corn and soybean biomass for biofuel production: A detailed dataset. Data in Brief 2024;54:110291. https://doi.org/10.1016/j.dib.2024.110291.

[188] United States Department of Agriculture. National Agricultural Statistics Service: Quick Stats 2023. https://quickstats.nass.usda.gov/ (accessed August 15, 2022).

[189] Greene JM, Quiroz D, Compton S, Lammers PJ, Quinn JC. A validated thermal and biological model for predicting algal productivity in large scale outdoor cultivation systems. Algal Research 2021;54:102224. https://doi.org/10.1016/j.algal.2021.102224.

[190] Quiroz D, Greene JM, McGowen J, Quinn JC. Geographical assessment of open pond algal productivity and evaporation losses across the United States. Algal Research 2021;60:102483. https://doi.org/10.1016/j.algal.2021.102483.

[191] Daioglou V, Woltjer G, Strengers B, Elbersen B, Barberena Ibañez G, Sánchez Gonzalez D, et al. Progress and barriers in understanding and preventing indirect land-use change. Biofuels, Bioproducts and Biorefining 2020;14:924–34. https://doi.org/10.1002/bbb.2124.

[192] USDA. USDA Forest Service FSGeodata Clearinghouse - Download National Datasets 2023. https://data.fs.usda.gov/geodata/edw/datasets.php (accessed September 14, 2023).

[193] Bessaad A, Bilger I, Korboulewsky N. Assessing Biomass Removal and Woody Debris in Whole-Tree Harvesting System: Are the Recommended Levels of Residues Ensured? Forests 2021;12:807. https://doi.org/10.3390/f12060807.

[194] Dumortier J, Elobeid A, Carriquiry M. Light-duty vehicle fleet electrification in the United States and its effects on global agricultural markets. Ecological Economics 2022;200:107536. https://doi.org/10.1016/j.ecolecon.2022.107536.

[195] Dewitz J. National Land Cover Database (NLCD) 2021 Products 2023. https://doi.org/10.5066/P9JZ7AO3.

[196] UNEP-WCMC. Protected Area Profile for United States of America from the World Database on Protected Areas. Protected Planet 2022. https://www.protectedplanet.net/country/USA (accessed October 11, 2022).

[197] IUCN Species Survival Commission, IUCN World Commission on Protected Areas, IUCN Global Species Programme. A Global Standard for the Identification of Key Biodiversity Areas. vol. 1.0. Gland, Switzerland and Cambridge, UK: International Union for Conservation of Nature and Natural Resources; 2016.

[198] United States Department of Agriculture. Conservation Practice Standard Stripcropping (Code 585) 2017.

[199] Miller G. Corn Suitability Ratings - An Index to Soil Productivity 2012.

[200] Northwest Natural Resource Group. A Field Guide to Harvest Equipment - Northwest Natural Resource Group 2021. https://www.nnrg.org/a-field-guide-to-harvest-equipment/ (accessed May 28, 2024).

[201] University of Washington Forest Engineering Senior Class, Spring 2003. Developing a Road System Strategy for the Tahoma State Forest. 2003.

[202] West T, Sessions J, Strimbu BM. Steep Slope Harvest System Models for Small to Large Trees. Forests 2022;13:305. https://doi.org/10.3390/f13020305.

[203] U.S., United States Geological Survey 3D Elevation Program. LANDFIRE Program: Data Products - Topographic - Slope Percent Rise n.d. https://www.landfire.gov/slope.php (accessed October 15, 2022).

[204] Esri. USA Counties 2022. https://hub.arcgis.com/datasets/esri::usa-counties/explore?location=24.781154,56.950742,4.00 (accessed July 7, 2022).

[205] Spawn SA, Sullivan CC, Lark TJ, Gibbs HK. Harmonized global maps of above and belowground biomass carbon density in the year 2010. Sci Data 2020;7:112. https://doi.org/10.1038/s41597-020-0444-4.

[206] Food and Agriculture Organization of the United Nations. Global Ecological Zones (second edition) - FAO 2012. https://data.apps.fao.org/map/catalog/srv/eng/catalog.search?id=47105&fname=gez2010.zip&access=private#/metadata/2fb209d0-fd34-4e5e-a3d8-a13c241eb61b (accessed January 19, 2023).

[207] Niels H Batjes. IPCC default soil classes derived from the Harmonized World Soil Data Base, version 1.2. 2021.

[208] Beal CM, Cuellar AD, Wagner TJ. Sustainability assessment of alternative jet fuel for the U.S. Department of Defense. Biomass and Bioenergy 2021;144:105881. https://doi.org/10.1016/j.biombioe.2020.105881.

[209] Plastina A. Estimated Costs of Crop Production in Iowa - 2018 2018.

[210] Wright S, Klonsky K, Stewart D. 2015 Sample Costs to Produce Field Corn in the San Joaquin Valley - South 2015.

[211] Perdue S, Hamer H. 2017 Census of Agriculture - United States - Summary and State Data - Volume 1 • Geographic Area Series • Part 51. 2019.

[212] Bigelow D, Borchers A, Hubbs T. U.S. Farmland Ownership, Tenure, and Transfer. 2016.

[213] Chen M, Smith PM. The U.S. cellulosic biofuels industry: Expert views on commercialization drivers and barriers. Biomass and Bioenergy 2017;102:52–61. https://doi.org/10.1016/j.biombioe.2017.05.002.

[214] Duffy MD. Estimated Costs for Production, Storage and Transportation of Switchgrass | Ag Decision Maker 2008.

[215] Hoque M, Artz G, Hart C. Estimated Cost of Establishment and Production of Miscanthus in Iowa | Ag Decision Maker. Iowa State University; 2014.

[216] Moore CE, von Haden AC, Burnham MB, Kantola IB, Gibson CD, Blakely BJ, et al. Ecosystem-scale biogeochemical fluxes from three bioenergy crop candidates: How energy sorghum compares to maize and miscanthus. GCB Bioenergy 2021;13:445–58. https://doi.org/10.1111/gcbb.12788.

[217] Buchman D, Jackson J, Berguson WE, McMahon BG, Nelson ND, DuPlissis J, et al. Grower's Guide for Hybrid Poplar Plantations for Biomass Production 2020.

[218] Heavey JP, Volk TA. Shrub Willow Fact Sheet Series: Planting and Maintenance 2016.

[219] McAloon A, Taylor F, Yee W. Determining the Cost of Producing Ethanol from Corn Starch and Lignocellulosic Feedstocks 2000.

[220] Cheng M-H, Rosentrater KA. Economic feasibility analysis of soybean oil production by hexane extraction. Industrial Crops and Products 2017;108:775–85. https://doi.org/10.1016/j.indcrop.2017.07.036.

[221] Swanson RM, Platon A, Satrio JA, Brown RC, Hsu DD. Techno-Economic Analysis of Biofuels Production Based on Gasification. National Renewable Energy Lab. (NREL), Golden, CO (United States); 2010. https://doi.org/10.2172/994017.

[222] Jiang Y, Jones SB, Zhu Y, Snowden-Swan L, Schmidt AJ, Billing JM, et al. Techno-economic uncertainty quantification of algal-derived biocrude via hydrothermal liquefaction. Algal Research 2019;39:101450. https://doi.org/10.1016/j.algal.2019.101450.

[223] Zhu Y, Biddy MJ, Jones SB, Elliott DC, Schmidt AJ. Techno-economic analysis of liquid fuel production from woody biomass via hydrothermal liquefaction (HTL) and upgrading. Applied Energy 2014;129:384–94. https://doi.org/10.1016/j.apenergy.2014.03.053.

[224] Tao L, Markham JN, Haq Z, Biddy MJ. Techno-economic analysis for upgrading the biomass-derived ethanol-to-jet blendstocks. Green Chem 2017;19:1082–101. https://doi.org/10.1039/C6GC02800D.

[225] Michaga MFR, Michailos S, Hughes KJ, Ingham D, Pourkashanian M. Techno-economic and life cycle assessment review of sustainable aviation fuel produced via biomass gasification. Sustainable Biofuels, Elsevier; 2021, p. 269–303. https://doi.org/10.1016/B978-0-12-820297-5.00012-8.

[226] Limb BJ, Smith J, Simske S, Quinn JC. Results Dataset for Addressing the SAF Grand Challenge: Economic and Environmental Insights from Feedstock Optimization 2024. https://doi.org/10.5281/zenodo.11521694.

[227] United States Department of Agriculture. 2023 USDA/NASS QuickStats County Land Rent Costs 2023. https://quickstats.nass.usda.gov/results/20A3FB36-FC5E-3D17-B9C2-110461C5D4F4 (accessed September 12, 2023).

[228] United States Department of Agriculture. 2023 USDA/NASS QuickStats State Land Rent Costs 2023. https://quickstats.nass.usda.gov/results/58B27A06-F574-315B-A854-9BF568F17652#7878272B-A9F3-3BC2-960D-5F03B7DF4826 (accessed September 12, 2023).

[229] U.S. Energy Information Administration. US Electricity Profile 2021 2022. https://www.eia.gov/electricity/state/archive/2021/index.php (accessed June 3, 2024).

[230] U.S. Energy Information Administration. Natural Gas Summary - Industrial Price 2024. https://www.eia.gov/dnav/ng/ng_sum_lsum_a_EPG0_PIN_DMcf_a.htm (accessed May 31, 2024).

[231] U.S. Energy Information Administration. U.S. Gasoline and Diesel Retail Prices 2024. https://www.eia.gov/dnav/pet/pet_pri_gnd_dcus_nus_a.htm (accessed May 31, 2024).

[232] U.S. Energy Information Administration. Glossary - U.S. Energy Information Administration (EIA) 2024. https://www.eia.gov/tools/glossary/index.php (accessed June 1, 2024).

[233] U.S. Energy Information Administration. Wholesale Propane Weekly Heating Oil and Propane Prices 2024. https://www.eia.gov/dnav/pet/pet_pri_wfr_a_EPLLPA_PWR_dpgal_w.htm (accessed June 1, 2024).

[234] IPCC. Climate Change 2022: Impacts, Adaptation and Vulnerability 2022.

[235] Baral A, Malins C. Comprehensive carbon accounting for identification of sustainable biomass feedstocks 2014.

[236] American Center for Life Cycle Assessment. ACLCA Guidance to Calculating Non-LCIA Inventory Metrics in Accordance with ISO 21930:2017. 2019.

[237] Brandao M, Heijungs R, Cowie AR. On quantifying sources of uncertainty in the carbon footprint of biofuels: crop/feedstock, LCA modelling approach, land-use change, and GHG metrics. Biofuel Research Journal 2022;9:1608–16. https://doi.org/10.18331/BRJ2022.9.2.2.

[238] Searchinger T, Heimlich R, Houghton RA, Dong F, Elobeid A, Fabiosa J, et al. Use of U.S. Croplands for Biofuels Increases Greenhouse Gases Through Emissions from Land-Use Change. Science 2008;319:1238–40. https://doi.org/10.1126/science.1151861.

[239] Finkbeiner M. Indirect land use change – Help beyond the hype? Biomass and Bioenergy 2014;62:218–21. https://doi.org/10.1016/j.biombioe.2014.01.024.

[240] Lark TJ, Hendricks NP, Smith A, Pates N, Spawn-Lee SA, Bougie M, et al. Environmental outcomes of the US Renewable Fuel Standard. Proc Natl Acad Sci USA 2022;119:e2101084119. https://doi.org/10.1073/pnas.2101084119.

[241] Wang M, Elgowainy A, Lee U, Baek KH, Bafana A, Benavides PT, et al. Summary of Expansions and Updates in GREET® 2022. Argonne National Laboratory (ANL), Argonne, IL (United States); 2022. https://doi.org/10.2172/1891644.

[242] Kwon H, Liu X, Dunn JB, Mueller S, Wander MM, Wang M. Carbon Calculator for Land Use and Land Management Change from Biofuels Production (CCLUB) Manual (Rev. 7). 2021.

[243] Kent J, Hartman MD, Lee DK, Hudiburg T. Simulated Biomass Sorghum GHG Reduction Potential is Similar to Maize. Environ Sci Technol 2020;54:12456–66. https://doi.org/10.1021/acs.est.0c01676.

[244] Handler RM, Shi R, Shonnard DR. Land use change implications for large-scale cultivation of algae feedstocks in the United States Gulf Coast. Journal of Cleaner Production 2017;153:15–25. https://doi.org/10.1016/j.jclepro.2017.03.149.

[245] U.S. Energy Information Administration. U.S. Kerosene-Type Jet Fuel Wholesale/Resale Price by Refiners (Dollars per Gallon) 2022. https://www.eia.gov/dnav/pet/hist/LeafHandler.ashx?n=PET&s=EMA_EPJK_PWG_NUS_DPG&f=M (accessed May 31, 2024).

[246] USDA/NASS QuickStats Ad-hoc Query Tool n.d. https://quickstats.nass.usda.gov/results/6D3F1A5B-2DC6-3D9B-B4A6-E0CBA61EBABB (accessed July 19, 2023).

[247] Ersi Data and Maps. USA Airports 2023.

[248] United States Department of Agriculture. Grain Truck and Ocean Rate Advisory 2023. https://www.ams.usda.gov/sites/default/files/media/GTOR1stQtr2023.pdf (accessed October 9, 2023).

[249] Distributed Evolutionary Algorithms in Python · GitHub n.d. https://github.com/DEAP (accessed May 2, 2024).

[250] Taheripour F, Sajedinia E, Karami O. Oilseed Cover Crops for Sustainable Aviation Fuels Production and Reduction in Greenhouse Gas Emissions Through Land Use Savings. Frontiers in Energy Research 2022;9.

[251] Field JL, Zhang Y, Marx E, Boote KJ, Easter M, George S, et al. Modeling Yield, Biogenic Emissions, and Carbon Sequestration in Southeastern Cropping Systems With Winter Carinata. Frontiers in Energy Research 2022;10.

[252] Bonabeau E. Agent-based modeling: Methods and techniques for simulating human systems. Proc Natl Acad Sci USA 2002;99:7280–7. https://doi.org/10.1073/pnas.082080899.

[253] Lan K, Yao Y. Integrating Life Cycle Assessment and Agent-Based Modeling: A Dynamic Modeling Framework for Sustainable Agricultural Systems. Journal of Cleaner Production 2019;238:117853. https://doi.org/10.1016/j.jclepro.2019.117853.

[254] Yang P, Cai X, Hu X, Zhao Q, Lee Y, Khanna M, et al. An agent-based modeling tool supporting bioenergy and bio-product community communication regarding cellulosic bioeconomy development. Renewable and Sustainable Energy Reviews 2022;167:112745. https://doi.org/10.1016/j.rser.2022.112745.

[255] Seymour K, Held M, Stolz B, Georges G, Boulouchos K. Future costs of power-to-liquid sustainable aviation fuels produced from hybrid solar PV-wind plants in Europe. Sustainable Energy & Fuels 2024;8:811–25. https://doi.org/10.1039/D3SE00978E.

[256] Foley JA, DeFries R, Asner GP, Barford C, Bonan G, Carpenter SR, et al. Global Consequences of Land Use. Science 2005;309:570–4. https://doi.org/10.1126/science.1111772.

[257] Moss B. Water pollution by agriculture. Philos Trans R Soc Lond B Biol Sci 2008;363:659–66. https://doi.org/10.1098/rstb.2007.2176.

[258] Grim RG, Tao L, Abdullah Z, Cortright R, Oakleaf B. The Challenge Ahead: A Critical Perspective on Meeting U.S. Growth Targets for Sustainable Aviation Fuel. 2024. https://doi.org/10.2172/2331423.

[259] Temple J. Why new ethanol aviation fuel tax subsidies aren't a clear climate win. MIT Technology Review 2024.

[260] Bioenergy Technologies Office. World's First Ethanol-To-Jet Fuel Plant Paves the Way for Commercial Production of Sustainable Aviation Fuels. EnergyGov 2024. https://www.energy.gov/eere/bioenergy/articles/worlds-first-ethanol-jet-fuel-plant-paves-way-commercial-production (accessed May 30, 2024).

[261] Alewell C, Ringeval B, Ballabio C, Robinson DA, Panagos P, Borrelli P. Global phosphorus shortage will be aggravated by soil erosion. Nat Commun 2020;11:4546. https://doi.org/10.1038/s41467-020-18326-7.

[262] Agri Drain Corporation. Inline Water Level Control Structure n.d.

[263] United States Department of Agriculture. Conservation Practice Standard Saturated Buffer (Code 604) 2020.

[264] The Board of Regents of the University of Nebraska. How to properly apply nitrogen fertilizer n.d. https://water.unl.edu/documents/Section%20G.pdf (accessed August 7, 2023).

[265] Lemus R. Annual Ryegrass Performance in Mississippi: Long-Term Yield Production n.d.

[266] Zhu Y, Tjokro Rahardjo SA, Valkenburt C, Snowden-Swan LJ, Jones SB, Machinal MA. Techno-economic analysis for the thermochemical conversion of biomass to liquid fuels. Pacific Northwest National Lab.(PNNL), Richland, WA (United States); 2011.

[267] Haarlemmer G, Boissonnet G, Imbach J, Setier P-A, Peduzzi E. Second generation BtL type biofuels – a production cost analysis. Energy Environ Sci 2012;5:8445–56. https://doi.org/10.1039/C2EE21750C.

[268] Tunå P, Hulteberg C. Woody biomass-based transportation fuels – A comparative techno-economic study. Fuel 2014;117:1020–6. https://doi.org/10.1016/j.fuel.2013.10.019.

[269] Sarkar S, Kumar A, Sultana A. Biofuels and biochemicals production from forest biomass in Western Canada. Energy 2011;36:6251–62. https://doi.org/10.1016/j.energy.2011.07.024.

[270] Anex RP, Aden A, Kazi FK, Fortman J, Swanson RM, Wright MM, et al. Techno-economic comparison of biomass-to-transportation fuels via pyrolysis, gasification, and biochemical pathways. Fuel 2010;89:S29–35. https://doi.org/10.1016/j.fuel.2010.07.015.

[271] Meerman JC, Ramírez A, Turkenburg WC, Faaij APC. Performance of simulated flexible integrated gasification polygeneration facilities, Part B: Economic evaluation. Renewable and Sustainable Energy Reviews 2012;16:6083–102. https://doi.org/10.1016/j.rser.2012.06.030.

[272] Huang E, Zhang X, Rodriguez L, Khanna M, de Jong S, Ting KC, et al. Multi-objective optimization for sustainable renewable jet fuel production: A case study of corn stover based supply chain system in Midwestern U.S. Renewable and Sustainable Energy Reviews 2019;115:109403. https://doi.org/10.1016/j.rser.2019.109403.

[273] Crawford JT, Shan CW, Budsberg E, Morgan H, Bura R, Gustafson R. Hydrocarbon bio-jet fuel from bioconversion of poplar biomass: techno-economic assessment. Biotechnol Biofuels 2016;9:141. https://doi.org/10.1186/s13068-016-0545-7.

[274] Michailos S, Bridgwater A. A comparative techno-economic assessment of three bio-oil upgrading routes for aviation biofuel production. International Journal of Energy Research 2019;43:7206–28. https://doi.org/10.1002/er.4745.

[275] Alves CM, Valk M, De Jong S, Bonomi A, Van Der Wielen LAM, Mussatto SI. Techno-economic assessment of biorefinery technologies for aviation biofuels supply chains in Brazil. Biofuels Bioprod Bioref 2017;11:67–91. https://doi.org/10.1002/bbb.1711.

[276] IPCC. 2019 Refinement to the 2006 IPCC Guidelines for National Greenhouse Gas Inventories - Chapter 11 - N2O Emissions from Managed Soils, and CO2 Emissions from Lime and Urea Application 2019.

[277] Moore CE, von Haden AC, Burnham MB, Kantola IB, Gibson CD, Blakely BJ, et al. Ecosystem-scale biogeochemical fluxes from three bioenergy crop candidates: How energy sorghum compares to maize and miscanthus. GCB Bioenergy 2021;13:445–58. https://doi.org/10.1111/gcbb.12788.

[278] Moretti C, López-Contreras A, de Vrije T, Kraft A, Junginger M, Shen L. From agricultural (by-)products to jet fuels: Carbon footprint and economic performance. Science

of The Total Environment 2021;775:145848.
https://doi.org/10.1016/j.scitotenv.2021.145848.

[279] Huq NA, Hafenstine GR, Huo X, Nguyen H, Tifft SM, Conklin DR, et al. Toward net-zero sustainable aviation fuel with wet waste–derived volatile fatty acids. Proceedings of the National Academy of Sciences 2021;118:e2023008118.
https://doi.org/10.1073/pnas.2023008118.

APPENDIX A

Appendix A Nomenclature

Variable	Description	Units
AECI	Annual Electricity Cost Increase	$ yr^{-1}
AFCI	Annual Fuel Cost Increase	$ yr^{-1}
AFOMC	Annual Fixed Operating and Maintenance Cost	$ yr^{-1}
B31B	NGCC + CCS power plant specified by NETL	-
CAISO	California Independent System Operator	-
CAP	Capital Investment	$
CBR	Construction Build Rate	% yr^{-1}
CC	Capital Cost	$
CCS	Carbon Capture and Storage	-
CIR	Construction Interest Rate	%
Comb	Combustor	
Cond. Pump	Condensate Pump	
Comp	Compressor	
CPD	Charging Power Decrease	MW
CS	Cold Storage	
CT	Cooling Tower	
DAC	Direct Air Capture	-
DCPD	Discharging Emissions Capture Percent Decrease	%
DF	Discount Factor	-
DFI	Discharging Fuel Increase	kg s^{-1}
DPI	Discharging Power Increase	MW
EC	Emissions Cost	$
ECC	Capital Cost All Equipment Other than Storage Mediums	$
ECP	Emissions Capture Percent	%
EES	Engineering Equation Solver	-
EF	Percent of Total Capital Paid in Equity	%
EQ	Equity	$
FC	Fuel Consumption	kg s^{-1}
FOM	Fixed Operating and Maintenance	-
FOMC	Fixed Operating and Maintenance Costs	$ yr^{-1}
GT	Gas Turbine	
HPHX	High-Pressure Heat Exchanger	
HPP	High-Pressure Pump	
HS	Hot Storage	
HRSG	Heat Recovery Steam Generator	-
INT	Interest	$
IPHX	Intermediate-Pressure Heat Exchanger	
IPP	Intermediate-Pressure Pump	

IPR	Intermediate Pressure Reheater	-
IPRH	Intermediate-Pressure Reheater	
IPT	Intermediate-Pressure Turbine	
LF	Percent of Capital Paid by Loan	%
LIR	Loan Interest Rate	%
LPCP	Loan Principle	$
LPEC	Low-Pressure Economizer	
LPHX	Low-Pressure Heat Exchanger	
LPMT	Loan Payment	$ yr^{-1}
LPT	Low-Pressure Turbine	
$\dot{m}$	Mass Flowrate	kg s^{-1}
MACRS	Modified Accelerated Cost Recovery System	-
MDR	MACRS Depreciation Rate	% yr^{-1}
NETL	National Energy Technology Laboratory	-
NGCC	Natural Gas Combined Cycle	-
NPV	Net Present Value	$
NYISO	New York Independent System Operator	
P	Pressure	kPa
PO	Power Output	MW
Pu	Pump	
$\dot{Q}$	Heat Transfer/Heat Duty	kW
REV	Revenue	$
SCC	Storage Medium Capital Cost	$ hr^{-1}
T	Temperature	°C
TAEC	Total Annual Emissions Cost	$ yr^{-1}
TAF	Total Annual Fuel Consumed	kg
TAR	Total Annual Revenue	$ yr^{-1}
TAVOMC	Total Annual Variable Operating and Maintenance Cost	$ yr^{-1}
TAX	Tax Amount Paid	$
TCC	Total Capital Cost	$
TES	Thermal Energy Storage	-
TI	Taxable Income	$
TR	Tax Rate	%
VOM	Variable Operating and Maintenance	-
VOMC	Variable Operating and Maintenance Costs	$ MWh^{-1}
$\dot{W}$	Mechanical Power	kW
X	Thermodynamic Quality	
Greek Symbols		
η	Efficiency	%
Subscripts		
a	Air	
AUX	Auxiliary	
BP	Base Plant	
CP	Condensate Pump	

CS	Cold Storage	
CSC	Cold Storage Charging	
CSD	Cold Storage Discharging	
CST	Cold Storage Technology	
f	Fuel	
g	Flue Gas	
GC	Gas Compressor	
GT	Gas Turbine	
HPP	High Pressure Pump	
HPT	High Pressure Turbine	
HRSG	Heat Recovery Steam Generator	
HS	Hot Storage	
HSC	Hot Storage Charging	
HSD	Hot Storage Discharging	
HSSG	Hot Storage Steam Generator	
HST	Hot Storage Technology	
I	Inlet	
IPP	Intermediate Pressure Pump	
IPT	Intermediate Pressure Turbine	
k	Designates a Given Year	
LPT	Low Pressure Turbine	
N	Neutral Operation Mode	
net	Net	
NGCC	Natural Gas Combined Cycle	
NPV	Designates a Component of the Net Present Value	
O	Outlet	
P	Pump	
SCP	Condensate Pump in the Base Plant Steam Cycle	
ST	Steam Turbine	

Modeling Assumptions

The following modeling assumptions were used for all technology configurations discussed in this paper and included in Appendix A:

1. Constant air volumetric flowrate
2. Constant ambient air temperature (15°C)
3. Constant compressor pressure ratios
4. Constant isentropic efficiency for each component (see power flow table below)

5. Constant combustor temperature
6. Constant reboiler duty in the CCS unit
7. No pressure drop occurs in the combustor, preheater, low pressure economizer, condenser, and configuration specific heat exchangers
8. Flue gas has the same thermodynamic properties as air
9. Five HRSG heat exchangers are used in lieu of the 19 specified on the NETL 2019 report for Case B31B. A surrogate HRSG model was used to validate the simplified model. HRSG temperature profiles of the surrogate model are included

Economic Modeling Details and Governing Equations

A discounted cash flow approach was needed to complete the 30-year NPV analysis.

Table A1 presents the economic assumptions used in this approach. A 3-year build period was assumed to occur before the start of the 30-year plant operation. Twenty percent of the plant capital costs is assumed to be paid in equity during the build period. A loan amount is then calculated to pay of the remaining capital throughout the lifetime of the plant. The revenue, fuel costs, emissions costs, FOM costs, and VOM costs determined in the optimization model in the first year of operation are used to determine the cash flow for the remaining years.

Table A1. Economic Assumptions

Item	Value	Units	Source
Loan Interest Rate	5.0	%	ATB
Loan Term	30	Years	ATB
Financed Amount	80	%	ATB
Equity Amount	20	%	ATB
Construction Interest Rate	3.5	%	ATB
Construction Period	3.0	Years	ATB
Construction Build Rate	80, 10, 10	%	ATB
MACRS Depreciation	15	Years	ATB
Tax Rate (Federal and State)	25	%	ATB
Internal Rate of Return	10	%	ATB

Natural Gas Price Increase	3.5	%/year	EIA
Electricity Price Increase	2.2	%/year	EIA

Equation (A.1) is used to determine the discount factor for each year in the analysis given the internal rate of return specified in

Table A1.

$$DF_k = \frac{1}{(1+IRR)^k} \quad \text{(A.1)}$$

The non-discounted revenue and fuel costs during the first year of plant operation are equal to the total annual revenue and total annual fuel costs, as shown in equations (A.2) and (A.3) respectively.

$$REV_{k=1} = TAR \quad \text{(A.2)}$$

$$FC_{k=1} = TAF \quad \text{(A.3)}$$

The non-discounted revenue and fuel costs are determined for the remaining twenty-nine years using the estimated annual increase in revenue and fuel costs specified in Table A1 and are calculated in equations (A.4) and (A.5) respectively.

$$REV_k = REV_{k-1}(1 + AECI) \quad \text{(A.4)}$$

$$FC_k = FC_{k-1}(1 + AFCI) \quad \text{(A.5)}$$

The non-discounted emissions costs, FOM costs, and VOM costs are set equal to the total annual emissions cost, the annual FOM cost, and the total annual VOM cost respectively for all 30 years of operation, as shown in equations (A.6) through (A.8).

$$EC_k = TAE\text{C} \quad \text{(A.6)}$$

$$FOMC_k = AFOMC \quad \text{(A.7)}$$

$$VOMC_k = TAVOMC \tag{A.8}$$

The discounted revenue, fuel cost, emissions cost, FOM cost, and VOM cost for the entire plant life are calculated using equations (A.9) through (A.13) respectively.

$$REV_{NPV} = \sum_{k=1}^{30} REV_k * DF_k \tag{A.9}$$

$$FC_{NPV} = \sum_{k=1}^{30} FC_k * DF_k \tag{A.10}$$

$$EC_{NPV} = \sum_{k=1}^{30} EC_k * DF_k \tag{A.11}$$

$$FOMC_{NPV} = \sum_{k=1}^{30} FOMC_k * DF_k \tag{A.12}$$

$$VOMC_{NPV} = \sum_{k=1}^{30} VOMC_k * DF_k \tag{A.13}$$

The total amount paid in equity is determined using equation (A.14) and the total interest paid during the construction period is determined using equation (A.15). The total capital cost contribution to NPV is assumed to be the sum of the equity and interest paid, as shown in equation (A.16).

$$EQ_{NPV} = TCC * EF * \sum_{k=-2}^{0} CBR_k * DF_k \tag{A.14}$$

$$INT_{NPV} = TCC * LF * CIR * \sum_{k=1}^{30} CBR_k * DF_k \tag{A.15}$$

$$CAP_{NPV} = EQ_{NPV} + INT_{NPV} \tag{A.16}$$

The annual non-discounted loan payment is determined using equation (A.17). The amount of loan principle is determined using equations (A.18) and (A.19). The discounted loan amount used for the NPV calculation is determined using equation (A.20).

$$LPMT = \frac{TCC*LIR*LF}{(1-LIR)^{-30}} \tag{A.17}$$

$$LPCP_{k=1} = LPMT * 30 \quad \text{(A.18)}$$

$$LPCP_k = LPCP_{k-1} - LPMT \quad \text{(A.19)}$$

$$LPMT_{NPV} = \sum_{k=1}^{30} LPMT * DF_k \quad \text{(A.20)}$$

The taxable income is determined using the annual non-discounted revenue and costs, as shown in equation (A.21). The tax paid contributing to the NPV calculation is determined using equation (A.22).

$$TI_k = REV_k - FC_k - EC_k - VOM_k - LIR * LPCP_k - MDR_k * TCC \quad \text{(A.21)}$$

$$TAX_{NPV} = TR * \sum_{k=1}^{30} TI_k * DF_k \quad \text{(A.22)}$$

The NPV is determined by subtracting each contributing discounted cost from the discounted revenue, as shown in equation (A.23).

$$NPV = REV_{NPV} - FC_{NPV} - EC_{NPV} - FOMC_{NPV} - VOMC_{NPV} - CAP_{NPV} - LPMT_{NPV} - TAX_{NPV} \quad \text{(A.23)}$$

Technology Modeling Details and Governing Equations

The technology configurations analyzed in this research use NETL case B31B NGCC+CCS power plant as a starting point. This powerplant was first replicated in EES so that the implications of each thermal storage design could be accurately understood. Figure A1 shows a process flow diagram of the base case B31B power plant as it is modeled in EES including temperature, pressure, quality, and mass flow rates at various points throughout the system.

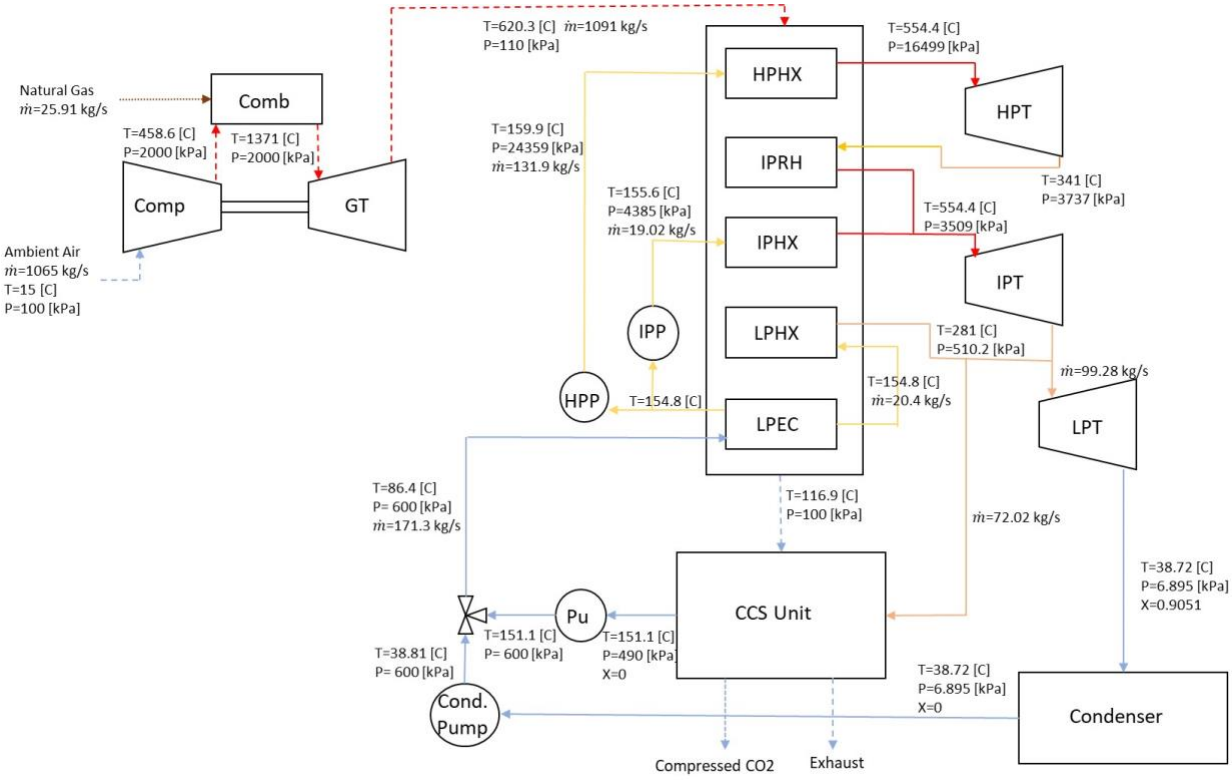

Figure A1. Model flow diagram for the NGCC+CCS base power plant (NETL Case B31B) including temperature, pressure, quality, and mass flow rates at various points throughout the system.

The model consists of a gas cycle, a steam cycle, and the CANSOLV carbon capture unit. The gas cycle includes the gas compressor, combustor, gas turbine, and HRSG. In this cycle, ambient air is compressed in the gas compressor, and then mixed with natural gas and ignited in the combustor. The resulting flue gas is expanded to create power in the gas turbine before its remaining heat is transferred to the water/steam in the HRSG. The gas exiting the HRSG then enters the carbon capture unit, which separates and compresses the CO_2 for transport.

The steam cycle includes a condensate pump, CCS pump, multiple HRSG internal heat exchangers, HP pump, IP pump, HP turbine, IP Turbine, LP turbine, and condenser. The internal HRSG heat exchangers include the LP economizer, LP heat exchanger, IP heat exchanger, IP

reheater, and HP heat exchanger. In this cycle, the water exiting the condensate pump is mixed with the water exiting the ccs pump, and the resulting stream is heated in the LP economizer. The LP economizer exit is split into 3 streams: one is boiled and superheated in the LP heat exchanger, one is pumped to a high pressure in the HP pump, and one is pumped to an intermediate pressure in the IP pump. The exit from the HP pump is boiled and superheated in the HP heat exchanger before being expanded to create power in the HP turbine. The exhaust from the HP turbine is reheated in the IP reheater. The exit stream from the IP pump is boiled and superheated in the IP heat exchanger, mixed with the IP reheater exit stream, and expanded to create power in the IP turbine. The exhaust from the IP turbine is mixed with the LP heat exchanger exit stream and split into two streams: One of which is condensed to provide the heat for solvent regeneration in the carbon capture unit and the other is expanded in the LP turbine to create power. The LP turbine exhaust is condensed in the condenser and then pressurized in the condensate pump. The condensate exiting the carbon capture unit is pressurized in the CCS pump, mixed with the exit stream of the condensate pump, and the steam cycle is restarted.

The internal operation of the CANSOLV carbon capture unit operation is proprietary, and therefore not reported by NETL or the current research. Instead, the capture unit is assumed to be a heat sink that requires a specific heat duty of condensing steam, delivered at a specified temperature and pressure, to enable the removal of CO_2. All CCS parameters are constrained in the model to be equal to those specified by NETL throughout the entirety of the plant operation. In addition, the amount of CO_2 captured is always held constant to keep the CANSOLV unit always operating at design point conditions. This means that any additional CO_2 created due to thermal storage discharge is vented to the atmosphere.

The base plant technology model outputs 9 parameters that are used in the operation model. These parameters are listed in Table A2. The power output and fuel consumption are calculated in the base plant, designated by the variables $\dot{W}_{BP}$ and $\dot{m}_f$ respectively. The capture percent, capital costs, fixed operating and maintenance (FOM) costs, and variable operating and maintenance (VOM) costs are identical to those reported by NETL.

Table A2. Base plant technology model outputs

Parameter	Variable
Power Output (MW)	PO_{BP}
Fuel Consumption (kg/s)	FC_{BP}
Emissions Captured (%)	ECP_{BP}
NGCC Capital Cost (MM$)	CC_{NGCC}
NGCC FOM (MM$/yr)	FOM_{NGCC}
NGCC VOM (MM$/MWh)	VOM_{NGCC}
CCS Capital Cost (MM$)	CC_{CCS}
CCS FOM (MM$/yr)	FOM_{CCS}
CCS VOM (MM$/tonne)	VOM_{CCS}

Governing Equations

The net power output of the base plant was calculated using the following equations:

$$\dot{W}_{BP} = \dot{W}_{net,GT} + \dot{W}_{ST} - \dot{W}_{AUX} - \dot{W}_{HPP} - \dot{W}_{IPP} - \dot{W}_{SCP} \quad \text{(A.24)}$$

$$\dot{W}_{net,GT} = \dot{W}_{GT} - \dot{W}_{GC} \quad \text{(A.25)}$$

$$\dot{W}_{GT} = \dot{m}_g(h_{g,GT,I} - h_{g,GT,O}) \quad \text{(A.26)}$$

$$\dot{W}_{GC} = \dot{m}_a(h_{a,GC,O} - h_{a,GC,I}) \quad \text{(A.27)}$$

$$\dot{W}_{ST} = \dot{W}_{HPT} + \dot{W}_{IPT} + \dot{W}_{LPT} \quad \text{(A.28)}$$

$$\dot{W}_{\_PT} = \dot{m}_{\_PT}(h_{s,\_PT,I} - h_{s,\_PT,O}) \quad \text{(A.29)}$$

$$\dot{W}_{AUX} = \dot{W}_{AUX,DP} - \dot{W}_{HPP} - \dot{W}_{IPP} - \dot{W}_{CP} \quad \text{(A.30)}$$

$$\dot{W}_{HPP} = \dot{m}_{HP}(h_{s,HPP,O} - h_{s,HPP,I}) \quad \text{(A.31)}$$

$$\dot{W}_{IPP} = \dot{m}_{IP}(h_{s,IPP,O} - h_{s,IPP,I}) \quad \text{(A.32)}$$

$$\dot{W}_{SCP} = \dot{m}_{LPT}(h_{s,CP,O} - h_{s,CP,I}) \quad \text{(A.33)}$$

The hot and cold storage models calculated the heat duty of the system. The working fluid and configuration design effected efficiencies, flow rates, and heat transfer coefficient. In general, equation A.34 was used to calculate heat duty in for the storage systems:

$$\dot{Q} = \dot{m}(h_I - h_O) \quad \text{(A.34)}$$

Table A3 presents the list of thermal energy storage parameters that are outputted by the technology model for use in the operation model.

Table A3. Thermal energy storage technology model outputs

Parameter	Hot Storage Variable	Cold Storage Variable
Charging Power Decrease (MW)	CPD_{HST}	CPD_{CST}
Discharging Power Increase (MW)	DPI_{HST}	DPI_{CST}
Discharging Fuel Increase (kg/s)	NA	DFI_{CST}
Discharging Emissions Capture Percent Decrease (%)	NA	$DCPD_{CST}$
Storage Capital Cost (MM$/hr discharge)	SCC_{HST}	SCC_{CST}
Other Equipment Capital Cost (MM$)	ECC_{HST}	ECC_{CST}
Fixed Operating and Maintenance (MM$/yr)	$FOMC_{HST}$	$FOMC_{CST}$
VOM (MM$/MWh)	$VOMC_{HST}$	$VOMC_{CST}$

The charging power decrease is the total amount of power required to charge the storage technologies. This value is determined for the hot and cold storage technologies in equations (A.35) and (A.36) respectively.

$$CPD_{HST} = \frac{\dot{Q}_{HST}}{1000} \tag{A.35}$$

$$CPD_{CST} = \frac{\dot{W}_c}{1000} \tag{A.36}$$

The discharging power increase is the difference in power between the discharge mode and the neutral mode for each storage technology. This value is determined for the hot and cold storage technologies in equations (A.37) and (A.38) respectively.

$$DPI_{HST} = \frac{\dot{W}_{BP,HSD} - \dot{W}_{BP,N} - \dot{W}_{B,HSD} - \dot{W}_P}{1000} \tag{A.37}$$

$$DPI_{CST} = \frac{\dot{W}_{BP,HSD} - \dot{W}_{BP,N} - \dot{W}_{B,HSD} - \dot{W}_P}{1000} \tag{A.38}$$

The discharging fuel increase is the difference in fuel consumption between the discharge mode and the neutral mode. This value is zero for the hot storage and is calculated using equation (A.39) for the cold storage.

$$DFI_{CST} = \dot{m}_{f,CSD} - \dot{m}_{f,N} \tag{A.39}$$

The discharging capture percent decrease is the difference in percent of CO_2 emissions captured between the discharging and neutral modes. This value is zero for the hot storage and is calculated using equation (A.40) for the cold storage.

$$DCPD_{CST} = ECP_{BP}(1 - \frac{\dot{m}_{f,N}}{\dot{m}_{f,CSD}}) \tag{A.40}$$

The power generated and heat duty of each component in the modeled base plant (Case B31B) is shown in Table A4 and Table A5, respectively. The HRSG temperature profiles of the surrogate model used to validate using 5 HRSG heat exchangers as an accurate representation of the 19 heat exchangers used in NETL's B31B is shown in Figure A2.

Table A4. Power generated and required by each component for the NGCC+CCS base power plant (NETL Case B31B)

Component	***Power [MW]***	***Isentropic Efficiency***
Gas Compressor	(490.077)	0.85
Gas Turbine	968.634	0.9
High-Pressure Turbine	48.740	0.85
Intermediate-Pressure Turbine	83.651	0.925
Low-Pressure Turbine	67.800	0.93
High-Pressure Pump	(4.821)	0.71
Intermediate-Pressure Pump	(0.113)	0.71
Condensate Pump	(0.103)	0.71
Carbon Capture Pump	(0.027)	0.71
Auxiliary Power	(38.936)	NA
Net Power	634.747	NA

Table A5. Heat duty of each component for the NGCC+CCS base power plant (NETL Case B31B)

Component	***Heat Duty [MW]***
Combustor	1163.000
High-Pressure Heat Exchanger	363.734
Intermediate-Pressure Heat Exchanger	55.458
Intermediate-Pressure Reheater	65.388
Low-Pressure Heat Exchanger	49.444
Low-Pressure Economizer	49.790
Heat Recovery Steam Generator Total	583.814
Condenser	216.591
Carbon Capture Unit	172.039

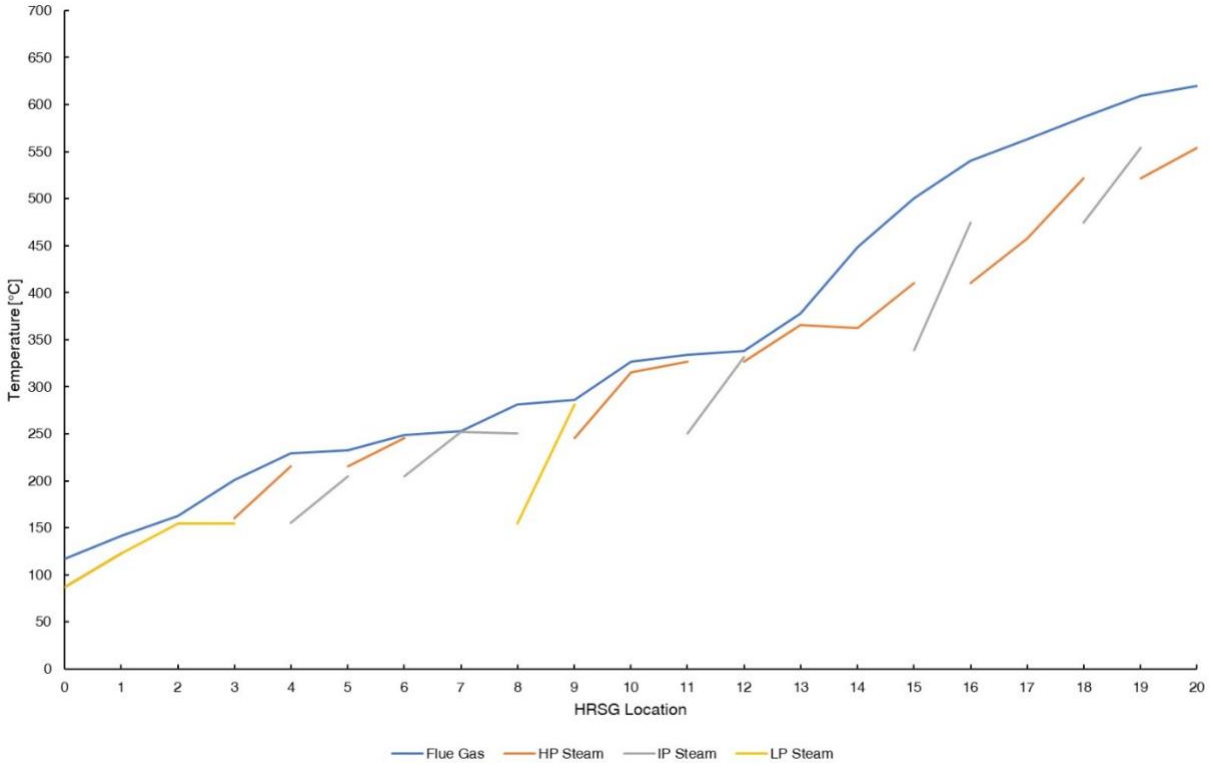

Figure A2. HRSG temperature profiles of the surrogate model used to validate using 5 HRSG heat exchangers was an accurate representation of the 19 heat exchangers used in NETL's B31B

Vapor – FG_S/HC Model

Figure A3 shows a process flow diagram of the thermal energy storage configuration Vapor - FG_S/HC in both charging and discharging modes as it is modeled in EES including temperature, pressure, quality, and mass flow rates at various points throughout the system. The power generated and heat duty of each component in thermal energy storage configuration Vapor - FG_S/HC is shown in Table A6 and Table A7, respectively.

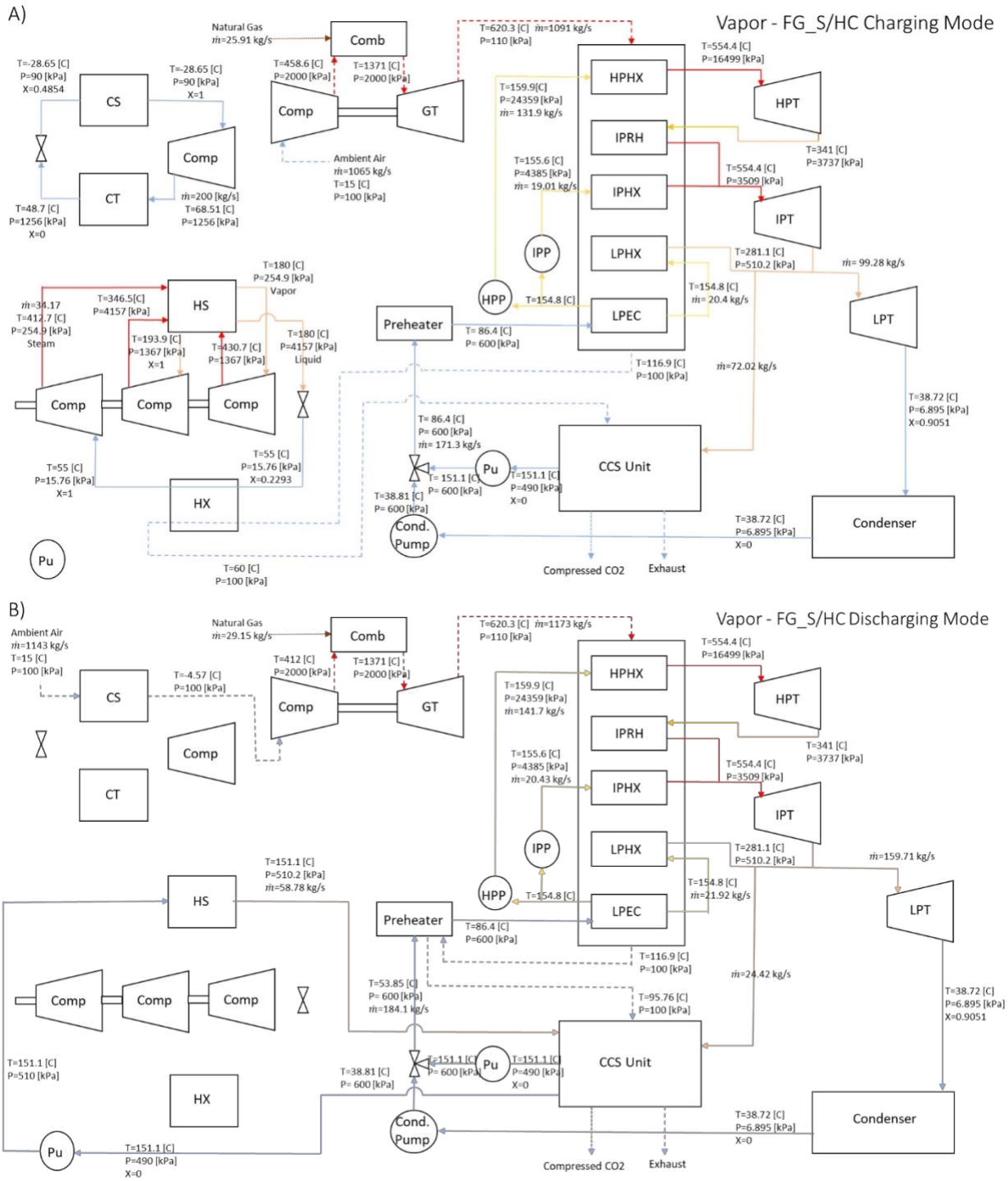

Figure A3. Model flow diagram for the thermal energy storage configuration Vapor - FG_S/HC in both A) charging and B) discharging modes. Diagrams include temperature, pressure, quality, and mass flow rates at various points throughout the system.

Table A6. Power generated and required by each component for thermal energy storage configuration Vapor - FG_S/HC.

Component	***Charging Power [MW]***	***Discharging Power [MW]***	***Isentropic Efficiency***
Gas Compressor	(490.077)	(490.902)	0.85
Gas Turbine	968.634	1041.000	0.90
High-Pressure Turbine	48.742	52.366	0.85
Intermediate-Pressure Turbine	83.653	89.872	0.925
Low-Pressure Turbine	67.795	108.985	0.93
High-Pressure Pump	(4.809)	(5.167)	0.71
Intermediate-Pressure Pump	(0.111)	(0.119)	0.71
Condensate Pump	(0.103)	(0.191)	0.71
Carbon Capture Pump	(0.027)	(0.009)	0.71
Hot Storage Pump	0.000	(0.002)	0.71
Hot Storage Compressor (Total)	(64.000)	0.000	0.85
Auxiliary Power	(39.053)	(39.053)	NA
Net Power	570.643	756.780	NA

Table A7. Heat duty of each component for thermal energy storage configuration Vapor - FG_S/HC.

Component	***Charging Heat Duty [MW]***	***Discharging Heat Duty [MW]***
Combustor	1,163.000	1,308.000
High-Pressure Heat Exchanger	363.753	390.797
Intermediate-Pressure Heat Exchanger	55.459	59.583
Intermediate-Pressure Reheater	65.391	70.252
Low-Pressure Heat Exchanger	49.414	53.087
Low-Pressure Economizer	49.798	53.500
Heat Recovery Steam Generator Total	583.814	627.219
Preheater	0.000	25.082
Condenser	250.773	401.420
Carbon Capture Unit	172.027	58.318
Hot Storage	113.709	0.000
Cold Storage	22.504	0.000
Hot Storage Heat Exchanger	62.709	0.000
Cooling Tower	35.504	0.000

HRSG IPT – S/HC Model

Figure A4 shows a process flow diagram of the thermal energy storage configuration HRSG – S/HC in both charging and discharging modes as it is modeled in EES including temperature, pressure, quality, and mass flow rates at various points throughout the system. The power generated and heat duty of each component in thermal energy storage configuration HRSG – S/HC is shown in Table A8 and Table A9, respectively.

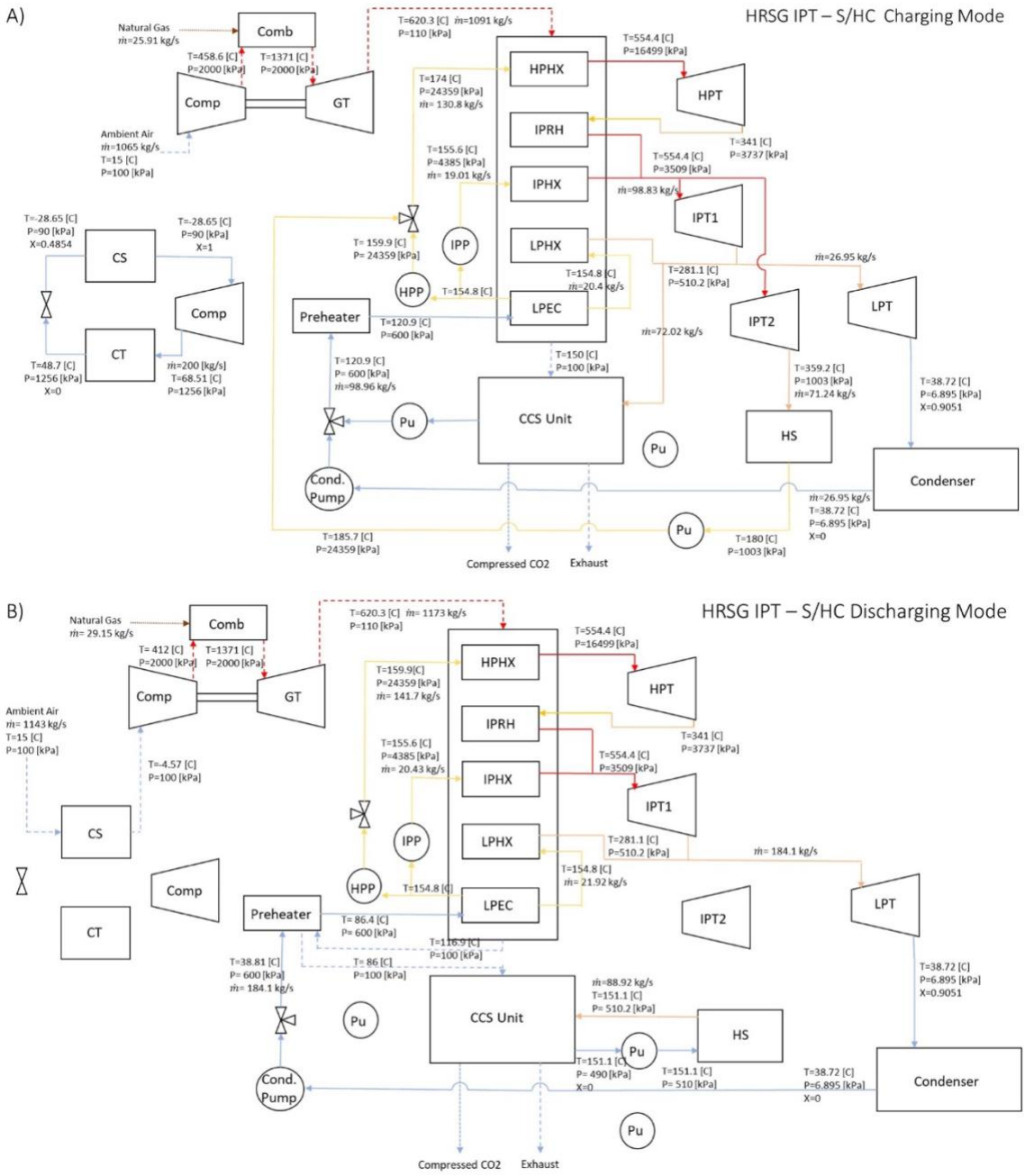

Figure A4. Model flow diagram for the thermal energy storage configuration HRSG – S/HC in both A) charging and B) discharging modes. Diagrams include temperature, pressure, quality, and mass flow rates at various points throughout the system.

Table A8. Power generated and required by each component for thermal energy storage configuration HRSG – S/HC.

Component	***Charging Power [MW]***	***Discharging Power [MW]***	***Isentropic Efficiency***
Gas Compressor	(490.077)	(490.902)	0.85
Gas Turbine	968.634	1041.000	0.9
High-Pressure Turbine	48.323	52.365	0.85
Intermediate-Pressure Turbine 1	43.544	89.872	0.925
Intermediate-Pressure Turbine 2	28.155	0.000	0.93
Low-Pressure Turbine	18.451	125.535	0.93
High-Pressure Pump	(2.171)	(5.167)	0.71
Intermediate-Pressure Pump	(0.111)	(0.119)	0.71
Condensate Pump	(0.023)	(0.155)	0.71
Carbon Capture Pump	(0.012)	0.000	0.71
Hot Storage Pump 1	0.000	(0.003)	0.71
Hot Storage Pump 2	(2.625)	0.000	0.71
Cold Storage Compressor	(13.000)	0.000	0.85
Auxiliary Power	(39.053)	(39.053)	NA
Net Power	560.035	773.382	NA

Table A9. Heat duty of each component for thermal energy storage configuration HRSG – S/HC.

Component	***Charging Heat Duty [MW]***	***Discharging Heat Duty [MW]***
Combustor	1,163.000	1,310.000
High-Pressure Heat Exchanger	352.755	390.796
Intermediate-Pressure Heat Exchanger	55.459	59.583
Intermediate-Pressure Reheater	64.828	70.252
Low-Pressure Heat Exchanger	49.414	53.087
Low-Pressure Economizer	24.690	53.502
Heat Recovery Steam Generator Total	547.146	627.219
Preheater	0.000	36.689
Condenser	25.336	401.419
Carbon Capture Unit	172.378	0.000
Hot Storage	176.037	0.000
Cold Storage	22.504	0.000

APPENDIX B

Additional methods and results are presented in this Appendix. Six subsections are included. The first subsection provides details on the total nutrient loads that green treatment technologies can achieve in the U.S. The second subsection details the optimum green infrastructure deployment across the contiguous United States (CONUS). The third subsection provides the results for the global warming potential (GWP) of gray and green treatment technologies across the CONUS. The fourth subsection details the total costs for gray and green technologies across the CONUS along with maps for carbon financing potential considering a $20 per tonne-CO2e carbon credit price and the net different between the costs of each technology if carbon financing is included. The fifth nutrient subsection provides a comparison between the minimum cost and minimum emission green treatment scenarios verses grey treatment technologies. The sixth subsection provides additional details on the methods used for this analysis. The seventh subsection provides additional details on the assumptions used for green treatment methods LCA estimates.

Nutrient Remediation Potential of Green Infrastructure

This analysis considers 7 primary green nutrient remediation methods, all of which are implemented on agricultural farmland. These include 3 barrier treatment methods which are applied at the edge of the field (saturated buffers, woodchip bioreactors, and constructed wetlands) and 4 land treatment methods (nutrient rate reduction, split nutrient application, cover crops, and no-till farming). Additionally, combinations of the green treatment methods were also considered which resulted in 63 unique combinations of green treatment methods being evaluated. Each green nutrient treatment method had unique infrastructure requirements, agricultural land limitations, and nutrient removal efficiencies. Therefore, each green treatment

method could treat different quantities of nitrogen and/or phosphorus. Maps of the nutrient treatment percentage in each waterbasin can be seen in Figure B1 for the Level 2 scenario, Figure B2 for the Level 3 scenario, Figure B3 for the Level 4 scenario, and in Figure 9 for the Level 5 scenario.

Figure B4 illustrates the total nutrient treatment which each green treatment method, or combination of methods, could achieve for the Level 2 scenario (a), Level 3 scenario (b), Level 4 scenario (c), and Level 5 scenario (d). Also provided is the maximum treatment potential of green treatment methods if the most productive treatment method is selected in each waterbasin and the percent of the required nutrient treatment necessary to achieve desired nutrient concentration goals in the CONUS. In total, 31.7% (530,255 tonnes N yr^{-1}) and 20.8% (54,110 tonnes P yr^{-1}) of the desired nitrogen and phosphorus treatment could be achieved using green infrastructure, respectively, for the Level 5 scenario. For the Level 2 scenario, Level 3 scenario, and Level 4 senario; results show that 36.8% (403,913 tonnes N yr^{-1}) and 22.5% (39,453 tonnes P yr^{-1}), 35.3% (447,888 tonnes N yr^{-1}) and 21.1% (50,147 tonnes P yr^{-1}), and 32.4% (505,953 tonnes N yr^{-1}) and 21.0% (52,457 tonnes P yr^{-1}) of the desired nitrogen and phosphorus treatment could be achieved using green infrastructure, respectively. The primary reason why green treatment methods cannot achieve higher nutrient treatment loads is due to limited agricultural land in the watershed, low nutrient removal efficiencies (which results in large land requirements), and limitations on geographic deployment (i.e., saturated buffers and woodchip bioreactors can only be used in locations with tile drainage which is predominately used in the corn belt, but not elsewhere in the US). This can be seen in Figure B4 because the treatment methods with high nutrient removal efficiencies and limited geographic constraints tend to

remove the most nutrients (constructed wetland + cover crops for nitrogen and all land treatment methods for phosphorus).

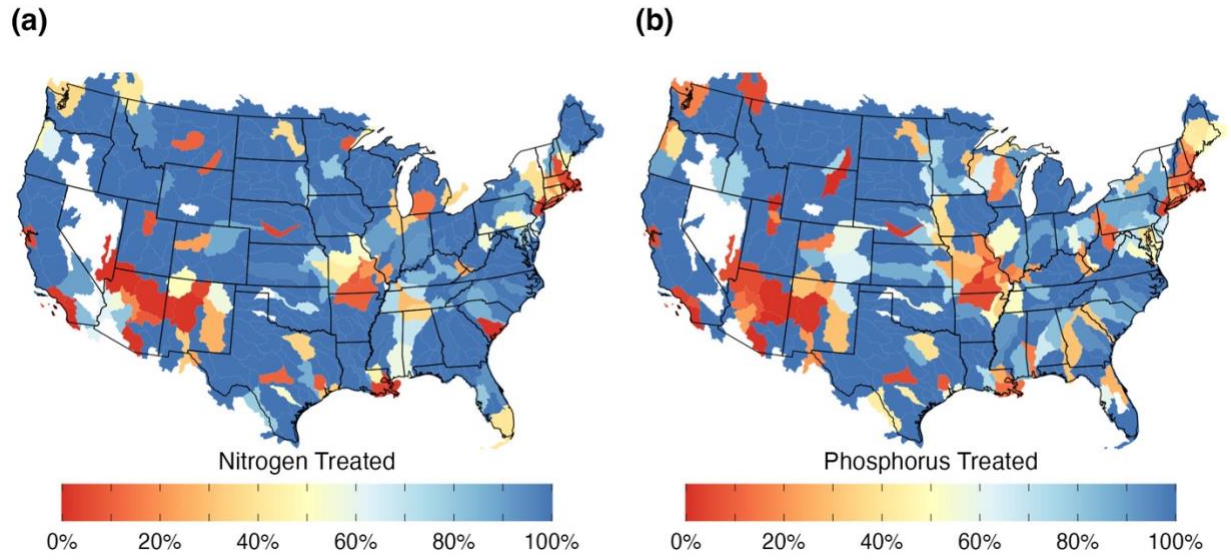

Figure B1. Percent of Nitrogen (a) and Phosphorus (b) treatment possible for green treatment technologies in each waterbasin for the Level 2 scenario of reducing mean nutrient concentrations to 8 mgN L^{-1} and 1 mgP L^{-1}.

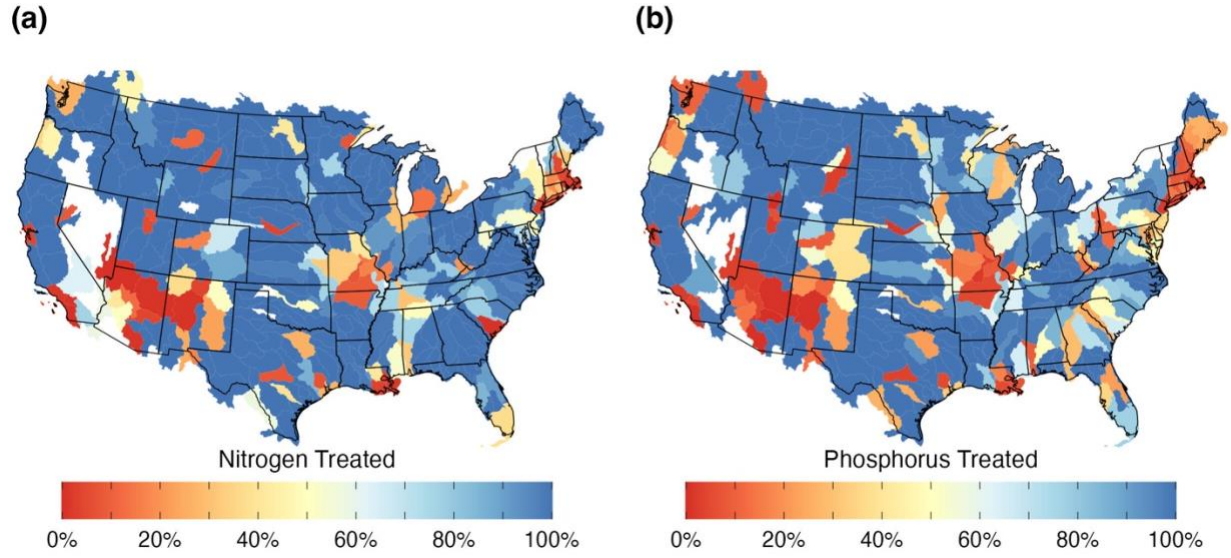

Figure B2. Percent of Nitrogen (a) and Phosphorus (b) treatment possible for green treatment technologies in each waterbasin for the Level 3 scenario of reducing mean nutrient concentrations to 6 mgN L^{-1} and 0.2 mgP L^{-1}.

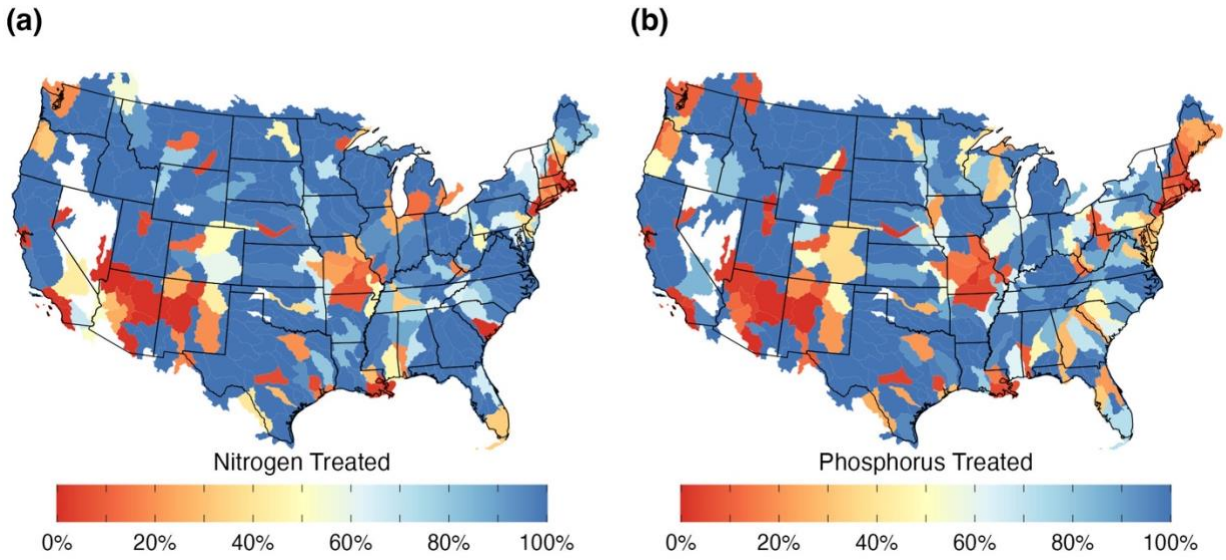

Figure B3. Percent of Nitrogen (a) and Phosphorus (b) treatment possible for green treatment technologies in each waterbasin for the Level 4 scenario of reducing mean nutrient concentrations to 3 mgN L^{-1} and 0.1 mgP L^{-1}.

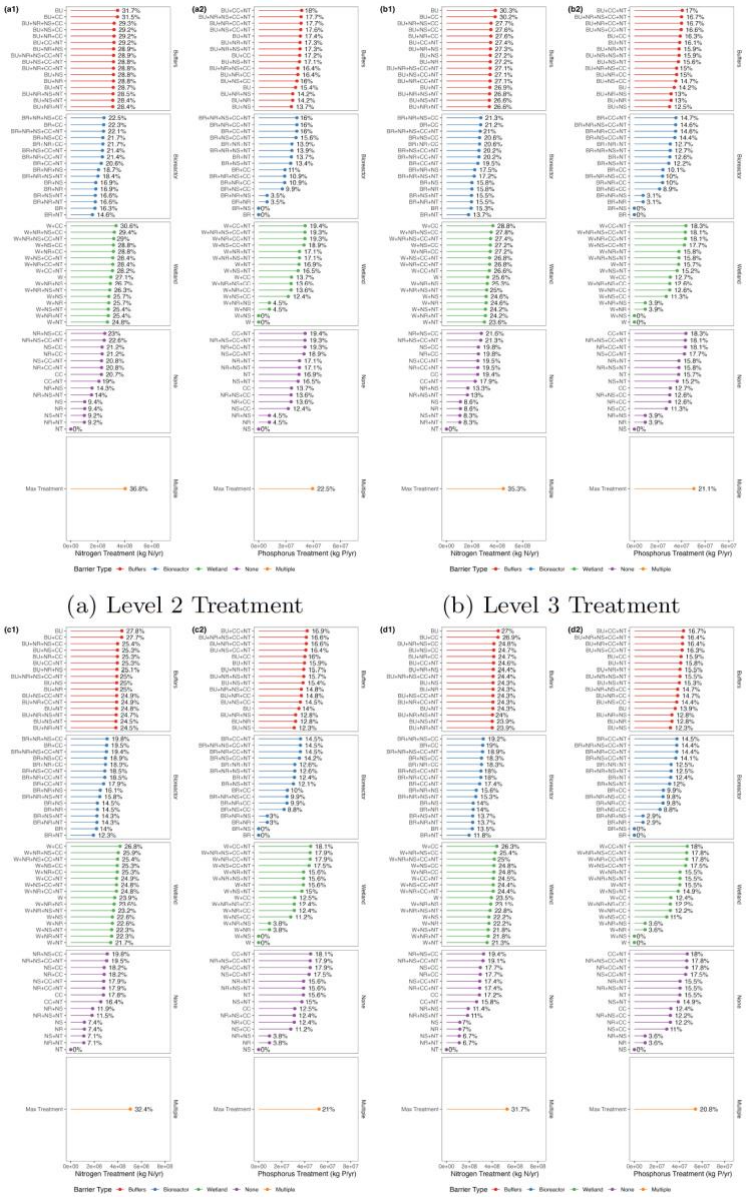

Figure B4. Maximum Nitrogen (1) and Phosphorus (2) treatment capacity of each green treatment technology or combinations of green technologies for the Level 2 (a), Level 3 (b), Level 4 (c), and Level 5 (d) scenarios. Percentage represents the percent of the total load needed to reduce mean concentration of all watersheds to 8 mg N L^{-1} and 1 mgP L^{-1} for Level 2, 6 mgN L^{-1} and 0.2 mgP L^{-1} for Level 3, 3 mgN L^{-1} and 0.1 mgP L^{-1} for Level 4, and 2 mgN L^{-1} and 0.02 mgP L^{-1} for Level 5. Labels represent Saturated Buffer (BU), Woodchip Bioreactor (BR), Constructed Wetland (W), Nitrogen Rate Reduction (NR), Split Nitrogen Application (NS), Cover Crop (CC), No-Till farming (NT), and the maximum treatment possible when optimizing for the most productive treatment method in each watershed (Max Treatment). Green treatment technologies are separated by common barrier treatment method: Buffers (saturated buffer), Bioreactor (woodchip bioreactor), Wetland (constructed wetland), None (only land treatment methods), or Multiple (optimum treatment method used in each location).

Optimal Green Infrastructure Deployment Across the US

One of the primary goals of this study was to capture the geospatial intricacies of green nutrient remediation methods. As such, Figure B5 illustrates the best green treatment methods to use in each waterbasin when prioritizing maximum nutrient treatment and minimum costs for the each of the nutrient treatment scenarios. The results between the scenarios are similar. In all cases, saturated buffers, reduced nitrogen application, and cover crops are used widely for both nitrogen and phosphorus remediation. Constructed wetlands and split nutrient application are used for nitrogen treatment and no-till farming is used widely for phosphorus treatment. In total, 49 of the modeled 63 green treatment combinations are used for either nitrogen or phosphorus in at least one of the scenarios.

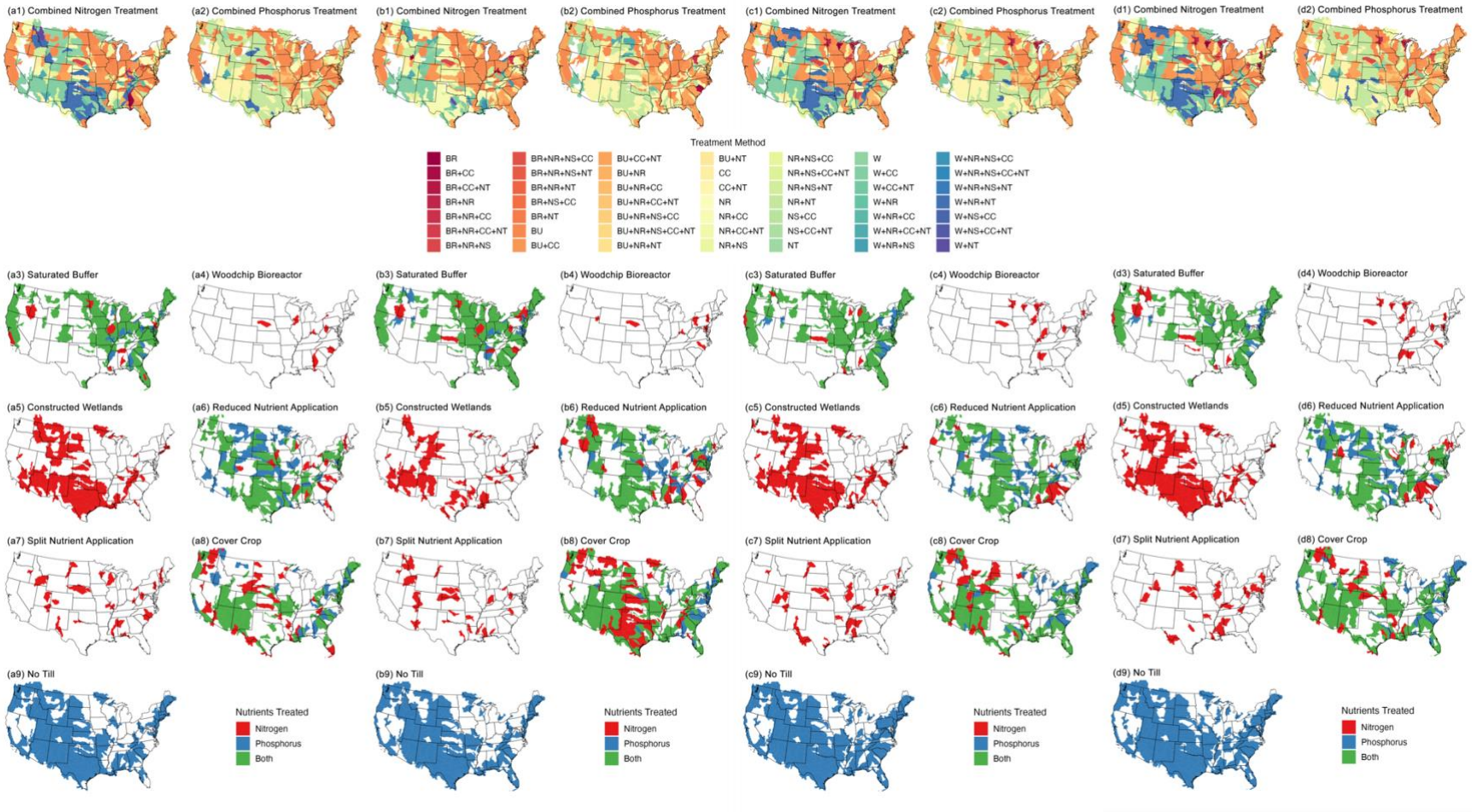

Figure B5. Geographic variability of treatment methods for the optimized green treatment scenario prioritizing minimum cost for the Level 2 scenario (a), Level 3 scenario (b), Level 4 scenario (c), and the Level 5 scenario (d). Labels represent Saturated Buffer (BU), Woodchip Bioreactor (BR), Constructed Wetland (W), Nitrogen Rate Reduction (NR), Split Nitrogen Application (NS), Cover Crop (CC), and No-Till farming (NT).

Global Warming Potential of Gray vs. Green Infrastructure

Similar results shown in Section 3.3.2 for the Level 5 scenario Figures B6, B7, and B8 show GWP of green versus gray technologies across the CONUS for the Level 2, Level 3, and Level 4 scenarios, respectively. In the Level 2 scenario, gray treatment technologies emit 11.9 MtCO2e while green treatment technologies sequester 3.4 MtCO2e annually which results in a annual carbon credit potential of 15.3 MtCO2e. In the Level 3 scenario, gray treatment technologies emit 17.4 MtCO2e while green treatment technologies sequester 3.8 MtCO2e annually which results in a annual carbon credit potential of 21.2 MtCO2e. In the Level 4 scenario, gray treatment technologies emit 18.5 MtCO2e while green treatment technologies sequester 3.9 MtCO2e annually which results in a annual carbon credit potential of 22.4 MtCO2e. Overall, GWP values are reduced in the Level 2-4 scenarios compared to the Level 5 scenario due to the reduction in nutrient treatment required.

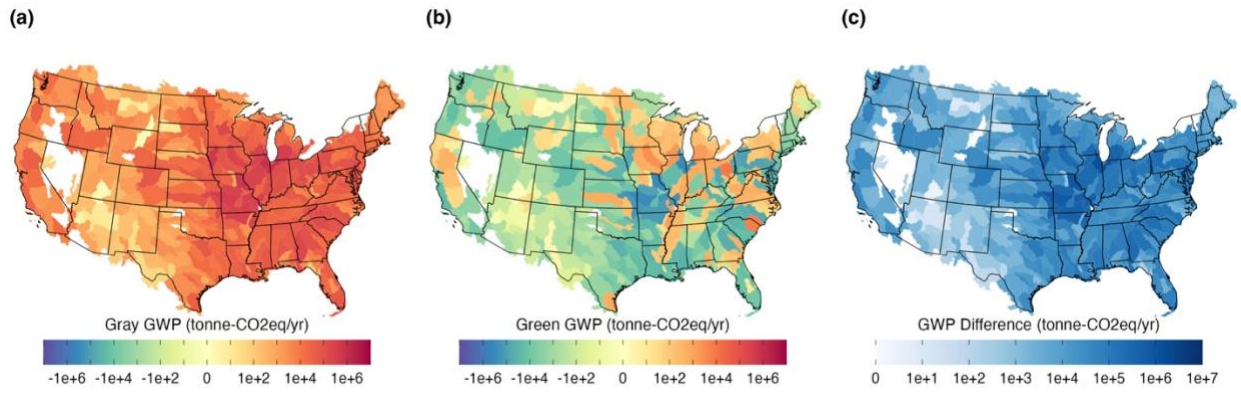

Figure B6. Continental United States global warming potential (GWP) in tonnes of CO2 equivalent emissions per year for removal of nitrogen (to 8 mg L^{-1}) and phosphorus (to 1 mg L^{-1}) using (a) gray treatment technologies (11.9 $MtCO2e\ year^{-1}$) and (b) green treatment technologies (-3.4 $MtCO2e\ year^{-1}$), and (c) net GWP representing potential carbon credit generation (15.3 $MtCO2e\ year^{-1}$).

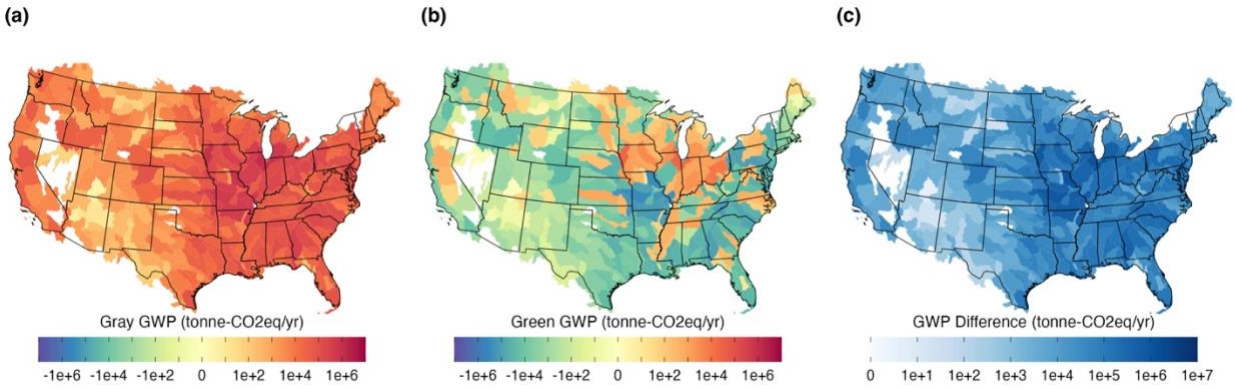

Figure B7. United States global warming potential (GWP) in tonnes of CO2 equivalent emissions per year for removal of nitrogen (to 6 mg L-1) and phosphorus (to 0.2 mg L^{-1}) using (a) gray treatment technologies (17.4 $MtCO2e\ year^{-1}$) and (b) green treatment technologies (-3.8 $MtCO2e\ year^{-1}$), and (c) net GWP representing potential carbon credit generation (21.2 $MtCO2e\ year^{-1}$).

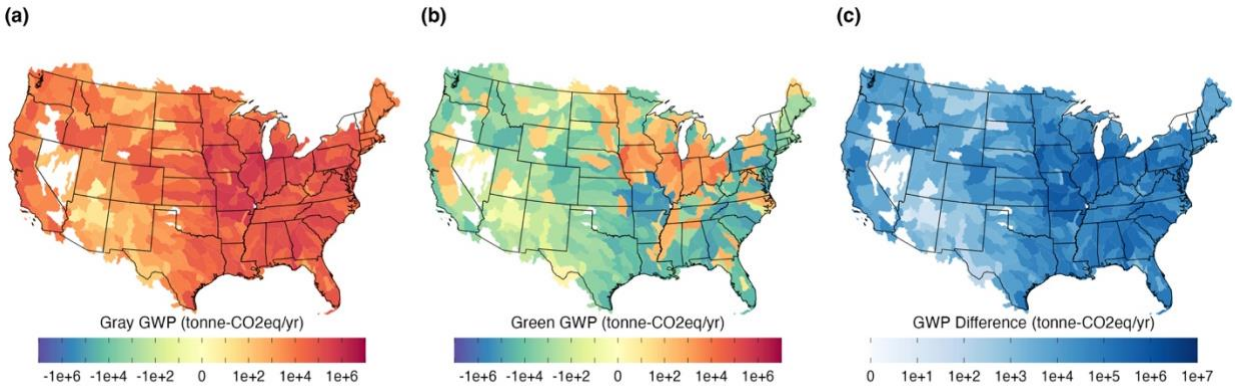

Figure B8. Continental United States global warming potential (GWP) in tonnes of CO2 equivalent emissions per year for removal of nitrogen (to 3 mg L^{-1}) and phosphorus (to 0.1 mg L^{-1}) using (a) gray treatment technologies (18.5 $MtCO2e\ year^{-1}$) and (b) green treatment technologies (-3.9 $MtCO2e\ year^{-1}$), and (c) net GWP representing potential carbon credit generation (22.4 $MtCO2e\ year^{-1}$).

Carbon Financing Potential Green Infrastructure

Similar results shown in Section 3.3.3 for the Level 2 and Level 5 scenarios, Figures B10 and B11 show costs of green versus gray technologies across the CONUS for the Level 3 and Level 4 scenarios, respectively. Nutrient treatment costs for the Level 3 scenario were \$18.3B $year^{-1}$ and \$12.4B $year^{-1}$ for gray and green technologies, respectively. Additionally, the carbon financing potential is \$424M $year^{-1}$ assuming a carbon credit price of \$20 $tonne\text{-}CO2eq^{-1}$ and the

total savings of green treatment technologies when compared to gray treatment and including carbon financing potential is \$6.3B year^{-1}. Of the 315 waterbasins in the CONUS which required nutrient treatment, 166 (53%) had green treatment costs cheaper than those of the gray treatment technologies excluding carbon financing revenues. If carbon financing revenue is added, 176 (56%) of waterbasins had green treatment costs cheaper than gray treatment technologies. However, when evaluated as a percent of total nutrients treated in the CONUS, 84.3% of nitrogen and 73.0% of phosphorus is treated in waterbasins where green treatment costs are cheaper than gray treatment technologies when carbon financing revenues are excluded. These values increase to 85.7% of nitrogen and 77.0% of phosphorus treated in the CONUS in waterbasins which green technologies are cheaper when carbon financing revenues are included. Similar to the other scenarios, green treatment costs were largely impacted by the farmer incentive payments. On a national level, farmer incentive payments make up 50% (\$6.2B year^{-1}) of the total green treatment costs.

Nutrient treatment costs for the Level 4 scenario were \$19.5B year^{-1} and \$13.2B year^{-1} for gray and green technologies, respectively. Additionally, the carbon financing potential is \$449M year^{-1} assuming a carbon credit price of \$20 tonne-CO2eq^{-1} and the total savings of green treatment technologies when compared to gray treatment and including carbon financing potential is \$6.8B year^{-1}. Of the 315 waterbasins in the CONUS which required nutrient treatment, 163 (52%) had green treatment costs cheaper than those of the gray treatment technologies excluding carbon financing revenues. If carbon financing revenue is added, 173 (55%) of waterbasins had green treatment costs cheaper than gray treatment technologies. However, when evaluated as a percent of total nutrients treated in the CONUS, 82.1% of nitrogen and 73.6% of phosphorus is treated in waterbasins where green treatment costs are

cheaper than gray treatment technologies when carbon financing revenues are excluded. These values increase to 86.1% of nitrogen and 78.5% of phosphorus treated in the CONUS in waterbasins which green technologies are cheaper when carbon financing revenues are included. Similar to the other scenarios, green treatment costs were largely impacted by the farmer incentive payments. On a national level, farmer incentive payments make up 49% ($6.5B year^{-1}) of the total green treatment costs.

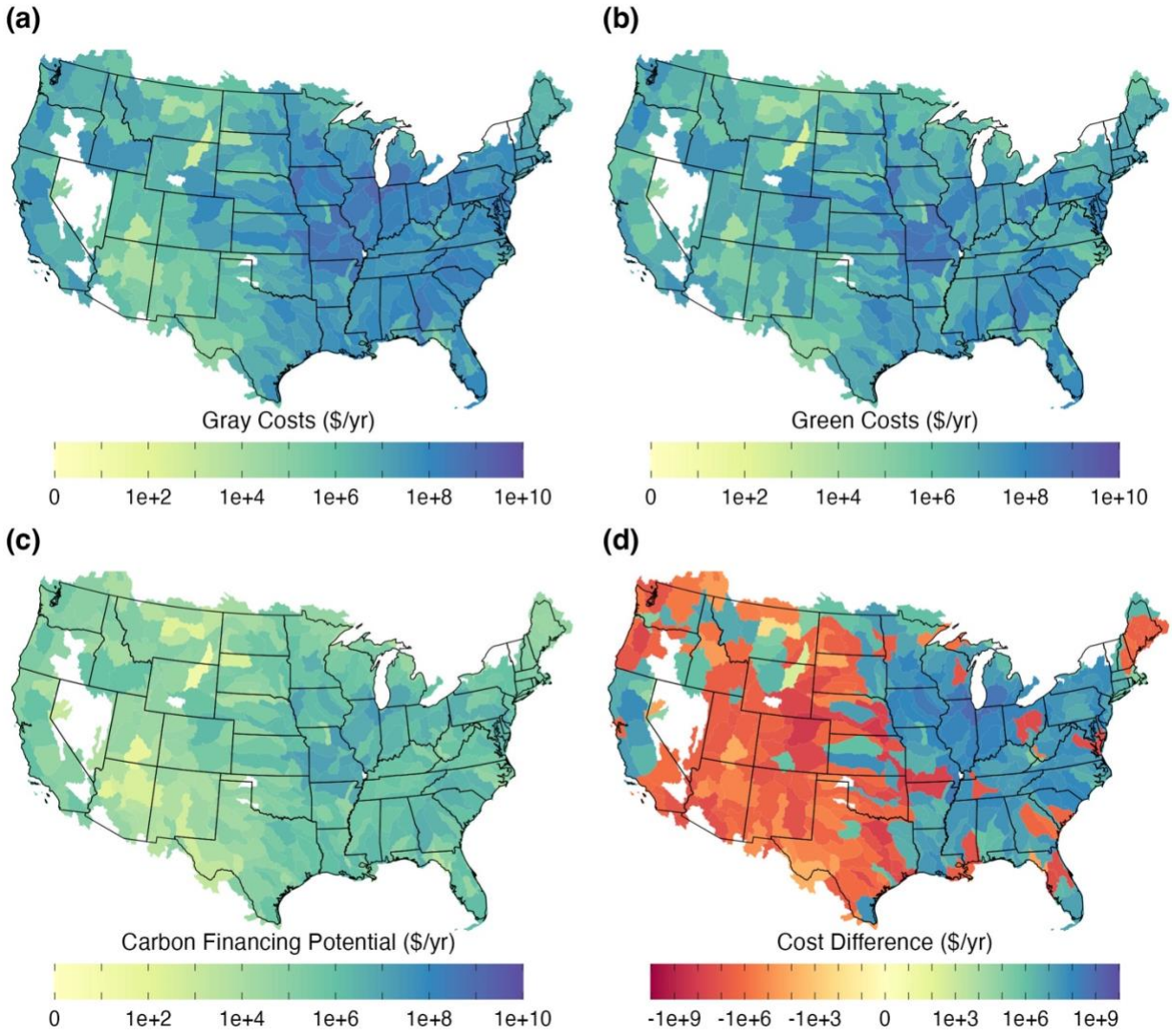

Figure B9. Continental United States water treatment costs for removal of nitrogen (to 8 mg L^{-1}) and phosphorus (to 1 mg L^{-1}) using (a) gray treatment technologies ($14.9B $year^{-1}$) and (b) green treatment technologies ($10.0B $year^{-1}$), (c) Potential carbon market revenue ($307M $year^{-1}$ at $20 per credit), and (d) net cost difference between gray and green treatment technologies when including carbon financing revenue ($5.2B $year^{-1}$). Negative cost differences show waterbasins where green technologies are more expensive than gray technologies. White space designates waterbasins which didn't have wastewater treatment facilities or didn't require nutrient treatment.

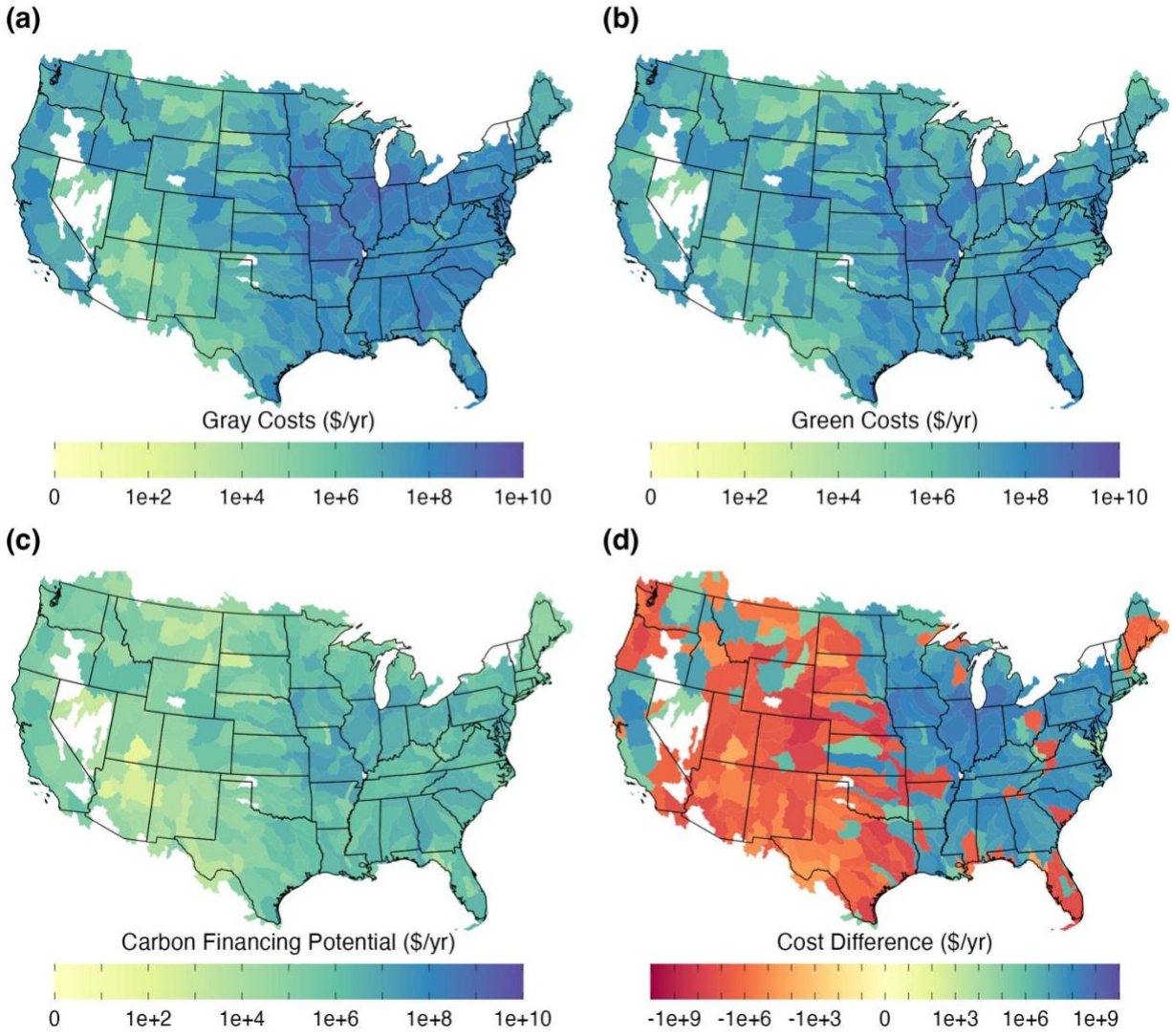

Figure B10. Continental United States water treatment costs for removal of nitrogen (to 6 mg L^{-1}) and phosphorus (to 0.2 mg L^{-1}) using (a) gray treatment technologies ($18.3B $year^{-1}$) and (b) green treatment technologies ($12.4B $year^{-1}$), (c) Potential carbon market revenue ($424M $year^{-1}$ at $20 per credit), and (d) net cost difference between gray and green treatment technologies when including carbon financing revenue ($6.3B $year^{-1}$). Negative cost differences show waterbasins where green technologies are more expensive than gray technologies. White space designates waterbasins which didn't have wastewater treatment facilities or didn't require nutrient treatment.

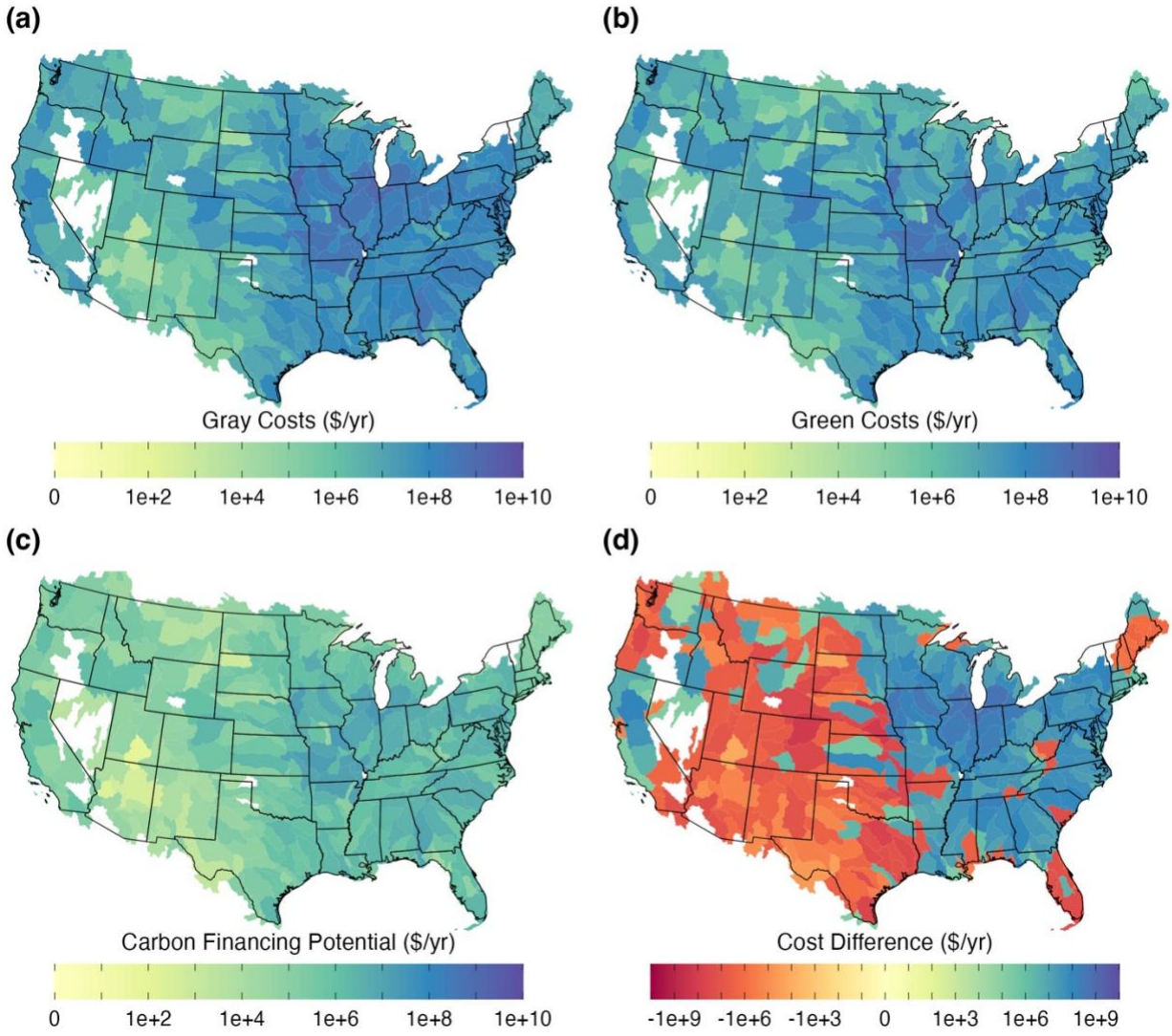

Figure B11. Continental United States water treatment costs for removal of nitrogen (to 8 mg L^{-1}) and phosphorus (to 1 mg L^{-1}) using (a) gray treatment technologies ($19.5B $year^{-1}$) and (b) green treatment technologies ($13.2B $year^{-1}$), (c) Potential carbon market revenue ($449M $year^{-1}$ at $20 per credit), and (d) net cost difference between gray and green treatment technologies when including carbon financing revenue ($6.8B $year^{-1}$). Negative cost differences show waterbasins where green technologies are more expensive than gray technologies. White space designates waterbasins which didn't have wastewater treatment facilities or didn't require nutrient treatment.

Cost and Emissions Comparison Between All Green and Gray Technologies

The primary goal of this work to was to evaluate the costs and GWP of nutrient remediation by building additional traditional wastewater treatment facilities (gray infrastructure) compared to green infrastructure. Figure B12 shows the costs and GWP required to treat the maximum amount of nitrogen and phosphorus treatment possible with green treatment technologies and all gray treatment technologies considered for the Levels 2-5 treatment scenarios.

Results show that green treatment technologies have the potential to have both less costs and less GWP than gray infrastructure in both scenarios. This result correlates with existing literature on the subject [26,27,129]. In the Level 2 scenario, the minimum cost green treatment method has total costs of \$10.0 billion yr^{-1} and total GWP of -3.4 $MtCO2\ yr^{-1}$ and the minimum emissions green treatment method has total costs of \$13.8 billion yr^{-1} and total GWP of -7.6 $MtCO2\ yr^{-1}$. In order to make the minimum emissions scenario financially competitive with the minimum cost scenario, a carbon price of \$927 would be required. Comparatively, the cheapest and least environmentally damaging gray treatment method was Anaerobic/Anoxic/Oxic with total costs of \$14.9 billion yr^{-1} and total GWP of 11.9 $MtCO2\ yr^{-1}$.

In the Level 3 scenario, the minimum cost green treatment method has total costs of \$12.4 billion yr^{-1} and total GWP of -3.8 $MtCO2\ yr^{-1}$ and the minimum emissions green treatment method has total costs of \$16.6 billion yr^{-1} and total GWP of -8.4 $MtCO2\ yr^{-1}$. In order to make the minimum emissions scenario financially competitive with the minimum cost scenario, a carbon price of \$928 would be required. Comparatively, the cheapest gray treatment method was the 4-Stage Bardenpho Membrane Bioreactor with total costs of \$18.3 billion yr^{-1} and total GWP

of 17.4 MtCO2 yr^{-1}. The least environmentally damaging gray treatment method was the Modified University of Cape Town Process with total costs of $18.8 billion yr^{-1} and total GWP of 16.1 MtCO2 yr^{-1}.

In the Level 4 scenario, the minimum cost green treatment method has total costs of $13.2 billion yr^{-1} and total GWP of -3.9 MtCO2 yr^{-1} and the minimum emissions green treatment method has total costs of $17.7 billion yr^{-1} and total GWP of -8.8 MtCO2 yr^{-1}. In order to make the minimum emissions scenario financially competitive with the minimum cost scenario, a carbon price of $946 would be required. Comparatively, the cheapest gray treatment method was the 4-Stage Bardenpho Membrane Bioreactor with total costs of $19.5 billion yr^{-1} and total GWP of 18.5 MtCO2 yr^{-1}. The least environmentally damaging gray treatment method was the 5-Stage Bardenpho with Denitrification Filter with total costs of $20.6 billion yr^{-1} and total GWP of 18.5 MtCO2 yr^{-1}.

In the Level 5 scenario, the minimum cost green treatment method has total costs of $13.6 billion yr^{-1} and total GWP of -4.2 MtCO2 yr^{-1} and the minimum emissions green treatment method has total costs of $18.2 billion yr^{-1} and total GWP of -9.1 MtCO2 yr^{-1}. In order to make the minimum emissions scenario financially competitive with the minimum cost scenario, a carbon price of $939 would be required. Comparatively, the cheapest gray treatment method was 5-Stage Bardenpho Membrane Bioreactor with Sidestream Reverse Osmosis Treatment with total costs of $28.5 billion yr^{-1} and total GWP of 29.8 MtCO2 yr^{-1}. The least environmentally damaging gray treatment method was 5-Stage Bardenpho with Sidestream Reverse Osmosis Treatment with total costs of $30.2 billion yr^{-1} and total GWP of 29.1 MtCO2 yr^{-1}.

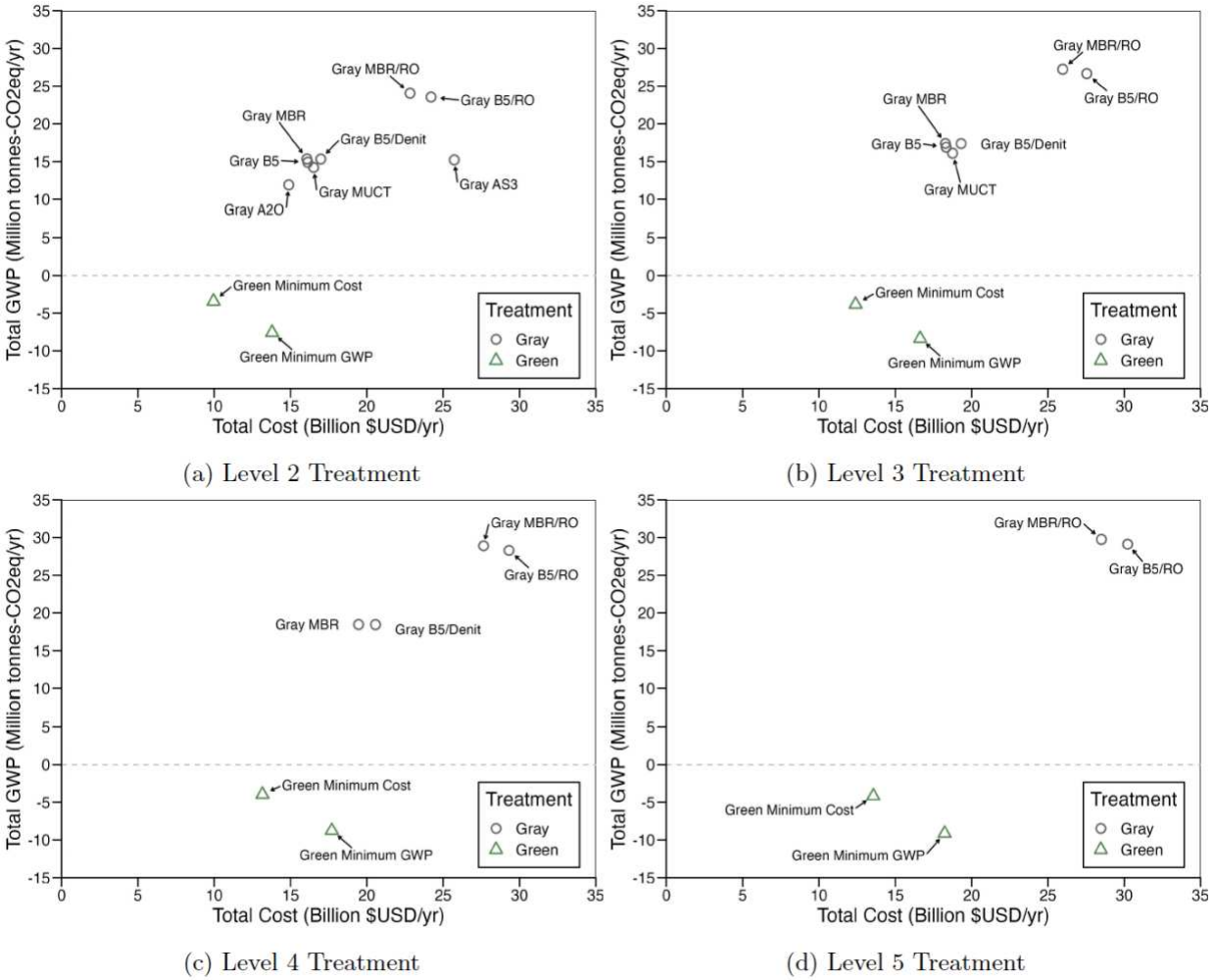

Figure B12. Total Cost and Global Warming Potential (GWP) of the optimum Green treatment methods and each Gray treatment method to meet desired nutrient concentration limits for the Level 2 scenario (a - 8 mgN L^{-1} and 1 mgP L^{-1}), Level 3 scenario (b - 6 mgN L^{-1} and 0.2 mgP L^{-1}), Level 4 scenario (c - 3 mgN L^{-1} and 0.1 mgP L^{-1}), and Level 5 scenario (d - 2 mgN L^{-1} and 0.02 mgP L^{-1}). Gray treatment methods include Anaerobic/Anoxic/Oxic (A2O), Activated 3-Sludge System (AS3), 5-Stage Bardenpho (B5), Modified University of Cape Town Process (MUCT), Denitrification Filter (Denit), 4-Stage Bardenpho Membrane Bioreactor (MBR), and Reverse Osmosis Treatment (RO).

Supplementary Methods Visuals

The following visualizations provide additional information about the methods used to complete this study. Table B1 outlines which green technologies require what base technologies in order to be used within the waterbasin. Figure B13 provides maps of the required technologies for the green treatment methods shown in Table B1. Figure B14 provides a diagram of the analysis process.

Table B1. Land limitations placed on green treatment technologies.

Name	Abbr.	Type	Tile Drain	Buffer	Wetlands	Fertilizer	Current Land Use (%)	Farmer Incentive Scaling
Buffers	BU	Barrier	Yes	Yes	No	No	0.01%	1/15
Bioreactors	BR	Barrier	Yes	No	No	No	0.01%	1/10
Wetland	W	Barrier	No	No	Yes	No	0.4%	1/40
N Rate Reduction	NR	Land	No	No	No	Yes	18.6%	1
Split N Application	NS	Land	No	No	No	Yes	18.6%	1
Cover Crop	CC	Land	No	No	No	No	Varies	1
No-till	NT	Land	No	No	No	No	Varies	1

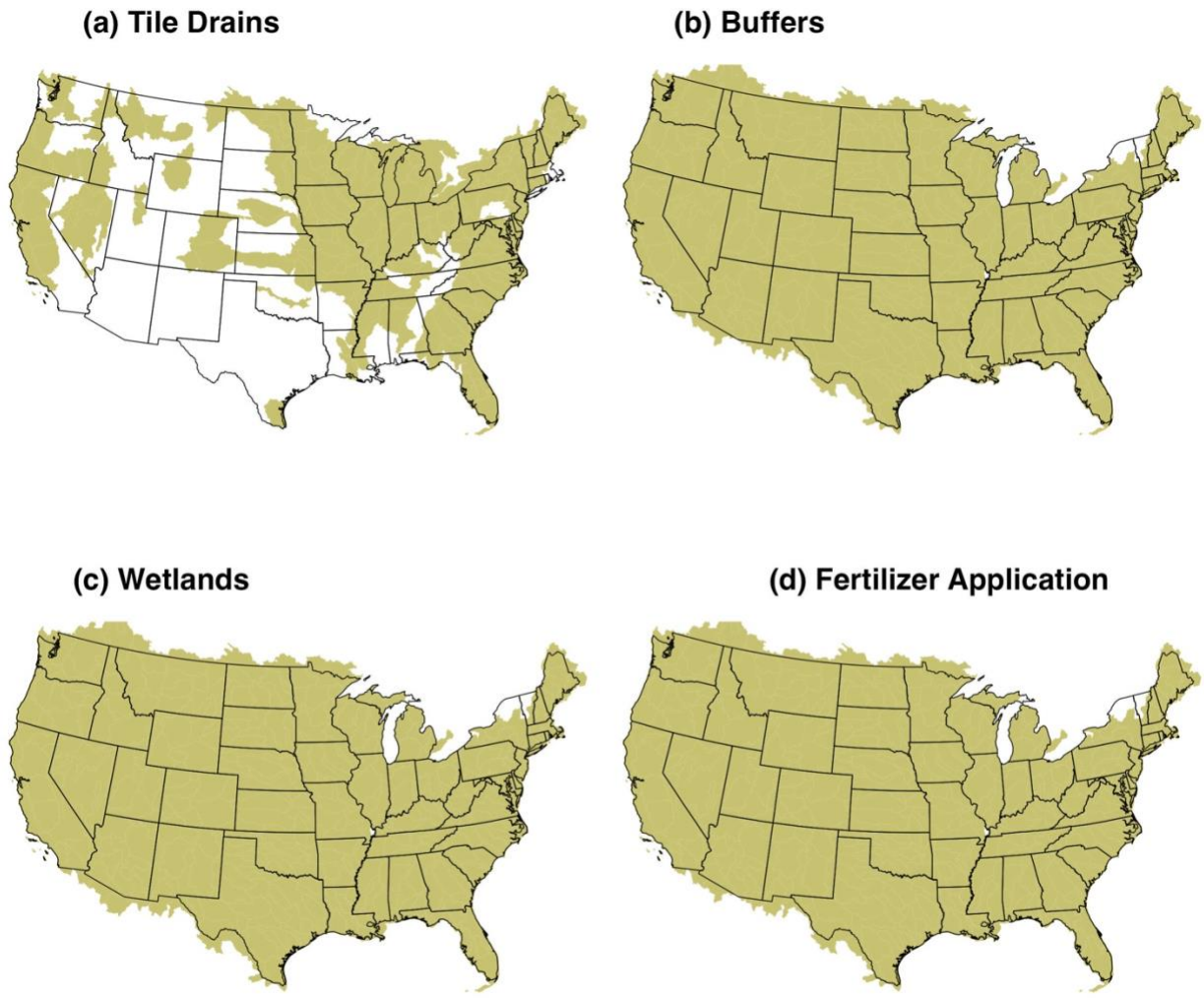

Figure B13. Green water treatment availability by waterbasin for technologies needing tile drainage (a), riparian buffers (b), wetlands (c), and supplemental fertilizer application (d). Data for waterbasin characteristics provided by the US EPA's EnviroAtlas [143].

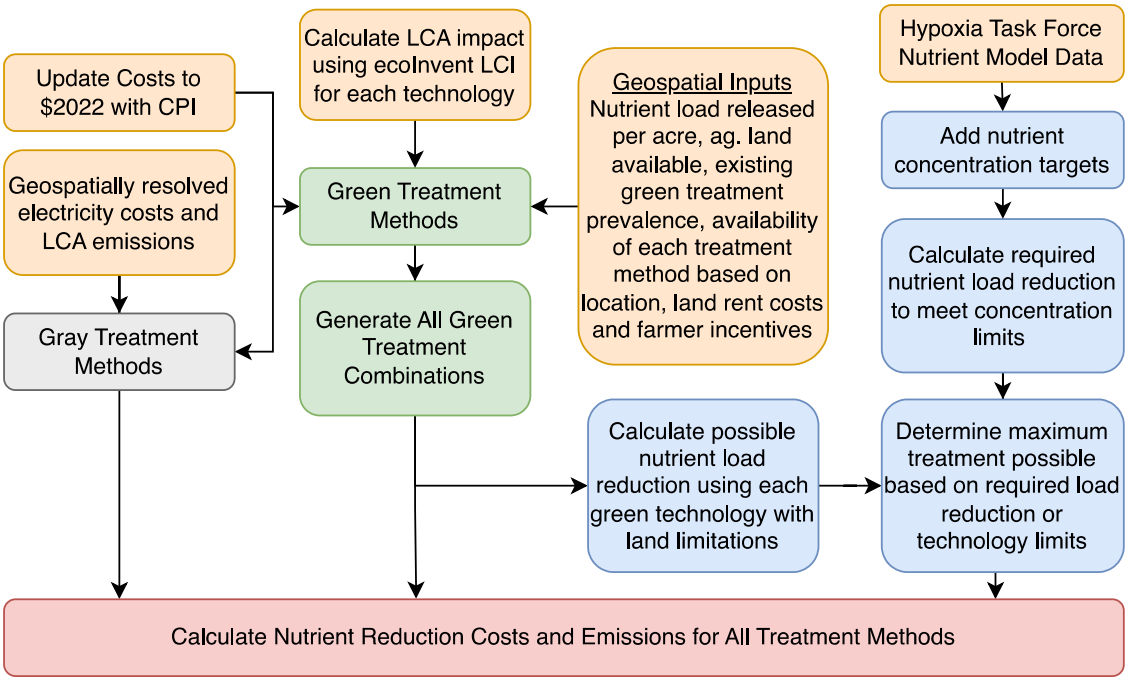

Figure B14. Diagram of the methods used for this study.

Life Cycle Emissions of Green Treatment Methods

Because of limited literature on life cycle emissions of green nutrient treatment scenarios, the GWP of each was estimated using life-cycle inventory data from the EcoInvent 3.71 database, using cut-off analysis, accessed through the software openLCA 1.10.3 (https://openlca.org), and calculated using the Traci 2.1 impact assessment methodology [166,167]. The GWP estimate for constructed wetlands includes direct land use change effects which were calculated using IPCC methodology [168]. Detailed assumptions for each of the treatment methods are presented in the following sections. The descriptions in the following sections are meant to be used in unison with the supplemental spreadsheet with LCA calculations. For all LCA estimates, calculations were performed for a 50 acre square farm with mean annual nutrient loss of 9.5 kg N $acre^{-1}$ and 0.65 kg P $acre^{-1}$ [154,261]. Costs and emissions

for green nutrient treatment technologies were assumed to scale linearly based on the number of acres treated, so the 50 acre farm was used to calculate per acre treatment emissions of all treated farmland. Additionally, all green treatment methods that needed a water control device were assumed to use one that was 9 feet tall, 1 foot wide, and 1 foot deep per 50 acres treated [262].

Saturated Buffer

A saturated buffer is an alternative method to drain the excess water from a farm that uses tile drainage systems. Instead of releasing the runoff directly to a stream, the runoff is released through a riparian buffer using perforated tubing running parallel to the stream. This allows the soil to trap some of the excess nutrients in the runoff before reaching the waterway. Therefore, the environmental impact associated with saturated buffers included the perforated drainage pipe, the water control device, and the excavator needed to install the system. Buffers were assumed to have a 15 year life [263].

Woodchip Bioreactor

A woodchip bioreactor is a large filtration system that uses woodchips to denitrify agricultural runoff. Assumptions used for the LCA of a woodchip bioreactor were gathered from Christianson et al. [154]. It was assumed that a 10 yard long, 5 yard wide, and 3 yard deep bioreactor would be required to treat 50 acres of farmland. This results in 150 cubic yards of woodchips and 165 cubic yards of excavation needed for both the bioreactor and the water control device. Additionally, it was assumed that 6 mil thick plastic would line the bioreactor and it would be covered on top with landscaping fabric. Life cycle emissions were included for all of these components and a 10 year lifetime was assumed.

Constructed Wetland

A constructed wetland consists of building a wetland on part of the farm and running the agricultural runoff through the wetland to trap some of the nutrients. For this, part of farm needs to be converted to a wetland. It was assumed that the wetland size requirement was 2% of treated land plus 2X the wetland size for a buffer [150]. Therefore 6% of the treated land was required for wetland construction. Emissions were included for the wetland's excavation, straw required to help establish the buffer, and seed to start wetland growth. Additionally, direct land use change emissions were also included for constructed wetlands and calculations were performed using IPCC methodology [168]. For these calculations, it was assumed that the farm resided in a cold temperate and dry location and that high activity clay soil existed at the farm location. It was assumed that all above ground biomass was removed and burned prior to creating the wetland. A 40 year wetland life was assumed.

Nutrient Rate Reduction

Nutrient rate reduction consists of farmers applying the proper amount of fertilizer to their field, instead of over fertilizing which eventually leads to extra nutrients running off farms and into streams. A 26.3% percent fertilizer reduction was assumed based on information provided by the University of Nebraska Board of Regents [264]. Reduced fertilizer use results in a net emissions savings compared to traditional nutrient applications because less fertilizer is required.

Split Nutrient Application

Split nutrient application consists of farmers applying part of their fertilizer in the fall and part in the spring. This results in more fertilizer being absorbed by the plants and soils which

results in less nutrient runoff. Therefore, the only emissions associated with treatment method were assumed to be that a second fertilizer application.

Cover Crop

Cover cropping is a method to plant a crop of fallow soil to prevent excess nutrient runoff. In this case, it was assumed that ryegrass would be used as the cover crop and emissions associated with ryegrass production were calculated using the EcoInvent inventory and an assumed yield of 700 lbs of ryegrass per acre [265].

No-Till Farming

Conventional tilled farming involves turning over the first 6 - 12 inches of soil before crops are planted. This makes the soil easier to work with, but also removes plant matter from the soil surface and increases erosion risk. Conversely, no-till farming involves not tilling the soil before planting. Therefore, the emissions associated with no-till farming were assumed to be the avoided emissions from not tilling the farmland. Due to the various methods for no-till farming, emissions associated with other no-till practices such as additional weed killer application were not included.

APPENDIX C

Discussion on Gasification/Hydroprocessing End Products

This supplementary discussion section is designed to provide an overview on our understanding of the literature of hydroprocessing end products which is in conflict to the assumptions used by Uludere Aragon et al. (2022) of the only end products being electricity and Jet-A fuel [33].

Uludere Aragon et al. reference a publication by de Jong et al. (2015) [50] for their conversion efficiency (0.175 kg Jet kg^{-1} Miscanthus).

de Jong et al. features a table of conversion factors and associated sources. They cite a number of studies including Ekbom et al. (2009) [52], Atsonios et al. (2015) [51], Zhu et al. (2011) [266], Swanson et al. (2010) [221], Haarlemmer et al. (2012) [267], Tunå and Hulteberg (2014) [268], Sarkar et al. (2011) [269], Anex et al. (2010) [270], and Meerman et al. (2012) [271]. Alphabetically, each of the cited papers indicate that jet fuel is *not* the only product made in Fischer-Tropsch processing.

Anex et al. (2010) [270]	"Both scenarios produce naphtha- and diesel-range stock fuel"
Atsonios et al. (2015) [51]	Table 8: even split in FT pathway between (av)gasoline and SAF
Ekbom et al. (2009) [52]	Table 4: Naphtha, Heavy Diesel, and Bio-jet listed as products
Meerman et al. (2012) [271]	"Four different outputs…FT-liquids (gasoline/diesel)"
Sarkar et al. (2011) [269]	"The yields of gasoline and diesel are assumed to be…"
Swanson et al. (2010) [221]	Table 8: Product distribution lists 4 different fuels
Tunå and Hulteberg (2014) [268]	"A large part of the produced hydrocarbons are out of the diesel range"
Zhu et al. (2011) [266]	Table 4-2: Diesel and Naphtha as fuel products

Of these papers, the most relevant to jet fuel are Atsonios et al. (2015) [51] and Ekbom et al. (2009) [52]. Both articles explicitly state the goal of producing fuel that is usable in the

aviation industry (the other publications do not). In Atsonios et al., the distinction between jet fuel and avgas is made in the second paragraph of the introduction. In Ekbom et al., Section 2 discusses at length the requirements for producing a suitable blendstock for use in a jet engine. Also of note is that de Jong et al. (which Uludere Aragon et al. cites) explicitly states that jet fuel is not the only product for the Fischer-Tropsch pathway (Table 4).

Still unconvinced, we reviewed additional publications. The takeaways of this review were that (1) most publications agree that the Hydroprocessing of Fischer-Tropsch liquids cannot be executed so many times as to reliably produce Jet-A in a cost-effective manner (Pearlson et al. [2013] [49] has the best discussion of this; Table 1) and that (2) there is a lot of uncertainty surrounding what can be used in jet engines and what can be classified as SAF (e.g., Huang et al. [2019] [272] claims diesel = SAF, which we disagree with). There are a couple of publications (Crawford et al. [2016] [273], Michailos and Bridgwater [2019] [274], Alves et al. [2016] [275]) that claim only primarily jet fuel can be produced through a different chemical processing technique. For each article which would claim 100% conversion to jet fuel, there were multiple others which state jet fuel can't be the only product. However, each of the papers which state 100% to jet fuel has a unique set of additional economic data that was not incorporated into Uludere Aragon et al.'s assumptions.

Based on the number publications which state the Fischer-Tropsch pathway cannot solely produce Jet-A fuel, we have assumed a conversion factor of 0.49 kg jet fuel for each kg of input biocrude for this study [225]. It is our hypothesis that the assumption by Huang et al. (2019) to use 100% biojet fuel as the end product has created confusion in the literature. Therefore, we recommend future studies carefully consider the pathways they are using and understand the literature landscape before selecting appropriate end products and conversion factors.

Corn Grain Cultivation (Inputs)	
Nitrogen Fert:	180 kg/year
Phosphorus Fert:	84 kg/year
Potassium Fert:	108 kg/year
Herbicide:	1 kg/year
Corn Seed:	18 kg/year
Diesel Use:	128 kg/year
Labor:	$82/year
Capital Cost:	$5,977

Starch Fermentation (Inputs)	
Corn Grain:	$10x10^3$ kg/year
Sodium Hydroxide:	55 kg/year
Lime:	13 kg/year
Sulfuric Acid:	22 kg/year
Natural Gas:	794 kg/year
Grid Electricity:	3,375 MJ/year
Labor:	$281/year
Capital Cost:	$1937

Ethanol-to-Jet (Inputs)	
Ethanol:	3,479 kg/year
Hydrogen:	36 kg/year
Cobalt:	7 kg/year
Grid Electricity:	2,108 MJ/year
Water:	4,935 kg/year
Labor:	$8/year
Capital Cost:	$525

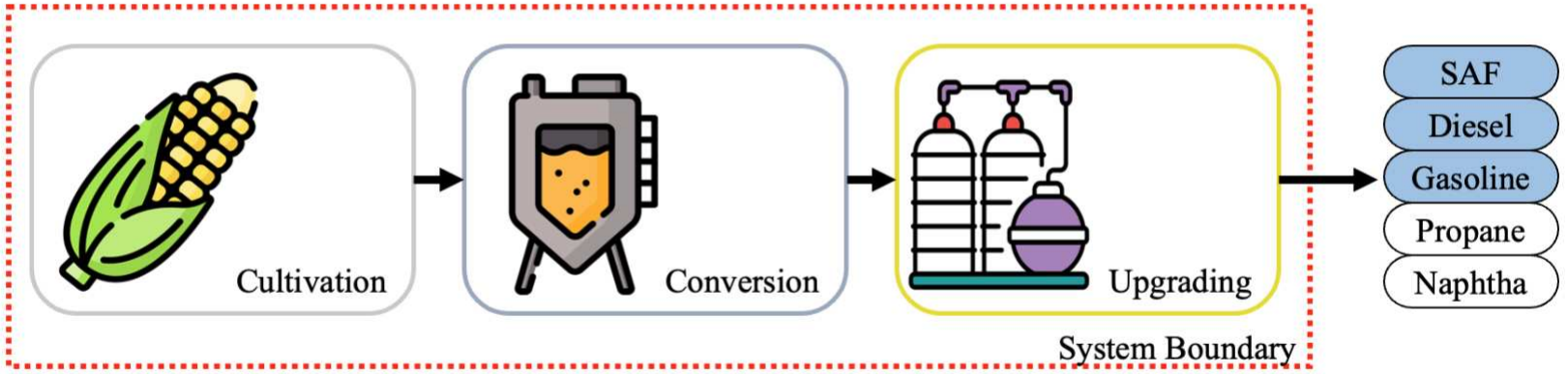

Corn Grain Cultivation (Outputs)	
N_2O Emissions:	4 kg/year
Corn Grain:	$10x10^3$ kg/year

Starch Fermentation (Outputs)	
Fuel Ethanol:	3,479 kg/year
DDGS:	3,781 kg/year
CO_2 Emissions:	3,714 kg/year

Ethanol-to-Jet (Outputs)	
Jet-A (SAF):	1,363 kg/year
Diesel, Produced:	162 kg/year
Gasoline, Produced:	282 kg/year
Wastewater:	4,936 kg/year

Figure C1. Process inputs, outputs, and references associated with the corn grain to sustainable aviation fuel pathway using the ethanol-to-jet process.[209,210,219,224,276]

Soybean Cultivation (Inputs)	
Nitrogen Fert:	6 kg/year
Phosphorus Fert:	11 kg/year
Potassium Fert:	34 kg/year
Herbicide:	2 kg/year
Soybean Seed:	111 kg/year
Diesel Use:	48 kg/year
Labor:	$62/year
Capital Cost:	$6,817

Hexane Extraction (Inputs)	
Soybeans:	3,017 kg/year
Water:	778 kg/year
Hexane:	3 kg/year
Natural Gas:	52 kg/year
Grid Electricity:	241 MJ/year
Labor:	$25/year
Capital Cost:	$997

Hydroprocessing (Inputs)	
Soybean Oil:	670 kg/year
Hydrogen:	27 kg/year
Natural Gas:	100 kg/year
Grid Electricity:	148 MJ/year
Water:	603 kg/year
Labor:	$3/year
Capital Cost:	$121

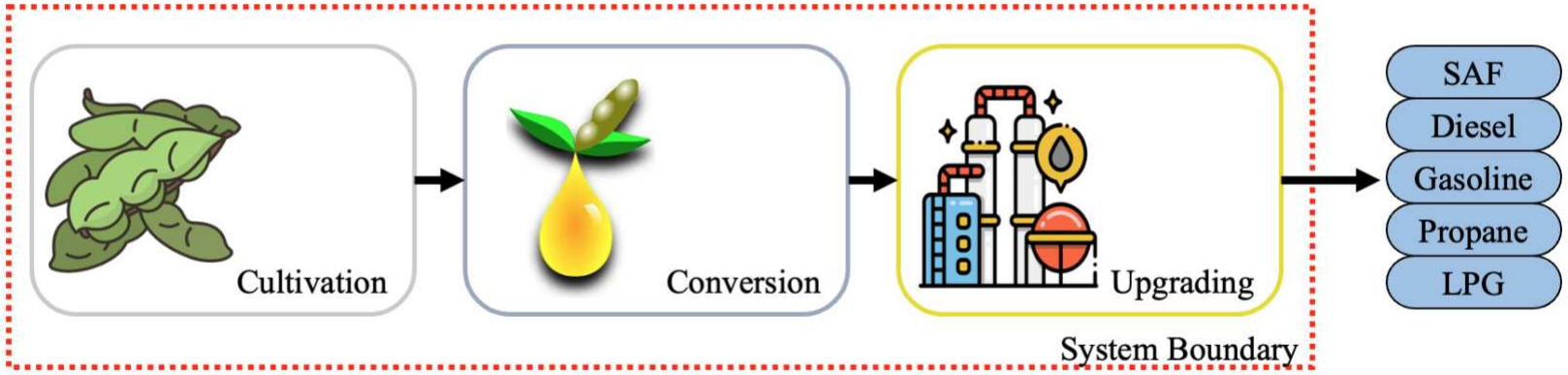

Soybean Cultivation (Outputs)	
N_2O Emissions:	2 kg/year
Soybean:	3,017 kg/year

Hexane Extraction (Outputs)	
Soybean Oil:	671 kg/year
Soybean Meal:	2,347 kg/year
Wastewater:	780 kg/year

Hydroprocessing (Outputs)	
Jet-A (SAF):	331 kg/year
Diesel, Produced:	156 kg/year
Propane, Produced:	28 kg/year
LPG, Produced:	40 kg/year
Gasoline, Produced:	47 kg/year
Wastewater:	604 kg/year

Figure C2. Process inputs, outputs, and references associated with the soybean to sustainable aviation fuel pathway using the hexane extraction process. [213,276,220,49]

Switchgrass Cultivation (Inputs)	
Nitrogen Fert:	135 kg/year
Phosphorus Fert:	13 kg/year
Potassium Fert:	110 kg/year
Ag Lime:	672 kg/year
Herbicide:	2 kg/year
Diesel Use:	16 kg/year
Labor:	$33/year
Capital Cost:	$2,300

Gasification-FT (Inputs)	
Switchgrass:	$16x10^3$ kg/year
Water:	8,816 kg/year
Cobalt:	2 kg/year
Air:	$23x10^3$ kg/year
Electricity:	$17x10^3$ MJ/year
Propane:	389 kg/year
Labor:	$97/year
Capital Cost:	$9,244

Hydroprocessing (Inputs)	
Biocrude:	2,410 kg/year
Grid Electricity:	1,100 MJ/year
Water:	1,596 kg/year
Labor:	$5/year
Capital Cost:	$67

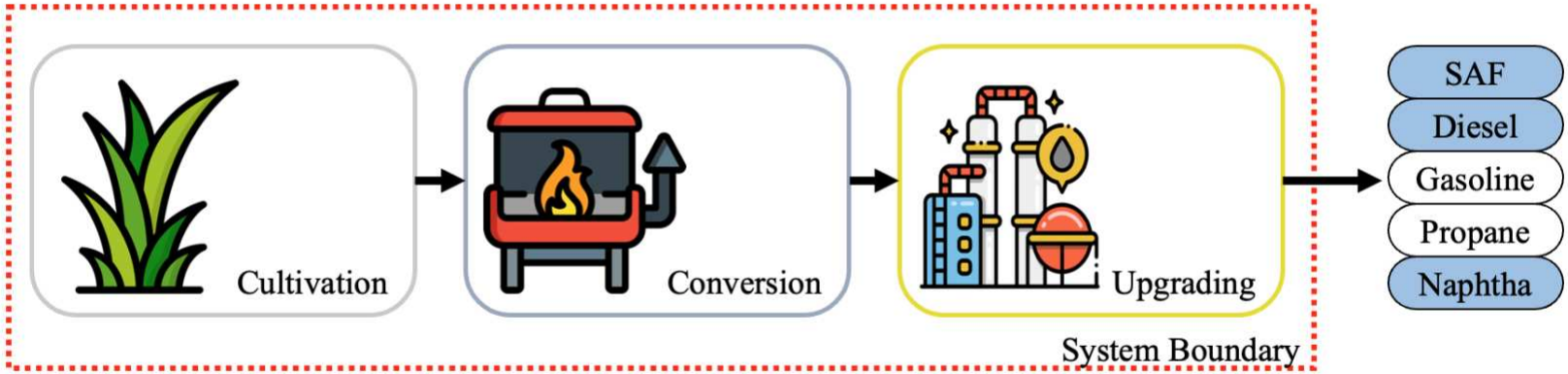

Switchgrass Cultivation (Outputs)	
N_2O Emissions:	3 kg/year
Switchgrass:	$16x10^3$ kg/year

Gasification-FT (Outputs)	
Biocrude:	2,410 kg/year
Slag:	916 kg/year
Hydrogen:	32 kg/year
CO_2 Emissions:	$16x10^3$ kg/year
Electricity, Gen.:	$25x10^3$ MJ/year
Wastewater:	9,529 kg/year

Hydroprocessing (Outputs)	
Jet-A (SAF):	1,421 kg/year
Diesel, Produced:	744 kg/year
Naphtha, Produced:	243 kg/year
Wastewater:	1,596 kg/year

Figure C3. Process inputs, outputs, and references associated with the switchgrass to sustainable aviation fuel pathway using the gasification Fischer-Tropsch process. [214,221,225,276]

Miscanthus Cultivation (Inputs)	
Nitrogen Fert:	88 kg/year
Phosphorus Fert:	17 kg/year
Potassium Fert:	88 kg/year
Ag Lime:	336 kg/year
Herbicide:	1 kg/year
Diesel Use:	16 kg/year
Labor:	$33/year
Capital Cost:	$1,346

Gasification-FT (Inputs)	
Miscanthus:	$22x10^3$ kg/year
Water:	$12x10^3$ kg/year
Cobalt:	3 kg/year
Air:	$32x10^3$ kg/year
Electricity:	$23x10^3$ MJ/year
Propane:	534 kg/year
Labor:	$134/year
Capital Cost:	$12,711

Hydroprocessing (Inputs)	
Biocrude:	3,313kg/year
Grid Electricity:	1,500 MJ/year
Water:	2,159 kg/year
Labor:	$7/year
Capital Cost:	$92

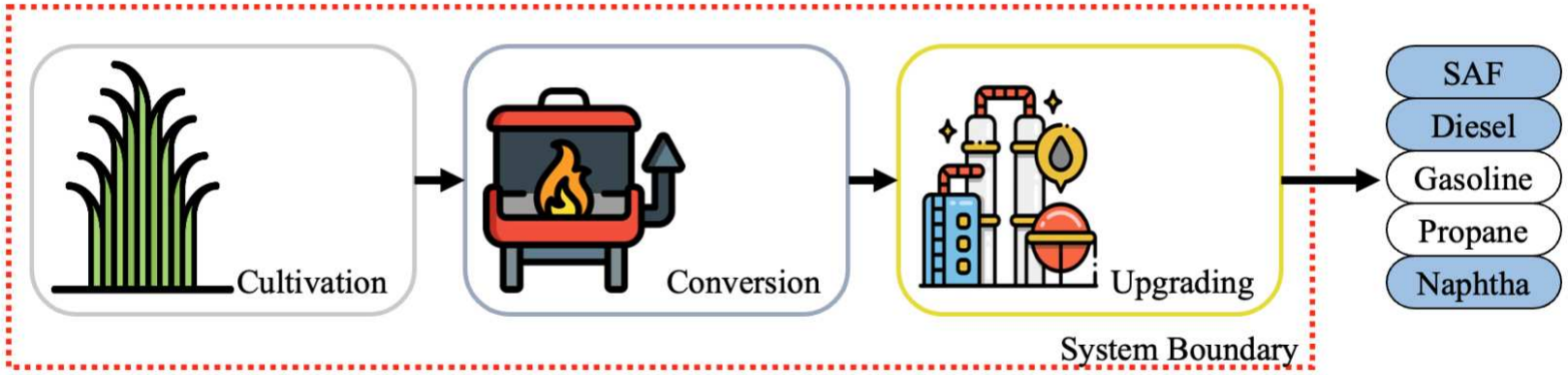

Miscanthus Cultivation (Outputs)	
N_2O Emissions:	2 kg/year
Miscanthus:	$22x10^3$ kg/year

Gasification-FT (Outputs)	
Biocrude:	3,313 kg/year
Slag:	1,260 kg/year
Hydrogen:	44 kg/year
CO_2 Emissions:	$22x10^3$ kg/year
Electricity, Gen.:	$35x10^3$ MJ/year
Wastewater:	$13x10^3$ kg/year

Hydroprocessing (Outputs)	
Jet-A (SAF):	1,955 kg/year
Diesel, Produced:	1,023 kg/year
Naphtha, Produced:	335 kg/year
Wastewater:	2,195 kg/year

Figure C4. Process inputs, outputs, and references associated with the miscanthus to sustainable aviation fuel pathway using the gasification Fischer-Tropsch process. [215,221,225,276]

Sorghum Cultivation (Inputs)	
Nitrogen Fert:	100 kg/year
Phosphorus Fert:	26 kg/year
Potassium Fert:	33 kg/year
Herbicide:	4 kg/year
Sorghum Seed:	4 kg/year
Diesel Use:	16 kg/year
Labor:	$33/year
Capital Cost:	$1,345

Gasification-FT (Inputs)	
Sorghum:	$19x10^3$ kg/year
Water:	$10x10^3$ kg/year
Cobalt:	2 kg/year
Air:	$28x10^3$ kg/year
Electricity:	$20x10^3$ kg/year
Propane:	462 kg/year
Labor:	$115/year
Capital Cost:	$10,977

Hydroprocessing (Inputs)	
Biocrude:	2,861 kg/year
Grid Electricity:	1,300 MJ/year
Water:	1,896 kg/year
Labor:	$7/year
Capital Cost:	$79

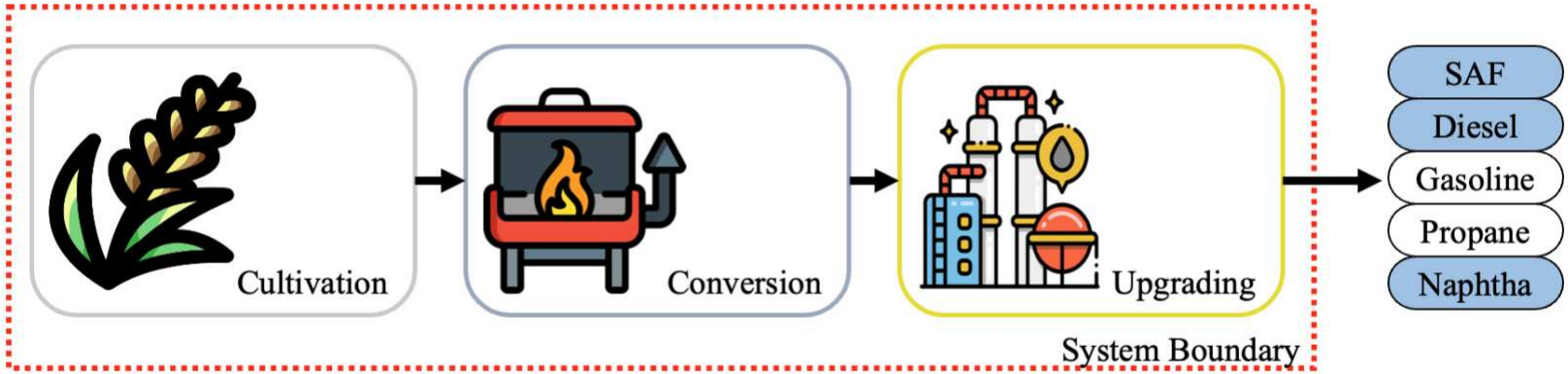

Sorghum Cultivation (Outputs)	
N_2O Emissions:	2 kg/year
Sorghum:	$19x10^3$ kg/year

Gasification-FT (Outputs)	
Biocrude:	2,861 kg/year
Slag:	1,088 kg/year
Hydrogen:	38 kg/year
CO_2 Emissions:	$19x10^3$ kg/year
Electricity, Gen.:	$30x10^3$ MJ/year
Wastewater:	$11x10^3$ kg/year

Hydroprocessing (Outputs)	
Jet-A (SAF):	1,688 kg/year
Diesel, Produced:	884 kg/year
Naphtha, Produced:	289 kg/year
Wastewater:	1,896 kg/year

Figure C5. Process inputs, outputs, and references associated with the sorghum to sustainable aviation fuel pathway using the gasification Fischer-Tropsch process. [221,225,276,277]

Poplar Cultivation (Inputs)	
Nitrogen Fert:	6 kg/year
Phosphorus Fert:	1 kg/year
Potassium Fert:	1 kg/year
Herbicide:	1 kg/year
Poplar Cuttings:	1,077 kg/year
Diesel Use:	417 kg/year
Labor:	$18/year
Capital Cost:	$1,183

Gasification-FT (Inputs)	
Poplar:	$12x10^3$ kg/year
Water:	6,350 kg/year
Cobalt:	1 kg/year
Air:	$17x10^3$ kg/year
Electricity:	$13x10^3$ MJ/year
Propane:	280 kg/year
Labor:	$70/year
Capital Cost:	$6,659

Hydroprocessing (Inputs)	
Biocrude:	1,736 kg/year
Grid Electricity:	800 MJ/year
Water:	1,150 kg/year
Labor:	$4/year
Capital Cost:	$48

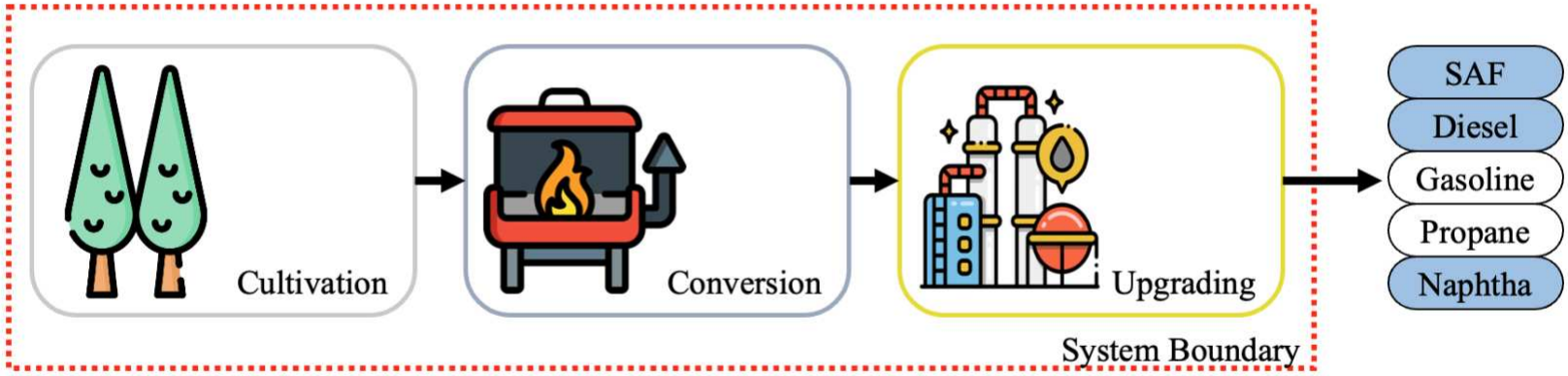

Poplar Cultivation (Outputs)	
N_2O Emissions:	1 kg/year
Poplar:	$12x10^3$ kg/year

Gasification-FT (Outputs)	
Biocrude:	1,736 kg/year
Slag:	660 kg/year
Hydrogen:	23 kg/year
CO_2 Emissions:	$11x10^3$ kg/year
Electricity, Gen.:	$19x10^3$ MJ/year
Wastewater:	6,864 kg/year

Hydroprocessing (Outputs)	
Jet-A (SAF):	1,024 kg/year
Diesel, Produced:	536 kg/year
Naphtha, Produced:	175 kg/year
Wastewater:	1,150 kg/year

Figure C6. Process inputs, outputs, and references associated with the poplar to sustainable aviation fuel pathway using the gasification Fischer-Tropsch process. [217,221,225,276]

Willow Cultivation (Inputs)	
Nitrogen Fert:	32 kg/year
Herbicide:	1 kg/year
Willow Cuttings:	1,295 kg/year
Sorghum Seed:	4 kg/year
Diesel Use:	459 kg/year
Labor:	$18/year
Capital Cost:	$1,183

Gasification-FT (Inputs)	
Willow:	8,781 kg/year
Water:	4,839 kg/year
Cobalt:	1 kg/year
Air:	13×10^3 kg/year
Electricity:	9×10^3 MJ/year
Propane:	213 kg/year
Labor:	$53/year
Capital Cost:	$5,074

Hydroprocessing (Inputs)	
Biocrude:	1,323 kg/year
Grid Electricity:	610 MJ/year
Water:	876 kg/year
Labor:	$3/year
Capital Cost:	$37

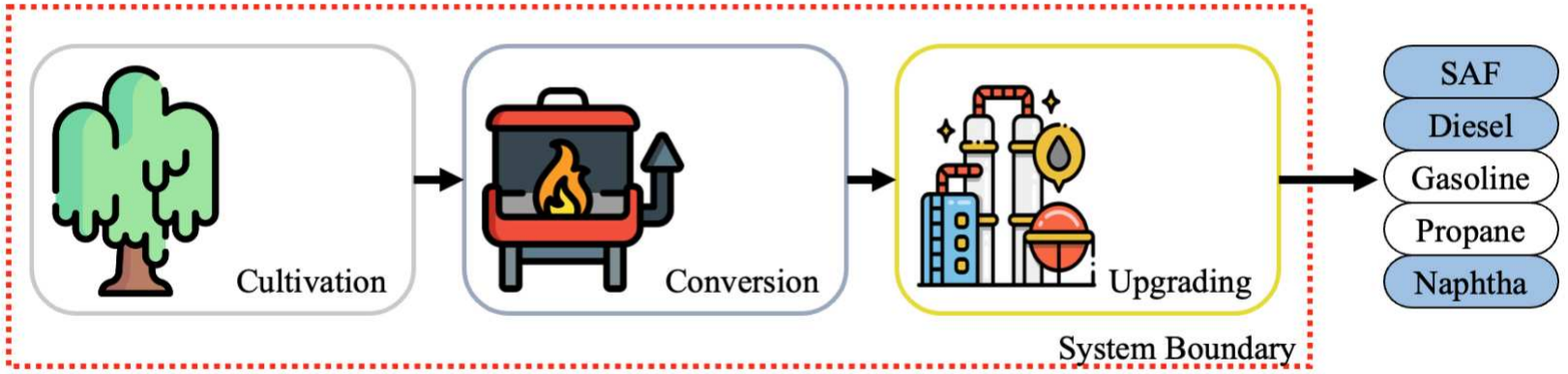

Willow Cultivation (Outputs)	
N_2O Emissions:	1 kg/year
Willow:	8,781 kg/year

Gasification-FT (Outputs)	
Biocrude:	1,323 kg/year
Slag:	503 kg/year
Hydrogen:	18 kg/year
CO_2 Emissions:	8,648 kg/year
Electricity, Gen.:	14×10^3 MJ/year
Wastewater:	5,230 kg/year

Hydroprocessing (Outputs)	
Jet-A (SAF):	780 kg/year
Diesel, Produced:	408 kg/year
Naphtha, Produced:	134 kg/year
Wastewater:	876 kg/year

Figure C7. Process inputs, outputs, and references associated with the willow to sustainable aviation fuel pathway using the gasification Fischer-Tropsch process. [218,221,225,276]

Algae Cultivation (Inputs)	
Nitrogen Fert:	757 kg/year
Phosphorus Fert:	93 kg/year
Atmospheric CO_2:	$82x10^3$ kg/year
LDPE:	1,153 kg/year
Seawater:	$85x10^6$ kg/year
Grid Electricity:	98,595 MJ/year
Labor:	$10,983/year
Capital Cost:	$359,504

Hydrothermal Liquefaction (Inputs)	
Algae Biomass:	$41x10^3$ kg/year
Grid Electricity:	$113x10^3$ MJ/year
Natural Gas:	210 kg/year
Labor:	$340/year
Capital Cost:	$30,843

Hydroprocessing (Inputs)	
Biocrude:	$20x10^3$ kg/year
Hydrogen:	815 kg/year
Natural Gas:	3,046 kg/year
Grid Electricity:	4,480 MJ/year
Water:	18,328 kg/year
Labor:	$99/year
Capital Cost:	$3,665

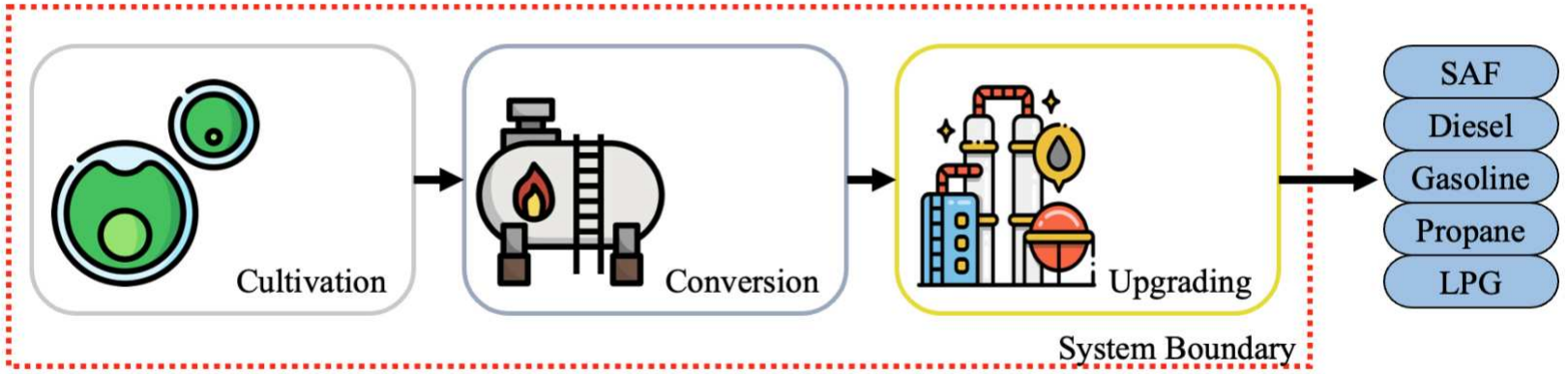

Algae Cultivation (Outputs)	
Seawater:	$85x10^6$ kg/year
CO_2 Emissions:	$59x10^3$ kg/year
Ash and Sludge:	1,153 kg/year
Algal Biomass:	$41x10^3$ kg/year

Hydrothermal Liquefaction (Outputs)	
Wastewater:	$20x10^3$ kg/year
Algal Biocrude:	$20x10^3$ kg/year

Hydroprocessing (Outputs)	
Jet-A (SAF):	$10x10^3$ kg/year
Propane, Produced:	855 kg/year
LPG, Produced:	1,222 kg/year
Diesel, Produced:	4,745 kg/year
Gas, Produced:	1,426 kg/year
CO_2 Emissions:	1,100 kg/year

Figure C8. Process inputs, outputs, and references associated with the microalgae to sustainable aviation fuel pathway using the hydrothermal liquefaction process. [49,189,190,266]

Table C1. Optimization results breakdown by crop for the 25-billion-gallon SAF scenario when optimized for minimum fuel costs.

	Jet Fuel (million gallons)	Jet Fuel Percentage	Land Use (ha)	Land Use Percentage (SAF)	Land Use Percentage (CONUS)	MFSP ($/gallon Jet)	GHG (gCO2e/MJ)	Carbon Price ($/tCO2e)
Algae	-	0.0%	-	0.0%	0.0%	$-	-	$-
Upland Switchgrass	-	0.0%	-	0.0%	0.0%	$-	-	$-
Lowland Switchgrass	-	0.0%	-	0.0%	0.0%	$-	-	$-
Miscanthus	12,582.2	50.3%	21,042,646	51.1%	2.7%	$3.23	48.68	$281.94
Poplar	-	0.0%	-	0.0%	0.0%	$-	-	$-
Corn	-	0.0%	-	0.0%	0.0%	$-	-	$-
Soy	160.3	0.6%	998,617	2.4%	0.1%	$3.13	(1.85)	$108.44
Willow	-	0.0%	-	0.0%	0.0%	$-	-	$-
Sorghum	12,257.5	49.0%	19,126,338	46.5%	2.5%	$3.26	46.18	$269.64

Table C2. Optimization results breakdown by land for the 25-billion-gallon SAF scenario when optimized for minimum fuel costs.

	Jet Fuel (million gallons)	Jet Fuel Percentage	Land Use (ha)	Land Use Percentage (SAF)	Land Use Percentage (CONUS)	MFSP ($/gallon Jet)	GHG (gCO2e/MJ)	Carbon Price ($/tCO2e)
Barren Land	-	0.0%	-	0.0%	0.0%	$-	-	$-
Deciduous Forest	7,822.8	31.3%	12,559,163	30.5%	1.6%	$3.19	55.72	$339.67
Evergreen Forest	1,620.9	6.5%	2,736,166	6.6%	0.4%	$3.25	75.56	$1,118.41
Mixed Forest	2,351.3	9.4%	3,897,129	9.5%	0.5%	$3.22	68.59	$624.41
Shrubland	2,447.6	9.8%	3,811,954	9.3%	0.5%	$3.23	61.81	$444.56
Grassland Herbaceous	6,612.2	26.4%	11,333,533	27.5%	1.5%	$3.28	39.99	$235.20
Cultivated Crops	4,145.3	16.6%	6,829,656	16.6%	0.9%	$3.31	10.34	$145.10

Table C3. Optimization results breakdown by crop for the 25-billion-gallon SAF scenario when optimized for minimum fuel emissions.

	Jet Fuel (million gallons)	Jet Fuel Percentage	Land Use (ha)	Land Use Percentage (SAF)	Land Use Percentage (CONUS)	MFSP ($/gallon Jet)	GHG (gCO2e/MJ)	Carbon Price ($/tCO2e)
Algae	-	0.0%	-	0.0%	0.0%	$-	-	$-
Upland Switchgrass	14.2	0.1%	57,278	0.1%	0.0%	$4.20	7.97	$228.94
Lowland Switchgrass	-	0.0%	-	0.0%	0.0%	$-	-	$-
Miscanthus	24,886.1	99.5%	89,708,257	99.1%	11.5%	$3.89	4.49	$189.02
Poplar	-	0.0%	-	0.0%	0.0%	$-	-	$-
Corn	0.7	0.0%	2,822	0.0%	0.0%	$7.23	1.10	$485.09
Soy	99.0	0.4%	714,804	0.8%	0.1%	$3.60	(12.75)	$133.34
Willow	-	0.0%	-	0.0%	0.0%	$-	-	$-
Sorghum	-	0.0%	-	0.0%	0.0%	$-	-	$-

Table C4. Optimization results breakdown by land for the 25-billion-gallon SAF scenario when optimized for minimum fuel emissions.

	Jet Fuel (million gallons)	Jet Fuel Percentage	Land Use (ha)	Land Use Percentage (SAF)	Land Use Percentage (CONUS)	MFSP ($/gallon Jet)	GHG (gCO2e/MJ)	Carbon Price ($/tCO2e)
Barren Land	-	0.0%	-	0.0%	0.0%	$-	-	$-
Deciduous Forest	169.3	0.7%	241,977	0.3%	0.0%	$3.13	13.96	$133.12
Evergreen Forest	61.2	0.2%	239,377	0.3%	0.0%	$3.96	13.85	$221.89
Mixed Forest	30.6	0.1%	43,882	0.0%	0.0%	$3.14	13.28	$133.03
Shrubland	5,416.0	21.7%	35,849,717	39.6%	4.6%	$4.53	4.09	$248.68
Grassland Herbaceous	9,880.4	39.5%	37,220,404	41.1%	4.8%	$3.88	7.88	$197.07
Cultivated Crops	9,442.5	37.8%	16,887,805	18.7%	2.2%	$3.53	0.74	$148.68

Table C5. Optimization results breakdown by crop for the 25-billion-gallon SAF scenario when optimized for minimum carbon price.

	Jet Fuel (million gallons)	Jet Fuel Percentage	Land Use (ha)	Land Use Percentage (SAF)	Land Use Percentage (CONUS)	MFSP ($/gallon Jet)	GHG (gCO2e/MJ)	Carbon Price ($/tCO2e)
Algae	-	0.0%	-	0.0%	0.0%	$-	-	$-
Upland Switchgrass	-	0.0%	-	0.0%	0.0%	$-	-	$-
Lowland Switchgrass	-	0.0%	-	0.0%	0.0%	$-	-	$-
Miscanthus	22,008.9	88.0%	56,246,039	90.8%	7.2%	$3.61	7.30	$168.31
Poplar	-	0.0%	-	0.0%	0.0%	$-	-	$-
Corn	-	0.0%	-	0.0%	0.0%	$-	-	$-
Soy	143.1	0.6%	913,642	1.5%	0.1%	$3.22	(6.11)	$111.58
Willow	-	0.0%	-	0.0%	0.0%	$-	-	$-
Sorghum	2,847.9	11.4%	4,776,606	7.7%	0.6%	$3.26	32.70	$199.24

Table C6. Optimization results breakdown by land for the 25-billion-gallon SAF scenario when optimized for minimum carbon price.

	Jet Fuel (million gallons)	Jet Fuel Percentage	Land Use (ha)	Land Use Percentage (SAF)	Land Use Percentage (CONUS)	MFSP ($/gallon Jet)	GHG (gCO2e/MJ)	Carbon Price ($/tCO2e)
Barren Land	-	0.0%	-	0.0%	0.0%	$-	-	$-
Deciduous Forest	1,909.0	7.6%	2,779,351	4.5%	0.4%	$3.12	31.61	$176.16
Evergreen Forest	35.2	0.1%	113,348	0.2%	0.0%	$3.71	15.75	$200.60
Mixed Forest	247.9	1.0%	364,922	0.6%	0.0%	$3.13	29.64	$170.94
Shrubland	2,074.9	8.3%	8,866,258	14.3%	1.1%	$3.92	6.07	$196.47
Grassland Herbaceous	11,351.7	45.4%	33,016,623	53.3%	4.2%	$3.62	14.56	$186.78
Cultivated Crops	9,381.4	37.5%	16,795,784	27.1%	2.2%	$3.52	0.73	$147.53

Table C7. Optimization results breakdown by crop for the 25-billion-gallon SAF scenario when optimized for minimum land use.

	Jet Fuel (million gallons)	Jet Fuel Percentage	Land Use (ha)	Land Use Percentage (SAF)	Land Use Percentage (CONUS)	MFSP ($/gallon Jet)	GHG (gCO2e/MJ)	Carbon Price ($/tCO2e)
Algae	25,587.5	100.0%	3,671,472	100.0%	0.5%	$8.65	62.76	$2,334.57
Upland Switchgrass	-	0.0%	-	0.0%	0.0%	$-	-	$-
Lowland Switchgrass	-	0.0%	-	0.0%	0.0%	$-	-	$-
Miscanthus	-	0.0%	-	0.0%	0.0%	$-	-	$-
Poplar	-	0.0%	-	0.0%	0.0%	$-	-	$-
Corn	-	0.0%	-	0.0%	0.0%	$-	-	$-
Soy	-	0.0%	-	0.0%	0.0%	$-	-	$-
Willow	-	0.0%	-	0.0%	0.0%	$-	-	$-
Sorghum	-	0.0%	-	0.0%	0.0%	$-	-	$-

Table C8. Optimization results breakdown by land for the 25-billion-gallon SAF scenario when optimized for minimum land use.

	Jet Fuel (million gallons)	Jet Fuel Percentage	Land Use (ha)	Land Use Percentage (SAF)	Land Use Percentage (CONUS)	MFSP ($/gallon Jet)	GHG (gCO2e/MJ)	Carbon Price ($/tCO2e)
Barren Land	3,857.2	15.1%	559,921	15.3%	0.1%	$8.84	62.76	$2,399.24
Deciduous Forest	23.9	0.1%	3,428	0.1%	0.0%	$8.59	64.17	$2,470.99
Evergreen Forest	484.5	1.9%	69,315	1.9%	0.0%	$8.54	64.60	$2,506.81
Mixed Forest	91.7	0.4%	13,068	0.4%	0.0%	$8.52	64.16	$2,443.84
Shrubland	16,554.9	64.7%	2,367,848	64.5%	0.3%	$8.62	62.73	$2,320.35
Grassland Herbaceous	4,575.3	17.9%	657,892	17.9%	0.1%	$8.62	62.65	$2,312.29
Cultivated Crops	-	0.0%	-	0.0%	0.0%	$-	-	$-

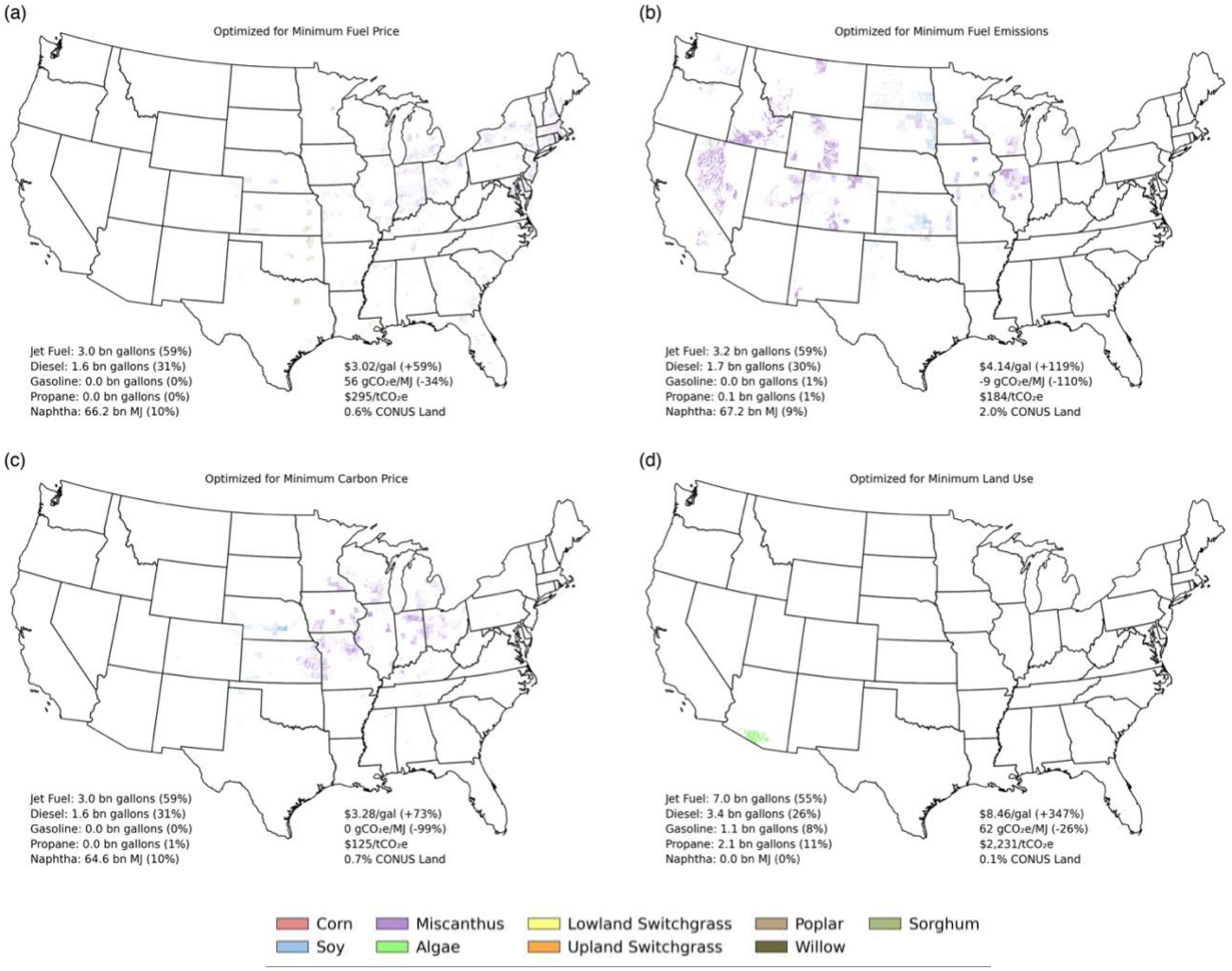

Figure C9. Multi-objective optimization maps of the optimal geographic feedstock deployment to meet 3 billion gallons of annual SAF production while minimizing fuel price (a), fuel emissions (b), breakeven carbon price (c), and land area (d). Percentages in parentheses for the fuel products represent the total percent of megajoules produced for that fuel type as a percentage of total megajoules of fuel produced by the feedstocks. Percentages in parentheses for the mean fuel selling price and mean fuel emissions represent the percent cost increase and percent emissions reduction, respectively, compared to petroleum jet fuel.

Table C9. Optimization results breakdown by crop for the 3-billion-gallon SAF scenario when optimized for minimum fuel costs.

	Jet Fuel (million gallons)	Jet Fuel Percentage	Land Use (ha)	Land Use Percentage (SAF)	Land Use Percentage (CONUS)	MFSP ($/gallon Jet)	GHG (gCO2e/MJ)	Carbon Price ($/tCO2e)
Algae	-	0.0%	-	0.0%	0.0%	$-	-	$-
Upland Switchgrass	-	0.0%	-	0.0%	0.0%	$-	-	$-
Lowland Switchgrass	-	0.0%	-	0.0%	0.0%	$-	-	$-
Miscanthus	2,191.2	73.0%	3,479,850	71.5%	0.4%	$3.01	59.40	$334.72
Poplar	-	0.0%	-	0.0%	0.0%	$-	-	$-
Corn	-	0.0%	-	0.0%	0.0%	$-	-	$-
Soy	57.1	1.9%	349,206	7.2%	0.0%	$2.77	(4.76)	$74.73
Willow	-	0.0%	-	0.0%	0.0%	$-	-	$-
Sorghum	751.7	25.1%	1,038,441	21.3%	0.1%	$3.05	49.84	$252.74

Table C10. Optimization results breakdown by crop for the 3-billion-gallon SAF scenario when optimized for minimum fuel emissions.

	Jet Fuel (million gallons)	Jet Fuel Percentage	Land Use (ha)	Land Use Percentage (SAF)	Land Use Percentage (CONUS)	MFSP ($/gallon Jet)	GHG (gCO2e/MJ)	Carbon Price ($/tCO2e)
Algae	-	0.0%	-	0.0%	0.0%	$-	-	$-
Upland Switchgrass	0.6	0.0%	4,230	0.0%	0.0%	$5.57	(8.92)	$298.75
Lowland Switchgrass	-	0.0%	-	0.0%	0.0%	$-	-	$-
Miscanthus	2,988.8	92.6%	13,820,699	86.8%	1.8%	$4.09	(8.13)	$179.92
Poplar	-	0.0%	-	0.0%	0.0%	$-	-	$-
Corn	0.4	0.0%	2,240	0.0%	0.0%	$9.04	(9.79)	$575.39
Soy	237.8	7.4%	2,095,237	13.2%	0.3%	$4.84	(13.20)	$228.72
Willow	-	0.0%	-	0.0%	0.0%	$-	-	$-
Sorghum	-	0.0%	-	0.0%	0.0%	$-	-	$-

Table C11. Optimization results breakdown by crop for the 3-billion-gallon SAF scenario when optimized for minimum carbon price.

	Jet Fuel (million gallons)	Jet Fuel Percentage	Land Use (ha)	Land Use Percentage (SAF)	Land Use Percentage (CONUS)	MFSP ($/gallon Jet)	GHG (gCO2e/MJ)	Carbon Price ($/tCO2e)
Algae	-	0.0%	-	0.0%	0.0%	$-	-	$-
Upland Switchgrass	-	0.0%	-	0.0%	0.0%	$-	-	$-
Lowland Switchgrass	-	0.0%	-	0.0%	0.0%	$-	-	$-
Miscanthus	2,872.3	95.7%	4,378,368	84.6%	0.6%	$3.29	0.65	$126.55
Poplar	-	0.0%	-	0.0%	0.0%	$-	-	$-
Corn	-	0.0%	-	0.0%	0.0%	$-	-	$-
Soy	127.7	4.3%	799,905	15.4%	0.1%	$3.06	(4.36)	$99.78
Willow	-	0.0%	-	0.0%	0.0%	$-	-	$-
Sorghum	-	0.0%	-	0.0%	0.0%	$-	-	$-

Table C12. Optimization results breakdown by crop for the 3-billion-gallon SAF scenario when optimized for minimum land use.

	Jet Fuel (million gallons)	Jet Fuel Percentage	Land Use (ha)	Land Use Percentage (SAF)	Land Use Percentage (CONUS)	MFSP ($/gallon Jet)	GHG (gCO2e/MJ)	Carbon Price ($/tCO2e)
Algae	6,976.8	100.0%	980,060	100.0%	0.1%	$8.46	62.39	$2,231.34
Upland Switchgrass	-	0.0%	-	0.0%	0.0%	$-	-	$-
Lowland Switchgrass	-	0.0%	-	0.0%	0.0%	$-	-	$-
Miscanthus	-	0.0%	-	0.0%	0.0%	$-	-	$-
Poplar	-	0.0%	-	0.0%	0.0%	$-	-	$-
Corn	-	0.0%	-	0.0%	0.0%	$-	-	$-
Soy	-	0.0%	-	0.0%	0.0%	$-	-	$-
Willow	-	0.0%	-	0.0%	0.0%	$-	-	$-
Sorghum	-	0.0%	-	0.0%	0.0%	$-	-	$-

Table C13. Optimization results breakdown by land for the 3-billion-gallon SAF scenario when optimized for minimum fuel costs.

	Jet Fuel (million gallons)	Jet Fuel Percentage	Land Use (ha)	Land Use Percentage (SAF)	Land Use Percentage (CONUS)	MFSP ($/gallon Jet)	GHG (gCO2e/MJ)	Carbon Price ($/tCO2e)
Barren Land	-	0%	-	0%	0%	$-	-	$-
Deciduous Forest	1,637.1	55%	2,512,045	52%	0%	$3.02	52.71	$267.11
Evergreen Forest	223.0	7%	360,741	7%	0%	$3.00	81.45	$2,526.46
Mixed Forest	409.6	14%	662,429	14%	0%	$3.00	70.56	$590.12
Shrubland	232.4	8%	332,556	7%	0%	$3.04	65.29	$448.52
Grassland Herbaceous	412.0	14%	608,303	12%	0%	$3.05	44.72	$219.39
Cultivated Crops	85.8	3%	391,423	8%	0%	$2.87	4.47	$92.39

Table C14. Optimization results breakdown by land for the 3-billion-gallon SAF scenario when optimized for minimum fuel emissions.

	Jet Fuel (million gallons)	Jet Fuel Percentage	Land Use (ha)	Land Use Percentage (SAF)	Land Use Percentage (CONUS)	MFSP ($/gallon Jet)	GHG (gCO2e/MJ)	Carbon Price ($/tCO2e)
Barren Land	-	0%	-	0%	0%	$-	-	$-
Deciduous Forest	0.0	0%	4	0%	0%	$3.99	(4.95)	$177.89
Evergreen Forest	-	0%	-	0%	0%	$-	-	$-
Mixed Forest	-	0%	-	0%	0%	$-	-	$-
Shrubland	868.2	27%	7,984,705	50%	1%	$5.01	(11.58)	$246.21
Grassland Herbaceous	489.9	15%	3,060,770	19%	0%	$4.31	(9.07)	$196.03
Cultivated Crops	1,869.5	58%	4,876,928	31%	1%	$3.70	(6.93)	$150.00

Table C15. Optimization results breakdown by land for the 3-billion-gallon SAF scenario when optimized for minimum carbon price.

	Jet Fuel (million gallons)	Jet Fuel Percentage	Land Use (ha)	Land Use Percentage (SAF)	Land Use Percentage (CONUS)	MFSP ($/gallon Jet)	GHG (gCO2e/MJ)	Carbon Price ($/tCO2e)
Barren Land	-	0%	-	0%	0%	$-	-	$-
Deciduous Forest	142.1	5%	200,779	4%	0%	$3.07	15.07	$128.32
Evergreen Forest	0.4	0%	560	0%	0%	$3.06	13.51	$124.33
Mixed Forest	21.3	1%	30,277	1%	0%	$3.08	13.41	$127.02
Shrubland	4.1	0%	8,692	0%	0%	$3.22	5.33	$127.53
Grassland Herbaceous	187.9	6%	301,659	6%	0%	$3.09	13.21	$127.88
Cultivated Crops	2,644.2	88%	4,636,304	90%	1%	$3.31	(1.38)	$125.05

Table C16. Optimization results breakdown by land for the 3-billion-gallon SAF scenario when optimized for minimum land use.

	Jet Fuel (million gallons)	Jet Fuel Percentage	Land Use (ha)	Land Use Percentage (SAF)	Land Use Percentage (CONUS)	MFSP ($/gallon Jet)	GHG (gCO2e/MJ)	Carbon Price ($/tCO2e)
Barren Land	6.0	0%	836	0%	0%	$8.29	62.08	$2,144.91
Deciduous Forest	2.1	0%	296	0%	0%	$8.41	63.34	$2,312.93
Evergreen Forest	73.4	1%	10,220	1%	0%	$8.33	63.70	$2,322.75
Mixed Forest	12.5	0%	1,744	0%	0%	$8.33	63.68	$2,321.84
Shrubland	6,150.8	88%	864,252	88%	0%	$8.46	62.38	$2,231.03
Grassland Herbaceous	731.9	10%	102,712	10%	0%	$8.45	62.35	$2,224.38
Cultivated Crops	-	0%	-	0%	0%	$-	-	$-

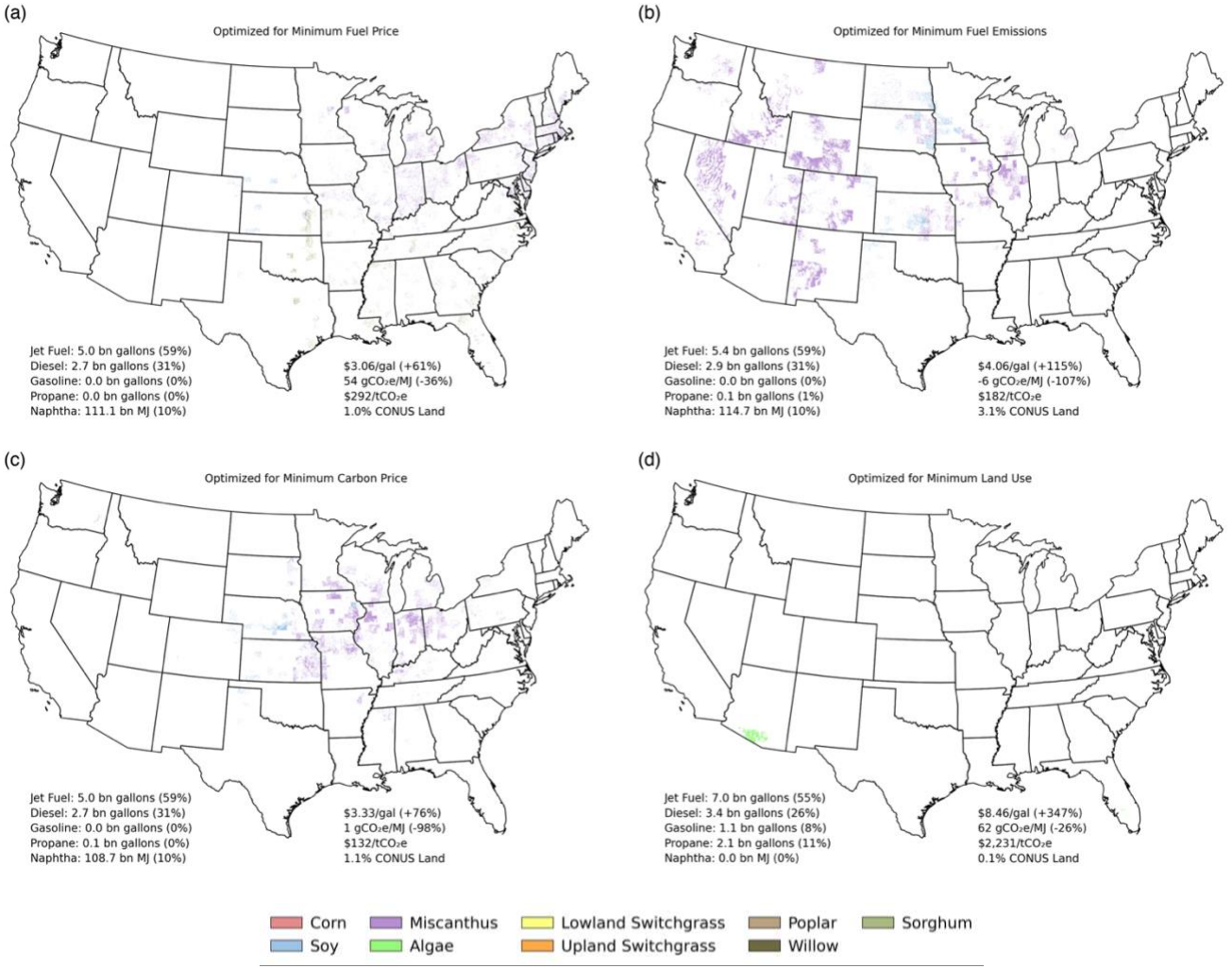

Figure C10. Multi-objective optimization maps of the optimal geographic feedstock deployment to meet 5 billion gallons of annual SAF production while minimizing fuel price (a), fuel emissions (b), breakeven carbon price (c), and land area (d). Percentages in parentheses for the fuel products represent the total percent of megajoules produced for that fuel type as a percentage of total megajoules of fuel produced by the feedstocks. Percentages in parentheses for the mean fuel selling price and mean fuel emissions represent the percent cost increase and percent emissions reduction, respectively, compared to petroleum jet fuel.

Table C17. Optimization results breakdown by crop for the 5-billion-gallon SAF scenario when optimized for minimum fuel costs.

	Jet Fuel (million gallons)	Jet Fuel Percentage	Land Use (ha)	Land Use Percentage (SAF)	Land Use Percentage (CONUS)	MFSP ($/gallon Jet)	GHG (gCO2e/MJ)	Carbon Price ($/tCO2e)
Algae	-	0.0%	-	0.0%	0.0%	$-	-	$-
Upland Switchgrass	-	0.0%	-	0.0%	0.0%	$-	-	$-
Lowland Switchgrass	-	0.0%	-	0.0%	0.0%	$-	-	$-
Miscanthus	3,525.1	70.5%	5,629,352	70.9%	0.7%	$3.05	56.79	$314.85
Poplar	-	0.0%	-	0.0%	0.0%	$-	-	$-
Corn	-	0.0%	-	0.0%	0.0%	$-	-	$-
Soy	57.2	1.1%	349,910	4.4%	0.0%	$2.77	(4.73)	$74.81
Willow	-	0.0%	-	0.0%	0.0%	$-	-	$-
Sorghum	1,417.6	28.4%	1,963,109	24.7%	0.3%	$3.08	51.06	$267.76

Table C18. Optimization results breakdown by crop for the 5-billion-gallon SAF scenario when optimized for minimum fuel emissions.

	Jet Fuel (million gallons)	Jet Fuel Percentage	Land Use (ha)	Land Use Percentage (SAF)	Land Use Percentage (CONUS)	MFSP ($/gallon Jet)	GHG (gCO2e/MJ)	Carbon Price ($/tCO2e)
Algae	-	0.0%	-	0.0%	0.0%	$-	-	$-
Upland Switchgrass	2.0	0.0%	10,586	0.0%	0.0%	$4.63	(3.67)	$235.81
Lowland Switchgrass	-	0.0%	-	0.0%	0.0%	$-	-	$-
Miscanthus	5,098.5	95.1%	21,729,229	90.5%	2.8%	$4.03	(5.68)	$179.46
Poplar	-	0.0%	-	0.0%	0.0%	$-	-	$-
Corn	0.4	0.0%	2,240	0.0%	0.0%	$9.04	(9.79)	$575.39
Soy	261.3	4.9%	2,270,961	9.5%	0.3%	$4.80	(11.79)	$229.18
Willow	-	0.0%	-	0.0%	0.0%	$-	-	$-
Sorghum	-	0.0%	-	0.0%	0.0%	$-	-	$-

Table C19. Optimization results breakdown by crop for the 5-billion-gallon SAF scenario when optimized for minimum carbon price.

	Jet Fuel (million gallons)	Jet Fuel Percentage	Land Use (ha)	Land Use Percentage (SAF)	Land Use Percentage (CONUS)	MFSP ($/gallon Jet)	GHG (gCO2e/MJ)	Carbon Price ($/tCO2e)
Algae	-	0.0%	-	0.0%	0.0%	$-	-	$-
Upland Switchgrass	-	0.0%	-	0.0%	0.0%	$-	-	$-
Lowland Switchgrass	-	0.0%	-	0.0%	0.0%	$-	-	$-
Miscanthus	4,832.6	96.7%	7,526,189	87.7%	1.0%	$3.34	1.62	$132.62
Poplar	-	0.0%	-	0.0%	0.0%	$-	-	$-
Corn	-	0.0%	-	0.0%	0.0%	$-	-	$-
Soy	167.4	3.3%	1,053,041	12.3%	0.1%	$3.14	(2.52)	$108.85
Willow	-	0.0%	-	0.0%	0.0%	$-	-	$-
Sorghum	-	0.0%	-	0.0%	0.0%	$-	-	$-

Table C20. Optimization results breakdown by crop for the 5-billion-gallon SAF scenario when optimized for minimum land use.

	Jet Fuel (million gallons)	Jet Fuel Percentage	Land Use (ha)	Land Use Percentage (SAF)	Land Use Percentage (CONUS)	MFSP ($/gallon Jet)	GHG (gCO2e/MJ)	Carbon Price ($/tCO2e)
Algae	6,976.8	100.0%	980,060	100.0%	0.1%	$8.46	62.39	$2,231.34
Upland Switchgrass	-	0.0%	-	0.0%	0.0%	$-	-	$-
Lowland Switchgrass	-	0.0%	-	0.0%	0.0%	$-	-	$-
Miscanthus	-	0.0%	-	0.0%	0.0%	$-	-	$-
Poplar	-	0.0%	-	0.0%	0.0%	$-	-	$-
Corn	-	0.0%	-	0.0%	0.0%	$-	-	$-
Soy	-	0.0%	-	0.0%	0.0%	$-	-	$-
Willow	-	0.0%	-	0.0%	0.0%	$-	-	$-
Sorghum	-	0.0%	-	0.0%	0.0%	$-	-	$-

Table C21. Optimization results breakdown by land for the 5-billion-gallon SAF scenario when optimized for minimum fuel costs.

	Jet Fuel (million gallons)	Jet Fuel Percentage	Land Use (ha)	Land Use Percentage (SAF)	Land Use Percentage (CONUS)	MFSP ($/gallon Jet)	GHG (gCO2e/MJ)	Carbon Price ($/tCO2e)
Barren Land	-	0%	-	0%	0%	$-	-	$-
Deciduous Forest	2,665.6	53%	4,105,069	52%	1%	$3.06	52.41	$273.43
Evergreen Forest	323.0	6%	523,103	7%	0%	$3.04	80.48	$2,022.23
Mixed Forest	640.0	13%	1,024,338	13%	0%	$3.04	67.01	$490.83
Shrubland	418.6	8%	604,882	8%	0%	$3.07	65.91	$476.44
Grassland Herbaceous	780.3	16%	1,164,603	15%	0%	$3.08	44.77	$225.81
Cultivated Crops	172.6	3%	520,375	7%	0%	$2.99	7.06	$107.18

Table C22. Optimization results breakdown by land for the 5-billion-gallon SAF scenario when optimized for minimum fuel emissions.

	Jet Fuel (million gallons)	Jet Fuel Percentage	Land Use (ha)	Land Use Percentage (SAF)	Land Use Percentage (CONUS)	MFSP ($/gallon Jet)	GHG (gCO2e/MJ)	Carbon Price ($/tCO2e)
Barren Land	-	0%	-	0%	0%	$-	-	$-
Deciduous Forest	0.0	0%	4	0%	0%	$3.99	(4.95)	$177.89
Evergreen Forest	0.0	0%	16	0%	0%	$3.15	(1.43)	$111.19
Mixed Forest	0.0	0%	4	0%	0%	$4.22	(3.01)	$201.94
Shrubland	1,458.0	27%	11,962,389	50%	2%	$4.84	(7.71)	$242.50
Grassland Herbaceous	817.3	15%	4,996,118	21%	1%	$4.32	(6.20)	$202.82
Cultivated Crops	3,086.9	58%	7,054,487	29%	1%	$3.63	(5.10)	$147.18

Table C23. Optimization results breakdown by land for the 5-billion-gallon SAF scenario when optimized for minimum carbon price.

	Jet Fuel (million gallons)	Jet Fuel Percentage	Land Use (ha)	Land Use Percentage (SAF)	Land Use Percentage (CONUS)	MFSP ($/gallon Jet)	GHG (gCO2e/MJ)	Carbon Price ($/tCO2e)
Barren Land	-	0%	-	0%	0%	$-	-	$-
Deciduous Forest	194.2	4%	275,694	3%	0%	$3.08	15.71	$131.20
Evergreen Forest	0.9	0%	1,272	0%	0%	$3.09	16.08	$133.21
Mixed Forest	44.1	1%	63,230	1%	0%	$3.11	15.72	$134.01
Shrubland	8.2	0%	15,341	0%	0%	$3.17	11.40	$132.88
Grassland Herbaceous	425.2	9%	760,556	9%	0%	$3.17	13.03	$135.86
Cultivated Crops	4,327.3	87%	7,463,137	87%	1%	$3.36	(0.46)	$131.45

Table C24. Optimization results breakdown by land for the 5-billion-gallon SAF scenario when optimized for minimum land use.

	Jet Fuel (million gallons)	Jet Fuel Percentage	Land Use (ha)	Land Use Percentage (SAF)	Land Use Percentage (CONUS)	MFSP ($/gallon Jet)	GHG (gCO2e/MJ)	Carbon Price ($/tCO2e)
Barren Land	6.0	0%	836	0%	0%	$8.29	62.08	$2,144.91
Deciduous Forest	2.1	0%	296	0%	0%	$8.41	63.34	$2,312.93
Evergreen Forest	73.4	1%	10,220	1%	0%	$8.33	63.70	$2,322.75
Mixed Forest	12.5	0%	1,744	0%	0%	$8.33	63.68	$2,321.84
Shrubland	6,150.8	88%	864,252	88%	0%	$8.46	62.38	$2,231.03
Grassland Herbaceous	731.9	10%	102,712	10%	0%	$8.45	62.35	$2,224.38
Cultivated Crops	-	0%	-	0%	0%	$-	-	$-

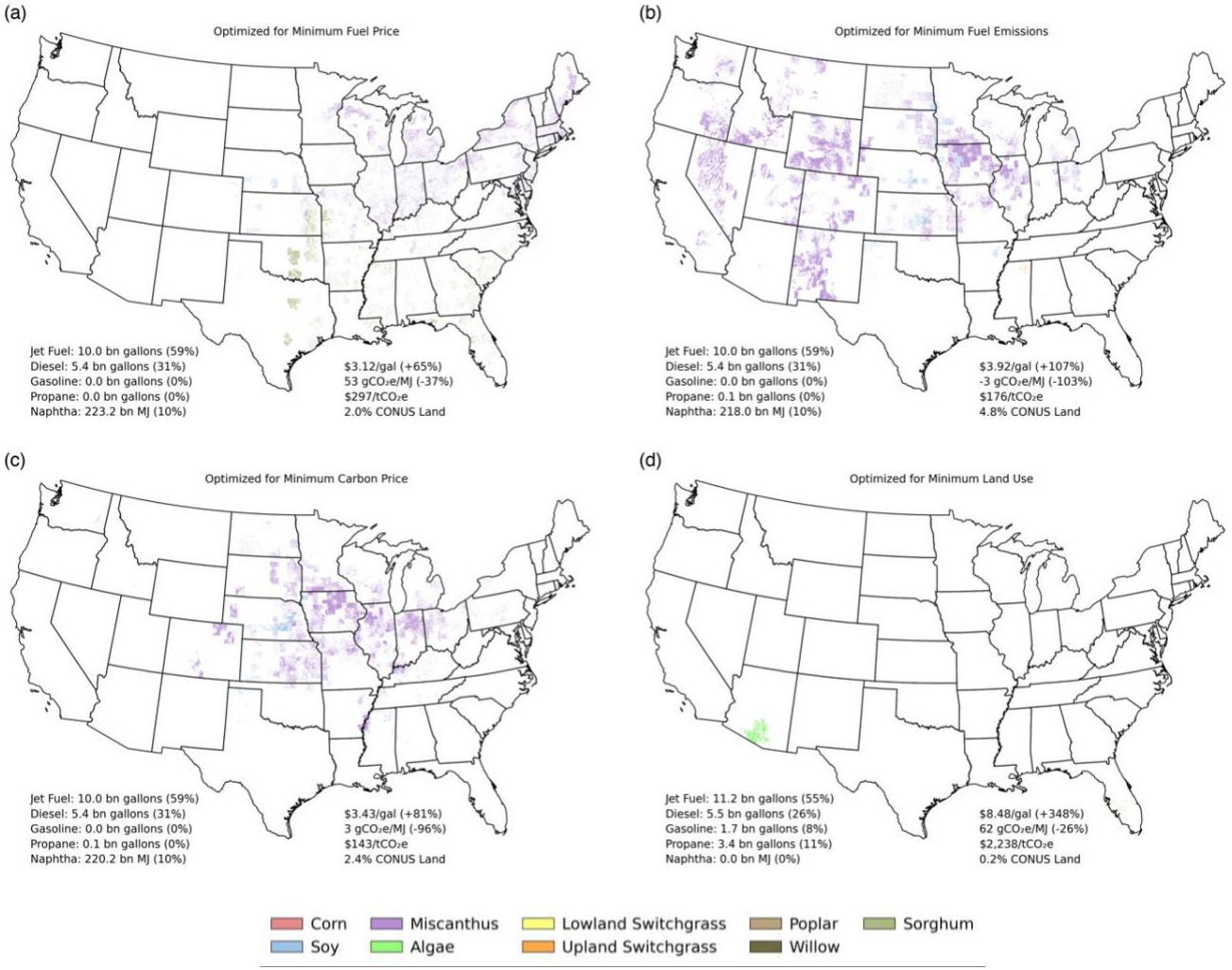

Figure C11. Multi-objective optimization maps of the optimal geographic feedstock deployment to meet 10 billion gallons of annual SAF production while minimizing fuel price (a), fuel emissions (b), breakeven carbon price (c), and land area (d). Percentages in parentheses for the fuel products represent the total percent of megajoules produced for that fuel type as a percentage of total megajoules of fuel produced by the feedstocks. Percentages in parentheses for the mean fuel selling price and mean fuel emissions represent the percent cost increase and percent emissions reduction, respectively, compared to petroleum jet fuel.

Table C25. Optimization results breakdown by crop for the 10-billion-gallon SAF scenario when optimized for minimum fuel costs.

	Jet Fuel (million gallons)	Jet Fuel Percentage	Land Use (ha)	Land Use Percentage (SAF)	Land Use Percentage (CONUS)	MFSP ($/gallon Jet)	GHG (gCO2e/MJ)	Carbon Price ($/tCO2e)
Algae	-	0.0%	-	0.0%	0.0%	$-	-	$-
Upland Switchgrass	-	0.0%	-	0.0%	0.0%	$-	-	$-
Lowland Switchgrass	-	0.0%	-	0.0%	0.0%	$-	-	$-
Miscanthus	6,259.3	62.6%	10,143,142	63.9%	1.3%	$3.11	55.52	$316.41
Poplar	-	0.0%	-	0.0%	0.0%	$-	-	$-
Corn	-	0.0%	-	0.0%	0.0%	$-	-	$-
Soy	71.7	0.7%	439,437	2.8%	0.1%	$2.85	(2.81)	$83.14
Willow	-	0.0%	-	0.0%	0.0%	$-	-	$-
Sorghum	3,669.0	36.7%	5,285,641	33.3%	0.7%	$3.14	50.96	$279.86

Table C26. Optimization results breakdown by crop for the 10-billion-gallon SAF scenario when optimized for minimum fuel emissions.

	Jet Fuel (million gallons)	Jet Fuel Percentage	Land Use (ha)	Land Use Percentage (SAF)	Land Use Percentage (CONUS)	MFSP ($/gallon Jet)	GHG (gCO2e/MJ)	Carbon Price ($/tCO2e)
Algae	-	0.0%	-	0.0%	0.0%	$-	-	$-
Upland Switchgrass	13.4	0.1%	44,384	0.1%	0.0%	$3.93	0.80	$184.66
Lowland Switchgrass	-	0.0%	-	0.0%	0.0%	$-	-	$-
Miscanthus	9,681.4	96.8%	35,210,222	93.6%	4.5%	$3.91	(2.63)	$175.71
Poplar	-	0.0%	-	0.0%	0.0%	$-	-	$-
Corn	0.4	0.0%	2,240	0.0%	0.0%	$9.04	(9.79)	$575.39
Soy	304.9	3.0%	2,360,852	6.3%	0.3%	$4.29	(6.77)	$199.22
Willow	-	0.0%	-	0.0%	0.0%	$-	-	$-
Sorghum	-	0.0%	-	0.0%	0.0%	$-	-	$-

Table C27. Optimization results breakdown by crop for the 10-billion-gallon SAF scenario when optimized for minimum carbon price.

	Jet Fuel (million gallons)	Jet Fuel Percentage	Land Use (ha)	Land Use Percentage (SAF)	Land Use Percentage (CONUS)	MFSP ($/gallon Jet)	GHG (gCO2e/MJ)	Carbon Price ($/tCO2e)
Algae	-	0.0%	-	0.0%	0.0%	$-	-	$-
Upland Switchgrass	-	0.0%	-	0.0%	0.0%	$-	-	$-
Lowland Switchgrass	-	0.0%	-	0.0%	0.0%	$-	-	$-
Miscanthus	9,773.9	97.7%	17,415,799	92.9%	2.2%	$3.43	3.23	$143.89
Poplar	-	0.0%	-	0.0%	0.0%	$-	-	$-
Corn	-	0.0%	-	0.0%	0.0%	$-	-	$-
Soy	205.4	2.1%	1,299,428	6.9%	0.2%	$3.25	(1.95)	$119.48
Willow	-	0.0%	-	0.0%	0.0%	$-	-	$-
Sorghum	20.7	0.2%	29,277	0.2%	0.0%	$3.06	29.32	$160.16

Table C28. Optimization results breakdown by crop for the 10-billion-gallon SAF scenario when optimized for minimum land use.

	Jet Fuel (million gallons)	Jet Fuel Percentage	Land Use (ha)	Land Use Percentage (SAF)	Land Use Percentage (CONUS)	MFSP ($/gallon Jet)	GHG (gCO2e/MJ)	Carbon Price ($/tCO2e)
Algae	11,202.7	100.0%	1,581,963	100.0%	0.2%	$8.48	62.39	$2,237.55
Upland Switchgrass	-	0.0%	-	0.0%	0.0%	$-	-	$-
Lowland Switchgrass	-	0.0%	-	0.0%	0.0%	$-	-	$-
Miscanthus	-	0.0%	-	0.0%	0.0%	$-	-	$-
Poplar	-	0.0%	-	0.0%	0.0%	$-	-	$-
Corn	-	0.0%	-	0.0%	0.0%	$-	-	$-
Soy	-	0.0%	-	0.0%	0.0%	$-	-	$-
Willow	-	0.0%	-	0.0%	0.0%	$-	-	$-
Sorghum	-	0.0%	-	0.0%	0.0%	$-	-	$-

Table C29. Optimization results breakdown by land for the 10-billion-gallon SAF scenario when optimized for minimum fuel costs.

	Jet Fuel (million gallons)	Jet Fuel Percentage	Land Use (ha)	Land Use Percentage (SAF)	Land Use Percentage (CONUS)	MFSP ($/gallon Jet)	GHG (gCO2e/MJ)	Carbon Price ($/tCO2e)
Barren Land	-	0%	-	0%	0%	$-	-	$-
Deciduous Forest	4,737.2	47%	7,416,308	47%	1%	$3.11	53.06	$291.92
Evergreen Forest	660.9	7%	1,070,836	7%	0%	$3.11	77.26	$1,231.75
Mixed Forest	1,167.0	12%	1,878,226	12%	0%	$3.10	65.80	$485.91
Shrubland	994.4	10%	1,473,639	9%	0%	$3.13	64.61	$467.64
Grassland Herbaceous	1,883.6	19%	2,896,376	18%	0%	$3.14	44.69	$236.14
Cultivated Crops	556.8	6%	1,132,836	7%	0%	$3.12	11.98	$128.67

Table C30. Optimization results breakdown by land for the 10-billion-gallon SAF scenario when optimized for minimum fuel emissions.

	Jet Fuel (million gallons)	Jet Fuel Percentage	Land Use (ha)	Land Use Percentage (SAF)	Land Use Percentage (CONUS)	MFSP ($/gallon Jet)	GHG (gCO2e/MJ)	Carbon Price ($/tCO2e)
Barren Land	-	0%	-	0%	0%	$-	-	$-
Deciduous Forest	0.0	0%	4	0%	0%	$3.99	(4.95)	$177.89
Evergreen Forest	0.1	0%	708	0%	0%	$4.15	1.41	$206.24
Mixed Forest	0.0	0%	28	0%	0%	$4.64	1.00	$249.76
Shrubland	2,176.7	22%	16,892,568	45%	2%	$4.75	(5.07)	$241.82
Grassland Herbaceous	1,527.8	15%	8,343,622	22%	1%	$4.22	(2.85)	$201.84
Cultivated Crops	6,295.3	63%	12,380,768	33%	2%	$3.57	(1.93)	$146.87

Table C31. Optimization results breakdown by land for the 10-billion-gallon SAF scenario when optimized for minimum carbon price.

	Jet Fuel (million gallons)	Jet Fuel Percentage	Land Use (ha)	Land Use Percentage (SAF)	Land Use Percentage (CONUS)	MFSP ($/gallon Jet)	GHG (gCO2e/MJ)	Carbon Price ($/tCO2e)
Barren Land	-	0%	-	0%	0%	$-	-	$-
Deciduous Forest	539.6	5%	771,377	4%	0%	$3.10	21.70	$146.02
Evergreen Forest	2.2	0%	3,136	0%	0%	$3.11	21.19	$145.96
Mixed Forest	89.9	1%	129,561	1%	0%	$3.11	20.88	$144.66
Shrubland	64.6	1%	313,824	2%	0%	$3.88	(15.54)	$150.92
Grassland Herbaceous	1,571.7	16%	3,921,530	21%	1%	$3.37	10.93	$152.55
Cultivated Crops	7,732.0	77%	13,605,076	73%	2%	$3.46	0.25	$141.53

Table C32. Optimization results breakdown by land for the 10-billion-gallon SAF scenario when optimized for minimum land use.

	Jet Fuel (million gallons)	Jet Fuel Percentage	Land Use (ha)	Land Use Percentage (SAF)	Land Use Percentage (CONUS)	MFSP ($/gallon Jet)	GHG (gCO2e/MJ)	Carbon Price ($/tCO2e)
Barren Land	182.8	2%	25,901	2%	0%	$8.49	62.40	$2,242.27
Deciduous Forest	9.1	0%	1,276	0%	0%	$8.45	63.70	$2,366.47
Evergreen Forest	230.9	2%	32,505	2%	0%	$8.43	63.94	$2,386.22
Mixed Forest	52.8	0%	7,444	0%	0%	$8.44	63.77	$2,370.90
Shrubland	9,119.9	81%	1,287,644	81%	0%	$8.48	62.36	$2,234.78
Grassland Herbaceous	1,607.2	14%	227,192	14%	0%	$8.48	62.30	$2,228.12
Cultivated Crops	-	0%	-	0%	0%	$-	-	$-

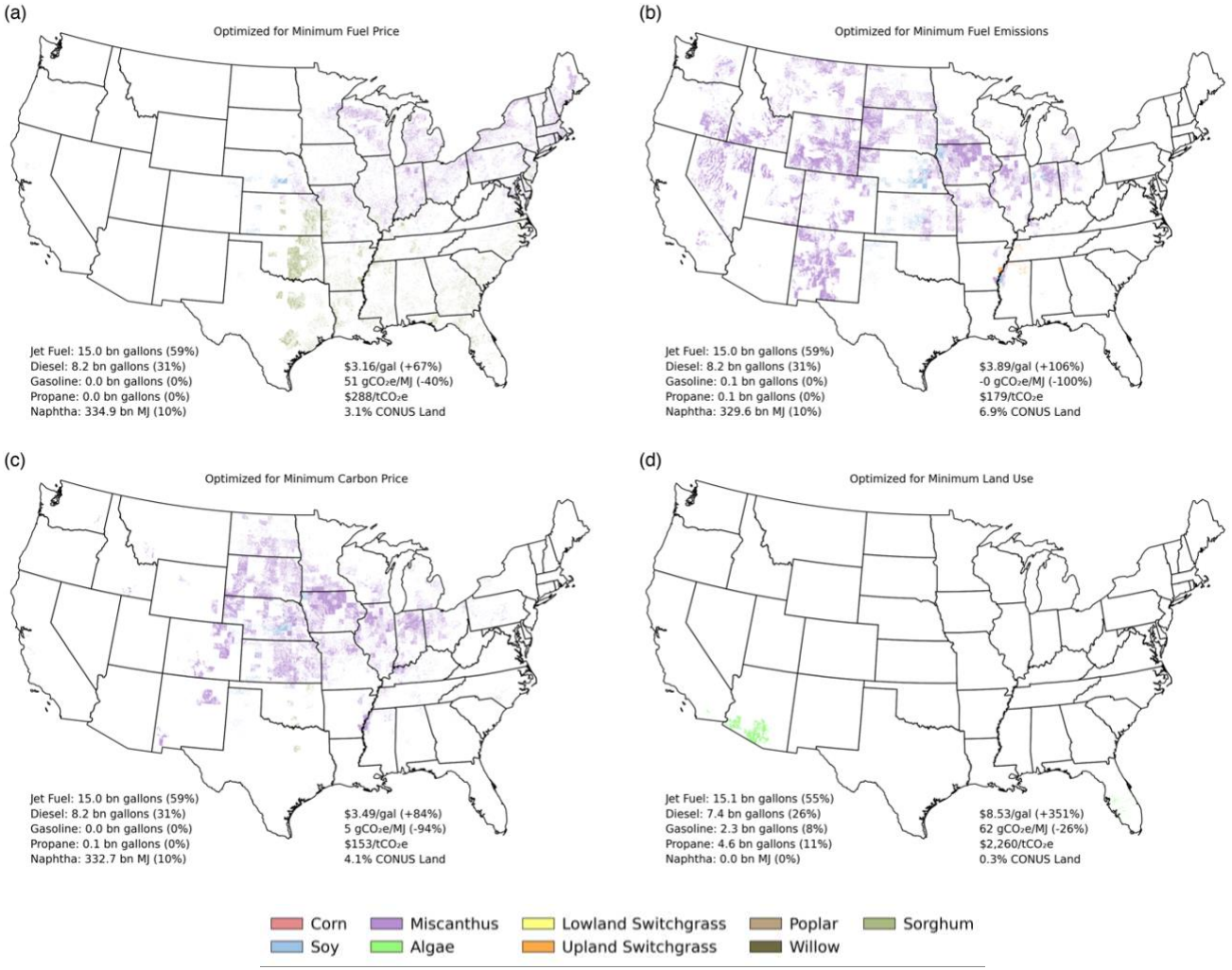

Figure C12. Multi-objective optimization maps of the optimal geographic feedstock deployment to meet 15 billion gallons of annual SAF production while minimizing fuel price (a), fuel emissions (b), breakeven carbon price (c), and land area (d). Percentages in parentheses for the fuel products represent the total percent of megajoules produced for that fuel type as a percentage of total megajoules of fuel produced by the feedstocks. Percentages in parentheses for the mean fuel selling price and mean fuel emissions represent the percent cost increase and percent emissions reduction, respectively, compared to petroleum jet fuel.

Table C33. Optimization results breakdown by crop for the 15-billion-gallon SAF scenario when optimized for minimum fuel costs.

	Jet Fuel (million gallons)	Jet Fuel Percentage	Land Use (ha)	Land Use Percentage (SAF)	Land Use Percentage (CONUS)	MFSP ($/gallon Jet)	GHG (gCO2e/MJ)	Carbon Price ($/tCO2e)
Algae	-	0.0%	-	0.0%	0.0%	$-	-	$-
Upland Switchgrass	-	0.0%	-	0.0%	0.0%	$-	-	$-
Lowland Switchgrass	-	0.0%	-	0.0%	0.0%	$-	-	$-
Miscanthus	7,974.8	53.2%	13,040,214	54.6%	1.7%	$3.14	52.51	$294.89
Poplar	-	0.0%	-	0.0%	0.0%	$-	-	$-
Corn	-	0.0%	-	0.0%	0.0%	$-	-	$-
Soy	106.1	0.7%	646,105	2.7%	0.1%	$2.98	(0.93)	$96.55
Willow	-	0.0%	-	0.0%	0.0%	$-	-	$-
Sorghum	6,919.1	46.1%	10,183,960	42.7%	1.3%	$3.19	50.51	$287.51

Table C34. Optimization results breakdown by crop for the 15-billion-gallon SAF scenario when optimized for minimum fuel emissions.

	Jet Fuel (million gallons)	Jet Fuel Percentage	Land Use (ha)	Land Use Percentage (SAF)	Land Use Percentage (CONUS)	MFSP ($/gallon Jet)	GHG (gCO2e/MJ)	Carbon Price ($/tCO2e)
Algae	-	0.0%	-	0.0%	0.0%	$-	-	$-
Upland Switchgrass	69.4	0.5%	229,431	0.4%	0.0%	$4.20	4.41	$218.91
Lowland Switchgrass	-	0.0%	-	0.0%	0.0%	$-	-	$-
Miscanthus	14,589.1	97.3%	51,238,705	95.1%	6.6%	$3.89	(0.35)	$178.90
Poplar	-	0.0%	-	0.0%	0.0%	$-	-	$-
Corn	0.4	0.0%	2,240	0.0%	0.0%	$9.04	(9.79)	$575.39
Soy	341.1	2.3%	2,433,217	4.5%	0.3%	$3.85	(3.08)	$169.71
Willow	-	0.0%	-	0.0%	0.0%	$-	-	$-
Sorghum	-	0.0%	-	0.0%	0.0%	$-	-	$-

Table C35. Optimization results breakdown by crop for the 15-billion-gallon SAF scenario when optimized for minimum carbon price.

	Jet Fuel (million gallons)	Jet Fuel Percentage	Land Use (ha)	Land Use Percentage (SAF)	Land Use Percentage (CONUS)	MFSP ($/gallon Jet)	GHG (gCO2e/MJ)	Carbon Price ($/tCO2e)
Algae	-	0.0%	-	0.0%	0.0%	$-	-	$-
Upland Switchgrass	-	0.0%	-	0.0%	0.0%	$-	-	$-
Lowland Switchgrass	-	0.0%	-	0.0%	0.0%	$-	-	$-
Miscanthus	14,590.4	97.3%	30,286,207	95.0%	3.9%	$3.50	5.13	$153.48
Poplar	-	0.0%	-	0.0%	0.0%	$-	-	$-
Corn	-	0.0%	-	0.0%	0.0%	$-	-	$-
Soy	203.6	1.4%	1,299,745	4.1%	0.2%	$3.32	(3.29)	$123.04
Willow	-	0.0%	-	0.0%	0.0%	$-	-	$-
Sorghum	206.1	1.4%	307,267	1.0%	0.0%	$3.09	31.60	$172.04

Table C36. Optimization results breakdown by crop for the 15-billion-gallon SAF scenario when optimized for minimum land use.

	Jet Fuel (million gallons)	Jet Fuel Percentage	Land Use (ha)	Land Use Percentage (SAF)	Land Use Percentage (CONUS)	MFSP ($/gallon Jet)	GHG (gCO2e/MJ)	Carbon Price ($/tCO2e)
Algae	15,090.6	100.0%	2,145,044	100.0%	0.3%	$8.53	62.45	$2,260.03
Upland Switchgrass	-	0.0%	-	0.0%	0.0%	$-	-	$-
Lowland Switchgrass	-	0.0%	-	0.0%	0.0%	$-	-	$-
Miscanthus	-	0.0%	-	0.0%	0.0%	$-	-	$-
Poplar	-	0.0%	-	0.0%	0.0%	$-	-	$-
Corn	-	0.0%	-	0.0%	0.0%	$-	-	$-
Soy	-	0.0%	-	0.0%	0.0%	$-	-	$-
Willow	-	0.0%	-	0.0%	0.0%	$-	-	$-
Sorghum	-	0.0%	-	0.0%	0.0%	$-	-	$-

Table C37. Optimization results breakdown by land for the 15-billion-gallon SAF scenario when optimized for minimum fuel costs.

	Jet Fuel (million gallons)	Jet Fuel Percentage	Land Use (ha)	Land Use Percentage (SAF)	Land Use Percentage (CONUS)	MFSP ($/gallon Jet)	GHG (gCO2e/MJ)	Carbon Price ($/tCO2e)
Barren Land	-	0%	-	0%	0%	$-	-	$-
Deciduous Forest	6,099.5	41%	9,570,312	40%	1%	$3.14	53.08	$299.64
Evergreen Forest	900.1	6%	1,464,750	6%	0%	$3.15	75.93	$1,079.13
Mixed Forest	1,484.7	10%	2,397,981	10%	0%	$3.14	65.89	$501.03
Shrubland	1,694.6	11%	2,529,262	11%	0%	$3.18	64.44	$482.64
Grassland Herbaceous	3,398.2	23%	5,360,483	22%	1%	$3.19	44.59	$245.30
Cultivated Crops	1,422.9	9%	2,547,490	11%	0%	$3.20	12.30	$137.66

Table C38. Optimization results breakdown by land for the 15-billion-gallon SAF scenario when optimized for minimum fuel emissions.

	Jet Fuel (million gallons)	Jet Fuel Percentage	Land Use (ha)	Land Use Percentage (SAF)	Land Use Percentage (CONUS)	MFSP ($/gallon Jet)	GHG (gCO2e/MJ)	Carbon Price ($/tCO2e)
Barren Land	-	0%	-	0%	0%	$-	-	$-
Deciduous Forest	0.1	0%	120	0%	0%	$3.23	3.93	$125.52
Evergreen Forest	0.3	0%	1,572	0%	0%	$3.97	2.94	$193.18
Mixed Forest	0.5	0%	724	0%	0%	$3.13	4.14	$116.42
Shrubland	2,906.4	19%	21,235,181	39%	3%	$4.66	(2.65)	$241.09
Grassland Herbaceous	3,756.5	25%	16,658,351	31%	2%	$4.07	1.49	$199.09
Cultivated Crops	8,336.2	56%	16,007,644	30%	2%	$3.55	(0.46)	$147.72

Table C39. Optimization results breakdown by land for the 15-billion-gallon SAF scenario when optimized for minimum carbon price.

	Jet Fuel (million gallons)	Jet Fuel Percentage	Land Use (ha)	Land Use Percentage (SAF)	Land Use Percentage (CONUS)	MFSP ($/gallon Jet)	GHG (gCO2e/MJ)	Carbon Price ($/tCO2e)
Barren Land	-	0%	-	0%	0%	$-	-	$-
Deciduous Forest	978.5	7%	1,411,296	4%	0%	$3.10	26.47	$157.58
Evergreen Forest	4.1	0%	6,012	0%	0%	$3.12	25.52	$157.30
Mixed Forest	145.4	1%	211,044	1%	0%	$3.11	25.23	$155.34
Shrubland	348.4	2%	1,420,981	4%	0%	$3.80	0.11	$171.20
Grassland Herbaceous	4,487.2	30%	12,568,687	39%	2%	$3.53	10.41	$167.65
Cultivated Crops	9,036.4	60%	16,275,199	51%	2%	$3.51	0.47	$145.80

Table C40. Optimization results breakdown by land for the 15-billion-gallon SAF scenario when optimized for minimum land use.

	Jet Fuel (million gallons)	Jet Fuel Percentage	Land Use (ha)	Land Use Percentage (SAF)	Land Use Percentage (CONUS)	MFSP ($/gallon Jet)	GHG (gCO2e/MJ)	Carbon Price ($/tCO2e)
Barren Land	407.2	3%	58,314	3%	0%	$8.70	60.87	$2,166.92
Deciduous Forest	14.2	0%	2,012	0%	0%	$8.51	64.21	$2,446.80
Evergreen Forest	309.1	2%	43,810	2%	0%	$8.48	64.14	$2,427.58
Mixed Forest	91.7	1%	13,060	1%	0%	$8.52	64.16	$2,443.70
Shrubland	12,212.4	81%	1,736,093	81%	0%	$8.53	62.45	$2,260.04
Grassland Herbaceous	2,056.0	14%	291,755	14%	0%	$8.50	62.40	$2,247.70
Cultivated Crops	-	0%	-	0%	0%	$-	-	$-

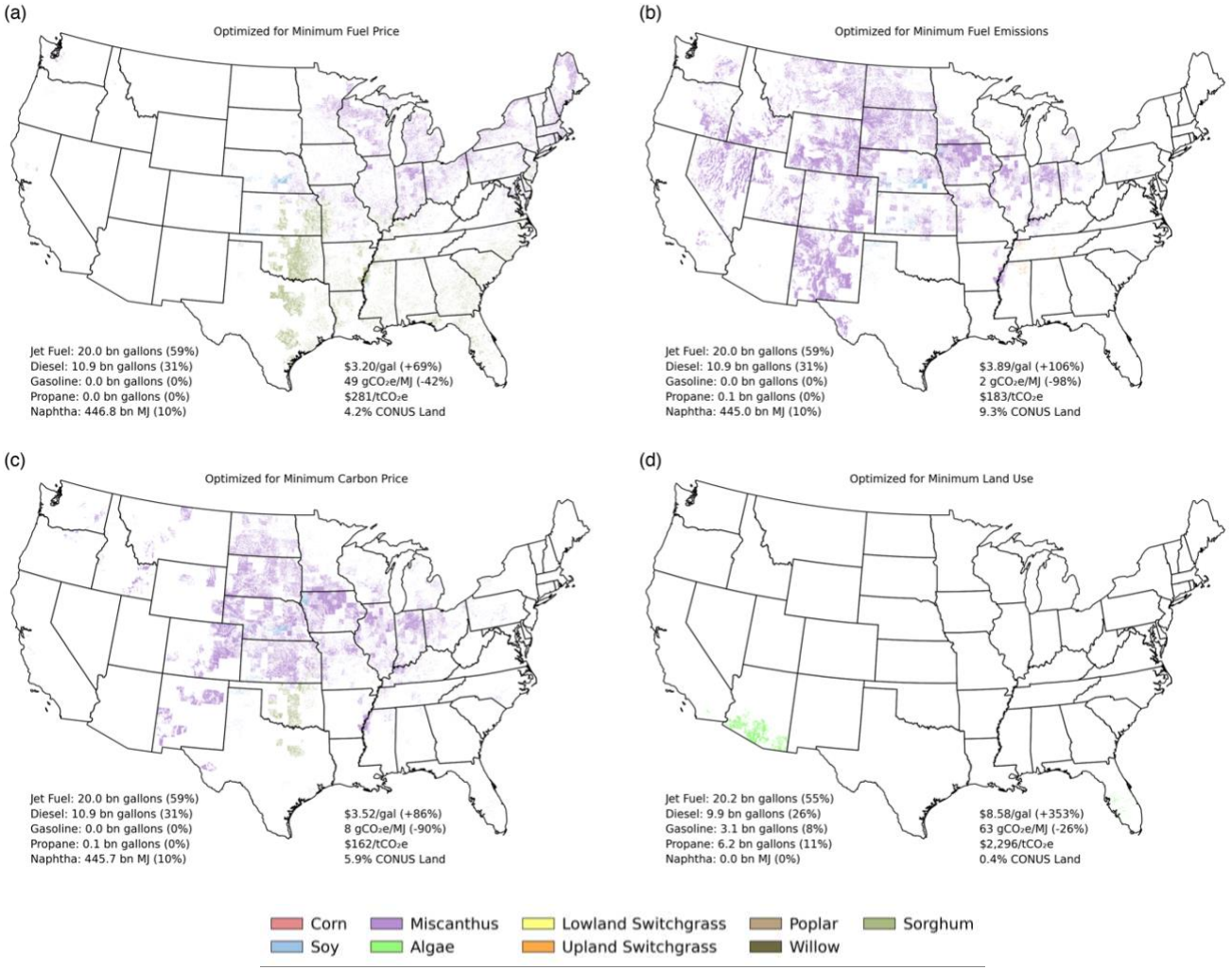

Figure C13. Multi-objective optimization maps of the optimal geographic feedstock deployment to meet 20 billion gallons of annual SAF production while minimizing fuel price (a), fuel emissions (b), breakeven carbon price (c), and land area (d). Percentages in parentheses for the fuel products represent the total percent of megajoules produced for that fuel type as a percentage of total megajoules of fuel produced by the feedstocks. Percentages in parentheses for the mean fuel selling price and mean fuel emissions represent the percent cost increase and percent emissions reduction, respectively, compared to petroleum jet fuel.

Table C41. Optimization results breakdown by crop for the 20-billion-gallon SAF scenario when optimized for minimum fuel costs.

	Jet Fuel (million gallons)	Jet Fuel Percentage	Land Use (ha)	Land Use Percentage (SAF)	Land Use Percentage (CONUS)	MFSP ($/gallon Jet)	GHG (gCO2e/MJ)	Carbon Price ($/tCO2e)
Algae	-	0.0%	-	0.0%	0.0%	$-	-	$-
Upland Switchgrass	-	0.0%	-	0.0%	0.0%	$-	-	$-
Lowland Switchgrass	-	0.0%	-	0.0%	0.0%	$-	-	$-
Miscanthus	10,246.0	51.2%	16,955,667	52.4%	2.2%	$3.19	50.77	$289.22
Poplar	-	0.0%	-	0.0%	0.0%	$-	-	$-
Corn	-	0.0%	-	0.0%	0.0%	$-	-	$-
Soy	131.4	0.7%	811,050	2.5%	0.1%	$3.06	(2.30)	$102.14
Willow	-	0.0%	-	0.0%	0.0%	$-	-	$-
Sorghum	9,622.6	48.1%	14,582,337	45.1%	1.9%	$3.23	48.25	$277.71

Table C42. Optimization results breakdown by crop for the 20-billion-gallon SAF scenario when optimized for minimum fuel emissions.

	Jet Fuel (million gallons)	Jet Fuel Percentage	Land Use (ha)	Land Use Percentage (SAF)	Land Use Percentage (CONUS)	MFSP ($/gallon Jet)	GHG (gCO2e/MJ)	Carbon Price ($/tCO2e)
Algae	-	0.0%	-	0.0%	0.0%	$-	-	$-
Upland Switchgrass	45.0	0.2%	142,502	0.2%	0.0%	$4.07	5.21	$208.26
Lowland Switchgrass	0.3	0.0%	3,742	0.0%	0.0%	$6.36	6.57	$434.47
Miscanthus	19,743.5	98.7%	70,581,191	97.8%	9.1%	$3.89	1.89	$183.76
Poplar	-	0.0%	-	0.0%	0.0%	$-	-	$-
Corn	0.4	0.0%	2,240	0.0%	0.0%	$9.04	(9.79)	$575.39
Soy	210.8	1.1%	1,465,845	2.0%	0.2%	$3.61	(4.62)	$146.40
Willow	-	0.0%	-	0.0%	0.0%	$-	-	$-
Sorghum	-	0.0%	-	0.0%	0.0%	$-	-	$-

Table C43. Optimization results breakdown by crop for the 20-billion-gallon SAF scenario when optimized for minimum carbon price.

	Jet Fuel (million gallons)	Jet Fuel Percentage	Land Use (ha)	Land Use Percentage (SAF)	Land Use Percentage (CONUS)	MFSP ($/gallon Jet)	GHG (gCO2e/MJ)	Carbon Price ($/tCO2e)
Algae	-	0.0%	-	0.0%	0.0%	$-	-	$-
Upland Switchgrass	-	0.0%	-	0.0%	0.0%	$-	-	$-
Lowland Switchgrass	-	0.0%	-	0.0%	0.0%	$-	-	$-
Miscanthus	18,349.0	91.7%	42,704,705	92.4%	5.5%	$3.55	6.49	$160.82
Poplar	-	0.0%	-	0.0%	0.0%	$-	-	$-
Corn	-	0.0%	-	0.0%	0.0%	$-	-	$-
Soy	179.7	0.9%	1,151,210	2.5%	0.1%	$3.34	(4.02)	$124.32
Willow	-	0.0%	-	0.0%	0.0%	$-	-	$-
Sorghum	1,471.4	7.4%	2,378,532	5.1%	0.3%	$3.20	32.13	$189.45

Table C44. Optimization results breakdown by crop for the 20-billion-gallon SAF scenario when optimized for minimum land use.

	Jet Fuel (million gallons)	Jet Fuel Percentage	Land Use (ha)	Land Use Percentage (SAF)	Land Use Percentage (CONUS)	MFSP ($/gallon Jet)	GHG (gCO2e/MJ)	Carbon Price ($/tCO2e)
Algae	20,225.5	100.0%	2,890,867	100.0%	0.4%	$8.58	62.63	$2,296.31
Upland Switchgrass	-	0.0%	-	0.0%	0.0%	$-	-	$-
Lowland Switchgrass	-	0.0%	-	0.0%	0.0%	$-	-	$-
Miscanthus	-	0.0%	-	0.0%	0.0%	$-	-	$-
Poplar	-	0.0%	-	0.0%	0.0%	$-	-	$-
Corn	-	0.0%	-	0.0%	0.0%	$-	-	$-
Soy	-	0.0%	-	0.0%	0.0%	$-	-	$-
Willow	-	0.0%	-	0.0%	0.0%	$-	-	$-
Sorghum	-	0.0%	-	0.0%	0.0%	$-	-	$-

Table C45. Optimization results breakdown by land for the 20-billion-gallon SAF scenario when optimized for minimum fuel costs.

	Jet Fuel (million gallons)	Jet Fuel Percentage	Land Use (ha)	Land Use Percentage (SAF)	Land Use Percentage (CONUS)	MFSP ($/gallon Jet)	GHG (gCO2e/MJ)	Carbon Price ($/tCO2e)
Barren Land	-	0%	-	0%	0%	$-	-	$-
Deciduous Forest	7,028.7	35%	11,161,439	35%	1%	$3.17	54.49	$319.68
Evergreen Forest	1,237.8	6%	2,080,385	6%	0%	$3.20	76.91	$1,262.50
Mixed Forest	1,898.4	9%	3,127,252	10%	0%	$3.18	68.03	$583.58
Shrubland	2,191.6	11%	3,367,605	10%	0%	$3.22	62.76	$457.00
Grassland Herbaceous	4,862.9	24%	7,971,064	25%	1%	$3.23	42.67	$241.98
Cultivated Crops	2,780.6	14%	4,641,307	14%	1%	$3.26	11.44	$142.30

Table C46. Optimization results breakdown by land for the 20-billion-gallon SAF scenario when optimized for minimum fuel emissions.

	Jet Fuel (million gallons)	Jet Fuel Percentage	Land Use (ha)	Land Use Percentage (SAF)	Land Use Percentage (CONUS)	MFSP ($/gallon Jet)	GHG (gCO2e/MJ)	Carbon Price ($/tCO2e)
Barren Land	-	0%	-	0%	0%	$-	-	$-
Deciduous Forest	34.0	0%	50,534	0%	0%	$3.14	9.67	$126.48
Evergreen Forest	6.1	0%	29,557	0%	0%	$3.92	7.60	$199.96
Mixed Forest	9.8	0%	14,009	0%	0%	$3.14	9.48	$126.02
Shrubland	4,010.1	20%	27,751,184	38%	4%	$4.58	0.48	$242.29
Grassland Herbaceous	6,798.8	34%	27,534,496	38%	4%	$3.97	4.66	$197.32
Cultivated Crops	9,141.2	46%	16,815,741	23%	2%	$3.54	0.29	$148.03

Table C47. Optimization results breakdown by land for the 20-billion-gallon SAF scenario when optimized for minimum carbon price.

	Jet Fuel (million gallons)	Jet Fuel Percentage	Land Use (ha)	Land Use Percentage (SAF)	Land Use Percentage (CONUS)	MFSP ($/gallon Jet)	GHG (gCO2e/MJ)	Carbon Price ($/tCO2e)
Barren Land	-	0%	-	0%	0%	$-	-	$-
Deciduous Forest	1,467.1	7%	2,131,891	5%	0%	$3.11	29.54	$167.77
Evergreen Forest	11.5	0%	33,961	0%	0%	$3.47	18.87	$181.89
Mixed Forest	214.0	1%	313,624	1%	0%	$3.13	28.10	$166.00
Shrubland	1,039.0	5%	4,435,021	10%	1%	$3.89	2.54	$184.59
Grassland Herbaceous	8,008.1	40%	22,637,690	49%	3%	$3.56	13.42	$178.06
Cultivated Crops	9,260.3	46%	16,682,260	36%	2%	$3.52	0.64	$146.84

Table C48. Optimization results breakdown by land for the 20-billion-gallon SAF scenario when optimized for minimum land use.

	Jet Fuel (million gallons)	Jet Fuel Percentage	Land Use (ha)	Land Use Percentage (SAF)	Land Use Percentage (CONUS)	MFSP ($/gallon Jet)	GHG (gCO2e/MJ)	Carbon Price ($/tCO2e)
Barren Land	861.7	4%	124,349	4%	0%	$8.66	61.68	$2,226.64
Deciduous Forest	14.2	0%	2,012	0%	0%	$8.51	64.21	$2,446.80
Evergreen Forest	421.8	2%	60,162	2%	0%	$8.52	64.55	$2,492.78
Mixed Forest	91.7	0%	13,060	0%	0%	$8.52	64.16	$2,443.70
Shrubland	15,365.9	76%	2,194,050	76%	0%	$8.58	62.68	$2,303.15
Grassland Herbaceous	3,470.3	17%	497,234	17%	0%	$8.55	62.36	$2,258.60
Cultivated Crops	-	0%	-	0%	0%	$-	-	$-

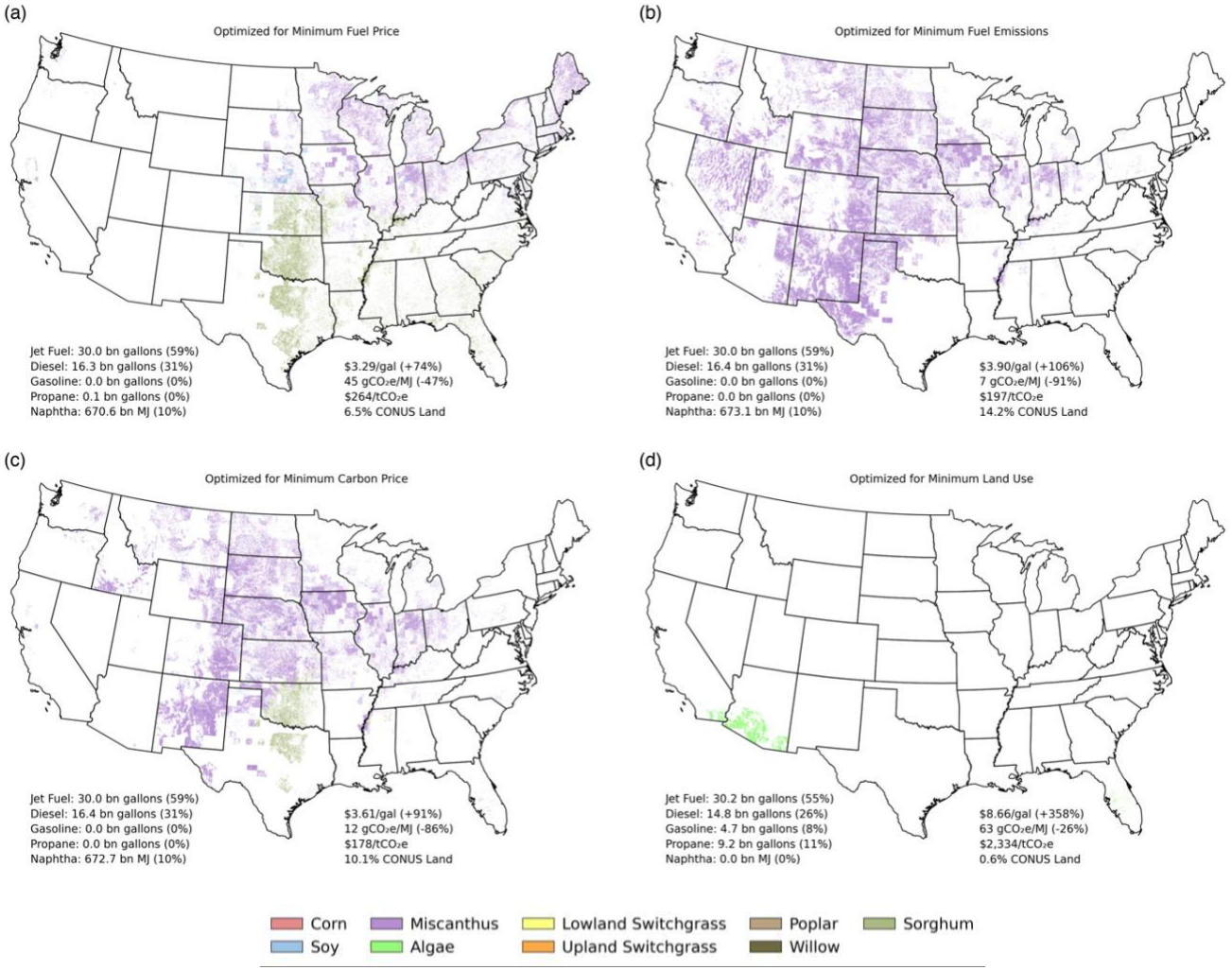

Figure C14. Multi-objective optimization maps of the optimal geographic feedstock deployment to meet 30 billion gallons of annual SAF production while minimizing fuel price (a), fuel emissions (b), breakeven carbon price (c), and land area (d). Percentages in parentheses for the fuel products represent the total percent of megajoules produced for that fuel type as a percentage of total megajoules of fuel produced by the feedstocks. Percentages in parentheses for the mean fuel selling price and mean fuel emissions represent the percent cost increase and percent emissions reduction, respectively, compared to petroleum jet fuel.

Table C49. Optimization results breakdown by crop for the 30-billion-gallon SAF scenario when optimized for minimum fuel costs.

	Jet Fuel (million gallons)	Jet Fuel Percentage	Land Use (ha)	Land Use Percentage (SAF)	Land Use Percentage (CONUS)	MFSP ($/gallon Jet)	GHG (gCO2e/MJ)	Carbon Price ($/tCO2e)
Algae	-	0.0%	-	0.0%	0.0%	$-	-	$-
Upland Switchgrass	-	0.0%	-	0.0%	0.0%	$-	-	$-
Lowland Switchgrass	-	0.0%	-	0.0%	0.0%	$-	-	$-
Miscanthus	15,181.7	50.6%	25,920,695	51.0%	3.3%	$3.28	45.09	$266.20
Poplar	-	0.0%	-	0.0%	0.0%	$-	-	$-
Corn	-	0.0%	-	0.0%	0.0%	$-	-	$-
Soy	178.9	0.6%	1,115,766	2.2%	0.1%	$3.20	(1.40)	$115.06
Willow	-	0.0%	-	0.0%	0.0%	$-	-	$-
Sorghum	14,639.3	48.8%	23,745,416	46.8%	3.0%	$3.29	44.80	$266.64

Table C50. Optimization results breakdown by crop for the 30-billion-gallon SAF scenario when optimized for minimum fuel emissions.

	Jet Fuel (million gallons)	Jet Fuel Percentage	Land Use (ha)	Land Use Percentage (SAF)	Land Use Percentage (CONUS)	MFSP ($/gallon Jet)	GHG (gCO2e/MJ)	Carbon Price ($/tCO2e)
Algae	-	0.0%	-	0.0%	0.0%	$-	-	$-
Upland Switchgrass	-	0.0%	-	0.0%	0.0%	$-	-	$-
Lowland Switchgrass	-	0.0%	-	0.0%	0.0%	$-	-	$-
Miscanthus	29,932.1	99.8%	110,044,617	99.6%	14.1%	$3.90	7.31	$196.82
Poplar	-	0.0%	-	0.0%	0.0%	$-	-	$-
Corn	8.9	0.0%	18,541	0.0%	0.0%	$5.15	15.64	$358.55
Soy	58.9	0.2%	432,761	0.4%	0.1%	$3.60	(22.59)	$121.02
Willow	-	0.0%	-	0.0%	0.0%	$-	-	$-
Sorghum	-	0.0%	-	0.0%	0.0%	$-	-	$-

Table C51. Optimization results breakdown by crop for the 30-billion-gallon SAF scenario when optimized for minimum carbon price.

	Jet Fuel (million gallons)	Jet Fuel Percentage	Land Use (ha)	Land Use Percentage (SAF)	Land Use Percentage (CONUS)	MFSP ($/gallon Jet)	GHG (gCO2e/MJ)	Carbon Price ($/tCO2e)
Algae	-	0.0%	-	0.0%	0.0%	$-	-	$-
Upland Switchgrass	-	0.0%	-	0.0%	0.0%	$-	-	$-
Lowland Switchgrass	-	0.0%	-	0.0%	0.0%	$-	-	$-
Miscanthus	25,795.2	86.0%	71,413,911	90.4%	9.2%	$3.66	8.31	$175.87
Poplar	-	0.0%	-	0.0%	0.0%	$-	-	$-
Corn	-	0.0%	-	0.0%	0.0%	$-	-	$-
Soy	83.3	0.3%	556,186	0.7%	0.1%	$3.20	(12.39)	$102.40
Willow	-	0.0%	-	0.0%	0.0%	$-	-	$-
Sorghum	4,121.5	13.7%	7,030,324	8.9%	0.9%	$3.28	33.26	$205.44

Table C52. Optimization results breakdown by crop for the 30-billion-gallon SAF scenario when optimized for minimum land use.

	Jet Fuel (million gallons)	Jet Fuel Percentage	Land Use (ha)	Land Use Percentage (SAF)	Land Use Percentage (CONUS)	MFSP ($/gallon Jet)	GHG (gCO2e/MJ)	Carbon Price ($/tCO2e)
Algae	30,174.2	100.0%	4,349,350	100.0%	0.6%	$8.66	62.71	$2,333.91
Upland Switchgrass	-	0.0%	-	0.0%	0.0%	$-	-	$-
Lowland Switchgrass	-	0.0%	-	0.0%	0.0%	$-	-	$-
Miscanthus	-	0.0%	-	0.0%	0.0%	$-	-	$-
Poplar	-	0.0%	-	0.0%	0.0%	$-	-	$-
Corn	-	0.0%	-	0.0%	0.0%	$-	-	$-
Soy	-	0.0%	-	0.0%	0.0%	$-	-	$-
Willow	-	0.0%	-	0.0%	0.0%	$-	-	$-
Sorghum	-	0.0%	-	0.0%	0.0%	$-	-	$-

Table C53. Optimization results breakdown by land for the 30-billion-gallon SAF scenario when optimized for minimum fuel costs.

	Jet Fuel (million gallons)	Jet Fuel Percentage	Land Use (ha)	Land Use Percentage (SAF)	Land Use Percentage (CONUS)	MFSP ($/gallon Jet)	GHG (gCO2e/MJ)	Carbon Price ($/tCO2e)
Barren Land	-	0%	-	0%	0%	$-	-	$-
Deciduous Forest	8,309.8	28%	13,483,849	27%	2%	$3.21	56.46	$353.28
Evergreen Forest	1,845.7	6%	3,165,906	6%	0%	$3.28	76.41	$1,258.19
Mixed Forest	2,759.2	9%	4,655,057	9%	1%	$3.26	70.07	$707.50
Shrubland	3,008.6	10%	5,085,561	10%	1%	$3.28	58.04	$395.49
Grassland Herbaceous	8,054.4	27%	14,606,351	29%	2%	$3.32	37.97	$231.67
Cultivated Crops	6,022.3	20%	9,785,154	19%	1%	$3.37	9.33	$149.02

Table C54. Optimization results breakdown by land for the 30-billion-gallon SAF scenario when optimized for minimum fuel emissions.

	Jet Fuel (million gallons)	Jet Fuel Percentage	Land Use (ha)	Land Use Percentage (SAF)	Land Use Percentage (CONUS)	MFSP ($/gallon Jet)	GHG (gCO2e/MJ)	Carbon Price ($/tCO2e)
Barren Land	-	0%	-	0%	0%	$-	-	$-
Deciduous Forest	408.9	1%	593,258	1%	0%	$3.14	18.74	$143.70
Evergreen Forest	84.6	0%	345,973	0%	0%	$3.99	16.48	$233.82
Mixed Forest	76.9	0%	111,652	0%	0%	$3.15	18.84	$144.57
Shrubland	7,424.3	25%	46,853,334	42%	6%	$4.47	9.00	$258.84
Grassland Herbaceous	12,459.4	42%	45,668,686	41%	6%	$3.86	10.53	$201.54
Cultivated Crops	9,545.9	32%	16,923,016	15%	2%	$3.53	0.96	$149.11

Table C55. Optimization results breakdown by land for the 30-billion-gallon SAF scenario when optimized for minimum carbon price.

	Jet Fuel (million gallons)	Jet Fuel Percentage	Land Use (ha)	Land Use Percentage (SAF)	Land Use Percentage (CONUS)	MFSP ($/gallon Jet)	GHG (gCO2e/MJ)	Carbon Price ($/tCO2e)
Barren Land	-	0%	-	0%	0%	$-	-	$-
Deciduous Forest	2,327.4	8%	3,407,107	4%	0%	$3.13	33.53	$183.56
Evergreen Forest	68.8	0%	194,539	0%	0%	$3.55	24.80	$209.89
Mixed Forest	285.8	1%	424,052	1%	0%	$3.13	31.37	$176.72
Shrubland	3,910.1	13%	16,757,275	21%	2%	$3.95	9.78	$209.00
Grassland Herbaceous	13,890.2	46%	41,397,563	52%	5%	$3.65	15.34	$193.18
Cultivated Crops	9,517.6	32%	16,819,886	21%	2%	$3.53	1.09	$148.51

Table C56. Optimization results breakdown by land for the 30-billion-gallon SAF scenario when optimized for minimum land use.

	Jet Fuel (million gallons)	Jet Fuel Percentage	Land Use (ha)	Land Use Percentage (SAF)	Land Use Percentage (CONUS)	MFSP ($/gallon Jet)	GHG (gCO2e/MJ)	Carbon Price ($/tCO2e)
Barren Land	3,887.0	13%	564,305	13%	0%	$8.84	62.77	$2,399.80
Deciduous Forest	24.4	0%	3,504	0%	0%	$8.59	64.20	$2,475.18
Evergreen Forest	624.2	2%	89,855	2%	0%	$8.58	64.87	$2,553.02
Mixed Forest	98.3	0%	14,029	0%	0%	$8.53	64.26	$2,460.46
Shrubland	20,688.3	69%	2,979,123	68%	0%	$8.64	62.69	$2,323.02
Grassland Herbaceous	4,852.0	16%	698,534	16%	0%	$8.64	62.45	$2,299.64
Cultivated Crops	-	0%	-	0%	0%	$-	-	$-

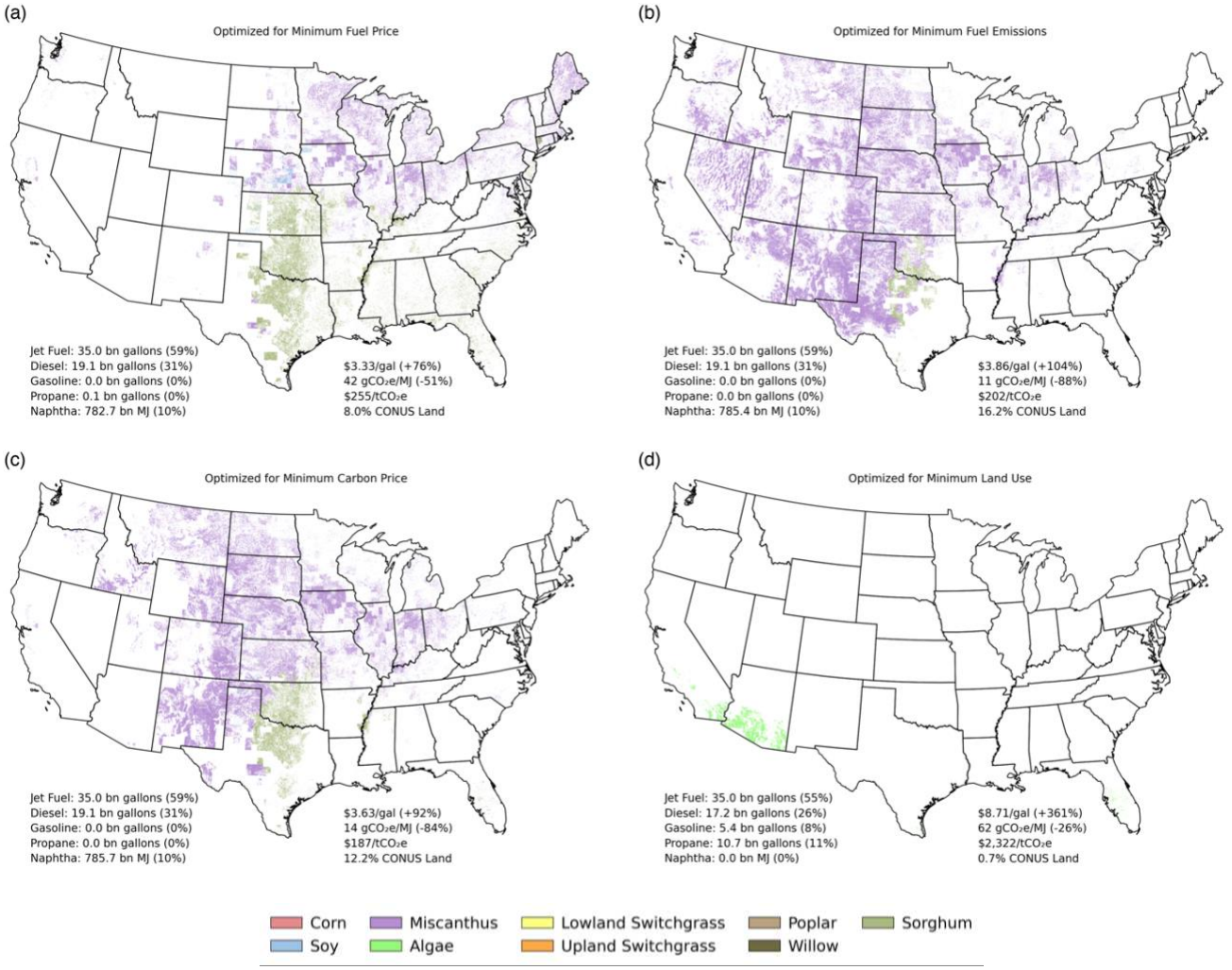

Figure C15. Multi-objective optimization maps of the optimal geographic feedstock deployment to meet 35 billion gallons of annual SAF production while minimizing fuel price (a), fuel emissions (b), breakeven carbon price (c), and land area (d). Percentages in parentheses for the fuel products represent the total percent of megajoules produced for that fuel type as a percentage of total megajoules of fuel produced by the feedstocks. Percentages in parentheses for the mean fuel selling price and mean fuel emissions represent the percent cost increase and percent emissions reduction, respectively, compared to petroleum jet fuel.

Table C57. Optimization results breakdown by crop for the 35-billion-gallon SAF scenario when optimized for minimum fuel costs.

	Jet Fuel (million gallons)	Jet Fuel Percentage	Land Use (ha)	Land Use Percentage (SAF)	Land Use Percentage (CONUS)	MFSP ($/gallon Jet)	GHG (gCO2e/MJ)	Carbon Price ($/tCO2e)
Algae	-	0.0%	-	0.0%	0.0%	$-	-	$-
Upland Switchgrass	-	0.0%	-	0.0%	0.0%	$-	-	$-
Lowland Switchgrass	-	0.0%	-	0.0%	0.0%	$-	-	$-
Miscanthus	17,731.0	50.7%	31,701,924	51.0%	4.1%	$3.33	40.38	$246.82
Poplar	-	0.0%	-	0.0%	0.0%	$-	-	$-
Corn	-	0.0%	-	0.0%	0.0%	$-	-	$-
Soy	191.3	0.5%	1,194,690	1.9%	0.2%	$3.23	(1.40)	$118.00
Willow	85.1	0.2%	150,534	0.2%	0.0%	$3.57	118.05	$(383.69)
Sorghum	16,992.6	48.6%	29,154,641	46.9%	3.7%	$3.33	43.48	$264.95

Table C58. Optimization results breakdown by crop for the 35-billion-gallon SAF scenario when optimized for minimum fuel emissions.

	Jet Fuel (million gallons)	Jet Fuel Percentage	Land Use (ha)	Land Use Percentage (SAF)	Land Use Percentage (CONUS)	MFSP ($/gallon Jet)	GHG (gCO2e/MJ)	Carbon Price ($/tCO2e)
Algae	-	0.0%	-	0.0%	0.0%	$-	-	$-
Upland Switchgrass	0.1	0.0%	1,492	0.0%	0.0%	$7.14	32.45	$763.66
Lowland Switchgrass	-	0.0%	-	0.0%	0.0%	$-	-	$-
Miscanthus	32,651.8	93.3%	121,091,242	95.9%	15.5%	$3.89	9.17	$201.27
Poplar	-	0.0%	-	0.0%	0.0%	$-	-	$-
Corn	20.1	0.1%	38,508	0.0%	0.0%	$5.07	16.23	$352.81
Soy	49.3	0.1%	363,555	0.3%	0.0%	$3.67	(22.91)	$125.54
Willow	-	0.0%	-	0.0%	0.0%	$-	-	$-
Sorghum	2,278.6	6.5%	4,775,150	3.8%	0.6%	$3.42	31.77	$218.88

Table C59. Optimization results breakdown by crop for the 35-billion-gallon SAF scenario when optimized for minimum carbon price.

	Jet Fuel (million gallons)	Jet Fuel Percentage	Land Use (ha)	Land Use Percentage (SAF)	Land Use Percentage (CONUS)	MFSP ($/gallon Jet)	GHG (gCO2e/MJ)	Carbon Price ($/tCO2e)
Algae	-	0.0%	-	0.0%	0.0%	$-	-	$-
Upland Switchgrass	-	0.0%	-	0.0%	0.0%	$-	-	$-
Lowland Switchgrass	-	0.0%	-	0.0%	0.0%	$-	-	$-
Miscanthus	28,111.9	80.3%	82,357,288	86.5%	10.6%	$3.70	9.04	$181.84
Poplar	-	0.0%	-	0.0%	0.0%	$-	-	$-
Corn	-	0.0%	-	0.0%	0.0%	$-	-	$-
Soy	59.7	0.2%	395,158	0.4%	0.1%	$3.05	(14.08)	$89.03
Willow	-	0.0%	-	0.0%	0.0%	$-	-	$-
Sorghum	6,828.5	19.5%	12,508,321	13.1%	1.6%	$3.35	33.93	$218.18

Table C60. Optimization results breakdown by crop for the 35-billion-gallon SAF scenario when optimized for minimum land use.

	Jet Fuel (million gallons)	Jet Fuel Percentage	Land Use (ha)	Land Use Percentage (SAF)	Land Use Percentage (CONUS)	MFSP ($/gallon Jet)	GHG (gCO2e/MJ)	Carbon Price ($/tCO2e)
Algae	35,011.8	100.0%	5,067,316	100.0%	0.7%	$8.71	62.43	$2,321.71
Upland Switchgrass	-	0.0%	-	0.0%	0.0%	$-	-	$-
Lowland Switchgrass	-	0.0%	-	0.0%	0.0%	$-	-	$-
Miscanthus	-	0.0%	-	0.0%	0.0%	$-	-	$-
Poplar	-	0.0%	-	0.0%	0.0%	$-	-	$-
Corn	-	0.0%	-	0.0%	0.0%	$-	-	$-
Soy	-	0.0%	-	0.0%	0.0%	$-	-	$-
Willow	-	0.0%	-	0.0%	0.0%	$-	-	$-
Sorghum	-	0.0%	-	0.0%	0.0%	$-	-	$-

Table C61. Optimization results breakdown by land for the 35-billion-gallon SAF scenario when optimized for minimum fuel costs.

	Jet Fuel (million gallons)	Jet Fuel Percentage	Land Use (ha)	Land Use Percentage (SAF)	Land Use Percentage (CONUS)	MFSP ($/gallon Jet)	GHG (gCO2e/MJ)	Carbon Price ($/tCO2e)
Barren Land	-	0%	-	0%	0%	$-	-	$-
Deciduous Forest	8,630.7	25%	14,085,480	23%	2%	$3.22	56.93	$363.19
Evergreen Forest	1,958.6	6%	3,418,143	5%	0%	$3.30	76.05	$1,223.29
Mixed Forest	2,853.9	8%	4,834,248	8%	1%	$3.27	70.83	$752.21
Shrubland	4,186.0	12%	8,409,121	14%	1%	$3.37	51.33	$336.72
Grassland Herbaceous	9,738.5	28%	18,966,305	30%	2%	$3.37	35.19	$226.17
Cultivated Crops	7,632.2	22%	12,488,493	20%	2%	$3.42	8.46	$152.26

Table C62. Optimization results breakdown by land for the 35-billion-gallon SAF scenario when optimized for minimum fuel emissions.

	Jet Fuel (million gallons)	Jet Fuel Percentage	Land Use (ha)	Land Use Percentage (SAF)	Land Use Percentage (CONUS)	MFSP ($/gallon Jet)	GHG (gCO2e/MJ)	Carbon Price ($/tCO2e)
Barren Land	-	0%	-	0%	0%	$-	-	$-
Deciduous Forest	943.1	3%	1,386,720	1%	0%	$3.14	25.42	$160.52
Evergreen Forest	110.5	0%	457,493	0%	0%	$3.98	19.57	$243.96
Mixed Forest	158.2	0%	232,265	0%	0%	$3.16	24.76	$161.05
Shrubland	9,432.7	27%	56,042,423	44%	7%	$4.38	13.52	$265.17
Grassland Herbaceous	14,785.1	42%	51,211,084	41%	7%	$3.80	13.77	$203.99
Cultivated Crops	9,570.4	27%	16,939,963	13%	2%	$3.54	1.03	$149.45

Table C63. Optimization results breakdown by land for the 35-billion-gallon SAF scenario when optimized for minimum carbon price.

	Jet Fuel (million gallons)	Jet Fuel Percentage	Land Use (ha)	Land Use Percentage (SAF)	Land Use Percentage (CONUS)	MFSP ($/gallon Jet)	GHG (gCO2e/MJ)	Carbon Price ($/tCO2e)
Barren Land	-	0%	-	0%	0%	$-	-	$-
Deciduous Forest	2,900.0	8%	4,294,240	5%	1%	$3.15	35.59	$193.81
Evergreen Forest	132.7	0%	361,153	0%	0%	$3.54	28.79	$224.54
Mixed Forest	327.9	1%	493,690	1%	0%	$3.14	33.08	$183.84
Shrubland	6,061.8	17%	25,359,875	27%	3%	$3.94	14.34	$220.94
Grassland Herbaceous	15,882.7	45%	47,877,740	50%	6%	$3.68	16.38	$199.35
Cultivated Crops	9,694.9	28%	16,874,068	18%	2%	$3.52	2.08	$149.79

Table C64. Optimization results breakdown by land for the 35-billion-gallon SAF scenario when optimized for minimum land use.

	Jet Fuel (million gallons)	Jet Fuel Percentage	Land Use (ha)	Land Use Percentage (SAF)	Land Use Percentage (CONUS)	MFSP ($/gallon Jet)	GHG (gCO2e/MJ)	Carbon Price ($/tCO2e)
Barren Land	4,301.3	12%	625,727	12%	0%	$8.86	62.38	$2,366.26
Deciduous Forest	25.9	0%	3,728	0%	0%	$8.60	64.16	$2,474.43
Evergreen Forest	729.1	2%	105,460	2%	0%	$8.60	65.04	$2,584.25
Mixed Forest	98.3	0%	14,033	0%	0%	$8.53	64.26	$2,460.46
Shrubland	24,145.7	69%	3,492,222	69%	0%	$8.69	62.38	$2,309.81
Grassland Herbaceous	5,711.5	16%	826,147	16%	0%	$8.71	62.28	$2,306.17
Cultivated Crops	-	0%	-	0%	0%	$-	-	$-

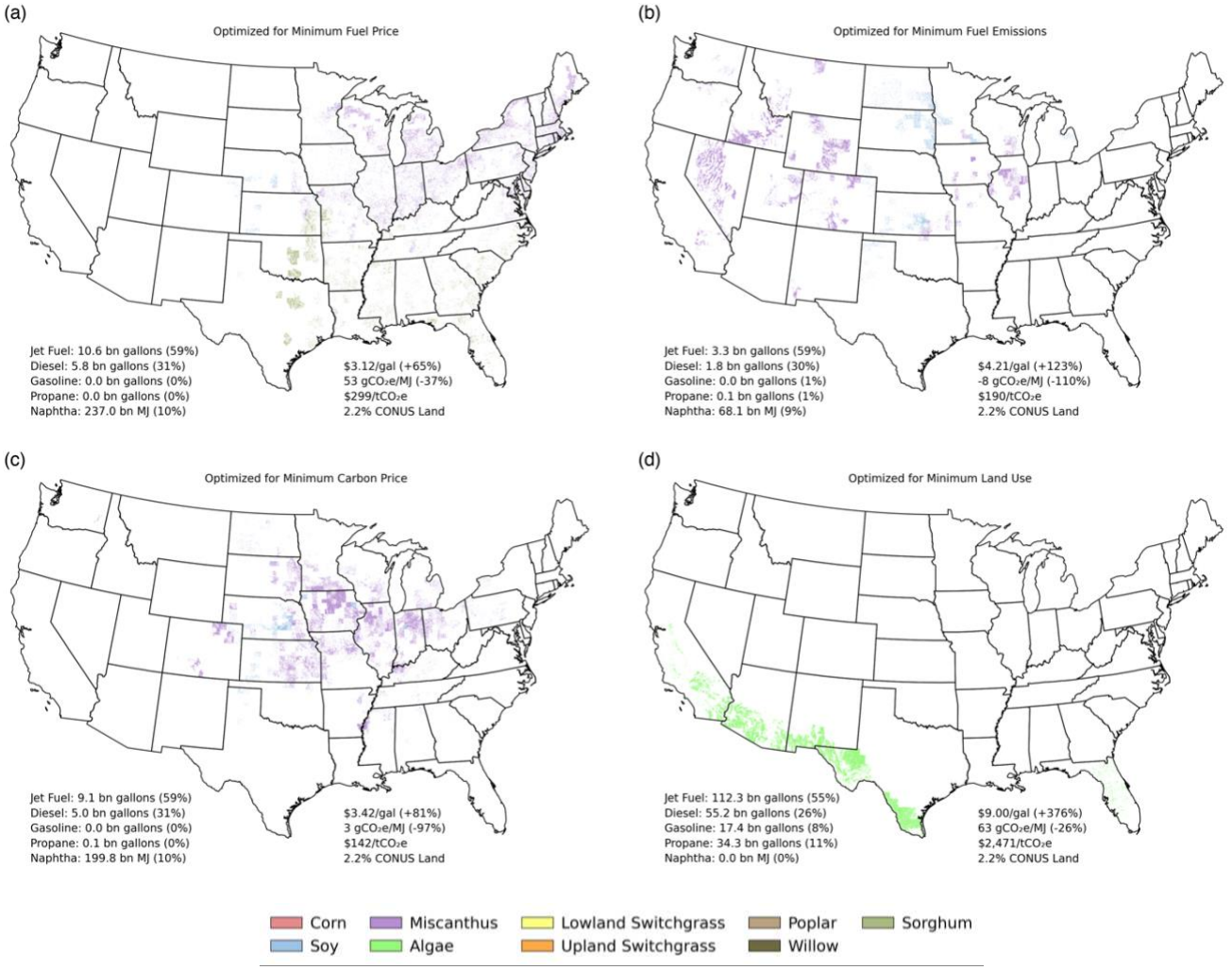

Figure C16. Multi-objective optimization maps of the optimal geographic feedstock deployment limited to existing bioenergy (corn ethanol and soybean biodiesel) land while minimizing fuel price (a), fuel emissions (b), breakeven carbon price (c), and land area (d). Percentages in parentheses for the fuel products represent the total percent of megajoules produced for that fuel type as a percentage of total megajoules of fuel produced by the feedstocks. Percentages in parentheses for the mean fuel selling price and mean fuel emissions represent the percent cost increase and percent emissions reduction, respectively, compared to petroleum jet fuel.

Table C65. Optimization results breakdown by crop for the bioenergy land limited scenario when optimized for minimum fuel costs.

	Jet Fuel (million gallons)	Jet Fuel Percentage	Land Use (ha)	Land Use Percentage (SAF)	Land Use Percentage (CONUS)	MFSP ($/gallon Jet)	GHG (gCO2e/MJ)	Carbon Price ($/tCO2e)
Algae	-	0.0%	-	0.0%	0.0%	$-	-	$-
Upland Switchgrass	-	0.0%	-	0.0%	0.0%	$-	-	$-
Lowland Switchgrass	-	0.0%	-	0.0%	0.0%	$-	-	$-
Miscanthus	6,663.2	62.7%	10,832,236	63.9%	1.4%	$3.11	55.52	$317.35
Poplar	-	0.0%	-	0.0%	0.0%	$-	-	$-
Corn	-	0.0%	-	0.0%	0.0%	$-	-	$-
Soy	84.4	0.8%	521,415	3.1%	0.1%	$2.90	(1.82)	$88.92
Willow	-	0.0%	-	0.0%	0.0%	$-	-	$-
Sorghum	3,877.5	36.5%	5,609,757	33.1%	0.7%	$3.15	51.13	$283.45

Table C66. Optimization results breakdown by crop for the bioenergy land limited scenario when optimized for minimum fuel emissions.

	Jet Fuel (million gallons)	Jet Fuel Percentage	Land Use (ha)	Land Use Percentage (SAF)	Land Use Percentage (CONUS)	MFSP ($/gallon Jet)	GHG (gCO2e/MJ)	Carbon Price ($/tCO2e)
Algae	-	0.0%	-	0.0%	0.0%	$-	-	$-
Upland Switchgrass	1.0	0.0%	8,371	0.0%	0.0%	$5.83	(8.57)	$321.29
Lowland Switchgrass	-	0.0%	-	0.0%	0.0%	$-	-	$-
Miscanthus	3,027.7	90.6%	14,364,068	83.4%	1.8%	$4.12	(7.70)	$183.40
Poplar	-	0.0%	-	0.0%	0.0%	$-	-	$-
Corn	0.4	0.0%	2,646	0.0%	0.0%	$9.62	(11.25)	$612.36
Soy	312.4	9.3%	2,850,810	16.5%	0.4%	$5.08	(13.17)	$247.60
Willow	-	0.0%	-	0.0%	0.0%	$-	-	$-
Sorghum	-	0.0%	-	0.0%	0.0%	$-	-	$-

Table C67. Optimization results breakdown by crop for the bioenergy land limited scenario when optimized for minimum carbon price.

	Jet Fuel (million gallons)	Jet Fuel Percentage	Land Use (ha)	Land Use Percentage (SAF)	Land Use Percentage (CONUS)	MFSP ($/gallon Jet)	GHG (gCO2e/MJ)	Carbon Price ($/tCO2e)
Algae	-	0.0%	-	0.0%	0.0%	$-	-	$-
Upland Switchgrass	-	0.0%	-	0.0%	0.0%	$-	-	$-
Lowland Switchgrass	-	0.0%	-	0.0%	0.0%	$-	-	$-
Miscanthus	8,878.9	97.3%	15,451,206	91.1%	2.0%	$3.42	2.75	$142.17
Poplar	-	0.0%	-	0.0%	0.0%	$-	-	$-
Corn	-	0.0%	-	0.0%	0.0%	$-	-	$-
Soy	236.3	2.6%	1,499,413	8.8%	0.2%	$3.26	(0.83)	$121.41
Willow	-	0.0%	-	0.0%	0.0%	$-	-	$-
Sorghum	8.3	0.1%	11,628	0.1%	0.0%	$3.05	30.05	$160.92

Table C68. Optimization results breakdown by crop for the bioenergy land limited scenario when optimized for minimum land use.

	Jet Fuel (million gallons)	Jet Fuel Percentage	Land Use (ha)	Land Use Percentage (SAF)	Land Use Percentage (CONUS)	MFSP ($/gallon Jet)	GHG (gCO2e/MJ)	Carbon Price ($/tCO2e)
Algae	112,321.1	100.0%	17,044,122	100.0%	2.2%	$9.00	62.90	$2,471.43
Upland Switchgrass	-	0.0%	-	0.0%	0.0%	$-	-	$-
Lowland Switchgrass	-	0.0%	-	0.0%	0.0%	$-	-	$-
Miscanthus	-	0.0%	-	0.0%	0.0%	$-	-	$-
Poplar	-	0.0%	-	0.0%	0.0%	$-	-	$-
Corn	-	0.0%	-	0.0%	0.0%	$-	-	$-
Soy	-	0.0%	-	0.0%	0.0%	$-	-	$-
Willow	-	0.0%	-	0.0%	0.0%	$-	-	$-
Sorghum	-	0.0%	-	0.0%	0.0%	$-	-	$-

Table C69. Optimization results breakdown by land for the bioenergy land limited scenario when optimized for minimum fuel costs.

	Jet Fuel (million gallons)	Jet Fuel Percentage	Land Use (ha)	Land Use Percentage (SAF)	Land Use Percentage (CONUS)	MFSP ($/gallon Jet)	GHG (gCO2e/MJ)	Carbon Price ($/tCO2e)
Barren Land	-	0%	-	0%	0%	$-	-	$-
Deciduous Forest	4,915.7	46%	7,716,227	45%	1%	$3.11	52.97	$292.03
Evergreen Forest	690.5	6%	1,127,258	7%	0%	$3.12	77.75	$1,323.46
Mixed Forest	1,195.1	11%	1,931,128	11%	0%	$3.11	65.61	$482.12
Shrubland	1,103.0	10%	1,637,233	10%	0%	$3.14	65.39	$489.96
Grassland Herbaceous	2,124.4	20%	3,293,558	19%	0%	$3.15	45.56	$243.20
Cultivated Crops	596.4	6%	1,258,005	7%	0%	$3.13	11.16	$127.93

Table C70. Optimization results breakdown by land for the bioenergy land limited scenario when optimized for minimum fuel emissions.

	Jet Fuel (million gallons)	Jet Fuel Percentage	Land Use (ha)	Land Use Percentage (SAF)	Land Use Percentage (CONUS)	MFSP ($/gallon Jet)	GHG (gCO2e/MJ)	Carbon Price ($/tCO2e)
Barren Land	-	0%	-	0%	0%	$-	-	$-
Deciduous Forest	0.0	0%	4	0%	0%	$3.99	(4.95)	$177.89
Evergreen Forest	-	0%	-	0%	0%	$-	-	$-
Mixed Forest	-	0%	-	0%	0%	$-	-	$-
Shrubland	918.1	27%	8,346,514	48%	1%	$4.99	(11.15)	$245.91
Grassland Herbaceous	575.8	17%	3,568,749	21%	0%	$4.33	(8.22)	$199.25
Cultivated Crops	1,847.6	55%	5,310,628	31%	1%	$3.79	(6.75)	$157.61

Table C71. Optimization results breakdown by land for the bioenergy land limited scenario when optimized for minimum carbon price.

	Jet Fuel (million gallons)	Jet Fuel Percentage	Land Use (ha)	Land Use Percentage (SAF)	Land Use Percentage (CONUS)	MFSP ($/gallon Jet)	GHG (gCO2e/MJ)	Carbon Price ($/tCO2e)
Barren Land	-	0%	-	0%	0%	$-	-	$-
Deciduous Forest	471.9	5%	673,441	4%	0%	$3.09	21.12	$143.55
Evergreen Forest	2.0	0%	2,876	0%	0%	$3.11	20.68	$144.44
Mixed Forest	79.7	1%	114,824	1%	0%	$3.11	19.85	$142.42
Shrubland	60.0	1%	299,735	2%	0%	$3.90	(17.26)	$150.13
Grassland Herbaceous	1,203.5	13%	2,920,345	17%	0%	$3.34	10.89	$148.75
Cultivated Crops	7,306.4	80%	12,951,026	76%	2%	$3.45	0.11	$140.41

Table C72. Optimization results breakdown by land for the bioenergy land limited scenario when optimized for minimum land use.

	Jet Fuel (million gallons)	Jet Fuel Percentage	Land Use (ha)	Land Use Percentage (SAF)	Land Use Percentage (CONUS)	MFSP ($/gallon Jet)	GHG (gCO2e/MJ)	Carbon Price ($/tCO2e)
Barren Land	7,650.8	7%	1,136,418	7%	0%	$9.00	61.81	$2,353.67
Deciduous Forest	269.3	0%	41,226	0%	0%	$8.97	63.94	$2,584.14
Evergreen Forest	1,527.9	1%	226,020	1%	0%	$8.74	65.16	$2,654.39
Mixed Forest	260.4	0%	39,149	0%	0%	$8.84	64.45	$2,598.32
Shrubland	78,899.0	70%	12,003,882	70%	2%	$9.01	62.91	$2,474.05
Grassland Herbaceous	23,713.8	21%	3,597,426	21%	0%	$9.00	63.05	$2,489.63
Cultivated Crops	-	0%	-	0%	0%	$-	-	$-

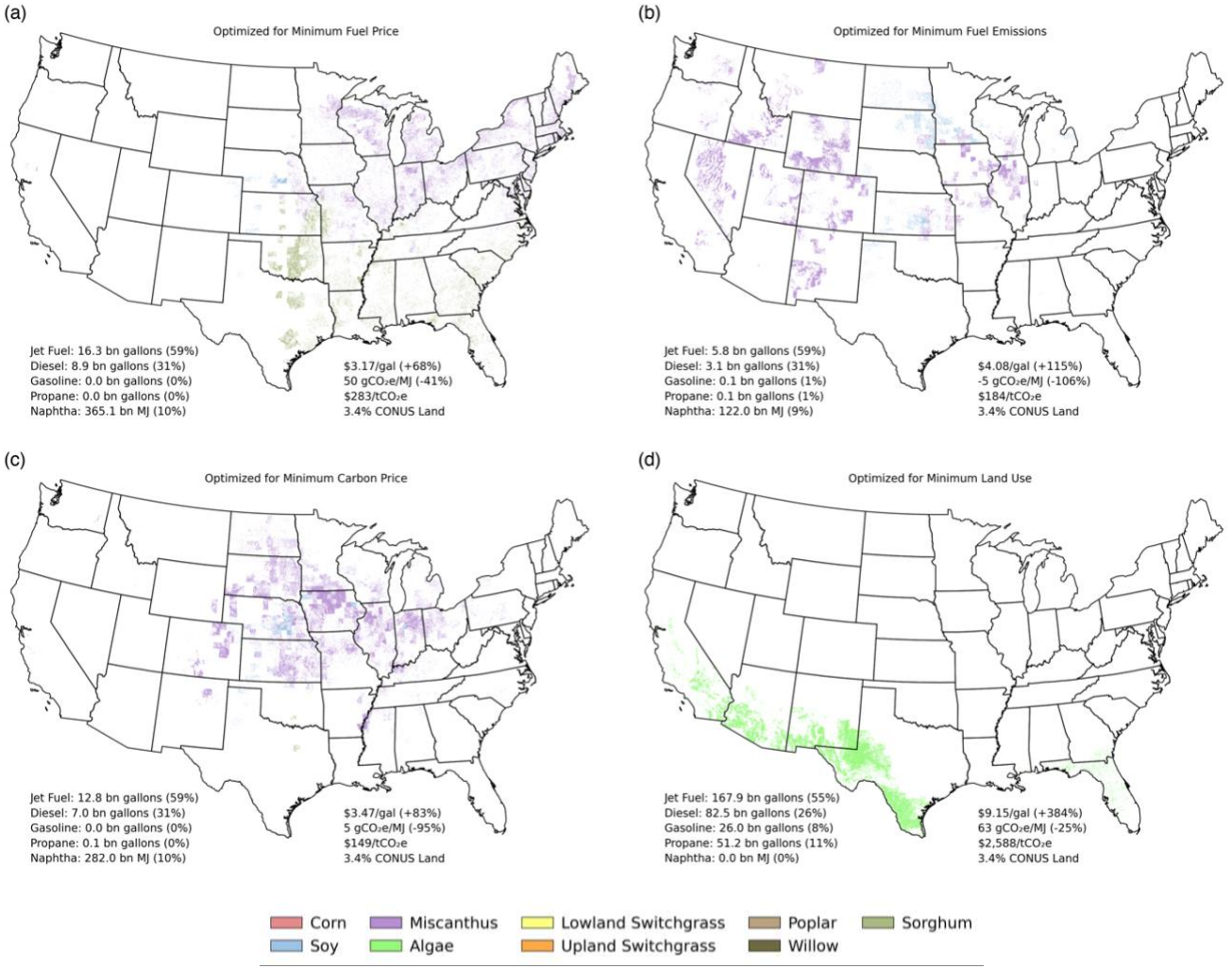

Figure C17. Multi-objective optimization maps of the optimal geographic feedstock deployment limited to existing bioenergy (corn ethanol and soybean biodiesel) land plus the historically mean annual land conversion to cropland for 30 years while minimizing fuel price (a), fuel emissions (b), breakeven carbon price (c), and land area (d). Percentages in parentheses for the fuel products represent the total percent of megajoules produced for that fuel type as a percentage of total megajoules of fuel produced by the feedstocks. Percentages in parentheses for the mean fuel selling price and mean fuel emissions represent the percent cost increase and percent emissions reduction, respectively, compared to petroleum jet fuel.

Table C73. Optimization results breakdown by crop for the bioenergy + mean conversion land limited scenario when optimized for minimum fuel costs.

	Jet Fuel (million gallons)	Jet Fuel Percentage	Land Use (ha)	Land Use Percentage (SAF)	Land Use Percentage (CONUS)	MFSP ($/gallon Jet)	GHG (gCO2e/MJ)	Carbon Price ($/tCO2e)
Algae	-	0.0%	-	0.0%	0.0%	$-	-	$-
Upland Switchgrass	-	0.0%	-	0.0%	0.0%	$-	-	$-
Lowland Switchgrass	-	0.0%	-	0.0%	0.0%	$-	-	$-
Miscanthus	9,083.5	55.6%	14,877,860	56.8%	1.9%	$3.16	51.29	$286.97
Poplar	-	0.0%	-	0.0%	0.0%	$-	-	$-
Corn	-	0.0%	-	0.0%	0.0%	$-	-	$-
Soy	108.7	0.7%	664,744	2.5%	0.1%	$2.98	(0.65)	$97.13
Willow	-	0.0%	-	0.0%	0.0%	$-	-	$-
Sorghum	7,152.7	43.8%	10,628,665	40.6%	1.4%	$3.20	50.00	$286.16

Table C74. Optimization results breakdown by crop for the bioenergy + mean conversion land limited scenario when optimized for minimum fuel emissions.

	Jet Fuel (million gallons)	Jet Fuel Percentage	Land Use (ha)	Land Use Percentage (SAF)	Land Use Percentage (CONUS)	MFSP ($/gallon Jet)	GHG (gCO2e/MJ)	Carbon Price ($/tCO2e)
Algae	-	0.0%	-	0.0%	0.0%	$-	-	$-
Upland Switchgrass	2.5	0.0%	14,761	0.1%	0.0%	$4.90	(4.44)	$256.92
Lowland Switchgrass	-	0.0%	-	0.0%	0.0%	$-	-	$-
Miscanthus	5,423.5	93.6%	22,930,935	87.4%	2.9%	$4.01	(4.96)	$179.91
Poplar	-	0.0%	-	0.0%	0.0%	$-	-	$-
Corn	0.4	0.0%	2,646	0.0%	0.0%	$9.62	(11.25)	$612.36
Soy	367.7	6.3%	3,288,144	12.5%	0.4%	$4.98	(11.47)	$244.04
Willow	-	0.0%	-	0.0%	0.0%	$-	-	$-
Sorghum	-	0.0%	-	0.0%	0.0%	$-	-	$-

Table C75. Optimization results breakdown by crop for the bioenergy + mean conversion land limited scenario when optimized for minimum carbon price.

	Jet Fuel (million gallons)	Jet Fuel Percentage	Land Use (ha)	Land Use Percentage (SAF)	Land Use Percentage (CONUS)	MFSP ($/gallon Jet)	GHG (gCO2e/MJ)	Carbon Price ($/tCO2e)
Algae	-	0.0%	-	0.0%	0.0%	$-	-	$-
Upland Switchgrass	-	0.0%	-	0.0%	0.0%	$-	-	$-
Lowland Switchgrass	-	0.0%	-	0.0%	0.0%	$-	-	$-
Miscanthus	12,449.6	97.1%	24,262,449	92.8%	3.1%	$3.47	4.43	$149.64
Poplar	-	0.0%	-	0.0%	0.0%	$-	-	$-
Corn	-	0.0%	-	0.0%	0.0%	$-	-	$-
Soy	274.0	2.1%	1,745,360	6.7%	0.2%	$3.32	(0.41)	$127.85
Willow	-	0.0%	-	0.0%	0.0%	$-	-	$-
Sorghum	93.7	0.7%	143,641	0.5%	0.0%	$3.09	30.60	$168.49

Table C76. Optimization results breakdown by crop for the bioenergy + mean conversion land limited scenario when optimized for minimum land use.

	Jet Fuel (million gallons)	Jet Fuel Percentage	Land Use (ha)	Land Use Percentage (SAF)	Land Use Percentage (CONUS)	MFSP ($/gallon Jet)	GHG (gCO2e/MJ)	Carbon Price ($/tCO2e)
Algae	167,929.6	100.0%	26,142,693	100.0%	3.4%	$9.15	63.44	$2,588.48
Upland Switchgrass	-	0.0%	-	0.0%	0.0%	$-	-	$-
Lowland Switchgrass	-	0.0%	-	0.0%	0.0%	$-	-	$-
Miscanthus	-	0.0%	-	0.0%	0.0%	$-	-	$-
Poplar	-	0.0%	-	0.0%	0.0%	$-	-	$-
Corn	-	0.0%	-	0.0%	0.0%	$-	-	$-
Soy	-	0.0%	-	0.0%	0.0%	$-	-	$-
Willow	-	0.0%	-	0.0%	0.0%	$-	-	$-
Sorghum	-	0.0%	-	0.0%	0.0%	$-	-	$-

Table C77. Optimization results breakdown by land for the bioenergy + mean conversion land limited scenario when optimized for minimum fuel costs.

	Jet Fuel (million gallons)	Jet Fuel Percentage	Land Use (ha)	Land Use Percentage (SAF)	Land Use Percentage (CONUS)	MFSP ($/gallon Jet)	GHG (gCO2e/MJ)	Carbon Price ($/tCO2e)
Barren Land	-	0%	-	0%	0%	$-	-	$-
Deciduous Forest	6,456.9	40%	10,204,135	39%	1%	$3.15	53.96	$310.50
Evergreen Forest	922.6	6%	1,513,480	6%	0%	$3.15	76.79	$1,198.55
Mixed Forest	1,540.7	9%	2,503,357	10%	0%	$3.14	66.10	$509.30
Shrubland	1,850.7	11%	2,803,556	11%	0%	$3.19	64.06	$477.40
Grassland Herbaceous	3,729.2	23%	5,980,594	23%	1%	$3.20	44.02	$243.82
Cultivated Crops	1,844.8	11%	3,166,146	12%	0%	$3.23	10.62	$136.89

Table C78. Optimization results breakdown by land for the bioenergy + mean conversion land limited scenario when optimized for minimum fuel emissions.

	Jet Fuel (million gallons)	Jet Fuel Percentage	Land Use (ha)	Land Use Percentage (SAF)	Land Use Percentage (CONUS)	MFSP ($/gallon Jet)	GHG (gCO2e/MJ)	Carbon Price ($/tCO2e)
Barren Land	-	0%	-	0%	0%	$-	-	$-
Deciduous Forest	0.0	0%	4	0%	0%	$3.99	(4.95)	$177.89
Evergreen Forest	0.0	0%	16	0%	0%	$3.15	(1.43)	$111.19
Mixed Forest	0.0	0%	4	0%	0%	$4.22	(3.01)	$201.94
Shrubland	1,555.2	27%	12,593,504	48%	2%	$4.81	(7.26)	$241.59
Grassland Herbaceous	960.6	17%	5,696,412	22%	1%	$4.27	(5.37)	$200.80
Cultivated Crops	3,278.3	57%	7,946,546	30%	1%	$3.67	(4.48)	$151.43

Table C79. Optimization results breakdown by land for the bioenergy + mean conversion land limited scenario when optimized for minimum carbon price.

	Jet Fuel (million gallons)	Jet Fuel Percentage	Land Use (ha)	Land Use Percentage (SAF)	Land Use Percentage (CONUS)	MFSP ($/gallon Jet)	GHG (gCO2e/MJ)	Carbon Price ($/tCO2e)
Barren Land	-	0%	-	0%	0%	$-	-	$-
Deciduous Forest	788.8	6%	1,130,850	4%	0%	$3.10	24.85	$152.86
Evergreen Forest	3.6	0%	5,140	0%	0%	$3.11	24.95	$154.26
Mixed Forest	115.0	1%	165,958	1%	0%	$3.11	22.97	$149.76
Shrubland	147.6	1%	605,275	2%	0%	$3.78	(4.02)	$161.72
Grassland Herbaceous	3,135.5	24%	8,436,962	32%	1%	$3.47	10.76	$162.20
Cultivated Crops	8,626.8	67%	15,807,266	60%	2%	$3.50	0.28	$144.64

Table C80. Optimization results breakdown by land for the bioenergy + mean conversion land limited scenario when optimized for minimum land use.

	Jet Fuel (million gallons)	Jet Fuel Percentage	Land Use (ha)	Land Use Percentage (SAF)	Land Use Percentage (CONUS)	MFSP ($/gallon Jet)	GHG (gCO2e/MJ)	Carbon Price ($/tCO2e)
Barren Land	8,283.0	5%	1,239,070	5%	0%	$9.05	61.85	$2,374.95
Deciduous Forest	438.5	0%	69,023	0%	0%	$9.14	64.79	$2,757.37
Evergreen Forest	1,852.1	1%	279,102	1%	0%	$8.87	65.14	$2,703.15
Mixed Forest	586.8	0%	93,043	0%	0%	$9.16	65.73	$2,899.95
Shrubland	125,809.7	75%	19,675,603	75%	3%	$9.17	63.48	$2,599.43
Grassland Herbaceous	30,934.6	18%	4,782,710	18%	1%	$9.12	63.57	$2,591.40
Cultivated Crops	24.9	0%	4,141	0%	0%	$9.57	64.49	$2,879.44

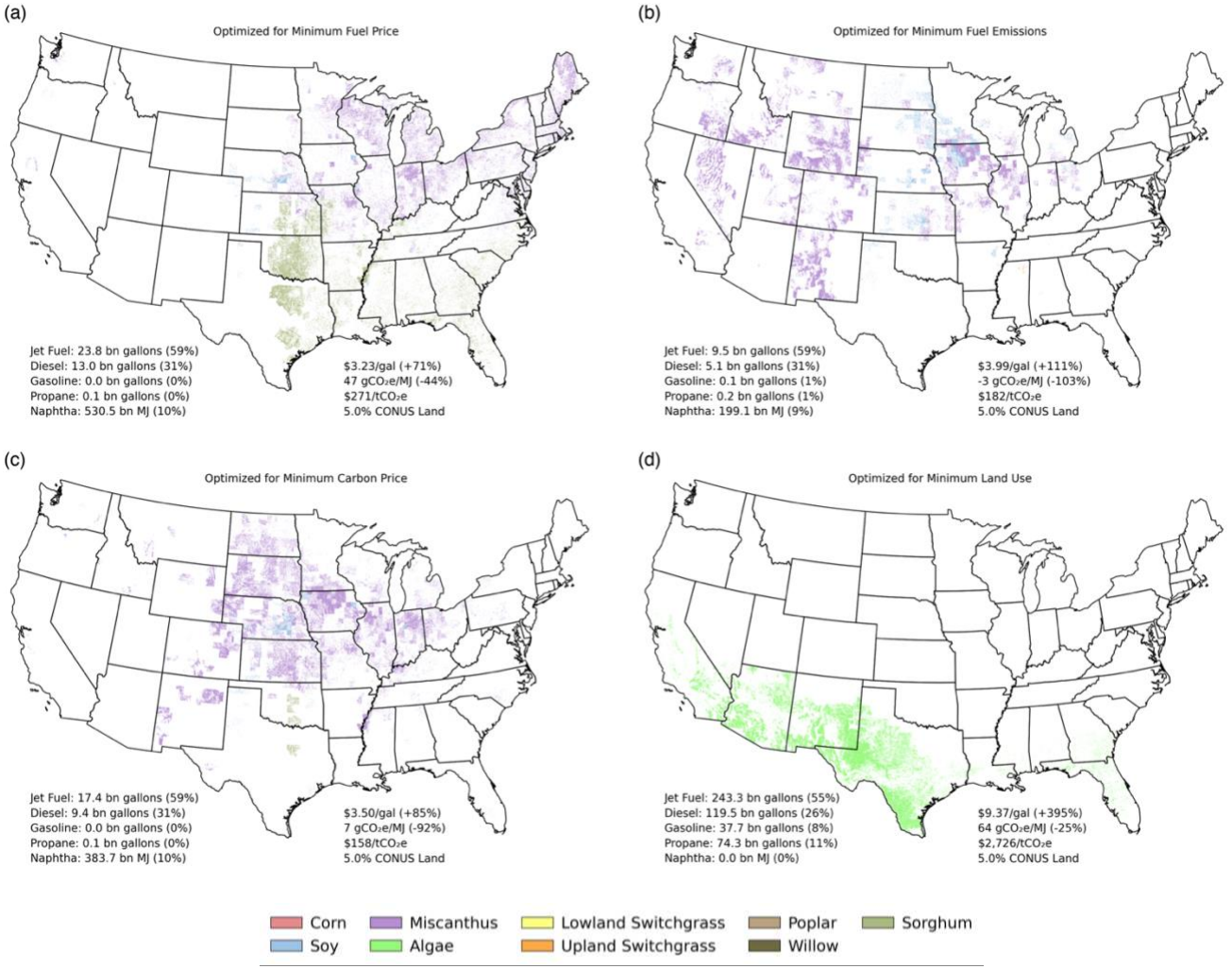

Figure C18. Multi-objective optimization maps of the optimal geographic feedstock deployment limited to existing bioenergy (corn ethanol and soybean biodiesel) land plus the historically max annual land conversion to cropland for 30 years while minimizing fuel price (a), fuel emissions (b), breakeven carbon price (c), and land area (d). Percentages in parentheses for the fuel products represent the total percent of megajoules produced for that fuel type as a percentage of total megajoules of fuel produced by the feedstocks. Percentages in parentheses for the mean fuel selling price and mean fuel emissions represent the percent cost increase and percent emissions reduction, respectively, compared to petroleum jet fuel.

Table C81. Optimization results breakdown by crop for the bioenergy + max conversion land limited scenario when optimized for minimum fuel costs.

	Jet Fuel (million gallons)	Jet Fuel Percentage	Land Use (ha)	Land Use Percentage (SAF)	Land Use Percentage (CONUS)	MFSP ($/gallon Jet)	GHG (gCO2e/MJ)	Carbon Price ($/tCO2e)
Algae	-	0.0%	-	0.0%	0.0%	$-	-	$-
Upland Switchgrass	-	0.0%	-	0.0%	0.0%	$-	-	$-
Lowland Switchgrass	-	0.0%	-	0.0%	0.0%	$-	-	$-
Miscanthus	12,362.9	52.0%	20,551,557	52.6%	2.6%	$3.21	48.66	$277.89
Poplar	-	0.0%	-	0.0%	0.0%	$-	-	$-
Corn	-	0.0%	-	0.0%	0.0%	$-	-	$-
Soy	176.4	0.7%	1,102,490	2.8%	0.1%	$3.13	(1.08)	$110.04
Willow	-	0.0%	-	0.0%	0.0%	$-	-	$-
Sorghum	11,229.4	47.2%	17,453,436	44.6%	2.2%	$3.26	46.24	$270.30

Table C82. Optimization results breakdown by crop for the bioenergy + max conversion land limited scenario when optimized for minimum fuel emissions.

	Jet Fuel (million gallons)	Jet Fuel Percentage	Land Use (ha)	Land Use Percentage (SAF)	Land Use Percentage (CONUS)	MFSP ($/gallon Jet)	GHG (gCO2e/MJ)	Carbon Price ($/tCO2e)
Algae	-	0.0%	-	0.0%	0.0%	$-	-	$-
Upland Switchgrass	12.0	0.1%	45,744	0.1%	0.0%	$4.15	(0.06)	$202.14
Lowland Switchgrass	-	0.0%	-	0.0%	0.0%	$-	-	$-
Miscanthus	8,840.3	93.3%	34,007,982	87.0%	4.4%	$3.94	(2.50)	$178.69
Poplar	-	0.0%	-	0.0%	0.0%	$-	-	$-
Corn	0.4	0.0%	2,646	0.0%	0.0%	$9.62	(11.25)	$612.36
Soy	623.4	6.6%	5,047,776	12.9%	0.6%	$4.60	(6.15)	$226.66
Willow	-	0.0%	-	0.0%	0.0%	$-	-	$-
Sorghum	-	0.0%	-	0.0%	0.0%	$-	-	$-

Table C83. Optimization results breakdown by crop for the bioenergy + max conversion land limited scenario when optimized for minimum carbon price.

	Jet Fuel (million gallons)	Jet Fuel Percentage	Land Use (ha)	Land Use Percentage (SAF)	Land Use Percentage (CONUS)	MFSP ($/gallon Jet)	GHG (gCO2e/MJ)	Carbon Price ($/tCO2e)
Algae	-	0.0%	-	0.0%	0.0%	$-	-	$-
Upland Switchgrass	-	0.0%	-	0.0%	0.0%	$-	-	$-
Lowland Switchgrass	-	0.0%	-	0.0%	0.0%	$-	-	$-
Miscanthus	16,448.6	94.8%	36,339,421	92.8%	4.7%	$3.52	6.12	$157.46
Poplar	-	0.0%	-	0.0%	0.0%	$-	-	$-
Corn	-	0.0%	-	0.0%	0.0%	$-	-	$-
Soy	288.0	1.7%	1,848,705	4.7%	0.2%	$3.36	(0.87)	$130.77
Willow	-	0.0%	-	0.0%	0.0%	$-	-	$-
Sorghum	616.5	3.6%	955,876	2.4%	0.1%	$3.15	32.59	$183.67

Table C84. Optimization results breakdown by crop for the bioenergy + max conversion land limited scenario when optimized for minimum land use.

	Jet Fuel (million gallons)	Jet Fuel Percentage	Land Use (ha)	Land Use Percentage (SAF)	Land Use Percentage (CONUS)	MFSP ($/gallon Jet)	GHG (gCO2e/MJ)	Carbon Price ($/tCO2e)
Algae	243,336.6	100.0%	39,218,827	100.0%	5.0%	$9.37	63.91	$2,726.40
Upland Switchgrass	-	0.0%	-	0.0%	0.0%	$-	-	$-
Lowland Switchgrass	-	0.0%	-	0.0%	0.0%	$-	-	$-
Miscanthus	-	0.0%	-	0.0%	0.0%	$-	-	$-
Poplar	-	0.0%	-	0.0%	0.0%	$-	-	$-
Corn	-	0.0%	-	0.0%	0.0%	$-	-	$-
Soy	-	0.0%	-	0.0%	0.0%	$-	-	$-
Willow	-	0.0%	-	0.0%	0.0%	$-	-	$-
Sorghum	-	0.0%	-	0.0%	0.0%	$-	-	$-

Table C85. Optimization results breakdown by land for the bioenergy + max conversion land limited scenario when optimized for minimum fuel costs.

	Jet Fuel (million gallons)	Jet Fuel Percentage	Land Use (ha)	Land Use Percentage (SAF)	Land Use Percentage (CONUS)	MFSP ($/gallon Jet)	GHG (gCO2e/MJ)	Carbon Price ($/tCO2e)
Barren Land	-	0%	-	0%	0%	$-	-	$-
Deciduous Forest	7,540.0	32%	12,073,069	31%	2%	$3.18	54.81	$327.02
Evergreen Forest	1,466.7	6%	2,476,560	6%	0%	$3.23	76.11	$1,171.67
Mixed Forest	2,236.0	9%	3,703,806	9%	0%	$3.21	68.54	$617.50
Shrubland	2,387.3	10%	3,701,690	9%	0%	$3.23	62.20	$450.61
Grassland Herbaceous	6,327.7	27%	10,769,764	28%	1%	$3.27	40.36	$235.99
Cultivated Crops	3,811.0	16%	6,382,593	16%	1%	$3.30	10.13	$143.64

Table C86. Optimization results breakdown by land for the bioenergy + max conversion land limited scenario when optimized for minimum fuel emissions.

	Jet Fuel (million gallons)	Jet Fuel Percentage	Land Use (ha)	Land Use Percentage (SAF)	Land Use Percentage (CONUS)	MFSP ($/gallon Jet)	GHG (gCO2e/MJ)	Carbon Price ($/tCO2e)
Barren Land	-	0%	-	0%	0%	$-	-	$-
Deciduous Forest	0.0	0%	12	0%	0%	$4.01	(0.56)	$188.95
Evergreen Forest	0.1	0%	708	0%	0%	$4.15	1.41	$206.24
Mixed Forest	0.2	0%	276	0%	0%	$3.13	2.78	$114.44
Shrubland	2,235.6	24%	17,167,514	44%	2%	$4.74	(4.86)	$241.40
Grassland Herbaceous	1,716.5	18%	9,080,182	23%	1%	$4.19	(2.22)	$200.67
Cultivated Crops	5,523.6	58%	12,855,456	33%	2%	$3.62	(2.04)	$151.40

Table C87. Optimization results breakdown by land for the bioenergy + max conversion land limited scenario when optimized for minimum carbon price.

	Jet Fuel (million gallons)	Jet Fuel Percentage	Land Use (ha)	Land Use Percentage (SAF)	Land Use Percentage (CONUS)	MFSP ($/gallon Jet)	GHG (gCO2e/MJ)	Carbon Price ($/tCO2e)
Barren Land	-	0%	-	0%	0%	$-	-	$-
Deciduous Forest	1,261.4	7%	1,829,528	5%	0%	$3.10	28.40	$163.63
Evergreen Forest	6.6	0%	13,945	0%	0%	$3.26	23.95	$170.58
Mixed Forest	182.1	1%	266,226	1%	0%	$3.12	26.74	$161.23
Shrubland	741.7	4%	3,074,990	8%	0%	$3.85	1.90	$180.03
Grassland Herbaceous	6,222.9	36%	17,410,055	44%	2%	$3.55	12.00	$172.92
Cultivated Crops	8,938.3	52%	16,549,257	42%	2%	$3.51	0.39	$145.94

Table C88. Optimization results breakdown by land for the bioenergy + max conversion land limited scenario when optimized for minimum land use.

	Jet Fuel (million gallons)	Jet Fuel Percentage	Land Use (ha)	Land Use Percentage (SAF)	Land Use Percentage (CONUS)	MFSP ($/gallon Jet)	GHG (gCO2e/MJ)	Carbon Price ($/tCO2e)
Barren Land	8,818.5	4%	1,331,782	3%	0%	$9.10	62.01	$2,407.46
Deciduous Forest	2,248.4	1%	383,774	1%	0%	$9.63	66.12	$3,152.23
Evergreen Forest	5,004.0	2%	825,943	2%	0%	$9.48	65.89	$3,055.74
Mixed Forest	1,410.4	1%	235,605	1%	0%	$9.47	66.47	$3,149.22
Shrubland	175,236.8	72%	28,225,561	72%	4%	$9.37	63.82	$2,712.69
Grassland Herbaceous	50,004.8	21%	8,110,074	21%	1%	$9.42	64.16	$2,774.71
Cultivated Crops	613.7	0%	106,089	0%	0%	$9.90	65.23	$3,114.74

Table C89. Estimation of annual sustainable aviation fuel (SAF) production potential from feedstock availability identified in the SAF Grand Challenge Roadmap and conversion factors from literature [28].

Feedstock	SAF Grand Challenge Biomass Availability (million tonnes year^{-1})	Conversion (gallon tonne^{-1})	Annual SAF (billion gallons)
Seed Oils (Soybeans)	9	37.42 [208]	0.31
Corn grain	148	46.04 [208]	6.18
Woody energy crops	71	12.11 [208]	0.78
Herbaceous energy crops	340	12.65 [208]	3.90
Algae	235	82.88 [208]	17.67
Agricultural Residue	176	7.59 [278]	1.21
Municipal solid waste	55	12.06 [208]	0.60
Forest waste	133	12.58 [208]	1.52
Fats, oils, and greases	7	161.44 [208]	1.03
Wet Wastes	78	48.12 [279]	3.40
Total	**1,252**		**36.60**

Impact of biorefinery location on economic and environmental impacts

Results presented in this main article and Appendix C assumed biomass transportation distances to agricultural distance centers for biorefining (see main article Section 4.2.6). Due to the uncertainty of future biorefinery locations, a sensitivity analysis was performed to is assumption by adjusting the placement of biorefineries to each county center. Under this alternate assumption, median biomass transportation distances decreased from 78.5 km to 20.1 km and SAF transportation distance increased marginally from 142.7 km to 144.8 km. However, these changes in biorefinery locations had minimal impact on overall results. In the county center biorefinery scenario, median minimum fuel selling price decreased by \$0.22 $gallon^{-1}$ on average (-3.9% change) and median fuel emissions decreased 1.3 $gCO_{2\text{-}eq}$ MJ^{-1} on average (-1.7% change). Full results for this alternative scenario are available in the associated open data package [226].